Titre: Title:	Application of biological ion exchange resins and gravity-driven membrane filtration process for drinking water treatment in remote areas
Auteur: Author:	Yaser Rasouli
Date:	2024
Type:	Mémoire ou thèse / Dissertation or Thesis
Référence: Citation:	Rasouli, Y. (2024). Application of biological ion exchange resins and gravity-driven membrane filtration process for drinking water treatment in remote areas [Thèse de doctorat, Polytechnique Montréal]. PolyPublie. https://publications.polymtl.ca/58017/

URL de PolyPublie: PolyPublie URL:	https://publications.polymtl.ca/58017/
Directeurs de recherche: Advisors:	Dominique Claveau-Mallet, & Benoit Barbeau
Programme: Program:	Génie civil

POLYTECHNIQUE MONTRÉAL

affiliée à l'Université de Montréal

Application of biological ion exchange resins and gravity-driven membrane filtration process for drinking water treatment in remote areas

YASER RASOULI

Département des génies civil, géologique et des mines

Thèse présentée en vue de l'obtention du diplôme de *Philosophiæ Doctor*

Génie civil

Avril 2024

POLYTECHNIQUE MONTRÉAL

affiliée à l'Université de Montréal

Cette thèse intitulée:

Application of biological ion exchange resins and gravity-driven membrane filtration process for drinking water treatment in remote areas

présenté par **Yaser RASOULI**

en vue de l'obtention du diplôme de *Philosophiæ Doctor*

a été dûment accepté par le jury d'examen constitué de:

Émilie BÉDARD, président

Dominique CLAVEAU-MALLET, membre et directrice de recherche

Benoît BARBEAU, membre et codirecteur de recherche

Sarah DORNER, membre

Patrick DROGUI, membre externe

DEDICATION

This thesis is dedicated to those whose unwavering support and encouragement have been instrumental in my academic journey. Their belief in my potential and their invaluable guidance have shaped this work and propelled me forward.

First and foremost, I extend my deepest gratitude to my supervisor, Dominique Claveau-Mallet. Your wisdom, expertise, and dedication to the pursuit of knowledge have been a constant source of inspiration. Your mentorship has not only enriched my academic experience but has also helped me grow as a researcher and an individual. I am profoundly grateful for your guidance throughout this journey.

I also want to express my sincere appreciation to my co-supervisor, Benoit Barbeau. Your insightful feedback, commitment to excellence, and collaborative spirit have played an essential role in the development of this thesis. Your mentorship has been instrumental in shaping my research and fostering a deeper understanding of the subject matter.

In the personal sphere, I owe a debt of gratitude to my beloved mother, Mesri. Your unwavering love, sacrifice, and unwavering belief in me have been a constant source of strength. Your resilience and determination have shown me the importance of perseverance in the face of challenges. This thesis is a testament to your enduring support.

To my loving wife, Tahmineh, I am profoundly grateful for your unwavering encouragement and understanding throughout this journey. Your patience, love, and unwavering belief in my abilities have been a constant source of motivation. Your presence in my life has made every step of this academic pursuit more meaningful.

To all of you, I dedicate this thesis with profound gratitude and appreciation. Your presence in my life has been a guiding light, and this work stands as a testament to our collective journey of growth, learning, and discovery.

With heartfelt thanks,

Yaser Rasouli

ACKNOWLEDGEMENTS

I would like to express my special gratitude to Dominique Claveau-Mallet and Benoit Barbeau because of their unlimited support during the PhD. I would like to thank to the Polytechnique Montreal technicians and research professionals, Gabriel St-Jean, Julie Philibert, Mélanie Bolduc, Tetiana Elyart, Jacinthe Mailly, and Yves Fontaine for their help in preparing the hybrid BIEX + GDCM setup and influent water and their technical support during this project. I intend to thank Noshin Reza from University of Waterloo for running and analyzing the LC-OCD samples. This project was funded by the Canada Research Chair for Decentralized and Small-Scale Water Treatment (file number 950-232871).

RÉSUMÉ

L'objectif principal de cette thèse était d'investiguer les processus de traitement de l'eau conçus pour être déployés dans des zones décentralisées et éloignées des systèmes centralisés. Par conséquent, les caractéristiques clés recherchées dans ces processus de traitement étaient une faible consommation d'énergie, une empreinte écologique réduite, des besoins d'entretien peu fréquents, aucune nécessité d'opérateurs qualifiés et une rentabilité globale. En conséquence, nous avons proposé l'utilisation de membrane à filtration frontale et gravitaire (GDM, avec des membranes en céramique et polymères) et de résines échangeuses d'ions (IEX), exploitées en mode biologique (BIEX), car leurs caractéristiques inhérentes correspondent aux exigences essentielles des systèmes de traitement décentralisés de l'eau.

Le premier objectif (article n° 1) de cette recherche était de synthétiser et caractériser trois types de membranes céramiques microfiltration (MF), avec différentes compositions de kaolin et alumine (M1 = 0 % wt d'alumine + 100 % wt de kaolin, M2 = 25 % wt d'alumine + 75 % wt de kaolin, et M3 = 50 % wt d'alumine + 50 % wt de kaolin), afin d'étudier leur application dans le processus membrane céramique entraînée par gravité (GDCM) lors de la filtration d'eau de rivière turbide, colorée et à forte teneur en matière organique naturelle (NOM). L'effet de la teneur en alumine a été évalué pour la filtration à long terme de l'eau de rivière en termes de flux membranaire et de qualité du perméat. De plus, les caractéristiques physiques de biofilm et la concentration de micro-organismes actifs dans le biofilm ont été étudiées. Les résultats pour les membranes fabriquées en laboratoire ont montré un flux stabilisé de 2,5 à 3,0 LMH indépendamment de l'alumine. Un enlèvement substantiel de l'UVA_{254}, de l'alcalinité et du COD pendant les premiers jours de filtration a été réalisé, ainsi que l'élimination de la turbidité après stabilisation du flux. Une couche de biofilm hétérogène et dispersée distincte avant la stabilisation du flux a été observée, suivie de la formation d'une couche de gâteau dense et irrégulière, confirmant la transformation du mécanisme du modèle de «blocage des pores» au modèle de «Formation de gâteau couche». Enfin, une forte concentration d'alumine dans la structure de la membrane (M3 avec 50 % wt d'alumine) a accru l'adsorption de carbone, renforçant l'activité biologique et l'épaisseur moyenne du biofilm formé à la surface de la membrane.

Le deuxième objectif (article n° 2) de cette thèse était d'intégrer une colonne BIEX en tant que prétraitement au processus GDCM (avec les mêmes types de membranes MF céramiques qu'à

l'objectif 1) afin d'augmenter le flux, la qualité du perméat et les caractéristiques du biofilm de l'effluent du processus hybride. Les résultats du processus hybride ont été comparés à ceux du processus GDCM sans prétraitement (à l'objectif 1). La colonne BIEX a éliminé environ 74 % du COD par rapport à l'eau influente, suivi de l'élimination de 27 % du COD en utilisant M3 par rapport à l'effluent de la colonne BIEX au jour 65 (6 240 BV), ce qui était remarquablement plus élevé que dans le processus GDCM sans prétraitement (~ 6 %). Le processus hybride BIEX + GDCM a réduit la turbidité de 2,20 UTN à 0,09 UTN. Le flux le plus stabilisé a atteint ~ 5,7 LMH, soit près de deux fois celui du GDCM sans prétraitement. Les biofilms membranaires dans le processus hybride présentaient une épaisseur et une rugosité inférieures à celles du GDCM sans prétraitement. Une concentration plus élevée d'EPS et une activité biologique accrue ont été observées pour M3 (50 % wt d'alumine + 50 % wt de kaolin), la membrane présentant le flux stabilisé le plus élevé et l'efficacité d'élimination du COD la plus élevée. Les conclusions suggèrent que l'approche hybride combinant BIEX et GDCM est une méthode résiliente, performante et conviviale capable d'améliorer à la fois le flux et la qualité du perméat dans les systèmes GDCM.

Dans le cadre du troisième objectif (article n° 3), l'effet du nettoyage physique et chimique sur des membranes céramiques et polymériques en termes de flux stabilisé, de récupération du flux après nettoyage physique/chimique, et de qualité du perméat a été étudié. Deux types de membranes MF et UF ont été utilisés (M1 = MF polymère, M2 = UF polymère, M3 = UF céramique, et M4 = MF céramique fabriquée en laboratoire) dans le processus hybride BIEX + GDM lors de la filtration du même affluent que dans les objectifs 1 et 2. Le nettoyage physique a été effectué sous forme de rétro-lavage air/eau avec deux débits et pressions différents, et le nettoyage chimique a utilisé NaOH à des concentrations de 20 et 40 mM, ainsi que NaOCl à des concentrations de 250 et 500 mg Cl_2/L. Les résultats ont montré un flux stabilisé de 3,8 à 5,2 LMH aussi bien avant qu'après le processus de nettoyage, suggérant que les matériaux membranaires ne jouent pas un rôle clé. Le flux stabilisé moyen des membranes polymériques a augmenté après le nettoyage, tandis que celui des membranes céramiques a diminué. Un débit et une pression accrus lors du rétro-lavage air/eau ont entraîné une élimination accrue de l'encrassement hydraulique réversible, considéré comme le type d'encrassement dominant. Les membranes céramiques ont révélé une plus grande élimination de l'encrassement hydraulique réversible que les membranes polymériques. Le nettoyage chimique a eu peu d'impact sur la récupération du flux; par conséquent, il est recommandé d'utiliser uniquement le nettoyage physique.

En résumé, les résultats de cette recherche non seulement contribuent à notre compréhension des processus de traitement de l'eau, mais offrent également des perspectives pratiques et des solutions adaptées aux petits systèmes décentralisés, contribuant ainsi à l'objectif de fournir des options de traitement de l'eau durables et accessibles pour les communautés éloignées et mal desservies.

ABSTRACT

The overarching goal of this thesis was to investigate water treatment processes designed for deployment in decentralized and remote areas, far from centralized systems. Consequently, the key characteristics sought in these treatment processes were low energy consumption, reduced footprint, infrequent maintenance requirements, no need for skilled operators, and overall cost-effectiveness. As a result, we proposed the utilization of gravity-driven membrane (GDM, with ceramic and polymeric membranes) and ion exchange (IEX) resins, operated in the biological mode (BIEX), as their inherent features align with the essential requirements of decentralized water treatment systems.

The first objective (paper # 1) of this research was to synthesize and characterize three types of ceramic microfiltration (MF) membranes with different compositions of kaolin clay and alumina (M1 = 0 % wt alumina + 100 % wt kaolin, M2 = 25 % wt alumina + 75 % wt kaolin, and M3 = 50 % wt alumina + 50 % wt kaolin) to study their applications in the gravity-driven ceramic membranes (GDCM) process during turbid, colored, and high natural organic matter (NOM) content river water filtration. The effect of alumina content was evaluated for long-term river water filtration in terms of membrane flux and permeate quality. Moreover, the physical characteristics of the biofouling layer and the concentration of active microorganisms in the biofilm were investigated. The results for the lab-made membranes showed a stabilized flux of 2.5 – 3.0 LMH which was independent of the alumina content. A substantial UVA_{254}, alkalinity, and DOC removal during the initial filtration days were achieved as well as the turbidity removal after flux stabilization. A distinct heterogeneous and scattered biofilm layer before flux stabilization was observed, followed by a dense and irregular cake layer formation, confirming the transformation of the mechanism from pore blocking model to cake layer formation model. Finally, a high concentration of alumina in the membrane structure (M3 with 50 % wt alumina) increased carbon adsorption, which enhances biological activity and mean biofilm thickness formed on the membrane surface.

The second objective (paper # 2) of this thesis was to integrate a BIEX column as a pre-treatment to the GDCM process (with the same ceramic MF membrane types as in objective 1) in order to increase the flux, permeate quality, and the biofilm characteristics of the hybrid process effluent. The hybrid process results were compared with those of the GDCM process without the BIEX pre-

treatment (in objective 1). The BIEX column removed approximately 74 % of the DOC compared with the influent water, followed by 27 % DOC removal using M3 compared with the BIEX column effluent on day 65 (6,240 BV), which was remarkably higher than that in the GDCM process without pre-treatment (~ 6%). The hybrid BIEX + GDCM process removed the turbidity from 2.20 NTU to 0.09 NTU. The most stabilized flux achieved ~ 5.7 LMH, which was almost two-fold compared to GDCM without pre-treatment. The membrane biofilms in the hybrid process showed lower thickness and roughness than that in GDCM without pre-treatment. Higher EPS concentration and biological activity were observed for M3 (50 % wt alumina + 50 % wt kaolin), the membrane with the highest stabilized flux and highest DOC removal efficiency. The findings suggest that the hybrid approach combining BIEX and GDCM proves to be a resilient, high-performing, and user-friendly method capable of enhancing both flux and permeate quality in GDCM systems.

In the third objective (paper # 3), the effect of physical and chemical cleaning on ceramic and polymeric membranes in terms of stabilized flux, flux recovery after physical/chemical cleaning, and permeate quality studied. Two types of MF and UF membranes were used (M1 = polymeric MF, M2 = polymeric UF, M3 = ceramic UF, and M4 = lab-made ceramic MF) in the hybrid BIEX + GDM process during filtration of the same influent water as in objectives 1 and 2. Physical cleaning was performed in the form of air/water backwash with two different flows and pressures, and chemical cleaning utilized NaOH at concentrations of 20 and 40 mM, as well as NaOCl at concentrations of 250 and 500 mg Cl_2/L. The results showed a stabilized flux of 3.8 – 5.2 LMH both before and after the cleaning process, suggesting that membrane materials do not play a key role. The mean stabilized flux of polymeric membranes experienced an increase after cleaning, whereas that of ceramics decreased. Enhanced air/water backwash flow and pressure resulted in increased removal of hydraulic reversible fouling, which was considered as the dominant fouling type. Ceramic membranes revealed higher removal of reversible hydraulic fouling than polymeric membranes. Chemical cleaning had a low impact on flux recovery; therefore, only employing physical cleaning is recommended.

In summary, the findings of this research not only contribute to our understanding of water treatment processes but also offer practical insights and solutions tailored for small-scale decentralized systems, thereby advancing the goal of providing sustainable and accessible water treatment options for remote and underserved communities.

TABLE OF CONTENTS

LIST OF TABLES

LIST OF FIGURES

LISTE OF SYMBOLS AND ABBREVIATIONS

GDM	Gravity-driven membrane
GDCM	Gravity-driven ceramic membrane
DOC	Dissolved organic carbon
TOC	Total organic carbon
UVA	Ultra-violet absorption
MF	Microfiltration
UF	Ultrafiltration
TMP	Transmembrane pressure
NF	Nanofiltration
RO	Reverse osmosis
BIEX	Biological ion exchange
IEX	Ion exchange
BV	Bed volume
GAC	Granular activated carbon
PAC	Powdered activated carbon
NOM	Natural organic matter
HS	Humic substances
BB	Building blocks
BP	Biopolymers
LMW	Low molecular weight
SiC	Silicon carbide
PVDF	Polyvinylidene difluoride
PES	Polyether sulfone

LMH	L m^{-2} h^{-1}
PTFE	Polytetrafluoroethylene
CLSM	Confocal laser scanning microscopy
OCT	Optical coherence tomography
QCM-D	Quartz crystal microbalance with dissipation
ATP	Adenosine triphosphate
EPS	Extracellular polymeric substances
THMs	Trihalomethanes
BAC	Biological activated carbon
BDOC	Biological dissolved organic carbon
CIEX	Chloride-form ion exchange
AOC	Assimilable organic carbon
GDMBR	Gravity-driven membrane bioreactor
XRD	X-ray diffraction
SEM	Scanning electron microscopy
DI water	Deionized water
USEPA	United States environmental protection agency
EBCT	Empty bed contact time
LC-OCD	Liquid chromatography – organic carbon detection
ANOVA	Analysis of variance
PS	Polysaccharide
PN	Protein

LIST OF APPENDICES

CHAPTER 1 Introduction

1.1 Objective of the thesis

Ensuring access to safe and clean drinking water sources is of utmost significance for every community. Traditionally, individuals residing in large urban centers have had the privilege of convenient access to treated water resources due to the presence of sophisticated centralized water treatment infrastructure. However, this privilege is not necessarily extended to small, remote communities situated far from urban centers. In these remote areas, the necessity for passive and decentralized water treatment systems becomes evident, primarily to mitigate the presence of hazardous contaminants such as Natural Organic Matter (NOM) and turbidity. Decentralized water treatment systems are designed to provide efficient water purification on a small scale, often for individual households or small communities. They are typically intended to serve populations ranging from a few individuals to a few hundred. These systems can be installed in various locations, including rural areas, peri-urban zones, or even in isolated facilities such as vacation camps or remote industrial sites.

Passive water treatment systems represent a viable solution in such contexts. Unlike conventional treatment methods, passive systems do not rely on the continuous addition of chemical reagents to carry out purification processes. Passive water treatment systems offer several advantages for addressing water quality concerns in remote communities. Firstly, they boast low operating and maintenance costs, making them an economically sustainable option for resource-constrained regions. Additionally, these systems are designed for long-term use, providing long-term solutions to water treatment needs. Furthermore, their operational requirements are minimal, reducing the need for constant supervision, which can be particularly beneficial in areas where human resources are limited (Derlon, Mimoso et al. 2014, Shao, Feng et al. 2017). Expanding upon the importance of passive water treatment systems in remote communities, it is crucial to consider their adaptability to varying environmental conditions. These systems can be tailored to suit the specific water quality challenges encountered in different geographic locations. Whether it be addressing high levels of NOM or reducing turbidity in surface water, passive water treatment systems can be customized to effectively target local contaminants. Passive systems often employ natural processes such as filtration and biological process, harnessing the inherent capacity of ecosystems

to purify water. This eco-friendly approach not only enhances water quality but also minimizes the ecological footprint of water treatment activities, aligning with sustainable and environmentally conscious practices (Zhang, Wang et al. 2020, Hafeez, Shamair et al. 2021).

Since the conventional coagulation, flocculation, and settling treatment processes are not considered as an option in the decentralized treatment due to continuous addition of chemicals, frequent required maintenance and supervision, the proposed solution is using gravity-driven membrane (GDM) process to remove color and turbidity in the decentralized water treatment. During the dead-end GDM process (MF/UF), water passes by gravity through the membrane in order to achieve a stable flux. Therefore, there is no need to use pump and the pilot would be simple to operate with minimal supervision. Conventionally, two types of polymeric and ceramic membranes can be used in the GDM process. Utilizing ceramic membranes instead of polymeric membranes offers several advantages owing to their superior mechanical, thermal, and chemical resilience, thereby extending their operational lifespan. The extended durability of ceramic membranes in long-term filtration processes holds critical significance, as it serves to reduce the capital cost required for plant installation, notwithstanding its elevated manufacturing expenses (Freeman and Shorney-Darby 2011). Hence, the advantages associated with the GDM process, which employs ceramic MF membranes for the removal of turbidity and color from surface water, motivated the pursuit of the first objective of this thesis.

The overall objective of this thesis was to explore water treatment methods tailored for implementation in decentralized water treatment systems. Accordingly, we recommended employing GDM with ceramic and polymeric membranes and ion exchange resins, operating in the biological mode (BIEX), as their intrinsic features align harmoniously with the fundamental necessities of decentralized water treatment systems. In the first objective, we focused on the GDM process while in the second objective, the hybrid BIEX + GDM process was investigated.

Objective 1: Synthesis, characterization, and application of kaolin/alumina based ceramic MF membranes in GDM process for the long-term treatment of colored and turbid surface water. In this objective, we have fabricated ceramic membranes in the laboratory with different kaolin and alumina contents to investigate the effect of alumina content on the stabilized flux, permeate quality, and biofilm characteristics formed on the membrane surface.

As mentioned above, NOM content in the drinking water is harmful for the human body and causes disinfection by products during disinfection process. Since the ceramic MF membranes in the GDM process are not high-performance in NOM elimination, to remove NOM from surface water in the decentralized environment, we have proposed biological ion exchange (BIEX) resin process as a pre-treatment for GDM process in the second objective. BIEX resin process is the ion exchange (IEX) resin process in which the regeneration occurs at longer intervals to promote secondary IEX in which NOM of the influent water displaced with bicarbonate and sulfate anions instead of chloride preloaded anions (primary IEX) (Liu, Lompe et al. 2020, Liu, Papineau et al. 2021). Postponing regeneration stage results in less production of spent brine and secondary pollution, minimum required supervision and maintenance, and lower operation cost.

Objective 2: Evaluation of BIEX performance as a pre-treatment step for GDM process during surface water treatment. Application of hybrid BIEX + GDM process with the same ceramic membranes, influent water, and operating conditions as in objective 1 was investigated in terms of stabilized flux, permeate quality, and biofilm characteristics to remove NOM using BIEX resin and turbidity by GDM process.

It is essential to carefully select the membrane type that maximizes productivity of the process and the quality of the effluent permeating from hybrid BIEX + GDM process. In assessing the permeability of polymeric and ceramic membranes, polymeric membranes frequently showed greater permeability compared to ceramic membranes (Moulin, Bourbigot et al. 1991, Bodzek and Konieczny 1998, Klomfas and Konieczny 2004). Fouling quantification however showed the same values (Oligny, Bérubé and Barbeau 2016) or lower fouling for ceramic membranes (Hofs, Ogier et al. 2011). To quantify the different fouling types causing flux decline in the GDM process and select the right membrane types, research (objective 3) is required to establish the optimal membrane cleaning conditions and the potential advantages of employing ceramic membranes to enable aggressive chemical washing of membranes that have been in operation for several months without cleaning.

Objective 3: Quantifying different fouling types causing flux decline in BIEX + GDM hybrid process in polymeric and ceramic MF/UF membranes. Furthermore, investigating the effect of increased and decreased physical (air/water backwash) and chemical cleaning (NaOH, NaOCl)

intensities on the stabilized flux, different fouling types, permeate quality, and biofilm characteristics. Finally, comparing the performance of polymeric and ceramic MF/UF membranes to select the right membrane type.

1.2 Content of this thesis

This paper-based thesis consists of three main objectives (mentioned above) and one published paper has been defined for each objective. In the literature review chapter (chapter 2), it was tried to cover the most recent advances achieved in the three objectives. Consequently, three main sections in the literature review chapter have been designed. For objective 1, the literature review highlighted the application of GDM process for drinking water treatment in the decentralized systems for remote areas. In the case of objective 2, recent advances related to application of BIEX resin in drinking water treatment in the decentralized systems were studied. Moreover, application of hybrid processes with GDM filtration in drinking water treatment in passive systems was reviewed to find the knowledge gaps in these fields. Finally, literature review in objective 3 focused on reviewing available knowledge related to comparing performance of ceramic and polymeric membrane, quantifying fouling types, and mitigating fouling in GDM process. The research objectives and hypothesis of the thesis are provided in chapter 3. The published papers for each objective are presented in chapter 4, chapter 5, and chapter 6 as follow:

Objective 1: **Rasouli, Y**., Maltais-Tariant, R., Barbeau, B., Lapointe, M., Boudoux, C., & Claveau-Mallet, D. (2023). Synthesis, characterization, and application of gravity-driven ceramic microfiltration membranes for surface water treatment. Journal of Water Process Engineering, 51, 103430.

Objective 2: **Rasouli, Y**., Maltais-Tariant, R., Barbeau, B., Peldszus, S., Boudoux, C., & Claveau-Mallet, D. (2024). Performance of biological ion exchange resin and gravity-driven ceramic membrane hybrid process for surface water treatment. Separation and Purification Technology, 332, 125769.

Objective 3: **Rasouli, Y.**; Barbeau, B.; Maltais-Tariant, R.; Boudoux, C.; Claveau-Mallet, D. Impact of Cleaning on Membrane Performance during Surface Water Treatment: A Hybrid Process

with Biological Ion Exchange and Gravity-Driven Membranes. Membranes 2024, 14, 33. https://doi.org/10.3390/membranes14020033

Finally, an overall integration of the thesis results is presented in chapter 7.

CHAPTER 2 Context and literature review

2.1 Application of GDM process without pretreatment using lab-made ceramic membranes (objective 1, paper 1)

The Gravity-Driven Membrane (GDM) process has garnered considerable attention over the past decade (Peter-Varbanets, Hammes et al. 2010). Notably, this process is distinguished by several unique features, including its reliance on low applied transmembrane pressure driven by gravity, the phenomenon of flux stabilization, and the formation of biofilm on the membrane surface.

The formation of biofilm on the membranes is a crucial aspect of the GDM process, as elucidated by Pronk et. al (Pronk, Ding et al. 2019). This biofilm plays a pivotal role in facilitating a stable flux, thereby enabling prolonged filtration periods without the need for frequent membrane cleaning procedures. Such a characteristic underscores the practicality and sustainability of the GDM process in various applications.

Given the inherent reliance on relatively low transmembrane pressure, the GDM process is predominantly operated in dead-end mode. Furthermore, it is pertinent to note that only membranes classified under the categories of MF and UF are utilized within the framework of the GDM process. This selective employment of membranes underscores the tailored approach adopted in GDM applications, further emphasizing its specialized nature.

For a comprehensive understanding of the GDM process, the literature review is segmented into three distinct subsections: I) Membrane module and configuration, II) The stable flux of GDM, and III) Characteristics of the biofilm formed on the membrane. This organizational structure aims to elucidate the multifaceted aspects of the GDM process, facilitating a nuanced analysis of its operational principles and performance characteristics.

2.1.1 Membrane module and configuration

In the GDM filtration process, fluid gravity serves as the driving force, typically employed in the dead-end mode. Two common configurations, external and submerged membranes, are utilized, as depicted schematically in Figure 2-1.

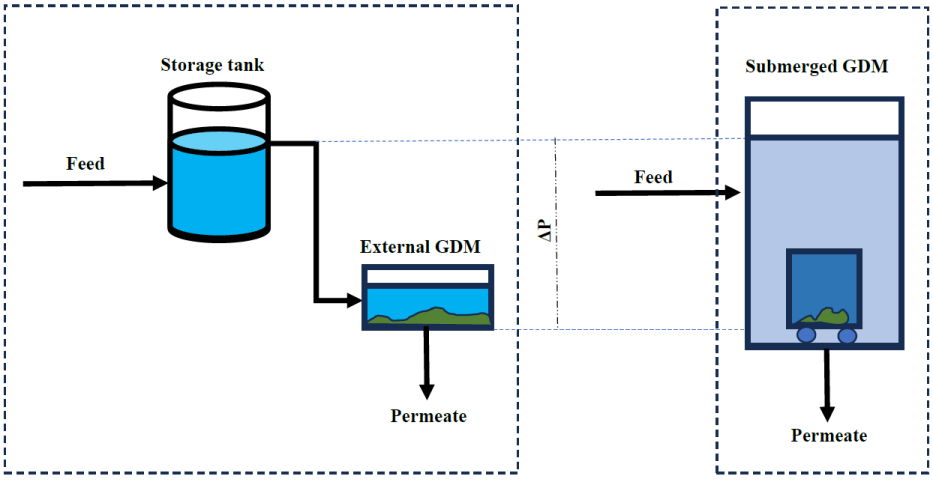

Figure 2-1. Two common configurations for GDM process, external GDM and submerged GDM (Pronk, Ding et al. 2019)

In the external GDM configuration, the storage tank is positioned above the membrane module, creating a pressure differential (ΔP) ranging from approximately 40 mbar to 100 mbar(Pronk, Ding et al. 2019). Similarly, in the submerged GDM setup, the same pressure difference can be achieved by submerging the membrane module in the feed solution.

Polymeric and ceramic membranes are regarded as reliable filters in drinking water treatment (Rasouli, Abbasi and Hashemifard 2019). While the use of polymeric membranes in tubular, flat sheet, or hollow fiber forms has been extensively studied in the GDM process, the application of ceramic membranes in this context remains relatively unexplored.

This research aims to investigate the performance of ceramic membranes in the GDM process. Consequently, the following sections will provide a brief overview of the synthesis and characteristics of ceramic membranes, laying the foundation for their potential application in GDM filtration.

2.1.1.1 Ceramic membrane materials

Ceramic membranes belong to the category of inorganic membranes and are primarily composed of oxides such as aluminum (Al), silicon (Si), titanium (Ti), or zirconium (Zr), along with materials like silicon carbide (SiC). They cover a wide range of filtration processes from MF to NF (Samaei, Gato-Trinidad and Altaee 2018). Compared to polymeric membranes, ceramic membranes offer several advantages, including greater mechanical, chemical, and thermal stability, as well as a

wider range of pH tolerance, easy cleaning procedures, and longer lifespan (Rasouli, Abbasi and Hashemifard 2019). These characteristics make ceramic membranes particularly suitable for demanding applications in various industries, including water treatment and filtration. To enhance cost-effectiveness, researchers have explored alternative materials for ceramic membrane production. Recently, clays such as Kaolin and natural zeolite have been investigated as potential raw materials. These natural resources offer economic benefits while maintaining the desired properties and performance of ceramic membranes (Rasouli, Abbasi and Hashemifard 2017). By leveraging the unique properties of ceramic membranes and exploring innovative approaches to their production, researchers aim to further improve the efficiency and affordability of membrane-based processes such as the GDM filtration. This research endeavor holds the promise of advancing sustainable water treatment solutions and expanding the applicability of ceramic membranes in diverse industrial and environmental contexts.

2.1.1.2 Ceramic membrane fabrication techniques

Phase-inversion, pressure casting, extruding and sintering techniques are among the most widely used methods of fabrication of ceramic membranes (Samaei, Gato-Trinidad and Altaee 2018). Generally, synthesis of ceramic membranes consists of preparation of 1) powder and suspension, 2) shaping by pressing; tape and slip casting; extrusion; phase inversion; foam techniques and leaching techniques, 3) heat treatment including pre-sintering, thermolysis and final sintering 4) additional layer deposition by dip or spin coating, sol-gel and chemical vapor deposition (Lee, Wu and Li 2015).

2.1.2 The flux stabilization in GDM process

The flux stabilization phenomenon which occurs in dead-end long-term filtration by postponing cleaning and backwashing stages, was first published in 2010 by Peter et. al (Peter-Varbanets, Hammes et al. 2010). In which, initially the flux declined rapidly until approximately 5 days of operation, then it reached a stable flux. Figure 2-2, illustrates the flux stabilization for two different feed water (river and lake) and wastewater (TOC of 12.5 and 4.8 mg C/L). The stable flux depends on some factors such as influent water characteristics, operating pressure by gravity, temperature and membrane module configuration (Pronk, Ding et al. 2019).

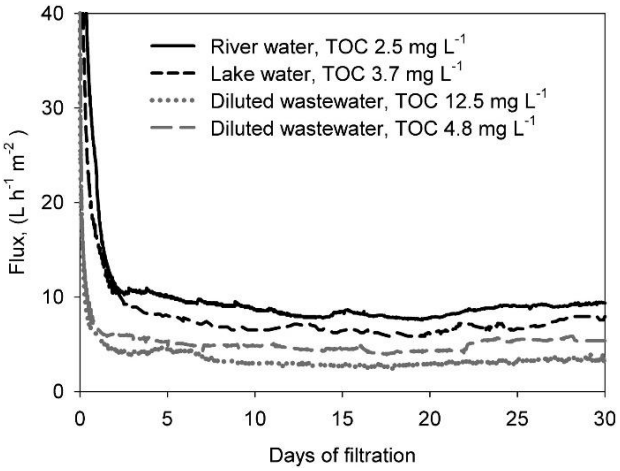

Figure 2-2. Flux stabilization phenomenon for two different water and wastewater using polyethersulfone 100 kDa (UF) membrane at ΔP = 65 mbar and T = 20°C (Peter-Varbanets, Hammes et al. 2010)

2.1.2.1 Influent water characteristics

The GDM process has found widespread application in various decentralized water treatment systems, where it is utilized to filter different types of water sources to produce potable water, as well as for non-potable applications such as wastewater treatment and seawater pre-treatment for reverse osmosis processes. In decentralized systems, GDM is employed to filter river water, rainwater, and greywater to produce potable water. Additionally, in non-potable applications, GDM is used for wastewater treatment to meet discharge standards and as a pre-treatment step for seawater prior to reverse osmosis processes. Table 2-1 provides a summary of influential studies in the literature that have investigated the effect of influent water characteristics on the stable flux in the GDM process. The results demonstrate that the stable flux is significantly influenced by the presence of organic contaminants in the influent water or wastewater. The organic content of the influent water, including dissolved organic carbon (DOC) and other organic compounds, can significantly impact the stabilized flux. High levels of organics can lead to fouling of the membrane surface, reducing flux over time. Organic fouling occurs when organic molecules adsorb onto the membrane surface and form a cake layer, hindering water flow through the membrane. Additionally, organic matter can provide nutrients for microbial growth, leading to biofilm formation, which further contributes to flux decline. Specifically, higher concentrations of organic substances lead to the formation of a more resistant biofilm, resulting in a sequence of permeate

flux as follows: diluted wastewater/greywater < rainwater < river water/seawater (Pronk, Ding et al. 2019).

2.1.2.2 Operating pressure

In pressure-driven membrane processes, such as reverse osmosis and ultrafiltration, there exists a linear correlation between the applied transmembrane pressure and membrane flux. However, the Gravity-Driven Membrane (GDM) process presents a unique behavior in this regard. Several studies (Peter-Varbanets, Hammes et al. 2010, Kus, Kandasamy et al. 2013, Akhondi, Wu et al. 2015) have reported that changing the transmembrane pressure in the GDM process does not significantly affect the stable flux. This phenomenon contrasts with the behavior observed in pressure-driven processes. The stability of flux in GDM despite variations in transmembrane pressure can be attributed to the formation of a biofilm layer on the membrane surface. Increasing the applied pressure may indeed enhance the fouling resistance of this biofilm layer, thereby maintaining a stable flux over time.

Table 2-1. Results of membrane filtration performance in the reported GDM systems fed with different types of water (Pronk, Ding et al. 2019).

Influent water	Stable flux (LMH)	Pore size	Module type	Applied pressure (mbar)	Hydraulic resistance (10^{-11} m^{-1})			References
					Membrane	Total	Biofilm	
River water	10	PES 100 KDa	Flat sheet	65	3	23.4	20.4	(Peter-Varbanets, Hammes et al. 2010)
Dil. Wastewater (125 mg TOC/L)	4	PES 100 KDa	Flat sheet	65	3	58.4	55.4	(Peter-Varbanets, Hammes et al. 2010)
River water treated by sand filtration	11.1	PES 100 KDa	Flat sheet	65	3	21	18	(Peter-Varbanets, Margot et al. 2011)
River water	8.0	PES 100 kDa	Flat sheet	40	3.0	18.0	15.0	(Derlon, Peter-Varbanets et al. 2012)
Pond/tap water	8	PVDF 40 nm	hollow fiber in-out	40	3	18.0	15.0	(Oka, Khadem and Bérubé 2017)

Table 2.1. Results of membrane filtration performance in the reported GDM systems fed with different types of water (Pronk, Ding et al. 2019) (cont'd).

Influent water	Stable flux (LMH)	Pore size	Module type	Applied pressure (mbar)	Hydraulic resistance (10^{-11} m^{-1})			References
					Membrane	Total	Biofilm	
No fouling control	*	PVDF 40 nm	hollow fiber in-out	*	33.1	157.7	124.6	(Oka, Khadem and Bérubé 2017)
Air sparging	*	PVDF 40 nm	hollow fiber in-out	*	33.1	82.8	49.7	(Oka, Khadem and Bérubé 2017)
Backwashing	*	PVDF 40 nm	hollow fiber in-out	*	28	57.1	29.1	(Oka, Khadem and Bérubé 2017)
Dil. Wastewater	4	PES 20 KDa	Flat sheet	45	5.4	-	-	(Wang, Fortunato et al. 2017)

*Membrane systems operated at constant flux instead of constant pressure.

Table 2.1. Results of membrane filtration performance in the reported GDM systems fed with different types of water (Pronk, Ding et al. 2019) (cont'd).

Influent water	Stable flux (LMH)	Pore size	Module type	Applied pressure (mbar)	Hydraulic resistance (10^{-11} m^{-1})			References
					Membrane	Total	Biofilm	
7.5 mg COD/L	4	PES 20 KDa	Flat sheet	45	-	40.4	35.0	(Wang, Fortunato et al. 2017)
15 mg COD/L	2	PES 20 KDa	Flat sheet	45	-	80.8	75.4	(Wang, Fortunato et al. 2017)
Greywater	2	PVDF 0.2 μm	hollow fiber in-out	30	3.1	107.8	104.7	(Jabornig and Podmirseg 2015)
Greywater	1	PVDF 0.2 μm	hollow fiber in-out	30	3.1	53.9	50.8	(Jabornig and Podmirseg 2015)

Table 2.1. Results of membrane filtration performance in the reported GDM systems fed with different types of water (Pronk, Ding et al. 2019) (cont'd).

Influent water	**Stable flux (LMH)**	**Pore size**	**Module type**	**Applied pressure (mbar)**	**Hydraulic resistance (10^{-11} m^{-1})**			**References**
					Membrane	**Total**	**Biofilm**	
Synthetic greywater	2	PES 150 KDa	Flat sheet	50	3	89.8	86.8	(Ding, Liang et al. 2016)
Rainwater	6	PES 150 KDa	Flat sheet	50	3	29.9	26.9	(Ding, Liang et al. 2017)
Seawater	18.6	PVDF 80 nm	Flat sheet	40	0.8	7.7	6.9	(Wu, Suwarno et al. 2017)
River water with addition of nematodes	18-20	Hydrophylized Polysulfone	Flat sheet	61.5	5.7	11.1	5.4	(Klein, Zihlmann et al. 2016)

2.1.2.3 Temperature

In the GDM process, temperature plays a significant role in influencing various aspects of membrane filtration performance. One crucial effect of temperature is its impact on water viscosity, which in turn affects membrane flux according to Darcy law. As temperature increases, water viscosity typically decreases, leading to lower resistance to flow through the membrane. This results in higher membrane flux rates, as predicted by Darcy law. The relationship between temperature and membrane flux is fundamental in understanding and optimizing the operation of GDM systems, particularly in applications where controlling flux rates is critical.

Furthermore, temperature also influences the growth and activity of microbial communities within the GDM system. Microbial growth can impact membrane fouling, a common challenge in membrane filtration processes. A study (Akhondi, Wu et al. 2015) has highlighted the effect of temperature on fouling resistance in the GDM process. Specifically, it has been reported that increasing the temperature from 21 to 29 ^{o}C resulted in approximately a 25% reduction in fouling resistance at a pressure driving force of 40 mbar. This reduction in fouling resistance suggests that higher temperatures may alter the composition of the biofilm layer on the membrane surface, thereby reducing fouling propensity. While higher temperatures may generally promote microbial growth, in the specific context of the observed reduction in fouling resistance, various mechanisms may interact to alter the dynamics of biofilm formation and thus reduce the risk of membrane fouling. In this study, the reduction in fouling resistance appears to be directly related to the decreasing viscosity of the influent water, rather than microbial activity.

2.1.2.4 Membrane module configuration

Membrane characteristics and module configuration such as pore size, membrane type (for example ceramic or polymeric), flat sheet or hollow fiber modules can affect the stable flux. Using the flat sheet membranes, with the pore sizes of 100 nm and 20 nm, the stable flux has been reported around 4 – 5 LMH despite a different initial obtained flux (Frechen, Exler et al. 2011). Wu et. al (Wu, Hochstrasser et al. 2016, Wu, Christen et al. 2017) used several types of MF and UF polymeric flat sheet membranes for seawater pre-treatment. The results of their investigation are summarized in the Table 2-2.

Table 2-2. Effect of membrane characteristics on the membrane performance in a dead-end GDM filtration during seawater pretreatment (Pronk, Ding et al. 2019)

	Flat sheet				**Hollow fiber**
Materials	PES	PVDF	PVDF	PVDF	PVDF
Brand	Microdyn-Nadir	Millipore	Millipore	-	GE
Pore size	100 kDa	0.22 μm	0.45 μm	0.08 μm	0.1 μm
Membranes Area (m^2)	0.0023	0.0023	0.0023	0.0023	0.0011
Contact angle (°)	81 ±3	77 ±1	74 ± 2	-	76 ± 2
Clean water flux at 40 mbar (LMH)	27.3 ± 0.4	227.1 ± 1.5	679.2 ± 46.2	182 ± 1.0	795.0 ± 18.3
Stabilized seawater flux at 40 mbar (LMH)	4.5 ± 0.1	8.4 ± 0.1	7.3 ± 0.4	2.7 ± 0.6	3.6 ± 0.3

According to the table, clean water flux varies between 27 to 795 LMH while the stabilized flux for seawater ranges from 4.5 to 8.4 LMH. Employing three UF membranes of PES-100 kDa, PVDF-120 kDa, and PVDF-100 kDa and one MF membrane of PTFE-0.3 μm in the GDM process for treatment of lake water, resulted to obtain an approximately equal flux data for the four membranes (Lee, Lee et al. 2019).

2.1.3 Characteristics of the biofilm formed on the membrane

During GDM filtration process, the microorganisms, colloidal material which are aggregated, and particulate organic and inorganic material in influent water or wastewater are not able to pass through the membrane and are concentrated on the membrane surface. Such chemical species (microorganisms and biomass) tend to form a very thin layer on the membrane surface which is called biofilm, biofouling layer, or cake/gel layer. The formed biofilm is considered as a mini ecological system. To characterize the layer, some different fields such as morphology, physical thickness, biological activity, community composition and their spatial distribution, such as prokaryotes (bacteria), eukaryotes including predators, composition of organic and inorganic constituents can be considered.

2.1.3.1 Biofilm morphology

It was found that the flux stabilization is occurring due to formation of biofilm in the membrane surface which was investigated using the confocal laser scanning microscopy (CLSM) (Peter-Varbanets, Hammes et al. 2010). Based on Figure 2-3, a flat and dense biofilm layer was observed in the first three days of operation. Then, the biofilm detached from the membrane after a week of filtration. Finally, heterogeneity and porosity of the layer increased with the formation of large voids between patches of biofilm (Peter-Varbanets, Margot et al. 2011).

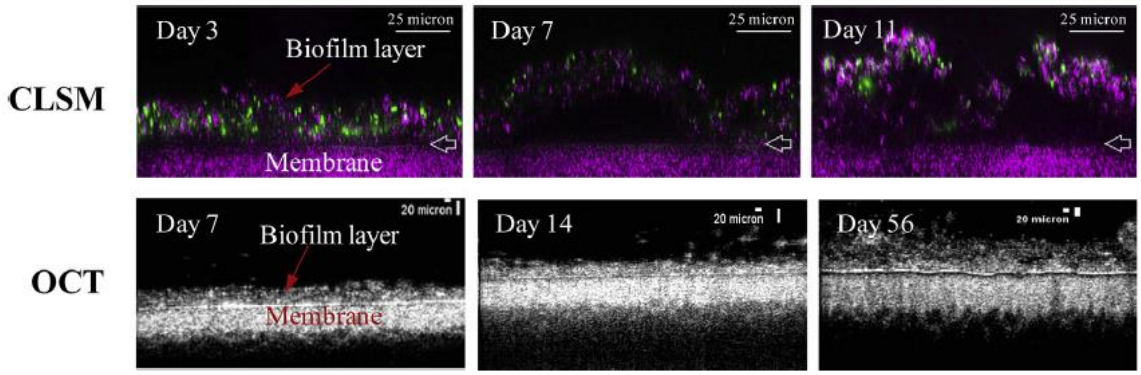

Figure 2-3. Studying the morphology of the biofilm formed on the membrane surface by CLSM and OCT images (Peter-Varbanets, Margot et al. 2011, Akhondi, Wu et al. 2015)

In addition to CLSM, Optical Coherence Tomography (OCT) has been employed widely in the characterization of biofilm. It provides images in the size of millimeter and micrometer. The image acquisition by OCT at the meso-scale has made it possible to provide details of important "structure/function" relationships (Martin, Bolster et al. 2014). In several studies which employed OCT technique (Derlon, Peter-Varbanets et al. 2012, Akhondi, Wu et al. 2015), a thicker, more heterogeneous and porous biofilm were reported by increasing filtration time, as Figure 2-3 illustrates. The results of the morphology studies using both CLSM and OCT methods indicates that as the filtration time increases, the biofilm structure characteristics such as roughness and porosity change dynamically regardless of the influent water (Pronk, Ding et al. 2019). Additionally, Raman spectroscopy has been used recently to characterize the composition of biofilms (Desmond, Best et al. 2018). It is a spectroscopic technique typically used to determine vibrational modes of molecules, although rotational and other low-frequency modes of systems

may also be observed. Raman spectroscopy is commonly used in chemistry to provide a structural fingerprint by which molecules can be identified (Graves and Gardiner 1989).

Quartz crystal microbalance with dissipation (QCM-D) method is a new tool to better understand and reduce ceramic membranes clogging. QCM-D is able to detect extremely small chemical, mechanical, and electrical changes taking place on the sensor surface and to convert them into electrical signals which can be investigated to study dynamic process (Dixon 2008). This device allows to measure the mass of NOM (or other colloids and compounds) over time on different sensors. This sensor is able to simulate the membrane surface. In other words, the device determines if compounds or different NOM fractions will be adsorbed or not on the membrane.

2.1.3.2 Biological composition and function

In the GDM process, the membrane biofilm layer is characterized by the biological parameters, such as amounts of live or dead cells, microbial community compositions, and predation behaviors (Pronk, Ding et al. 2019). Among all the methods in order to investigate the amounts of live and dead cells in the GDM biofilms, ATP analysis (Peter-Varbanets, Hammes et al. 2010) and CLSM live/dead staining are the predominant methods. The results of past studies showed that the biofilm layer formed on the membranes displayed a high viability. The viable cells were found to be related to the heterogeneity of the biofilm layer, i.e., leading to the formation of cavities and channels inside of the biofilm (Peter-Varbanets, Hammes et al. 2010, Akhondi, Wu et al. 2015).

As a result of the literature review in GDM section, there is a knowledge gap in the literature regarding the use ceramic membranes in this process. It is very interesting to prepare ceramic membranes with different contents and investigate the long-term performance of them in terms of permeate quality, stable flux, and biofilm characterization.

2.2 Application of BIEX process and hybrid processes with GDM filtration in decentralized systems (objective 2, paper 2)

Although the performance of IEX resin filtration has been extensively studied, research related to the BIEX resin filters is highly limited in literature. In this section, the past studies on IEX and BIEX resins are reviewed, and the results are compared.

The process of regular ion exchange involves the utilization of ion exchange resins to eliminate ions or NOM from influent water by exchanging them with ions of similar charge within the resin. These resins may either be cation exchange or anion exchange resins, depending on the targeted ions for removal. In the case of IEX resin, frequent regeneration of the resin is necessary to maintain its high capacity. However, with BIEX resin, regeneration is not as frequent; instead, the resin is allowed to exhaust according to the pre-charged ion in the primary ion exchange region, subsequently functioning in the secondary ion exchange region (BIEX mode). This occurs through the displacement of sulfate and/or bicarbonate ions. Using BIEX resin leads to a reduction in the required amount of chemicals and spent brine. Additionally, maintenance needs are decreased, resulting in lower transportation costs and a more cost-effective process overall. Given these advantages, BIEX resin appears to be an excellent fit for decentralized water treatment systems.

2.2.1 IEX and BIEX performance during NOM removal from water

DOC is considered as a major problem in drinking water because it directly affects color, odor, and taste of water. Indirectly, the reaction of DOC with the most used disinfectant, chlorine, causes the formation of harmful disinfection by-products (DBPs) like trihalomethanes (THMs). These compounds are classified as probable or possible human carcinogens (Rook and JJ 1974, Sadrnourmohamadi and Gorczyca 2015). The DOC content of the influent and effluent are usually measured using TOC meters and spectrophotometers.

IEX and BIEX resins performance in term of DOC removal from influent river water containing 7 mg C/L DOC has been investigated previously (Amini, Papineau et al. 2018). The results showed that IEX can achieve approximately 80% removal which is more than the removal value of BIEX resins (62%). This is far higher than the removal percentage of the granular activated carbon under biological mode, BAC (5%). From this study, it can be shown that BIEX resins can be considered as a reliable alternative operation to IEX resins to reduce spent brine production while still achieving high DOC removal.

In another investigation (Schulz, Winter et al. 2017), the performance of BIEX and IEX resin columns in term of DOC removal are compared. Before regeneration of resins, the biotic condition (BIEX) showed a higher DOC elimination (approximately 60%) while the abiotic operation (IEX) removed DOC content by approximately 45%.

DOC can be removed by anion, cation exchange resins or by employing both resins simultaneously. It is reported that using combined anion and cation exchange can lead to reduce the DOC content of influent water from 11 – 15 mg C/L to 3 – 7 mg C/L. Utilizing IEX only, the DOC was achieved from 11 – 15 mg C/L to 2 – 6 mg C/L (Arias-Paic, Cawley et al. 2016). However, some other researchers have reported that there is no DOC benefit can be gained by employing different types of IEX resins for water treatment (Humbert, Gallard et al. 2005).

The application of BIEX resins have been compared to three different types of GAC and BAC adsorbents during treatment of the influent water (Liu, Lompe et al. 2020). The outcomes of the research showed 29 – 36% DOC removal for BIEX resins while GAC and BAC removed 13 – 24% in the almost total operation time. In the depth of more than 30 cm of the adsorption columns, total DOC removal achieved equal to 81% whereas GAC/BAC filters reported 62 – 66% at the same depth.

In 2021 (Liu, Papineau et al. 2021), parallel pilot-scale bicarbonate-form and chloride-form BIEX resin were fed with surface water (DOC of 7 mg C/L). The findings indicated that when comparing bicarbonate-form BIEX with chloride-form BIEX, the former exhibited a slightly reduced removal of DOC at a median rate of 49% in contrast to 53% for the latter. Additionally, bicarbonate-form BIEX demonstrated a higher removal efficiency for biodegradable DOC (BDOC) with an average rate of 50%, as opposed to 33% for chloride-form BIEX. However, both forms of BIEX showed similar capabilities in removing precursors responsible for DBPs formation.

As a result of these limited number of studies on the performance of BIEX resins for DOC removal from influent water, BIEX resin in the most cases showed an equal or higher removal characteristics to regular IEX resin. Regarding the postponing of the regeneration stage and lower spent brine reduction, it seems that operation of ion exchange resins in biological mode is a reliable method in contaminant removal in the decentralized water treatment systems. In this case, there is still a need to carry out further studies aiming to increase DOC elimination.

2.2.2 Hybrid processes with GDM

To increase NOM removal, reduce membrane clogging, increase the final permeate quality, stabilized flux, and consequently increase the membrane lifetime in GDM process, it can be

integrated by some other processes such as ion exchange, coagulation/flocculation and adsorption. Integration of such processes can reduce organic substances physically or by biodegradation.

2.2.2.1 BIEX – GDM hybrid process

The impact of BIEX pretreatment on fouling of ultrafiltration membranes was investigated by Schulz et. al (Schulz, Winter et al. 2017). They used PVDF membranes with a pore size of 0.02 µm which are operated in the dead-end mode. The flux and temperature kept constant at 50 LMH and 22 ^{o}C, respectively. In this study, the impact of the NOM composition variation because of BIEX pre-treatment on the subsequent UF membrane fouling was investigated. Pre-treatment decreased the total and irreversible fouling significantly during filtration. Such decrease was reported due to the effective elimination of NOM with medium and low molecular weight.

2.2.2.2 Adsorption – GDM hybrid process

A layer of GAC, PAC and sand on the membrane surface in the GDM process for rainwater treatment is added on the surface of polyether sulfone membranes with a nominal cut-off of 150 kDa. The removal of organics increased 20 – 25% due to GAC or PAC layer which effectively adsorbs organic matters while the presence of GAC layer decreased the value of stable flux compared to GDM without adsorbent. This is because bio-fouling layer becomes denser with higher amount of biomass and extracellular polymeric substances contents (Ding, Wang et al. 2018).

Shao et. al (Shao, Feng et al. 2017) added a layer of PAC and IEX resins on the flat sheet PVDF membranes with a 100 KDa pore size for river water treatment. In the adsorption – GDM hybrid process, the adsorption of the PAC and IEX resins increased the removal efficiency of NOM by 7.2 – 43.5%. Moreover, the presence of adsorbent particles increased the number of microorganisms in the biofilm, consequently increasing the removal efficiency of assimilable organic carbon (AOC) by 20.1 – 34.4%.

In a study, effect of pre-treatment by bio filtration column packed with GAC on the performance of GDM process using PVDF hollow fiber 150 KDa membranes for seawater treatment were studied (Lee, Suwarno et al. 2019). GAC column removed soluble organic substances by bio sorption/biodegradation, leading to superior permeate quality from GAC + GDM and subsequently

lower RO fouling than GDM without pre-treatment. In addition, GAC column reduced the amounts and diversity of prokaryotes and eukaryotes in the membrane biofilm of GAC + GDM.

2.2.2.3 Coagulation – GDM hybrid process

In situ coagulation with the GDMBR process for application in treating synthetic sewage is studied by Ding et. al (Ding, Wang et al. 2017). The results showed that in situ coagulation roughly doubled the permeability, compared to the GDMBR without coagulation pretreatment. This is because of the existence of the dosed aluminum preventing formation of microbial metabolites and helping avoid membrane pore blocking.

2.3 Comparing performance of ceramic and polymeric membranes and membrane cleaning process in BIEX + GDM filtration (objective 3, paper 3)

Selection of the best membrane type is a crucial step in designing GDM process for the decentralized water treatment systems. To select the best membrane type for the long-term operation, there are some criteria to consider such as membrane lifetime, fouling effect and type, and cleanability. In this section, the mentioned factors will be explained.

On the one hand, polymeric membranes showed a higher clean water permeability than ceramic ones according to the different module design (hollow fiber vs monolithic for ceramic). Moreover, polymeric membranes production cost normally is less than ceramic membranes (Moulin, Bourbigot et al. 1991, Bodzek and Konieczny 1998, Klomfas and Konieczny 2004). On the other hand, lifetime of the ceramic membrane is considered more than two-fold of the polymeric ones (Alresheedi, Barbeau and Basu 2019, Jarvis, Carra et al. 2022). Ceramic membranes show lower susceptibility to organic fouling compared to polymeric membranes, primarily owing to their inherent hydrophilic properties. In a study (Alresheedi, Barbeau and Basu 2019), it was observed that the fouling rate of silicon carbide ceramic membranes was lower than that of PES membranes when filtering various synthetic influent water solutions containing sodium alginate, humic acid, bovine serum albumin, or their combinations. This difference in fouling behavior was attributed to the superior hydrophilicity and reduced surface charge of the tested ceramic membrane compared to the PES membrane. Comparing four ceramic Al_2O_3, ZrO_2, TiO_2, SiC membranes and a PES/PVP

polymeric MF membrane (Hofs, Ogier et al. 2011) under constant flux of 150 LMH in pressure driven process showed a reversible fouling in the order of polymeric ≈ Al2O3 ≈ ZrO2 > TiO2 > SiC, and for irreversible fouling polymeric > ZrO2 > Al2O3 > TiO2 > SiC. Comparing alumina composite ceramic membrane with a PES membrane for the pressure driven filtration of bentonite and water (Guerra and Pellegrino 2013) showed a gradual increase of the TMP over the duration of the experiment for the alumina membrane while the PES membrane showed negligible TMP increase until a critical condition was reached. In another study (Lee, Dilaver et al. 2013), fouling of ceramic and polymeric MF membranes were compared during treatment of different influent water types in pressure driven filtration process. The results showed that the cake resistance was the dominant form of the total resistance for ceramic membranes under the conditions tested, and it was removable by physical cleaning.

Moreover, the presence of functional groups on the membrane surface can also play a significant role in determining how membranes interact with foulants. A comparative study on ceramic and polymeric membranes to investigate how membrane properties impact fouling behavior and the rejection of micropollutants has been conducted (Zhao, Wang et al. 2018). Results indicated a lower irreversible fouling of ceramic membrane than the polymeric membrane. Furthermore, physical and chemical cleaning by water and NaOH showed to be more effective for flux recovery of ceramic membrane than polymeric counterparts.

The existing research suggests that ceramic membranes exhibit superior hydraulic performance compared to their polymeric counterparts. Additionally, ceramic membranes possess resistance to chlorine, a common cleaning agent employed for flux recovery in membrane processes. This resilience is attributed to the chemical inertness of ceramic materials, which prevents oxidation or degradation when exposed to potent oxidants such as chlorine and ozone (Hofs, Ogier et al. 2011, Lee, Dilaver et al. 2013, Lee and Kim 2014, Murić, Petrinić and Christensen 2014, Zhao, Wang et al. 2018, Alresheedi, Barbeau and Basu 2019). Conversely, prolonged exposure to potent oxidizing agents (such as chlorine) can have adverse effects on polymeric membranes. In a conducted research on the impact of chlorine exposure on polyamide polymeric membranes (Do, Tang et al. 2012) the findings revealed the chlorine integration into the polyamide membrane matrix was the dominant mechanism, at pH levels below 7, leading to alterations in membrane hydrophilicity and pollutant rejection. The use of hypochlorite for cleaning purpose of PES membranes was reported

to detrimentally affect the membrane performance and characteristic. Chemical cleaning resulted in a decline in the mechanical strength of PES membranes (Arkhangelsky, Kuzmenko and Gitis 2007). Likewise, some other studies reported of the degradation of polymeric membranes following exposure to chlorine (Do, Tang et al. 2012, Stolov and Freger 2019).

The literature review in this section reveals the fact that all the studies in comparing performance of the membrane types, the fouling, and cleaning performance of the membrane conducted in the pressure driven cross flow process while there is a serious knowledge gap in the field of GDM process. According to a low-pressure dead-end nature of GDM process and the fact that it is intended to be used in the long-term application in the decentralized systems, comparing performance of ceramic and membrane types in terms of fouling and cleaning needs to be investigated for deep insights.

CHAPTER 3 RESEARCH OBJECTIVES, HYPOTHESES AND METHODOLOGY

3.1 Research objectives and hypotheses

In this section, the general and specific objectives of this research will be outlined, followed by a discussion on the hypotheses and the unique aspects of the current study.

3.1.1 Objective of the research

The general objective of this study is to select and evaluate an appropriate decentralized and passive drinking water process for small and remote communities which are far from the centralized and complex water treatment systems. In this regard, we have selected BIEX and GDM processes as their characteristics are in harmonious alignment with the ones required by the decentralized water treatment systems. As mentioned before, there are three main objectives (one published paper per objective) in this thesis.

The specific and detailed objectives in “application of GDM process without pretreatment using lab-made ceramic membranes (objective 1, paper 1)” are:

- Synthesis of ceramic MF membranes by different compositions of kaolin/alumina which are intended to be used in the GDM process for the treatment of turbid and colored river water purpose.
- Characterization of the synthesized ceramic MF membranes to ensure the desired specifications.
- Investigation of the effect of membranes structure variation on NOM, turbidity, and stabilized flux. In GDM section, biofilm structure and composition are studied by morphological studies of biofilm formed on the membrane surface. Optical coherence tomography is employed in order to study the morphology of the biofilm formed on the membrane surface.
- Modeling of flux – time data to study the fouling mechanism before and after flux stabilization phenomenon.

The specific and detailed objectives in “BIEX + GDM hybrid process (objective 2, paper 2)” are:

- Investigating the BIEX resin performance in terms of organic removal
- Studying BIEX performance in the primary (NOM exchange with chloride) and secondary ion exchange (NOM exchange with sulfate/bicarbonate) regions
- Studying dynamic of exchange of most important anions such as sulfate, chloride, bicarbonate, and nitrate during the operation.
- Studying feasibility of using BIEX as a pre-treatment for gravity-driven ceramic membranes (hybrid BIEX + GDCM process). In this section, the application of BIEX resin is evaluated in terms of DOC, turbidity, and UVA_{254} removal as well as NOM fraction removals. Moreover, the BIEX impact on improving stabilized flux, permeate quality, and the biofilm characteristics of the membrane section are studied and compared to the GDCM process without BIEX pre-treatment.

The specific and detailed objectives in “comparing performance of ceramic and polymeric membranes and membrane cleaning process in BIEX + GDM process (objective 3, paper 3)” are:

- Comparing performance of polymeric and ceramic MF/UF membranes in terms of stabilized flux, flux recovery, permeate quality, and cleanability in the GDM process integrated with BIEX pretreatment.
- Quantifying different fouling types and studying the predominant fouling mechanism causing flux decline in the GDM process.
- Studying membrane cleaning by physical and chemical wash to investigate the effect of enhanced or decreased physical and chemical cleaning conditions on the stabilized flux, flux recovery, fouling removal, and permeate quality.

3.1.2 Hypotheses and originality of the research

The Research hypotheses section which shows the originality of this research, are divided in the three sections of 1) Application of GDM process without pretreatment using lab-made ceramic membranes (objective 1, paper 1), 2) BIEX + GDM hybrid process (objective 2, paper 2), and 3)

comparing performance of ceramic and polymeric membrane and membrane cleaning process in BIEX + GDM process (objective 3, paper 3).

3.1.2.1 Application of GDM process without pretreatment using lab-made ceramic membranes (objective 1, paper 1)

- Ceramic membranes which are produced using different contents of starting materials such as kaolin, and alumina in GDM process, show high performance in terms of organic, turbidity, UVA_{254} removal, and stabilized flux.

Originality: In GDM process, there is not any study focused on using synthesized ceramic membranes, therefore this hypothesis is considered very novel.

Refusal: The hypothesis will be refused if the removal values and the stable flux of the synthesized membranes exhibit an inferior performance.

- Increasing alumina composition in the structure of the membranes could increase the removal of turbidity and organics as well as improving the stable flux obtained by the membranes.

Originality: Although there are some studies regarding the use of adsorbents such as alumina as raw materials for ceramic MF/UF membrane synthesis in the crossflow pressure-driven process, the use of ceramic membranes synthesized with clays (kaolin) and adsorbents (alumina) have not been investigated in the GDM process yet.

Refusal: The hypothesis will be discarded if the membrane with a higher alumina composition reveals lower organic, turbidity, and UVA_{254} removal, and decreased stabilized flux compared to the membranes with less alumina content.

- Increasing alumina content in the ceramic membranes structure increases the mean biofilm thickness and biological activity of microorganisms in the biofilm, leading to an improved organic removal efficiency as well as the stabilized flux.

Originality: While research exploring the impact of coating a layer of GAC and PAC on the surface of polymeric membranes with respect to biofilm characteristics is scarce, this hypothesis is distinctive in its aim to utilize alumina within the membrane structure as raw material rather than

as a surface coating. Furthermore, the influence of alumina composition within the ceramic membrane structure on biofilm characteristics remains unexplored in existing literature.

Refusal: The hypothesis will be refused if the membrane with higher alumina composition shows a less dense biofilm and a decreased mean thickness (lower biofilm resistance).

3.1.2.2 BIEX + GDM hybrid process (objective 2, paper 2)

- Pre-treatment by BIEX process shows a decrease in the fouling resistance of the membranes, subsequently, the stable flux of the synthesized ceramic membranes in the GDM process increases compared to GDM process without pre-treatment.

Originality: There are highly limited studies in pre-treatment of influent water by BIEX for GDM process, especially with ceramic membranes. A comprehensive study is required to study the influence of the BIEX pre-treatment on the performance of the ceramic MF/UF GDM in the dead operation.

Refusal: The hypothesis will be rejected if the BIEX pre-treatment leads to an augmentation in fouling resistance, consequently resulting in a reduction of the stable flux exhibited by membranes within GDM section.

- Applying BIEX pre-treatment before GDM process results in a marked increase in the organics removal and turbidity of the effluent of the GDM section.

Originality: As there is highly limited research employing BIEX as a pre-treatment for the GDM process, this hypothesis is considered original to study the effect of BIEX pre-treatment on the organics and turbidity removal by ceramic membranes.

Refusal: The hypothesis will be refused if BIEX pre-treatment affects the overall permeate quality of the hybrid process (i.e., decrease the removal of organics and turbidity in the final effluent) adversely.

- BIEX pre-treatment decreases the biofilm physical characteristics such as mean thickness as well as the biofilm activity.

Originality: There are no studies reporting the use of BIEX as a pretreatment for GDM process with ceramic membranes. Therefore, the impact of BIEX on the subsequent biofilm formed on the membrane surface has not been investigated.

Refusal: The hypothesis will be discarded when BIEX pretreatment increases the physical membrane biofilm properties and activity.

3.1.2.3 Comparing performance of ceramic and polymeric membranes and membrane cleaning process in BIEX + GDM process (objective 3, paper 3)

- The stabilized flux of the ceramic membranes is higher than that of the polymeric membranes in the BIEX + GDM hybrid process.

Originality: Comparing performance of polymeric and ceramic membranes have not been researched in the GDM without pretreatment or BIEX + GDM process. Therefore, this hypothesis is considered unique for the present research.

Refusal: This hypothesis will be refused if ceramic membranes show a decreased stabilized flux compared to that of the polymeric ones.

- The permeate quality (organic, turbidity, and UVA_{254} removal) of the ceramic membranes is higher than that of the polymeric membranes in the BIEX + GDM hybrid process.

Originality: No study has focused on comparing ceramic and polymeric membranes in the GDM/ BIEX + GDM process. Consequently, this hypothesis is unique.

Refusal: This hypothesis will be refused if ceramic membranes show a decreased permeate quality compared to that of the polymeric ones.

- Flux recovery of the ceramic membranes is higher than that of the polymeric membranes in the BIEX + GDM hybrid process.

Originality: There is no study to compare the performance of polymeric and ceramic membranes in the GDM without pretreatment or BIEX + GDM process.

Refusal: This hypothesis will be refused if ceramic membranes show a decreased flux recovery compared to that of the polymeric ones.

- Increasing intensity of the physical and chemical cleaning increases the stabilized flux, permeate quality, and flux recovery of the membranes.

Originality: There is no study focusing on the membrane cleaning in the GDM or BIEX + GDM process.

Refusal: This hypothesis will be refused if enhanced cleaning condition does not influence the stabilized flux, permeate quality, and flux recovery.

- The hydraulic reversible fouling is the predominant fouling mechanism of the membranes in the BIEX + GDM hybrid process.

Originality: There is no study to investigate the fouling mechanism of the membranes in the GDM or BIEX + GDM process.

Refusal: This hypothesis will be refused if the other types of fouling are the predominant fouling mechanism responsible for flux decline.

- The physical cleaning method involving backwash with air and water demonstrates a greater efficacy in membrane flux recovery compared to chemical cleaning (with NaOH and NaOCl) techniques.

Originality: There is no study to investigate the effectiveness of physical and chemical cleaning on the flux recovery in the GDM or BIEX + GDM process

Refusal: This hypothesis will be refused if chemical cleaning demonstrates higher flux recovery than that of physical cleaning.

3.2 Research Strategy and Methodology

The experimental approach was designed in three main sections to validate or invalidate the research hypotheses.

Table 3-1. The main sections and methodologies used in each section

Sections	Methodologies
Application of GDM process without pretreatment using lab-made ceramic membranes (objective 1, paper 1):	• Synthesis of ceramic MF membranes in the laboratory. • Characterization of the synthesized membranes. • Preparation of the GDM pilot to investigate their performance in river water treatment. • Sampling of the river water. • Conducting a long-term filtration experiments and monitoring flux, permeate quality, and biofilm characteristics.
BIEX + GDM hybrid process (objective 2, paper 2):	• Employing the same ceramic membrane types, operating condition, and influent water type as in objective 1 • Preparation of the BIEX + GDM pilot to investigate the hybrid process performance in river water treatment. • Sampling of the river water. • Conducting a long-term filtration experiment and monitoring flux, permeate quality, and biofilm characteristics of both BIEX resin column and membrane section (GDM section).
Comparing performance of ceramic and polymeric membranes and membrane cleaning process in BIEX + GDM process (objective 3, paper3):	• Using Commercial polymeric MF (0.1 µm) and UF (0.03 µm) and ceramic UF (300 kDa) membranes • Producing two-layer (support + coating layer) ceramic membrane in the laboratory • Characterization of the synthesized membrane. • Preparation of two BIEX + GDM pilots • Conducting a long-term filtration experiments and monitoring flux, permeate quality, and biofilm characteristics of both BIEX resin column and membrane section (GDM section). • Performing physical and chemical cleaning with the enhanced (on pilot 1) and decreased (on pilot 2) intensities. • Measuring stabilized flux, permeate quality, and biofilm characteristics of the polymeric and ceramic membranes prior and after the cleaning. • Calculating flux recovery and different fouling types of the two membrane types.

For each of the three objectives, the experimental protocols are outlined, referencing the particular analysis conducted.

3.2.1 Application of GDM process without pretreatment using lab-made ceramic membranes (objective 1, paper 1):

To validate or invalidate the hypothesis in this section, three types of ceramic MF membranes using pressure casting and sintering method were synthesized in the lab with 0 – 50% alumina and 50 – 100% kaolin clay. The membranes were then subjected to characterization techniques such as SEM, XRD, contact angle, pore size and porosity measurement. After that, GDM pilot was designed to regularly monitor the long-term performance of the membranes such as effluent quality (DOC, turbidity, UVA_{254}, alkalinity), flux, and biofilm characteristics (by taking OCT images regularly from the biofilm).

The influent water utilized in this study was sourced from Des Prairies River and specifically collected from the Pont-Viau water treatment plant prior to the commencement of the experimental procedures. It was consistently maintained below 4°C within the refrigerator throughout the experiments. The characteristics of the influent water, encompassing turbidity, temperature, DOC, UVA_{254}, and alkalinity, were meticulously examined and continuously monitored throughout the course of the investigation. The Des Prairies River was selected for this research due to its notable turbidity, coloration, and organic content. While it may not be the most extreme in these aspects compared to some other bodies of water, it is recognized for its significant levels of these parameters, making it a relevant and representative choice for assessing membrane performance under challenging conditions. Consequently, the membrane performance can be assessed under a challenging and rigorous conditions, providing valuable insights into its efficacy.

3.2.2 BIEX + GDM hybrid process (objective 2, paper 2)

To substantiate the hypothesis outlined in this objective, the same ceramic membrane types, operating conditions, and influent water as in objective 1 (paper 1), were utilized. This approach enables a direct comparison between the BIEX + GDM hybrid process and the GDM-only process. The BIEX + GDM pilot was designed with a filtration rate of 4 BV/h, resin BV of 52 mL, and EBCT of 15 min. A commercial ceramic MF membrane was used as well along with the three lab-made membranes to enable the comparison between the performance of the synthesized and commercial membranes. The long-term experimental tests were conducted by regularly monitoring

of BIEX resin column (DOC, UVA_{254}, alkalinity, anion concentration, NOM fraction removal) and membrane section (flux, DOC, UVA_{254}, alkalinity, turbidity, pH, NOM fraction removal) performance. Finally, the flux, permeate quality, and biofilm characteristics of the BIEX + GDM process were compared to the ones in GDM-only process.

3.2.3 Comparing performance of ceramic and polymeric membranes and membrane cleaning process in BIEX + GDM process (objective 3, paper 3)

In the final objective, two distinct types of commercial polymeric membranes with pore sizes of 0.1 µm (MF) and 0.03 µm (UF), along with a commercial ceramic membrane of 300 kDa (UF), were employed. Additionally, a laboratory-synthesized two-layer ceramic membrane, comprising a kaolin support and alumina layer, was created through the pressure casting and sintering method. This lab-made membrane underwent thorough characterization process involving SEM, EDX, porosity, and pore size measurements.

Subsequently, two identical BIEX + GDM pilots were set up, using the same influent water as in objectives 1 and 2. The experiments extended over a 30-day period. Following this initial phase, physical (air and water backwash) and chemical cleaning (NaOH and NaOCl) procedures were implemented with enhanced intensity on one pilot 1 and decreased intensity on the other (pilot 2). This aimed to investigate the impact of cleaning intensity on stabilized flux, permeate quality, flux recovery, various fouling types, and biofilm characteristics. The experiments were then extended beyond 70 days, allowing for a comprehensive comparison of stabilized flux and permeate quality of ceramic and polymeric membranes before and after cleaning.

CHAPTER 4 Article 1: Synthesis, Characterization, and Application of Gravity-driven Ceramic Microfiltration Membranes for Surface Water Treatment

Yaser Rasouli, Raphaël Maltais-Tariant, Benoit Barbeau, Mathieu Lapointe, Caroline Boudoux, Dominique Claveau-Mallet. Synthesis, characterization, and application of gravity-driven ceramic microfiltration membranes for surface water treatment (publication date: Jan 5, 2023). *Journal of Water Process Engineering*, *51*, 103430.

4.1 Abstract

Gravity-driven ceramic microfiltration (MF) disk-shaped membranes were synthesized using kaolin and different alumina contents (0 % wt, 25 % wt, and 50 % wt). The pure water flux, mean pore size, porosity and contact angle of membranes were measured. Their structure and composition were characterized by scanning electron microscopy (SEM) and X-ray diffraction (XRD). The effect of alumina content was evaluated for long-term river water filtration in terms of permeate flux, turbidity, dissolved organic carbon (DOC), UVA $_{254}$, pH, and alkalinity removal. The physical characteristics of the biofouling layer, such as thickness and roughness, were studied using optical coherence tomography (OCT) imaging and the concentration of active microorganisms in the biofilm. The results showed acceptable turbidity removal after the flux stabilization period and relatively high performance for DOC, and UV removal and alkalinity reduction during the first three days of filtration. Flux stabilized at 2.5–3 LMH on day 24 of filtration, indicating that the alumina content does not considerably affect the stable flux. As the flux modeling data showed, prior to the flux stabilization time, the fouling was controlled by the pore blocking mechanism. This was confirmed by OCT imaging that showed a very outspread biofilm layer with a low relative roughness; the layer became more compact with a higher relative roughness over time, showing that the cake layer is dominant after the flux stabilization period. Increasing the alumina content of the membranes increased the number of active microorganisms in the biofilm layer, possibly because of an increased adsorption of nutrients in the biofouling layer.

4.2 Introduction

Although it is of paramount importance for every community to access safe drinking water, achieving this goal can be challenging for small and remote communities that have limited access to trained operators. Providing passive water treatment systems is an appealing option for small systems, as they minimize human intervention and maintenance needs. Consequently, these systems require lower operation and maintenance costs and provide long-term treatment options and minimal supervision (Derlon, Mimoso et al. 2014, Shao, Feng et al. 2017).

Gravity-driven membrane (GDM) filtration, initially proposed by Peter-Varbanets et al. (2010), is a passive water treatment process that requires a very simple setup and low transmembrane pressure (TMP). A low TMP (normally below 0.1 bar) enables gravity-fed operation and leads to a low stable flux, roughly between 1 and 15 LMH (Pronk, Ding et al. 2019). During long-term filtration, a biofilm grows on the membrane surface, and its presence is considered an important factor in flux stabilization (Truttmann, Su et al. 2020). Numerous studies have demonstrated the possibility of using polymeric membranes in GDM applications, including river water (Peter-Varbanets, Hammes et al. 2010, Klein, Zihlmann et al. 2016), pond and tap water (Oka, Khadem and Bérubé 2017, Shao, Feng et al. 2017), rainwater (Ding, Liang et al. 2017), and seawater (Wu, Suwarno et al. 2017). Among the past investigations, some focused on the relationship between stabilized flux and biofilm (Akhondi, Wu et al. 2015), while others investigated the effect of biofilm on permeate quality (Derlon, Mimoso et al. 2014) and some studied biofilm structure (Derlon, Koch et al. 2013). However, to date, only a limited number of researchers have studied the application of gravity-driven ceramic microfiltration membranes (GDCM) despite the fact that ceramic membranes have high mechanical, chemical, and thermal resistance and a prolonged lifespan (Issaoui and Limousy 2019, Du, Liu et al. 2021). Using kaolin as a starting material decreases the sintering temperature, which in turn decreases the synthesis cost. In some cases, kaolin-based ceramic membranes are more cost-effective compared to polymeric membranes (Hubadillah, Othman et al. 2018). In this regard, Du et al. (2021) studied manganese removal from synthetic water (mixing double-distilled water with $MnSO_4$, $CaCl_2$, $NaHCO_3$, and NaCl) using commercial disk-shaped 300-kDa ZrO_2/TiO_2 membranes (pre-coated with manganese oxides) and 15-kDa ZrO_2/TiO_2 membranes. Their results showed that surface modification (pre-coating with manganese) was beneficial and enabled 75%

manganese removal. They also investigated manganese removal following pre-deposition of manganese oxides and powdered activated carbon on the GDCM surface (Du, Liu et al. 2021). Pre-deposition improved the rejection and concentration of manganese oxidizing bacteria on the membrane surface. There is a scientific gap in the use of cost-effective kaolin-based ceramic membranes for GDM filtration in drinking water applications.

The general objective of this study was to investigate the feasibility of using affordable kaolin-based ceramic membranes operated in a gravity-driven mode to filter colored surface water. The sub-objectives were to 1) investigate the effect of alumina concentration in the membrane structure on the flux, permeate quality, and biofilm layer properties and 2) study the fouling mechanisms of the membranes by flux-decline data modeling and biofilm characterization. To achieve these objectives, disk-shaped ceramic microfiltration (MF) membranes composed of kaolin and alumina were synthesized using pressure casting and sintering. Virgin and colonized membranes were characterized, and their performances in treating surface water were assessed and compared. Biofilm development was studied using OCT and adenosine triphosphate (ATP) methods.

4.3 Materials and Methods

4.3.1 Membrane synthesis

Ceramic MF membranes were synthesized using the pressure casting and sintering method (Hubadillah, Othman et al. 2018). Pure kaolin clay (Sheffield Pottery, Sheffield, MA, USA, Table 4-1), alumina powder (Fisher Scientific, Switzerland; Al_2O_3, 40–300 μm, CAS: 1344-28-1, Mw = 101.96 g mol^{-1}), boric acid (Ward's Science, Rochester, NY, USA; H_3BO_3, CAS: 10043-35-3, crystals), and deionized (DI) water were used as the starting materials for membrane synthesis.

Table 4-1. Composition of kaolin used to synthesize membranes.

Compounds	**Value (%)**	**Compounds**	**Value (%)**
SiO_2	45.73	CaO	0.18
Al_2O_3	37.36	MgO	0.01
Fe_2O_3	0.79	Na_2O	0.06
TiO_2	0.37	K_2O	0.33
P_2O_5	0.24	Loss on ignition (LOI)	13.91

To make a suitable dough for molding, DI water was gradually added to the kaolin and alumina powder, and then boric acid was added at 10% by wt of kaolin. Boric acid was used to increase the mechanical strength of the membrane. The mixture was mixed for 10 minutes using a high-power mechanical mixer at 100 rpm (Masterflex L/S® Analog Variable-Speed Modular Drive, Cole-Parmer Instrument Co., Canada) with four blades to obtain a uniform dough. The dough was transferred to a disk-shaped mold, and pressure was applied using a clamp. Each disk-shaped membrane had a diameter, thickness, and area of 43 mm, 5 mm, and 14 cm^2, respectively. The membranes were kept at 22-25 ˚C for at least 24 hours to dry. The dried membranes were sintered in a programmable electrical furnace (Ney Vulcan, 3-550). Table 4-2 summarizes the calcination steps. After calcination, the membranes remained in the furnace for at least 8 hours to avoid sudden changes in the temperature leading to membrane breakage. The ratios of the kaolin/alumina used in membranes M1, M2, and M3 are listed in Table 4-3. Three membranes of each type (M1, M2, and M3) were synthesized for filtration experiments and membrane characterization.

Table 4-2. Membrane sintering procedure

Temperature range	**Temperature ramp**
25 °C –550 °C	3 °C/min
550 °C	0 (for 2 hours)
550 °C–750 °C	3 °C/min
750 °C	0 (for 2 hours)
750 °C–1100 °C	2 °C/min
1100 °C	0 (for 2 hours)

Table 4-3. Composition of different types of synthesized membrane

Membrane type	**Wt% kaolin**	**Wt% alumina**
M1	100	0
M2	75	25
M3	50	50

4.3.2 Influent water source

Influent water was collected in August 2021 from the Pont-Viau drinking water treatment plant (Laval, Canada), which is fed by the des Prairies River. The influent stock barrel was maintained at 4 °C. To ensure a constant temperature in the system, 20 L of the influent water was collected from the stock barrel every week and incubated at room temperature for 5 hours prior to use. The influent water characteristics are listed in Table 4-4.

Table 4-4. Influent water characterization

Parameters	Mean value	Max value	Min value	Standard deviation	Number of samples
DOC (mg L^{-1})	6.51	7.76	5.82	0.43	22
Turbidity (NTU)	2.30	2.45	2.05	0.13	21
pH	7.58	7.68	7.49	0.06	21
Alkalinity (mg $CaCO_3$ L^{-1})	18	22	12	4.80	21
UVA_{254} (cm^{-1})	0.18	0.22	0.16	0.01	21

4.3.3 Gravity-driven filtration experiments

Three membrane modules were fed in parallel with influent water for 65 days, as shown in Figure 4-1 and Figure A.1. A constant head of 90 mbar (~ 90 cm H_2O) was maintained by continuously pumping influent water from the influent water tank into the overhead tank with a permanent overflow. Permeates were collected daily for quality measurements and flux calculations. The temperature was monitored using a thermometer placed in the overhead tank and controlled by a laboratory air conditioning system. The mean temperature was 22 °C during the experiment (minimum 21 °C and maximum 24 °C). To avoid algae growth in the system, the entire setup (such as tanks, pipes, permeate containers) was covered by a layer of dark tape and a layer of aluminum foil. Makeup influent water was added to the influent water tank weekly.

The membrane modules were made from polyethylene with a sight glass to allow for visual tracking of cake layer growth and obtain OCT images without removing the membranes from their cells. During OCT imaging, the filtration cells were removed from the system for approximately

an hour (without removing the membranes) and replaced after imaging. The permeate weight was measured daily using a digital balance (Sartorius, LC1201S, Germany).

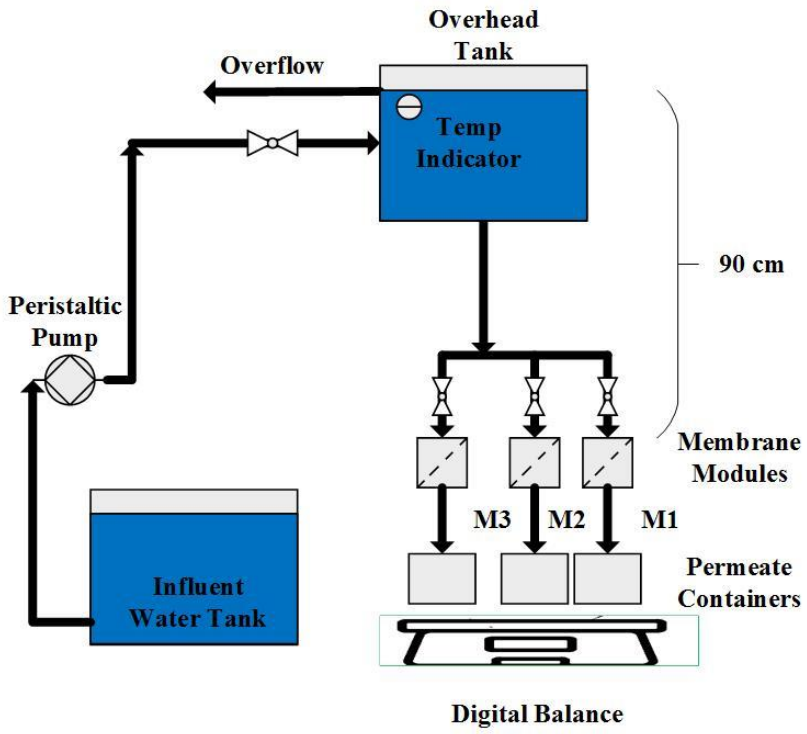

Figure 4-1. Schematic representation of the experimental setup

4.3.4 Permeate quality characterization

The influent and permeate were sampled daily for the first week of filtration and then twice a week for the remaining testing period. The collected permeate samples were measured for DOC, turbidity, UVA_{254} index, alkalinity, and pH. The samples that could not be analyzed immediately were stored at 4 °C. A DOC analysis was performed on samples filtered with prewashed (1 L) membranes (PES, 0.45-µm, 47 mm, Pall Corporation, Washington, NY, USA) using an online TOC analyzer (Sievers M5310 C, Trevose, PA, USA). UVA_{254} was measured in a 1-cm quartz cell using a UV-visible spectrophotometer (Cary 100 Scan, Varian Inc.). A turbidity meter (TL2300, Hach, USA) was used to measure the turbidity. Before each use, the device was calibrated using standard samples. A pH meter (Accumet AB 15 basic, Fisher Scientific, Waltham, MA, USA) was used to measure the pH. Before each use, the electrode was carefully washed with demineralized water and calibrated using standard solutions (pH = 4, 7, 11). For the alkalinity measurement, 50

ml of the sample was titrated using a 0.02 N H_2SO_4 solution to obtain a pH of 4.5 and then 4.2; alkalinity was calculated using Equation 3.1.

$$Alkalinity\ (\frac{mg}{l}CaCO_3) = \frac{(2B-C)\times 0.02 \times 50{,}000}{V} \quad (3.1)$$

where B is the consumed volume of H_2SO_4 to reach a pH of 4.5, C is the total volume of H_2SO_4 consumed to reach a pH of 4.2, and V is the volume of the sample.

4.3.5 Membrane characterization

4.3.5.1 Pure water flux

Before the start of the filtration experiment, demineralized water was used to obtain the pure water flux expressed in LMH at a mean temperature of 22 °C at 90 mbar. The fluxes were normalized to 20 °C.

4.3.5.2 Contact angle

The membrane surface was first cleaned with ethanol and dried with Kimwipes™ and pressurized air. The contact angle was measured with a droplet of water using a goniometer (OCA20, Dataphysiscs, Germany) equipped with a video camera. Based on the recorded videos (not shown), the membranes were categorized as highly hydrophilic, with contact angles lower than 5°.

4.3.5.3 Membrane structure characterization using scanning electron microscopy

Approximately one-quarter of the clean membranes were carefully cut and subjected to SEM analyses. The samples were prepared by vacuum coating with a very thin layer of gold (~60 nm, because the membrane materials are not electron conductive, Polaron SC502 sputter coater) at a pressure of approximately 10 bar and current of 10 mA. The samples were observed on a device (Jeol, JSM-7600TFE, JEOL Ltd., Japan) using low electron voltages (5–10 kV).

4.3.5.4 Crystalline phase characterization by X-ray diffraction

The clean membranes were crushed to obtain fine powders suitable for XRD analysis using a Brucker D8 Advanced device. The XRD patterns were obtained using Cu-Kα radiation at a rate of 0.2° per step and a time frame of one second per step.

4.3.5.5 Membrane porosity

Membrane porosity was calculated based on the water mass adsorbed in the membrane structure after immersion in a water bath. The dry membranes were initially weighed (W_1), and then soaked for 72 hours in pure water at a fixed ambient temperature. After soaking, the outer surface dried using Kimwipes™ and weighed again (W_2). The membrane porosity was calculated as follows (Arzani, Mahdavi et al. 2016):

$$Porosity = \left(\frac{W_2 - W_1}{\rho_m V_m}\right) \tag{3.2}$$

where ρ_m and V_m are the density of pure water at the corresponding temperature and membrane volume, respectively.

4.3.5.6 Membrane mean pore size

The membrane mean pore radius (R_m) was calculated using the Guerout-Elford-Ferry equation (Zhang, Lang et al. 2015), where ε is the membrane porosity, L is the membrane thickness, μ is the water viscosity at the filtration temperature, J is the membrane flux, and ΔP is the pressure.

$$R_m = \sqrt{\frac{(2.9 - 1.75\,\epsilon) 8\mu\, L\, J}{\varepsilon\, \Delta P}} \tag{3.3}$$

4.3.6 Biofilm characterization

4.3.6.1 Biofilm growth characterization by OCT

The OCT device used for characterization was the same as that used by the previously published study (Maltais-Tariant, Boudoux and Uribe-Patarroyo 2020). Briefly, a commercial 1310-nm OCT was operated with a balanced detector imaging module. The raw OCT images were processed, then analyzed using ImageJ software (NIH, USA) to obtain the relative thickness of the biofilm layer. The thickness was measured by determining manually the position of the membrane surface over 4 scans taken over 10.9 mm on different areas of the membranes. The pixel thickness was then converted into optical thickness (Z_f) using the μm/pixel ratio. Since OCT measures optical distance axially, the physical thickness (Z_i) was calculated using Equation 3.4 (Drexler and Fujimoto 2008) as follows:

$$Z_i = \frac{z_f}{n_f} \tag{3.4}$$

where n_f is the biofilm refractive index. Because of the high-water content of the biofilm, its refractive index can be assumed to be equal to that of water (n_f = 1.333) (Bakke, Kommedal and Kalvenes 2001). The mean biofilm layer thickness ($\overline{Z}$ in μm), absolute roughness (Ra in μm), and relative roughness coefficient ($\overline{R}_a$) were calculated according to Equations 3.5 to 3.7, respectively (Derlon, Peter-Varbanets et al. 2012, Akhondi, Wu et al. 2015). In this study, the thickness was calculated using OCT images only at the end of the filtration time (on day 65).

$$\overline{Z} = \frac{1}{n} \sum_{i=1}^{n} Z_i \tag{3.5}$$

$$R_a = \frac{1}{n} \sum_{i=1}^{n} (\left| Z_i - \overline{Z} \right|) \tag{3.6}$$

$$\overline{R}_a = \frac{1}{n} \sum_{i=1}^{n} (\frac{\left| Z_i - \overline{Z} \right|}{\overline{Z}}) \tag{3.7}$$

Here, n is the number of calculated thicknesses, and Z_i (in μm) is the biofilm thickness at each point.

4.3.6.2 Biofilm activity characterization using ATP method

Briefly, approximately one-eighth of the membranes after the filtration experiment were carefully cut and placed in 50 ml of sterile phosphate buffer saline, which was sonicated for 2 minutes at 40 W power and 20 KHz (Cole-Parmer Ultrasonic processor, Canada). This procedure was repeated six times, each time with fresh 50 mL sterile phosphate buffer. Thereafter, 30 mL of composite sample was produced by mixing equivalent volumes from each sonicated sub-sample. To measure the extracellular ATP, the composite sample was filtered through a syringe filter (0.2-μm, Quench-Gone, DIS-SFQG-25, LuminUltra, USA) to retain any microorganisms on the filter, and then lysed using Ultralyse 7 solution (LuminUltra, USA) to recover the intracellular ATP of the biofilm. Next, a TriStar2 Multimode Reader LB 942 (BERTHOLD Technologies) was used to read the luminescence in RLU/s units after washing the microplate reader with six cycles of ultrapure water and six cycles of luminase. Finally, using a developed calibration curve (0, 10, 25, 100, 250, 500, and 1000 pg/ml, R^2 = 0.9999) by dilution with Ultracheck solution (1000 pg/ml, LuminUltra, USA), the ATP values were reported as a standard ratio of ATP weight (pg)/sample weight (Pg).

4.3.7 Quartz crystal microbalance with dissipation

The affinities between the natural organic matter (NOM) and membrane-like surfaces were evaluated using a quartz crystal microbalance with dissipation monitoring (QCM-D) (QSense Explorer). The NOM deposition rates were measured on silica (SiO_2; QSense) and alumina sensors (Al_2O_3; QSense). The Sauerbrey equation (Sauerbrey 1959) can be used to describe the relationship between the deposited mass (in ng/cm^2) and the variation in the resonance frequency of the material (SiO_2 or Al_2O_3 sensor for this study):

$$\Delta m = -\frac{C_{QCM}}{n}\Delta f \tag{3.8}$$

where Δm is the change in the mass deposited on the sensor, C_{QCM} is the mass sensitivity constant (e.g., 17.7 ng cm^{-2} Hz $^{-1}$ for a 5 MHz quartz crystal), n is the overtone number (1, 3, 5, 7, and 9), and Δf (Hz) is the shift in resonance frequency at overtone n (Akanbi, Hernandez et al. 2018).

Before each QCM-D experiment, the SiO_2 and Al_2O_3 sensors were cleaned by soaking them in 2% Hellmanex. The sensors were then bath sonicated for 20 minutes, rinsed 10 times with DI water, rinsed three times with ethanol, rinsed again 10 times with DI water, and dried with nitrogen gas. The sensors were UV-exposed for 2 hours (UV chamber, Bioforce Nanosciences) to remove residual contaminants. DI water and all solutions used during the washing procedure were pre-filtered (0.1-µm cellulose acetate membrane, Corning® 500 mL) to avoid (nano)particles and undesired negative frequency shifts associated with contamination. The experiments were conducted at room temperature, and a peristaltic pump was used to enable operation under laminar flow conditions, while avoiding air bubbles (flow rate of 100 µL/min). Before entering the QCM-D module, the NOM was pre-filtered with a 0.45-µm membrane to avoid larger colloids and erratic deposition rates (Lapointe, Farner et al. 2020).

4.3.8 Flux calculation and fouling resistance modeling

The flux was calculated by dividing the daily volume of the permeate by the membrane area. The total fouling resistance of the membranes (m^{-1}, R) was obtained using Darcy's law: $R_{total} = \Delta P/ (\mu_T J_T)$, where μ_T is the permeate viscosity at temperature T, J_T is the measured permeate flux at temperature T, and ΔP is the hydrostatic pressure. The clean membrane resistance (R_{clean}) was calculated using the same procedure as that used for the pure water flux. The fouling resistance

(biofilm and irreversible resistance) was calculated by subtracting the clean membrane resistance (R_{clean}) from the total fouling resistance (R_{total}).

Hermia's model was used to identify the membrane fouling mechanism during filtration (Hermia 1982). The model can be described by Equation 3.9, where t is the time of filtration, V is the collected permeate volume, and K is a proportionality constant.

$$\frac{d^2t}{dv^2} = K\left(\frac{dt}{dv}\right)^n \tag{3.9}$$

In this equation, n depends on the fouling type, as listed in Table A.1. A schematic representation of these mechanisms is shown in Figure A.2.

4.4 Results

4.4.1 Effect of alumina content on membrane properties

The mean porosities of membranes M1, M2, and M3 are listed in Table 4-5. The mean porosities of M1 and M2 were calculated to be approximately 42% and 44%, respectively, and the difference between them was not significant ($p = 0.11$). However, a significant ($p = 0.02$) increase in porosity (~12%) was observed after increasing the alumina content to 50% in M3. Because alumina is integrated in the membrane structure between kaolin particles, it increases the porosity, pore size, and flux, as shown previously (Rasouli, Abbasi and Hashemifard 2017).

Table 4-5. Results of membrane characterization

Membrane type	M1	M2	M3
Contact angle	<5°	<5°	<5°
Porosity (%)	41.9 ± 0.99	43.6 ± 1.88	54.7 ± 2.1
Mean pore size (µm) (calculated)	0.43 ± 0.01	0.48 ± 0.01	0.98 ± 0.03
Mean pore size (µm) (from SEM)	0.37 ± 0.24	0.58 ± 0.23	0.98 ± 0.35
Pure water permeability (LMH/bar) at 90 mbar	101 ± 3	375 ± 18	3851 ± 35
Clean membrane resistance (m^{-1})	$3.48 \times 10^9 \pm 8.22 \times 10^7$	$9.75 \times 10^8 \pm 3.28 \times 10^7$	$8.87 \times 10^7 \pm 1.55 \times 10^6$
Major phase*	Boromullite	Aluminum borate	Aluminum borate
Minor phase*	SiO_2	SiO_2	SiO_2

*From the XRD analysis.

All membranes were highly hydrophilic, as indicated by their low contact angles (Table 4-5). The mean pore sizes of M1 and M2 ranged 0.43–0.48 µm and were not statistically different ($p = 0.05$). M3, with the highest alumina content, had a significantly higher mean pore size of 0.98 µm ($p = 0.001$). The XRD patterns of the membranes are illustrated in Figure A.3. For M1, the major phase was $Al_9BSi_2O_{19}$ (boromullite), whereas the minor phase detected was SiO_2. For M2 and M3, the phases were identified as aluminum borate and SiO_2, respectively. During the calcination process at 550 °C, kaolin clay was transformed into metakaolin by dihydroxylation, which is the anhydrous form of kaolin, according to Equation 3.10.

$$2\ Al_2Si_2O_5(OH)_4 \rightarrow 2\ Al_2Si_2O_7 + 4\ H_2O \qquad (3.10)$$

Increasing the temperature to 1050 °C leads to the formation of a mullite phase according to Equation 3.11 (Rasouli, Abbasi and Hashemifard 2019).

$$3\ (Al_2O_3.\ 2SiO_2) \rightarrow 3\ Al_2O_3.\ 2\ SiO_2 + 4\ Si \qquad (3.11)$$

Mullite can react with boric acid (which is added to increase the mechanical strength of the membrane) to form a boromullite phase, according to Equations 12 and 13 (Hernández, Violini et al. 2020). The presence of a boromullite phase after membrane calcination indicates the formation of a mullite phase during membrane calcination, which is the major phase in kaolin-based membranes (Rashad, Logesh et al. 2021), indirectly confirming the correct calcination procedure.

$$H_3BO_3 \rightarrow B_2O_3 + H_2O \text{ (boric acid decomposition)} \quad (3.12)$$

$$3\ Al_2O_3.\ 2SiO_2 + B_2O_3 \rightarrow Al_4.5SiB_{0.5}O_{9.5} \text{ (boromullite)} \quad (3.13)$$

The surface micrographs of the membranes are shown in Figure 4-2. A rough and porous structure was observed for the M3 membrane, confirming the porosity calculated using the wet and dry membrane weights. The porosity results showed that the M3 had the highest porosity. Moreover, as the circles in the micrograph indicate, the approximate pore sizes were 1 μm, which confirms the calculated mean pore sizes. A smoother, porous, and more compact structure was observed for M2. The SEM observations of the M2 samples showed a mean pore size lower than that of the M3 membrane. The general pattern and structure of the membrane were roughly the same as those of M1, although they were less porous and had a smaller pore size than the M3 membrane.

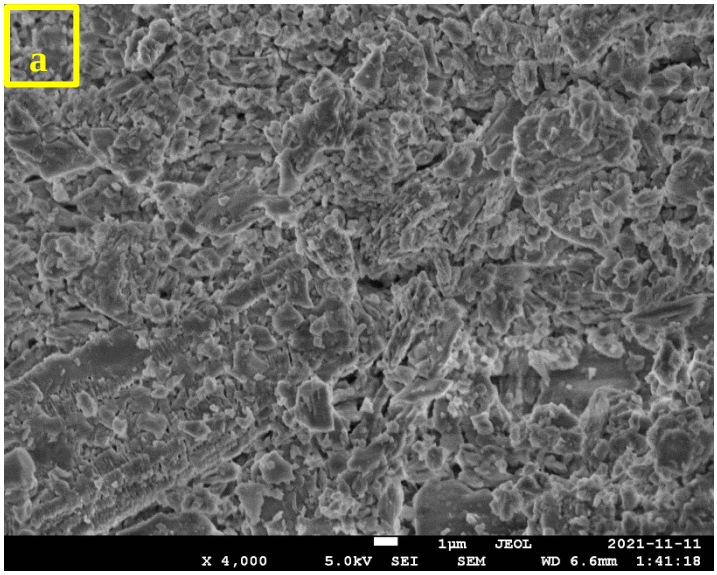

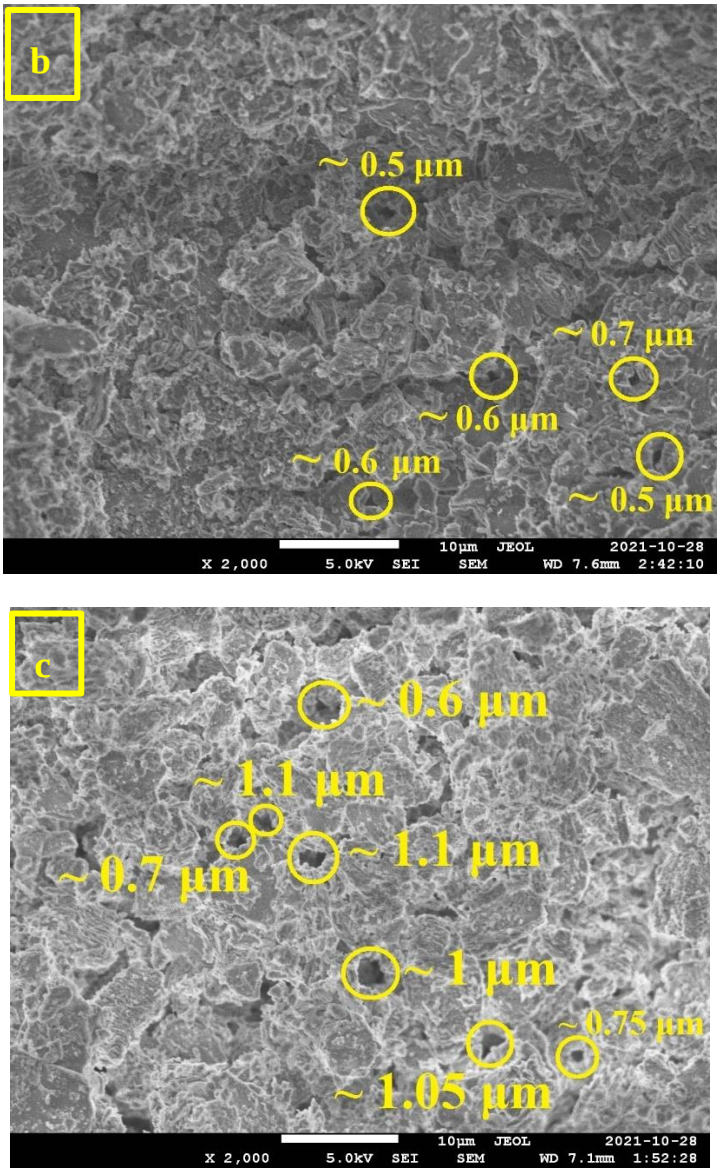

Figure 4-2. SEM images from the surface of M1 (kaolin only), M2 (75 Wt% kaolin + 25 Wt% alumina), and M3 (50 Wt% kaolin + 50 Wt% alumina) membranes.

At an operating pressure of 90 mbar, the lowest permeability of the pure water was roughly 100 LMH/bar for M1, which then roughly quadrupled for M2 (375 LMH/bar); for the M3, it increased more than 10 times to reach a peak of approximately 3850 LMH/bar, as expected from the results of porosity and mean pore sizes.

4.4.2 Effect of alumina content on membrane sorption affinity

The results of the NOM deposition in the QCM analysis are presented in Figure 4-3. The SiO_2 sensor mimics the kaolin-based membrane M1 with high Si content, whereas the Al_2O_3 sensor represents the kaolin plus alumina-based membranes M2 and M3. The frequency shift, representing the NOM deposition on the sensor, is low for SiO_2, which confirms that the soluble NOM molecules in the influent water have low surface interaction with the SiO_2 surface. The NOM deposition rate on the Al_2O_3 sensor was higher than that on the SiO_2 sensor, indicating that the NOM had a higher affinity toward Al-based oxides than Si-based oxides.

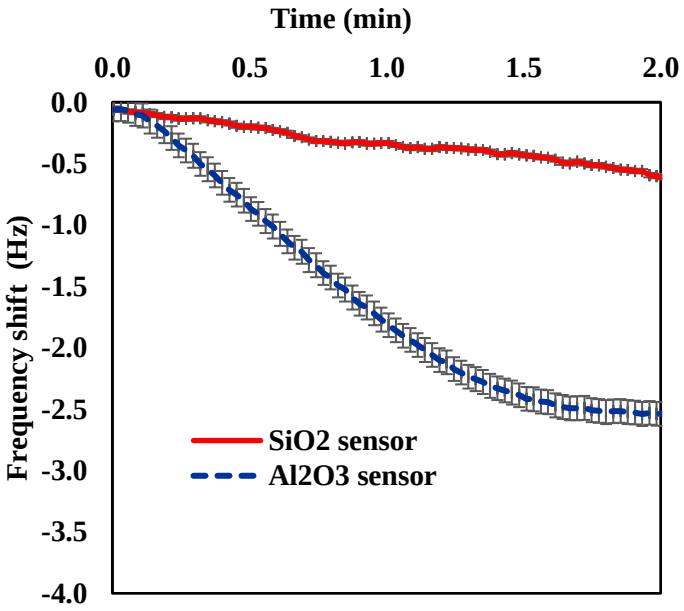

Figure 4-3. Frequency shift as an indicator of NOM deposition rates on SiO_2 and Al_2O_3 sensors mimicking kaolin-based membrane (M1, red curve) and kaolin + alumina-based membrane (M2 and M3, blue curve), respectively.

4.4.3 Permeate flux and fouling resistance

The flux decline rates for the tested membranes are shown in Figure 4-4a (or Figure A.4 for improved resolution). The figure can be divided into four phases. The first phase is characterized by a steep flux decrease related to rapid membrane pore blocking. During this phase, the permeate flux dropped from 45 to approximately 2.5 LMH, 17 to 2.2 LMH, and 7 to 2.1 LMH for M3, M2,

and M1, respectively. During the second phase, a stable flux was reached after 24 days of filtration for all the membranes.

During the third phase, a slight increase in flux was observed before a stable flux was reached again in the fourth phase, which can be attributed to biofilm growth on the membrane surface that has been shown to improve membrane flux (Du, Liu et al. 2021). The stable fluxes of M1, M2, and M3 were approximately 2.4, 2.5, and 3.0 LMH, respectively.

The same trend was observed for fouling resistance (Figure 4-4b). For the synthesized M1, M2, and M3 membranes, it first increased sharply to reach a peak of approximately 1.5×10^{10} m^{-1} and then decreased to achieve a stable value of approximately 1.3×10^{10} m^{-1}.

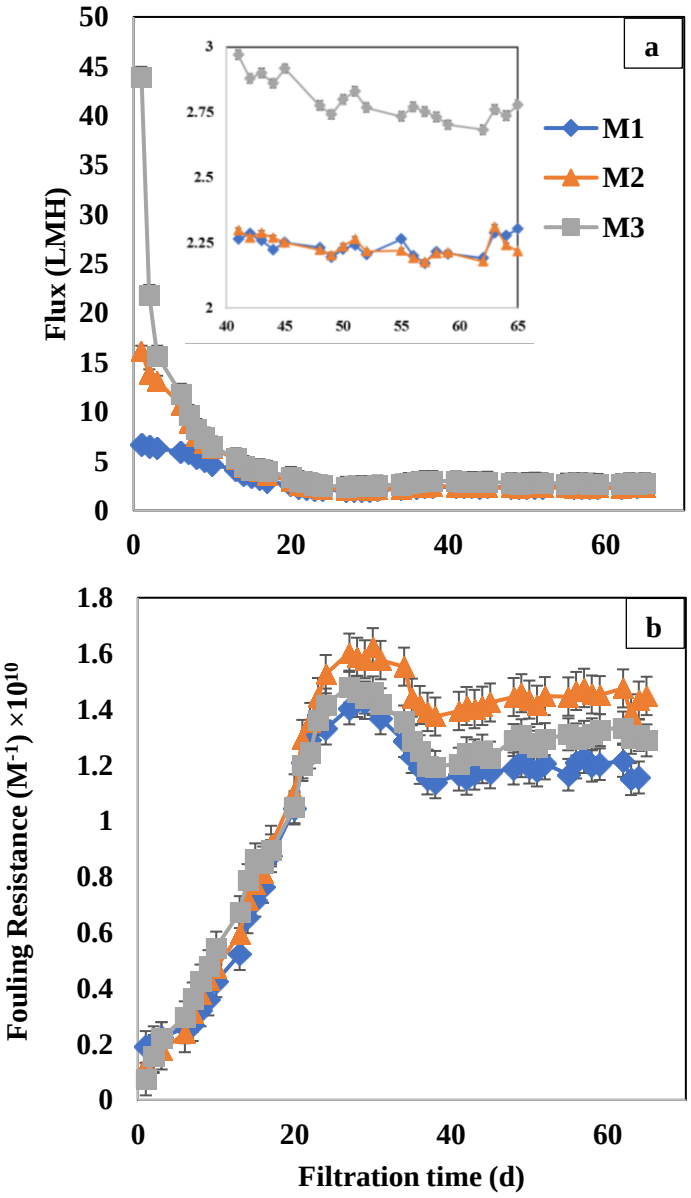

Figure 4-4. Evolution of a) permeate flux and b) fouling resistance for M1 (kaolin only), M2 (75 Wt% kaolin + 25 Wt% alumina), and M3 (50 Wt% kaolin + 50 Wt% alumina) membranes.

4.4.4 Membrane fouling mechanisms

The modeling of the flux-time data using pore blocking and cake layer formation mechanisms before reaching the stable flux time are shown in Figure 4-5, and the percentages of errors between

the experimental and modeled fluxes are listed in Table A.2. For M1, the standard and complete pore blocking models showed the minimum error between the experimental and modeled data, as approximately 18% and 15%, respectively. Likewise, for M2, the complete pore blocking model showed the best fit with an error of approximately 14%. For M3, the intermediate pore blocking model with an error of 5% was the best model. Furthermore, the error between the cake layer formation model and experimental data decreased with time. This suggests that in the initial days of filtration, before a stable flux was reached, the internal area of the membrane pores was clogged, and a biofilm layer started to form on the membrane surface toward the flux stabilization time.

4.4.5 Permeate quality

Permeate turbidity as a function of time is shown in Figure 4-6a. The highest variations were observed during the first 14 days of filtration. After the first day of filtration, M1 showed a turbidity of approximately 0.9 NTU, which dropped continuously to reach a minimum of approximately 0.2 NTU, followed by a fluctuating trend ranging between 0.2 and 0.3 NTU. Likewise, for M2, the general trend was the same; it started at approximately 0.45 NTU and decreased to approximately 0.1 NTU, finally reaching a stable value of 0.15 NTU. For M3, the turbidity was initially approximately 0.3 NTU, which decreased to around 0.15 NTU and then stabilized at 0.2 NTU. According to the United States Environmental Protection Agency (USEPA), the turbidity of the permeate should be lower than 0.15 NTU. This result suggests that it would be desirable for future assays to use membranes with lower porosities to improve turbidity rejection results.

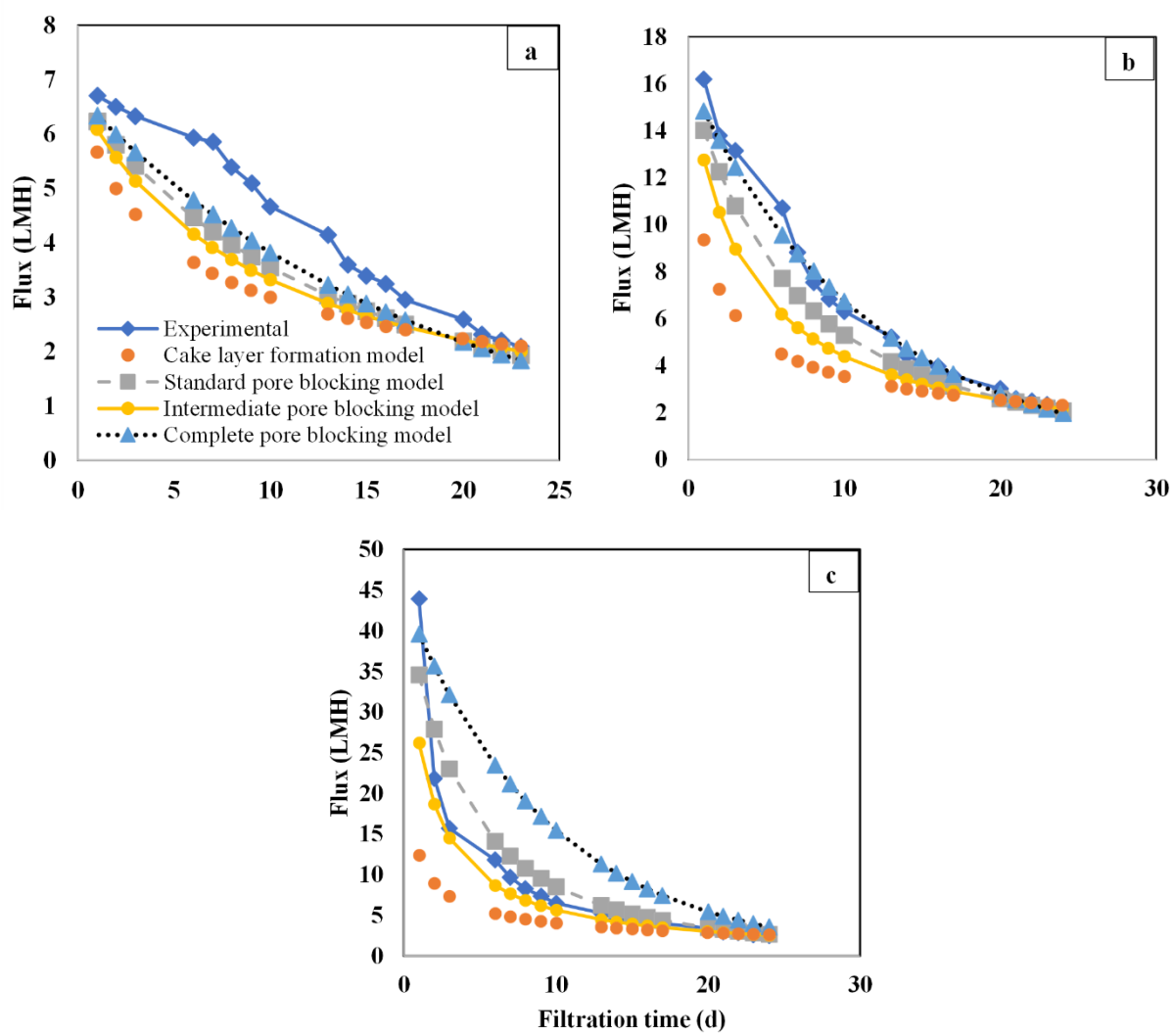

Figure 4-5. Flux decline modeling for a) M1 (kaolin only), b) M2 (75 Wt% kaolin + 25 Wt% alumina), and c) M3 (50 Wt% kaolin + 50 Wt% alumina) membranes

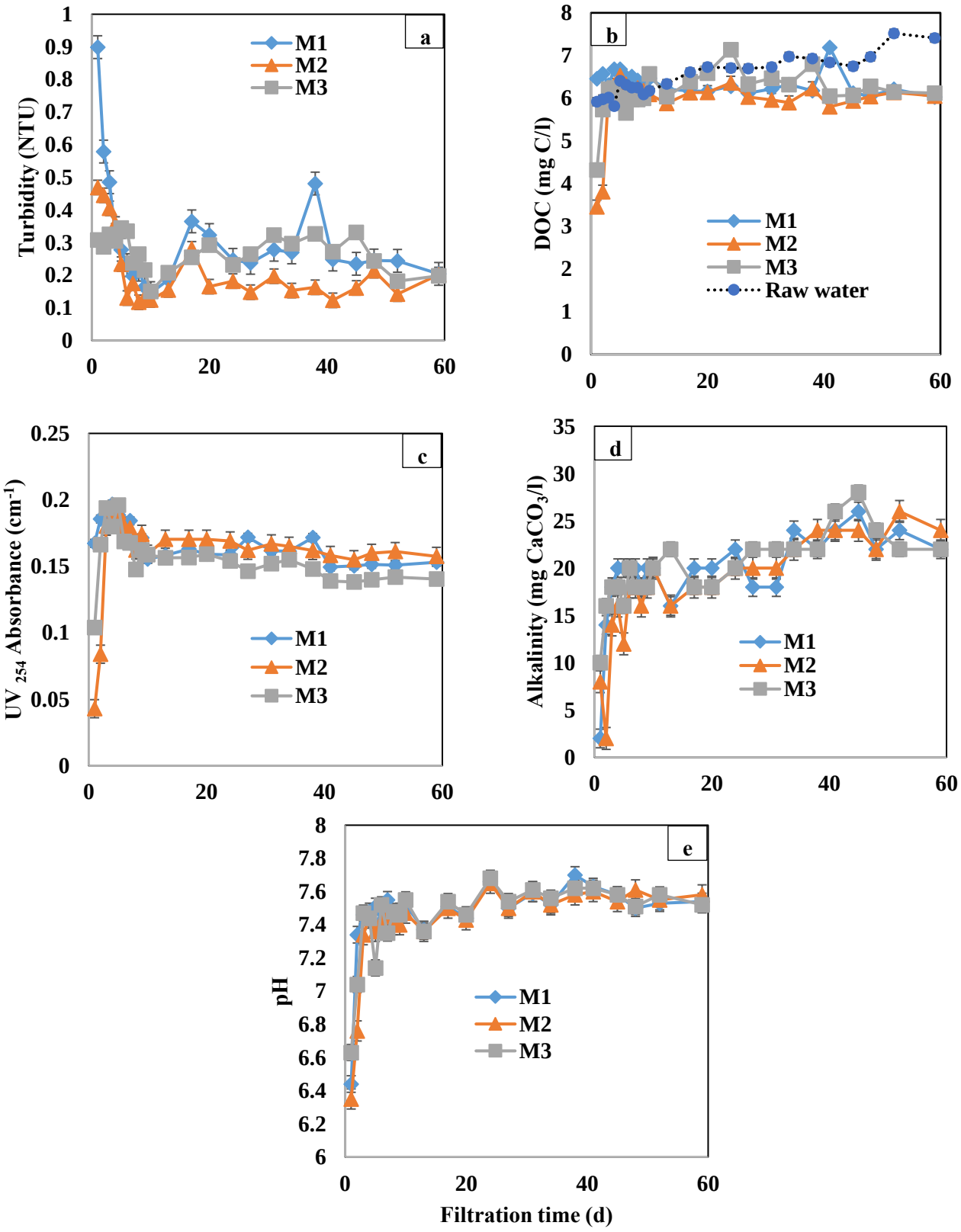
a
Turbidity (NTU)
M1
M2
M3
b
DOC (mg C/l)
M1
M2
M3
Raw water
c
UV 254 Absorbance (cm-1)
M1
M2
M3
d
Alkalinity (mg CaCO3/l)
M1
M2
M3
e
pH
M1
M2
M3
Filtration time (d)

Figure 4-6. Permeate quality variations by time using the three membrane types: M1 (kaolin only), M2 (75 Wt% kaolin + 25 Wt% alumina), and M3 (50 Wt% kaolin + 50 Wt% alumina) a) Turbidity (NTU), b) DOC (mg C/L), c) UV254 index, d) alkalinity (mg/L CaCO3), and e) pH

Figure 4-6b shows the evolution of DOC in the three permeates and the influent water. At the initial filtration time, the permeates of M2 and M3 showed a lower DOC content of approximately 3.4 and 4.5 mg C/L, respectively, compared to the influent water (~ 6 mg C/L). However, the NOM removal reached a stable value, fluctuating around 6 mg C/L after one week of operation, which was slightly lower than the DOC influent water. For M1, a different trend was observed. In the initial filtration time, the initial DOC was 6.5 mg C/L, followed by a slight decrease and finally fluctuating to around 6 mg C/L (similar to M2 and M3 membranes).

The UV_{254} absorbance versus time is plotted in Figure 4-6c. The general scheme was similar to that of the DOC evolution. Initially, M2 and M3 exhibited significant UV_{254} removal, reaching a minimum value of 0.05 and 0.1, respectively. However, after rapid exhaustion of the alumina adsorption capacity, there was a steep increase in the UVA_{254} trend, and a stable state with 0.16 and 0.14 absorbance units was achieved for M2 and M3 permeates, respectively. For the M1, the initial UVA_{254} of the permeate was 0.17 cm^{-1}, followed by a slight increase up to 0.19 cm^{-1} and then a decrease to reach a stable value of approximately 0.14 cm^{-1}.

The evolution of alkalinity and pH is presented in Figure 4-6d and Figure 4-6e, respectively. The trends followed a pattern similar to those of DOC and UV_{254}. The M1, M2, and M3 membranes showed a decrease in alkalinity from approximately 20 mg/L $CaCO_3$ (influent water) to 2 mg/L$CaCO_3$, 2 mg/L $CaCO_3$, and 10 mg/L $CaCO_3$, respectively. This may be because acidic moieties present in fresh membrane pores transform bicarbonate ions (HCO_3^-) into H_2CO_3 and eventually CO_2, as the pH of the influent water is always 7.4 –7.6; therefore, the wide alkalinity range was due to the presence of bicarbonate ions. After this short initial period, the alkalinity trend fluctuated to reach a stable value of approximately 22 mg/L $CaCO_3$, which is approximately equal to that of the influent water alkalinity. In the initial days of filtration, the pH of the M1, M2, and M3 permeates showed a minimum value of 6.3 – 6.6, which is based on the alkalinity graph. The pH data were consistent with those obtained for alkalinity. The pH stabilized at a value equivalent to that of the influent (7.5) once the initial neutralization period of the membranes was complete.

4.4.6 Biofilm characterization results

To discriminate the biofouling layer using OCT, an image without a biofilm layer (virgin membrane) was compared with another image with the biofilm layer on the membrane surface (Figure A.5). Digital camera photos of the synthesized membranes after 65 days of filtration (the last day of the experiment) are shown in Figure 4-7. The OCT images of membranes M1, M2, and M3 after 15, 30, and 45 days of filtration are shown in Figure A.6. The images taken on the last filtration day (day 65) are shown in Figure 4-8. According to the images taken after 15 days of filtration (Figure A.6 a, b, c), a distinct heterogeneous and outspread layer of biofilm was observed. After day 30, a denser, more compact, and aggregated biofouling layer was observed as shown in Figure A.6d-h, especially for the M2 and M3 membranes (for M1 membranes, there was still an outspread biofilm structure on day 30). At the end of the experiment, based on the images taken on day 65 (Figure 4-8 a, b, c), the most compact and dense biofilm structure was observed on the membrane surface.

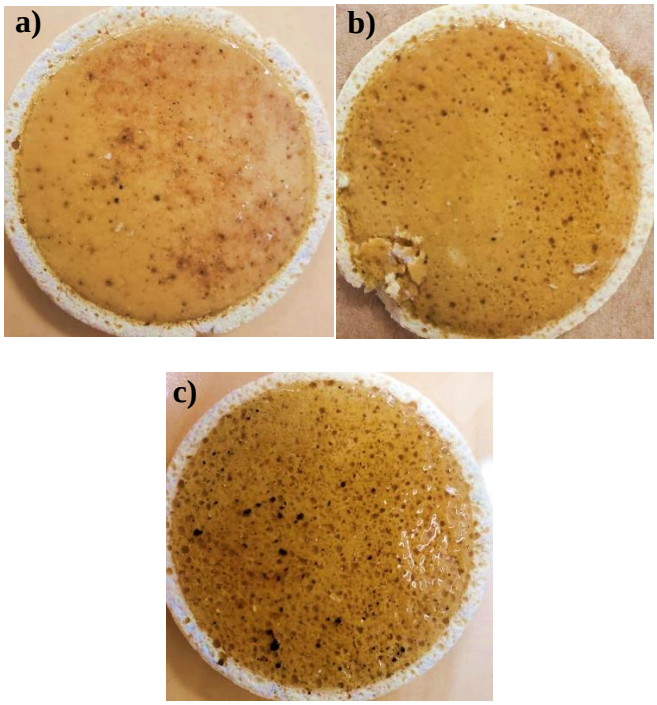

Figure 4-7 Digital photographs of a) M1 (kaolin only), b) M2 (75 Wt% kaolin + 25 Wt% alumina), and c) M3 (50 Wt% kaolin + 50 Wt% alumina) membranes on day 65

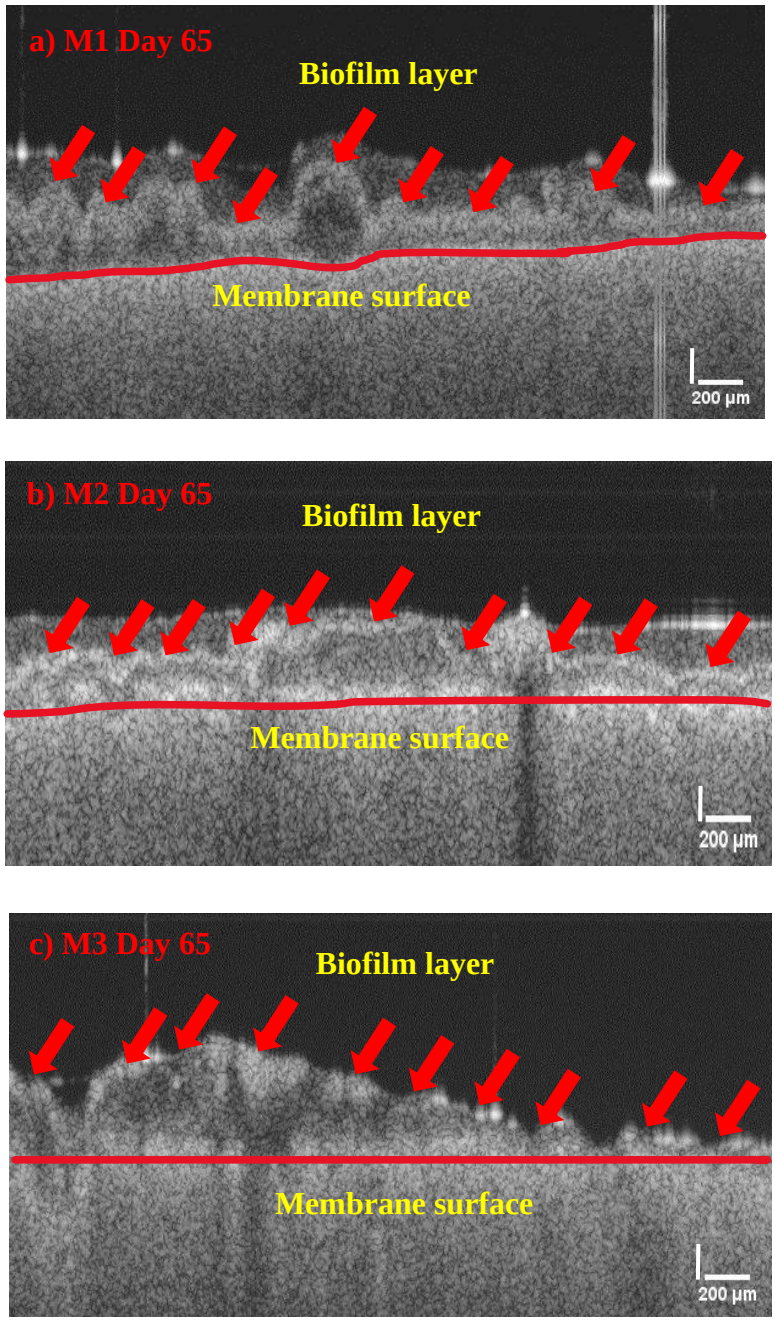

Figure 4-8 OCT images of a) M1 (kaolin only), b) M2 (75 Wt% kaolin + 25 Wt% alumina), and c) M3 (50 Wt% kaolin + 50 Wt% alumina) membrane surfaces on day 65

To study the effect of the membrane structure on biofilm formation, the absolute and relative roughness and mean thickness of the biofilm layer were determined (Table 4-6), using the OCT images acquired at the end of the experiment (day 65). For the membrane without alumina in its

structure (M1), the mean thickness and absolute roughness were 371 and 104 μm, respectively. For the membrane with 25% wt alumina (M2), the absolute roughness and mean thickness were calculated to be 224 and 70 μm, respectively. For M3, the mean biofilm layer thickness was 315 μm, and the absolute roughness was 173 μm. The relative roughness values for M1, M2, and M3 were calculated to be 0.28, 0.31, and 0.55, respectively.

Table 4-6 Mean biofilm thickness and relative and absolute roughness of the biofilm based on the OCT images acquired on day 65

Parameter	**M1**	**M2**	**M3**
$\bar{Z}$ **(μm)**	371	224	315
R_a**(μm)**	104	70	173
$\overline{R_a}$	0.28	0.31	0.55

To quantify the total active microorganisms present in the biofouling layer, the ATP concentration was measured in the biofilm layer (Figure 4-9). According to the graph, the mATP/m membrane ratio for M3 had the highest value of 6.3×10^{-8}, which is approximately three times more than that for M2 (2×10^{-8}) and ten times higher than that for M1.

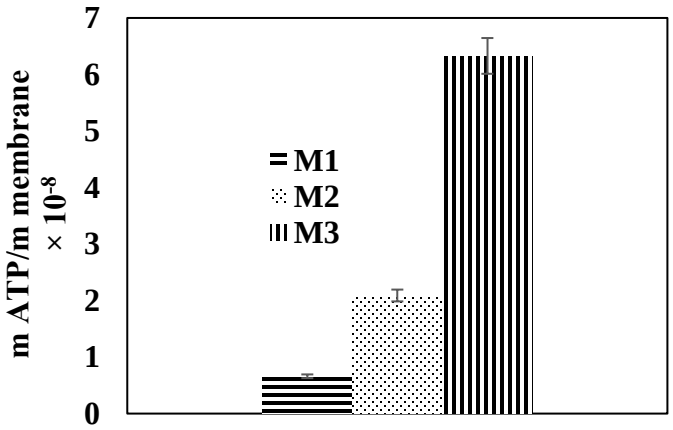

Figure 4-9 Ratio of m_{ATP}/ $m_{membrane}$ for the three synthesized membranes: M1 (kaolin only), M2 (75 Wt% kaolin + 25 Wt% alumina), and M3 (50 Wt% kaolin + 50 Wt% alumina)

4.5 Discussion

4.5.1 OCT observations confirm the flux decline modeling results

Based on the images acquired on day 15 of filtration, before reaching a stable flux (Figure A.6a, b, c), a distinct heterogeneous and outspread layer of biofilm was observed. As explained in the flux modeling section (section 4.4.4), before reaching a stable flux (approximately before day 24 for the synthesized membranes), the fouling mechanism is controlled by pore blocking mechanisms (standard, intermediate, and complete), not the cake layer, which were confirmed by the OCT observations, showing a scattered and sporadic biofilm structure. During the initial period, the steep flux decline might be related to the decrease in the effective membrane pore volume (i.e., pore blocking mechanisms) (Akanbi, Hernandez et al. 2018). After flux stabilization for the synthesized membranes, it was possible to observe a more compact and aggregated cake layer based on Figure A.6d, e, and f. After blocking the inside volume of the pores, it was expected that the contaminants accumulate on the membrane surface; consequently, a more compact biofouling/cake layer was observed. The transition of the pore blocking models to cake layer formation makes it possible to achieve a stable flux (Figure A.6 g, h, i), as reported elsewhere in the literature (Akanbi, Hernandez et al. 2018).

According to the images taken on day 65 (Figure 4-8 a, b, c), the most compact cake layer structure was observed on the membrane surface. In fact, in long-term and continuous filtration, the interaction between contaminant particles in the influent water on the membrane surface and the force exerted by the TMP were the factors compressing the biofouling layer formed on the membrane surface. Therefore, a relatively high-level biofilm layer with a dense internal structure is observed during long-term filtration (Derlon, Peter-Varbanets et al. 2012, Derlon, Koch et al. 2013, Shi, Liu et al. 2020). Based on these observations, it is more realistic to discuss the roughness and thickness of the biofilm at the end of the filtration time, where the most compact biofouling structure was observed.

Consistent with the values listed in Table 4-6, the relative biofilm roughness for M1, M2, and M3 showed an ascending trend for increasing alumina concentration in the membrane structure. The relative roughness coefficient indicated the homogeneity and uniformity of the biofilm. Increasing the alumina concentration in the membrane structure increased the heterogenicity of the biofilm

structure formed on their surfaces. Therefore, in the case of M3, at the end of filtration (day 65), the relative roughness showed the highest value, indicating the formation of the most heterogeneous biofilm structure.

4.5.2 Increase in biomass concentration in the biofilm is due to increased membrane adsorption capacity

Owing to the presence of higher alumina content in the M3 structure, which improves the adsorption conditions of the particles and contaminants, more biomass can accumulate on the membrane surface, which eventually enhances the microbial activity in the biofilm (Figure 4-9). Furthermore, increased adsorption of organic matter on the alumina-enriched membrane leads to an increase in the nutrient concentration on the membrane surface consumed by the microorganisms present in the biofilm, which finally increases the number of microbial species in M3 (Vieira and Melo 1995, Shao, Feng et al. 2017).

4.5.3 Effect of membrane structure on permeate flux and fouling resistance

In this study, a four-stage flux flow was observed for all synthesized membranes, regardless of their structure and alumina concentration. The four stages consisted of: i) a steep flux decline section before reaching the stabilized flux, ii) a constant flux section, iii) a slight flux increase, and iv) a constant flux regime. Therefore, no effect of the alumina concentration and membrane structure was observed on the general flux decline diagram behavior. However, the effect of increasing the alumina concentration in the membrane structure (M1 = 0 Wt% alumina, M2 = 25 Wt% alumina, and M3 = 50 Wt%) on the flux was clearly observed in the initial days of filtration, before reaching a stable flux. In this stage, the greater the alumina content in the membrane structure was, the higher the flux and the steeper the flux decline curve were. However, after reaching a stable flux, the alumina concentration had a negligible effect, as the flux at the end of the filtration time was roughly the same for the synthesized membranes (2.5 LMH for M1 and M2 and 3 LMH for M3). These results suggest that increasing alumina content in the membrane structure can increase the permeate flux prior to the section of reaching a stable flux. However, stable flux is roughly independent of the membrane structure, as reported for polymeric membranes (Frechen, Exler et al. 2011, Lee, Lee et al. 2019). Nevertheless, in the literature both flux rise or

drop can be found following modifications of surface properties or structure. The pre-deposition of zeolite on the surface of UF membranes showed an increased membrane fouling in both short-term and long-term GDM, however a higher stable flux was observed for GDM using zeolite and powdered activated carbon adsorbents combined with the membrane (Ding, Song et al. 2021). Furthermore, altering membrane characteristics by depositing a layer of granular activated carbon on the membrane surface resulted in an improved organic removal, decreased stable flux and increased hydraulically reversible resistance (Ding, Wang et al. 2018). The researchers in another study (Jiang, Zhao et al. 2019) modified the matrix of Polyvinylidene Fluoride membranes using synthetic tailored amphiphilic multi-arms polymer poly (propylene glycol)-silane-poly (ethylene glycol). The results revealed an increased porosity and hydrophilicity of the membranes compared to membranes without modification. The water flux of modified membranes in GDM process increased from 4.6 LMH to 12.1 LMH compared to control membranes (without modification).

Likewise, the general trend of fouling resistance for all the membranes followed three stages: i) a steep increase roughly to the flux stabilization point, ii) a decrease, and iii) eventually reaching a stable value. In the case of the synthesized membranes, regardless of their alumina content, the values of fouling resistance were approximately equal for most of the filtration time, indicating that increasing the alumina concentration in the membrane structure does not markedly affect the fouling resistance. However, it has been reported that using adsorption of a granular activated carbon as a thin layer on the polymeric membrane surface can increase fouling resistance (Ding, Wang et al. 2018).

4.5.4 Effect of membrane structure and bio-clogging on permeate quality

Permeate quality can be affected by two main factors: adsorption (by alumina in the membrane structure) and biodegradation/biosorption (by the biofilm/cake layer). Regarding permeate turbidity, during the initial filtration days before reaching a flux stabilization time, a poor cake layer effect occurred, as revealed by the OCT images and flux modeling results. Therefore, adsorption played a key role in turbidity removal, as M1 (0 Wt% alumina), M2 (25 Wt% alumina) and M3 (50 Wt% alumina).

The highest and lowest turbidity values are shown in Figure 4-6a. After reaching a stable flux and a compact biofilm structure, the turbidity removal values increased. This can be related to the

formation of a biofilm/cake layer on the membrane surface, which acts as a bio-filter medium, decreasing the turbidity content (Akanbi, Hernandez et al. 2018).

Likewise, the higher DOC and UV_{254} absorbance removal in M2 and M3 compared with that in M1, at the beginning of filtration, can be attributed to their higher adsorption capacity. Moreover, the QCM confirmed the higher affinity of the alumina-based membranes (M2 and M3) toward NOM (higher NOM deposition on the Al_2O_3 sensors). DOC and UV_{254} rejection after reaching a stable flux can be attributed to the formation of a cake layer on the membrane surface that operates as an extra filter medium (Discart, Bilad et al. 2014). The DOC removal of M3 was slightly lower than M2, despite the increased alumina content of M3 compared to M2. Generally, a higher NOM removal is expected by the membrane with the enhanced adsorption capacity (M3), however increasing alumina concentration in the membrane structure increased the porosity and membrane pore size, which decreases the organic rejection of the membrane. Moreover, in the case of M3 with the highest flux (especially in the initial filtration time) the contact time for the adsorption of NOM is less than that of M2. The less contact time could impact the NOM removal negatively.

The mechanism of increasing permeate quality after reaching a stable flux is mainly due to the biological activity of the biofilm layer on the membrane surface (Pronk, Ding et al. 2019). During the GDCM process, the porous membrane is responsible for rejecting larger contaminants in the influent water, such as colloidal matter (turbidity removal), and the formed biofilm is expected to improve the removal of dissolved organic matter, because the biofilm can act as a secondary membrane or biodegradation agent for organic matter (Chawla, Zwijnenburg et al. 2017, Pronk, Ding et al. 2019).

4.6 Conclusions

In this study, three types of ceramic microfiltration membranes based on kaolin clay and different alumina contents were synthesized, and their performance for gravity-driven filtration of river water was investigated. The membrane characteristics were studied using different methods (SEM, XRD, mean pore size and porosity calculations, and contact angle). The effects of alumina content and biofouling on steady-state flux and permeate quality (turbidity, DOC, UV_{254}, pH, and alkalinity) were investigated. The following conclusions were drawn:

- For the synthesized membranes (M1, M2, and M3), the stable flux was roughly the same at the end of the filtration (2.5–3.0 LMH), indicating that the stable flux state is independent of the alumina content.
- The synthesized membranes showed significant UVA_{254}, alkalinity, and DOC removal during the initial filtration days, as well as turbidity removal after flux stabilization.
- The modeling flux decline revealed that the dominant membrane fouling mechanism before reaching a stable flux corresponds to pore blocking. After reaching a stable flux, fouling was dominated by cake layer formation.
- The OCT imaging observations showed a distinct heterogeneous biofilm layer before a stable flux was achieved, followed by a dense and irregular cake layer formation, confirming the transformation of the mechanism from pore blocking model to cake layer formation model.
- Increasing the alumina content in the membrane structure leads to enhanced carbon adsorption, resulting in the deposition of more nutrients in the biofilm layer, which enhances the biological activity, as measured through the ATP method.

For future objectives, smaller pore size membranes (0.1–0.2 µm) should be tested to reach a permeate turbidity below 0.1 NTU. Moreover, according to the flux and fouling resistance results, the physical and chemical cleaning stages and pretreatment such as resins which are operating in biological mode could be added to increase the sustainability of the process.

4.7 Acknowledgements

The authors would like to express their gratitude to the Polytechnique Montreal technicians and research professionals, Gabriel St-Jean, Julie Philibert, Mélanie Bolduc, Tetiana Elyart, Jacinthe Mailly, and Yves Fontaine for their help in preparing the gravity-driven membrane filtration setup and raw water and for their technical support during this project. The authors would like to thank Nathalie Tufenkji for sharing the QCM equipment used in this study. This project was funded by the Canada Research Chair for Decentralized and Small-Scale Water Treatment (file number 950-232871).

CHAPTER 5 Article 2: Performance of biological ion exchange resin and gravity-driven ceramic membrane hybrid process for surface water treatment

Yaser Rasouli, Raphaël Maltais-Tariant, Benoit Barbeau, Sigrid Peldszus, Caroline Boudoux, Dominique Claveau-Mallet. Performance of biological ion exchange resin and gravity-driven ceramic membrane hybrid process for surface water treatment (publication date: Nov 19, 2023). *Separation and Purification Technology*, *332*, 125769.

5.1 Abstract

In this study, the performance of a biological ion exchange (BIEX) resin and gravity-driven ceramic membrane (GDCM) filtration hybrid process in terms of membrane permeate quality, flux, and membrane biofilm characteristics during river water treatment for drinking water was investigated. The hybrid process results were compared with those of the GDCM process without the BIEX pre-treatment. Three types of previously synthesized microfiltration membranes were used: M1 (100 wt% kaolin), M2 (75 wt% kaolin + 25 wt% alumina), M3 (50 wt% kaolin + 50 wt% alumina), and M4 (commercial ceramic microfiltration membrane). In terms of permeate quality, the BIEX column removed approximately 74% of the dissolved organic carbon (DOC) compared with the influent water, followed by 27% DOC removal using M3 compared with the BIEX column effluent on day 65 (6,240 BV), which was mainly due to the removal of humic and fulvic acids. BIEX removed turbidity of the influent water from 2.20 NTU to 0.77 NTU, which was further decreased to 0.09 NTU by membranes. The maximum stabilized flux of the membranes was approximately 5.7 LMH, which was almost doubled compared to GDCM without pre-treatment. The membrane biofilm showed lower thickness and roughness in the hybrid process than that in GDCM without pre-treatment. Higher extracellular polymeric substance (EPS) concentration and biological activity were observed for M3, the membrane with the highest stabilized flux and highest DOC removal efficiency. The results indicate that the hybrid BIEX + GDCM is a robust, high-performance, and easy-to-use process that can increase the flux and permeate quality of GDCM systems.

5.2 Introduction

Decentralized drinking water treatment systems are an appealing option for water supply of remote communities (Zhang, Wang et al. 2020, Hafeez, Shamair et al. 2021). However, given the lack of expertise available for maintenance and operation, such systems should be as passive as possible. Eliminating natural organic matter (NOM) in decentralized water treatment systems is a major challenge as most treatment options involve the use of chemicals such as coagulants, granular activated carbon (GAC), which has a limited capacity to absorb NOM, or high-pressure membranes processes. The abatement of NOM improves the organoleptic properties of water (color, taste, and odor) and mitigates the formation of organo-chlorinated disinfection byproducts (Ødegaard, Østerhus et al. 2010). An improved process targeting simultaneous passive disinfection and NOM removal from water is required to expand the deployment of decentralized drinking water systems.

Utilization of gravity-driven membrane (GDM) filtration is attractive because of its high particle removal performance, low energy consumption, reduced need for chemical or physical washing, and ability to reach a stabilized flux, making it suitable for long-term passive filtration (Issaoui and Limousy 2019, Du, Liu et al. 2021). Typically, stabilized GDM flux varies between 4 to 10 LMH according to the influent water composition, and the transmembrane pressure is below 0.1 bar (Pronk, Ding et al. 2019). The two critical limitations of this process are its relatively low flux (compared with conventional low-pressure membrane filtration) and very low NOM removal (Pronk, Ding et al. 2019). To overcome these disadvantages, we propose that integrating a passive NOM pre-treatment process with ceramic membranes could benefit the development of GDM filtration in decentralized water systems.

The longevity of ceramic membranes during long-term filtration is considered an essential factor because it decreases the capital costs of a plant, despite high production costs. For example, Metawater, a Japanese company, has supplied ceramic membranes for 160 installations worldwide. In one plant, the membranes have been in operation since 1998 with no breakage events (Jarvis, Carra et al. 2022).

Kaolin-based ceramic membranes are cost-effective (capital / production cost) compared with other ceramic membrane types, primarily because of the lower calcination temperature required for kaolin, which is attributed to the membrane structure and starting materials. In certain cases, they

are more cost-effective than polymeric membranes in term of total production cost (Hubadillah, Othman et al. 2018).

Although ion-exchange resins with regular regeneration have shown good NOM removal performance, there are concerns regarding the challenges with the management of spent brine and transportation of regeneration chemicals (Amini, Papineau et al. 2018). Biological Ion Exchange (BIEX) is an ion-exchange resin process that operates with an infrequent regeneration to promote secondary ion exchange (IEX) (e.g., NOM displacing sulfate and bicarbonate). Elimination of the regeneration step results in the formation and growth of biofilms, which increase the biological activity of the media (Winter, Wray et al. 2018). BIEX resins provide a suitable environment for the growth of microorganisms, although two recent studies (Liu, Solliec et al. 2022, Zimmermann, Li and Mohseni 2022) state that the main NOM removal mechanism is IEX and not biodegradation.

The traditional coagulation, flocculation, and sedimentation chains are not considered an option in the small water treatment systems because of their limitations such as online injection of chemicals (Arora, Malano et al. 2015). Therefore, researchers have widely suggested membrane filtration (MF/UF) processes in gravity driven mode (GDM) without pretreatment (Arora, Malano et al. 2015, Tang, Ding et al. 2016, Lee, Badoux et al. 2021) or integrated with GAC and/or PAC, while integration of BIEX with GDM has not been developed yet. In the hybrid BIEX + gravity-driven ceramic membrane (GDCM) filtration process, BIEX is mainly responsible for NOM removal, whereas GDCM filtration (MF/UF) principally targets particulate removal. These two treatment strategies are relatively new. The effect of BIEX pre-treatment on the fouling of polymeric ultrafiltration membranes has also been investigated (Schulz, Winter et al. 2017). BIEX has been reported to remove 50% of the different types of NOMs, such as humic substances, building blocks, and low-molecular-weight acids (from a pond water in Vancouver, Canada pre-filtered through 1 μm filters and diluted by tap-water to achieve 5 mg C/L of DOC), leading to a substantial reduction in total and irreversible UF fouling. However, the UF was conducted at a higher flux (50 LMH) than expected in the GDCM. In wastewater treatment applications, a hybrid process consisting of a biofilm reactor with submerged GDM can increase the flux compared to a single GDM process owing to improved organic matter removal (Wu, Hochstrasser et al. 2016). Two studies have focused on integrating granular and powdered activated carbon with a GDM process developed for rainwater treatment (Ding, Wang et al. 2018, Ding, Wang et al. 2018). In these studies, a layer of

granular and powdered activated carbon or sand was coated on the membrane surface. The presence of a granular activated carbon (GAC) layer increased the NOM removal by 25%; however, it decreased the stable flux (3.2 LMH) compared to that of the membrane without a coating layer (4.5 LMH). Finally, the effect of in situ coagulation on the performance of a GDM bioreactor intended for wastewater treatment enhanced the permeability by more than two-fold compared to the control process without coagulation. However, no flux stabilization was observed (Ding, Wang et al. 2017). In summary, previous studies suggest that lowering the NOM is beneficial in reducing membrane fouling. However, the effect of BIEX pre-treatment on the stabilized flux achieved by GDCM filtration has not yet been investigated.

The general objective of this research was to study the performance of the BIEX + GDCM hybrid process for the decentralized treatment of river water with high NOM concentration. In this study, two original sub-objectives were pursued. Firstly, the impact of BIEX pre-treatment on the permeate water quality and stabilized GDCM flux was investigated. Secondly, ceramic membranes were selected in the GDM process according to their extended lifetime expectancy which is aligned with the decentralized water treatment requirements. To achieve these objectives, a commercial anionic exchange resin operated without regeneration was used as a pre-treatment prior to kaolin-based microfiltration (MF) ceramic membranes. The performance of the hybrid process (BIEX + GDCM) was compared with that of a negative control consisting of only the GDCM step.

5.3 Materials and Methods

5.3.1 Membrane synthesis

Disk-shaped ceramic MF membranes with different kaolin and alumina contents were synthesized using a pressure casting and sintering method, as previously described (Rasouli, Maltais-Tariant et al. 2023). Briefly, kaolin (Sheffield Pottery, Sheffield, MA, USA) and alumina (Fisher Scientific, Switzerland; Al_2O_3, 40–300 μm, CAS: 1344-28-1, Mw = 101.96 g mol^{-1}) in predefined proportions (M1–M3) were mixed with deionized water to prepare a dough that was transferred to a disk-shaped mold. After applying 7.3 MPa pressure (SPI low-pressure sensor, NJ, USA) and drying at room temperature (20 – 25 °C), the membranes were calcined at 1100 °C for 2 h. The previously published membrane characteristics are presented in Table 5-1. Briefly, the goniometer (OCA20, Dataphysiscs, Germany) equipped with a video camera was used to measure the contact

angle by placing a water droplet on the membrane surface. Porosity was measured by determining the difference between wet and dry membrane weights. The membrane mean pore size was calculated using the Guerout-Elford-Ferry equation (Zhang, Lang et al. 2015) by measuring DI water flux at different pressure heads. Pore size of visible holes calculated using scanning electron microscopy (SEM) micrographs taken by Jeol, JSM-7600TFE, JEOL Ltd., Japan device using low electron voltages (5–10 kV) after sample preparation procedures. Minor and major crystalline phases appeared after membrane calcination procedure determined using a Brucker D8 Advanced X-ray diffraction (XRD) device by Cu-Kα radiation at a rate of 0.2° per second. Three membranes of each type were used for all the characterization techniques except XRD (one sample was used). A commercial ceramic MF (0.8 µm ZrO_2/TiO_2, disk shape, area 16 cm^2, Tami Industries, France, referred hereafter as M4) was tested along the alumina/kaolin ones to compare the performance of the membranes.

Table 5-1. Membrane characterization results (Rasouli, Maltais-Tariant et al. 2023)

Membrane type	**M1**	**M2**	**M3**	**M4**
Membrane contents	100 wt% kaolin 0 wt% alumina	75 wt% kaolin + 25 wt% alumina	50 wt% kaolin + 50 wt% alumina	ZrO_2/TiO_2
Contact angle	<5°	<5°	<5°	<5°
Porosity (%)	41.9 ± 2.48 [1]	43.6 ± 4.68	54.7 ± 5.21	21.2 ± 8.72
Mean pore size (µm) (calculated)	0.43 ± 0.03	0.48 ± 0.05	0.98 ± 0.07	0.8 [2]
Mean pore size (µm) (from SEM)	0.37 ± 0.03	0.58 ± 0.09	0.98 ± 0.13	-
Pure water permeability (LMH/bar) at 90 mbar	101 ± 7.60	375 ± 45.07	3,851 ± 87.07	141 ± 12.91
Major phase [3]	Boromullite	Aluminum borate	Aluminum borate	-
Minor phase [3]	SiO_2	SiO_2	SiO_2	-

[1] Mean ± 95% confidence interval
[2] According to the manufacturer
[3] From the XRD analysis

5.3.2 Influent water characteristics

Approximately 400 L of Des Prairies River water was collected in March 2022 from the influent of the Pont-Viau water treatment plant (after traversing through the water screen and before low-pressure pumps), which is located in Laval (Canada). The water was stored at 4 °C in a refrigerator (20 buckets, 20 L capacity) for the whole operation period. During the operation, DOC, turbidity, UVA_{254}, pH, alkalinity and the anions were monitored carefully by testing an average of 25 samples. The 95% confidence interval of the distributions (or standard deviations) confirmed fairly stable properties of the influent water during the operation. Influent water (40 L) was removed from the fridge weekly and incubated at room temperature for at least 5 h before being added to the system. The physicochemical composition of the influent water was monitored approximately thrice per week. The mean composition of the influent water during the study is presented in Table 5-2. The water exhibited a substantial DOC concentration and aromaticity, moderate turbidity, and a low concentration of competitive anions such as sulfate and nitrate (Liu, Papineau et al. 2021).

Table 5-2. Physico-chemical characterizations of the influent water

Parameters	Mean Value ± 95% confidence interval	Max Value	Min Value	Number of samples
DOC (mg C/L)	7.43 ± 0.05	7.67	7.12	27
Turbidity (NTU)	2.20 ± 0.07	2.72	1.89	27
pH	7.39 ± 0.06	7.62	7.14	27
Alkalinity (mg $CaCO_3$/L)	25.22 ± 0.37	28	24	27
UVA_{254} (cm^{-1})	0.25 ± 0.003	0.26	0.23	27
Nitrate (mg/L)	2.23 ± 0.18	3.02	1.73	19
Sulfate (mg/L)	4.53 ± 0.12	5.2	4.09	24
Chloride (mg/L)	4.78 ± 0.27	7.2	4.03	24

5.3.3 Biological ion exchange resin and gravity-driven filtration experiments

The experimental setup consisted of a BIEX step followed by a GDCM step, as shown in Figure 5-1. The membranes described in section 5.3.1 were used in the GDCM section. In the BIEX section, Purolite® A860, an anionic strong base resin, was packed into a transparent PVC column with a 63 cm height and 1.27 cm (0.5 inches) diameter. Approximately 42 cm of the column was

filled with resin to obtain a total bed volume (BV) of 52 cm^3. The empty-bed contact time (EBCT) was 15 min. The column was continuously fed with influent water at a constant filtration rate of 3.47 mL/min (~ 5L/d, 4 BV/h) for 65 days (6,240 BV). The resin column effluent was characterized for DOC, alkalinity, pH, UV absorbance, anions chromatography, and turbidity analyses daily in the first week of operation and twice per week for the remainder of the study.

To investigate the dynamic mechanism of exchange of different anions and NOM between the influent water and resin, the anion loading on the IEX resin charge was calculated using equation (1), where q (eq/L resin) is the cumulative anion loading on the resin, C_{inlet} and C_{outlet} are the concentrations (eq/L) of each anion in the influent/effluent of the resin column, V_{resin} is the total resin volume in the column (52 mL), Q is the flowrate (5 L/d), $\Delta t = (t_i - t_{i-1})$ is the time between each anion and DOC measurement (d), and i is the number of anion and DOC concentration measurements during the experiment. The loadings were calculated for chloride, sulfate, bicarbonate, and nitrate, which are the major inorganic anions present in the influent water (Liu, Lompe et al. 2020).

$$q = \sum_{i=1}^{24} \frac{\left(Average\,(C_{inlet,\ i},\ C_{inlet,\ i-1}) - Average\,(C_{outlet,\ i},\ C_{outlet,\ i-1})\right) \times Q \times (t_i - t_{i-1})}{V_{resin}} \qquad (4.1)$$

For converting the concentration from mg C/L to eq/L, the charge density of DOC (NOM) was considered to be 10 meq/g C at a pH of 6.5 (Boyer, Singer et al. 2008). Initially, the resin was loaded with chloride ions at a concentration of approximately 0.9 eq/L of resin.

In the GDCM step, the resin column effluent overflowed into a 10 L tank to maintain a constant transmembrane pressure of 90 cm (~ 93 mbar). To prevent algal growth in the system owing to natural light, the raw water tank, resin effluent receiver, and permeate containers were covered with an aluminum foil layer. Membrane holders were constructed from polyethylene equipped with a sight glass on top which allowed visually tracking of the biofilm growth and Optical Coherence Tomography (OCT) imaging without removing membranes from the holders. During the OCT imaging, the membrane holders were removed from the system for approximately 30 min and then installed back in place. The permeate was recovered in a covered container to minimize evaporation and weighed daily using an analytical balance (Ohaus Adventure Pro, Parsippany, NJ, USA). The

temperature of the laboratory air conditioning system was set to 20 °C and the real temperature of air was monitored daily (21.5 °C ± 0.5).

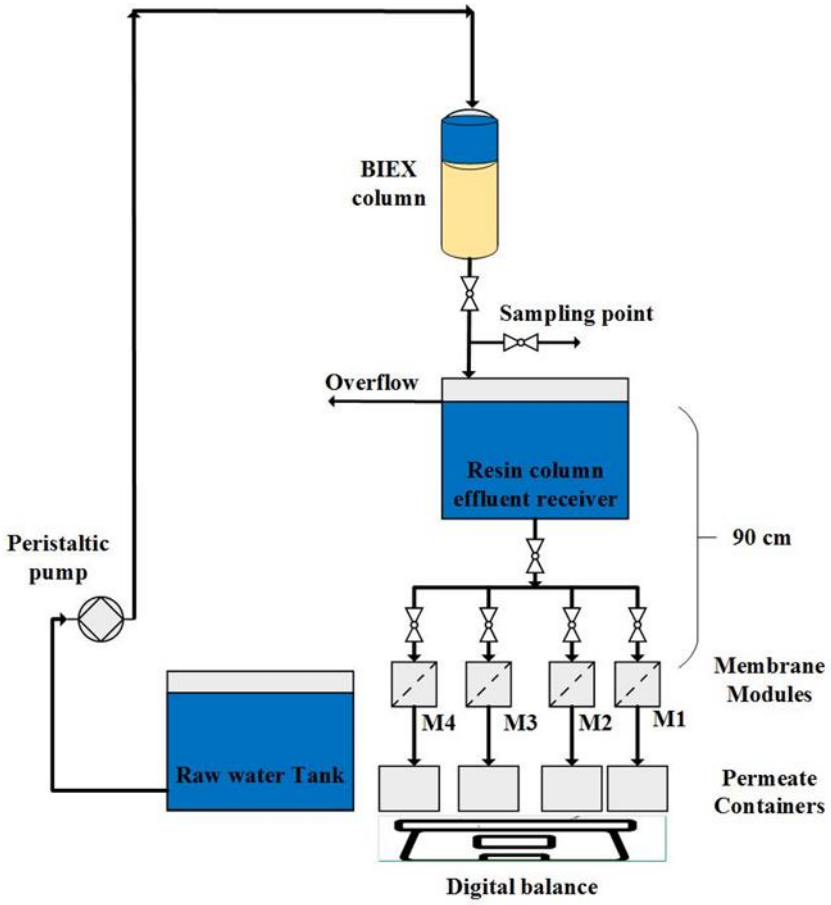

Figure 5-1. Schematic representation of the experimental setup showing two main sections of BIEX and GDCM. Figure adopted from (Rasouli, Maltais-Tariant et al. 2023).

The membrane flux was measured and normalized to 20 °C by transforming the permeate weight to a volume corresponding to 20 °C and divided by the membrane area. Darcy's law was used to calculate membrane fouling resistance. Fouling resistance (biofilm and irreversible resistance) was determined by subtracting the clean membrane resistance from the total fouling resistance (Akhondi, Wu et al. 2015). It is worth noting that the viscosity correction during calculation of fouling resistance in this study was negligible as the working temperature was fairly 20 °C. For experiments in the lower temperature, it is essential to consider such correction.

5.3.4 Analytical methods for water samples

DOC was measured by filtering samples through a prewashed 0.45 µm filter (PES, 0.45-µm, 47 mm, Pall Corporation, Washington, NY, USA) and then using an online TOC analyzer (Sievers M5310C, Trevose, PA, USA). The turbidity of the samples was measured using a TL2300 (Hach, USA) turbidity meter after calibration with standard samples. A UV-visible spectrophotometer (Cary 100 Scan, Varian Inc., USA) was utilized to measure UVA_{254} in a 1-cm quartz cells on filtered samples (0.45 µm filter, PES, 0.45-µm, 47 mm, Pall Corporation, Washington, NY, USA). A pH meter (Accumet AB 15 basic; Fisher Scientific, Waltham, MA, USA) was used to measure the pH after calibration with standard solutions. 50 mL of the sample was titrated using a 0.01 N H_2SO_4 solution to obtain a pH of 4.5, and then 4.2; alkalinity was calculated using Equation 2.

$$Alkalinity\ (\frac{mg}{l}CaCO_3) = \frac{(2B-C)\times 0.01\times 50{,}000}{V} \quad (4.2)$$

Where B is the consumed volume of H_2SO_4 to reach a pH of 4.5, C is the total volume of H_2SO_4 consumed to reach a pH of 4.2, and V is the volume of the sample.

To measure the anions, water samples were filtered through 0.45 µm syringe filters and analyzed using an ion chromatography device (ICS 5000 AS-DP DIONEX, Thermo Scientific, Waltham, MA, USA).

A liquid chromatography organic carbon detection (LC-OCD) device (DOC Labor Huber, Stuttgart, Germany) with three detectors (UV absorbance at 254 nm, organic carbon, and organic nitrogen) was used to quantify the NOM fractions in the duplicate samples of influent water, BIEX column effluent, and membrane permeates (Huber, Balz et al. 2011). The samples were filtered through a 0.45 µm filter before analysis.

5.3.5 Membrane Biofilm characterization

5.3.5.1 Biofilm growth by optical coherence tomography

The OCT device, method of analyzing images, and correlation between real and imaged biofilm thicknesses have been described comprehensively in a previous study (Rasouli, Maltais-Tariant et al. 2023). Briefly, a commercial 1310-nm OCT equipped with a Thorlabs SL1310V1, Newton, USA laser (with resolution of 8.1 µm) and a balanced detector imaging module were used. Three

random areas (~ 7 mm × 4 mm) were selected for each membrane type during each OCT B-scan. Then, using a developed MATLAB code, the raw images were processed and then analyzed using ImageJ software (NIH, USA) to obtain the optical biofilm thickness (Z_f in μm) which was subsequently used to calculate the physical (real) biofilm thickness (Z_i in μm) by considering the refractive index (n_f) equal to 1.333 due to the high water content of the biofilm (Bakke, Kommedal and Kalvenes 2001).

$$Z_i = \frac{Z_f}{n_f} \tag{4.3}$$

Finally, mean physical biofilm thickness ($\overline{Z}$ in μm), absolute (R_a in μm) roughness, and relative ($\overline{R_a}$) roughness coefficient were calculated using equations 4.4 – 4.6.

$$\overline{Z} = \frac{1}{n} \sum_{i=1}^{n} Z_i \tag{4.4}$$

$$R_a = \frac{1}{n} \sum_{i=1}^{n} (\left| Z_i - \overline{Z} \right|) \tag{4.5}$$

$$\overline{R}_a = \frac{1}{n} \sum_{i=1}^{n} (\frac{\left| Z_i - \overline{Z} \right|}{\overline{Z}}) \tag{4.6}$$

5.3.5.2 Biological activity of biofilm

At the end of the overall experiment, six sonication cycles (40 W power and 20 KHz, Cole-Parmer Ultrasonic processor, Canada) were performed on a piece of membrane, and each cycle was performed in 50 mL of phosphate buffered saline to ensure biofilm detachment from the membrane surface. Thereafter, 90 mL of the composite sample was obtained by mixing 15 ml supernatant from each sonicated subsample. A portion of the composite sample was then filtered through a syringe filter (0.2-μm, Quench-Gone, DIS-SFQG-25, LuminUltra, USA) to maintain microorganisms on the filter to measure the extracellular ATP. Intracellular ATP in the biofilm was then quantified by lysing a portion of the composite samples using Ultralyse 7 solution (LuminUltra, USA). Finally, using a luminometer (PhotonMaster, LuminUltra, USA) and sterilized test tubes, the luminescence (RLU/s) was read and then converted to ng ATP/cm^2 using a calibration curve prepared with a standard Ultracheck solution (1000 pg/ml, LuminUltra, USA) (Amini, Papineau et al. 2018).

5.3.5.3 Extracellular polymeric substances in the biofilm

EPS were extracted from the biofilm using sonication and centrifugation approach (Desmond, Best et al. 2018). The sonication step is described in section 5.3.5.2. Next, 45 mL of the composite sample was centrifuged twice (Avanti JXN-26; Beckman Coulter, Indianapolis, IN, USA) at 4000 × g for 20 min. The supernatants were collected for EPS quantification. The total EPS content in the extract was determined using protein (PN) and polysaccharide (PS) measurements (Jiang, Shang et al. 2020). The enhanced test tube protocol for the bicinchoninic acid (BCA) assay (Thermo Fisher Scientific, Waltham, MA, USA) was used for protein quantification, with bovine serum albumin as the standard solution. Polysaccharides were measured using the classic phenol-sulfuric acid method, with glucose as the standard solution (Dubois, Gilles et al. 1956).

5.3.6 Statistical analysis of data

Membranes with the highest mean stabilized flux, the lowest mean permeate turbidity, DOC, and UVA_{254} were identified as control and then the values were compared to the other membranes using an analysis of variance (ANOVA) with Tukey multiple comparison tests in GraphPad Prism® 10.0. 2 software to determine whether the differences were statistically significant at $p = 0.05$.

5.3.7 Gravity-driven ceramic membrane filtration without pre-treatment

To investigate the effect of BIEX pre-treatment on membrane flux, permeate quality, and biofouling layer characteristics formed on the membrane surface, the results of the hybrid BIEX + GDCM process (present study) were compared to those of the GDCM process without pre-treatment as a negative control (from the previous study of the authors, which was conducted using the same types of membranes, influent water, and operating conditions (Rasouli, Maltais-Tariant et al. 2023)).

5.4 Results

5.4.1 Dynamic of ion exchange on the resin

Figure 5-2a shows the dynamics of anion exchange for chloride, sulfate, bicarbonate, nitrate, and DOC (NOM) in relation to the operation time and cumulative waterbed volume. The fresh resin

capacity (on day 0 and 0 BV) was approximately 0.9 eq/L in the chloride form. Prior to 2,000 BV (~ day 21), chloride continuously exchanged with NOM from the influent water leading to a decrease in resin chloride loading from 0.9 to 0 eq/L resin, which causes exhaustion of resin according to the pre-charged anion (chloride). This can be considered an endpoint for primary IEX and initiation of secondary IEX, referred to as the BIEX mode. Meanwhile, the bicarbonate, sulfate, and nitrate concentrations on the resin increased to 0.78, 0.18, and 0.04 eq/L resin at 2,000 BV (day 21), respectively. The resin capacity was therefore completely exhausted from the chloride form by mostly bicarbonate and sulfate.

After 2,000 BV (~ day 21), the resin began exchanging bicarbonate and sulfate with the NOM present in the influent (BIEX mode). Therefore, the NOM loading on the resin continuously increased, whereas the bicarbonate and sulfate concentrations on the resin decreased. At the end of operation (6,240 BV = day 65), the anion loadings of NOM, chloride, bicarbonate, sulfate, and nitrate were 0.36, 0, 0.57, 0.12, and 0 eq/L resin, respectively. In this study, the experiment was not continued until the total resin exhaustion time (secondary exhaustion due to bicarbonate and sulfate). However, if the experiment continues to the exhaust point in the secondary IEX region (0 eq/L resin for bicarbonate and sulfate), the DOC of the resin effluent can reach the same level as that of the influent water (Liu, Papineau et al. 2021). It is worth noting that between 1,920 – 6,240 BV, the total anion loading on the resin was approximately 1.1 eq/L resin which was slightly higher than that of the obtained fresh resin capacity. This could be firstly related to the higher experimental error associated with our bicarbonate measurements compared to the other anions and DOC. Moreover, swelling of polymeric matrix of the resin which is described as the process of penetration of the influent water into a polymer matrix causing a change in the volume due to endosmosis phenomenon (diffusing water molecules from outside to inside the resin matrix). Therefore, a resin with greater swelling will demonstrate an increased rate of anion diffusion into the matrix core, resulting in a reduced reaction time and enhanced chemical conversion efficiency (Metze, Sant et al. 2023). The alkalinity and pH trends of the influent water and BIEX column effluent are shown in

Figure 5-2b. Prior to 2,300 BV (day 24), in the primary IEX region, the BIEX column effluent alkalinity varied in a lower range than that of the influent water, which confirmed the uptake of bicarbonate by the resin. Accordingly, pH showed a lower range (4.3 – 6.5) compared to that of

the influent water. After 2,300 BV (day 24), in the secondary IEX region, the BIEX column effluent alkalinity increased and exceeded that of the influent water, confirming the release of bicarbonate by the resin (bicarbonate exchange with NOM in the influent water).

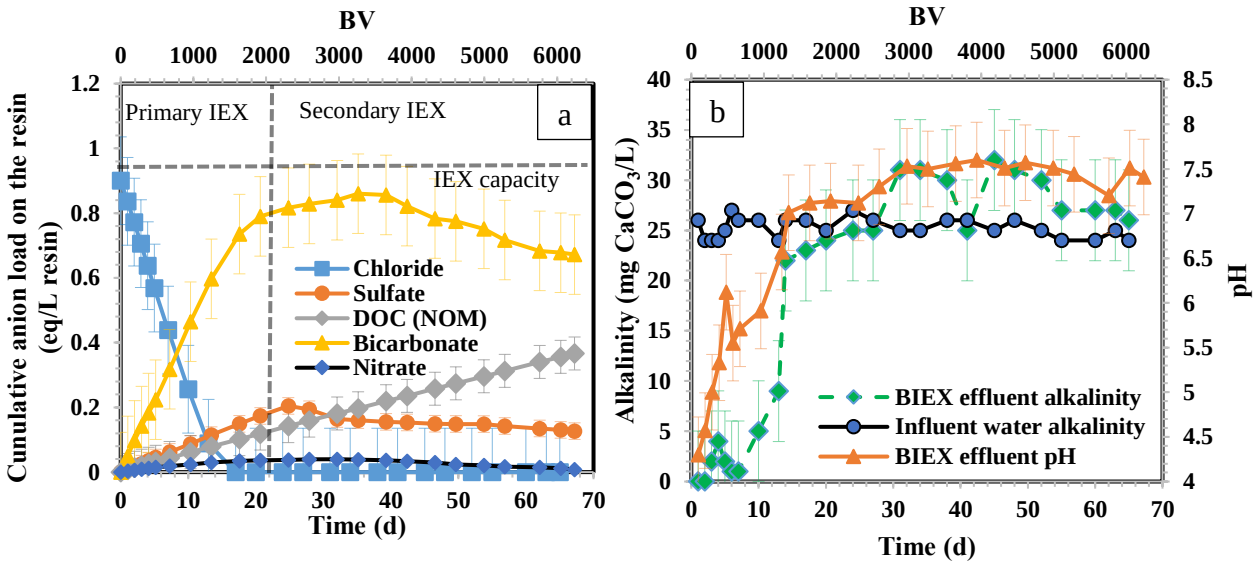

Figure 5-2. Variation of a) chloride, sulfate, DOC, bicarbonate, and nitrate concentration on the resin by operating time and bed volume, b) alkalinity and pH of BIEX column effluent, and alkalinity of influent water during the operation period. Error bars show 95% confidence intervals.

5.4.2 Effluent quality of BIEX column and membranes

5.4.2.1 Dissolved organic carbon removal

The DOC of the BIEX column effluent and membrane permeates are presented in Figure 5-3a. In the primary IEX region (prior to day 24 and 2,300 BV), the DOC concentration was at 0.57 mg C/L (~ 92% removal), then rose progressively and peaked at 2.03 mg C/L (~ 73% removal) at 2,304 BV. Until day 5 (480 BV), the chloride release was stable at 24 – 26 mg/L (Figure 5-3c). The chloride release then dropped markedly from 26 to 5.9 mg/L by day 24 (2,300 BV). Simultaneously, a breakthrough in the DOC of the BIEX column effluent was observed (2.03 mg C/L – 73% removal). This breakthrough in the DOC concentration indicates the end of the primary IEX region (chloride exchange with NOM), where the chloride concentration in the resin is almost completely released (Amini, Papineau et al. 2018, Liu, Lompe et al. 2020, Liu, Papineau et al. 2021). In the secondary IEX region (from 2,300 to 6,240 BV), the DOC concentration of the BIEX

effluent initially decreased because of bicarbonate and sulfate ion exchange with NOM. The concentration then fluctuated until approximately 4,000 BV before increasing again to 2.05 mg C/L (~ 74% removal) at the end of the experiment (day 65, 6,240 BV). In summary, BIEX pre-treatment provides an effective treatment option to remove NOM for 65 d without any regeneration.

The DOC concentration of the membrane permeate followed the general trend of the BIEX effluent. However, incremental DOC removal was achieved in all four membranes investigated. At the beginning of the experiment, membranes M1, M2, and M3 exhibited similar DOC concentrations. However, M3 (50 wt% kaolin and 50 wt% alumina) exhibited the best DOC removal performance at the end of the experiment. At the end of filtration (day 65), the DOC concentrations in the M1, M2, M3, and M4 permeates were 1.82, 1.71, 1.48, and 1.82 mg C/L, respectively, which corresponded to approximately 10%, 16%, 27%, and 10% DOC removal calculated against the DOC of the BIEX column effluent. According to Figure 5-4a, the mean DOC concentration of the M3 permeate (1.23 ± 0.11 mg C/L, mean ± 95% confidence interval) was statistically different compared to that of other membrane types (M1 = 1.45 ± 0.15 mg C/L, mean ± 95% confidence interval, p (M3 – M1) <0.001; M2 = 1.38 ± 0.15 mg C/L, mean ± 95% confidence interval, p (M3 – M2) = 0.003; M4 = 1.38 ± 0.12 mg C/L, mean ± 95% confidence interval, p (M3 – M4) = 0.006). We attribute this performance to the enhanced sorption provided by the higher alumina content of membrane M3. The hybrid BIEX + GDCM (using M3) process removed approximately 81% of DOC from the influent water at the end of the experiment.

5.4.2.2 UVA_{254} reduction

UVA_{254} in the BIEX effluent and membrane permeate are shown in Figure 5-3b. The general trend was the same as that of DOC in both the primary and secondary IEX regions. Regarding the BIEX effluent, in the primary IEX region (prior to 2,300 BV, day 24), UVA_{254} increased continuously as the operation commenced (day 0, 0.003 cm^{-1}) to 960 BV (day 10, 0.023 cm^{-1}) and then fluctuated before peaking at only 0.024 cm^{-1} on day 24 (2,300 BV). Similarly, the breakthrough in UVA_{254} confirmed the end of the primary IEX region (the endpoint of chloride release). Considering the constant UVA_{254} for the influent water (0.25 cm^{-1} ± 0.003, mean ± 95% confidence interval) during the experiment, the UVA_{254} removal at the end of the primary IEX region was approximately 90%. In the secondary IEX region (from days 24 to 65/ 2,300 to 6,240 BV), the removal initially

increased due to the exchange of sulfate and bicarbonate anions with the DOC from the influent water. UVA_{254} stabilized from 2,500 to 4,300 BV (days 27 to 45) before increasing to 0.031 cm^{-1} at the end of the operation (6,240 BV on day 65, with a corresponding removal of ~ 88%).

At the start of the experiment, the UVA_{254} in the membrane permeates was approximately the same as that in the BIEX effluent. The membrane long-term permeation decreased UVA_{254} below that of the BIEX effluent. UVA_{254} were 0.023, 0.024, 0.016, and 0.027 cm^{-1} in the permeates of M1, M2, M3, and M4, respectively, on day 65, corresponding to 25%, 22%, 48%, and 13% UVA_{254} removal compared to the BIEX. As shown in Figure 5-4b, the mean UVA_{254} of M3 (0.012 ± 0.002 cm^{-1}, mean ± 95% confidence interval) was lower than that of the other membranes and BIEX column effluent. However, the obtained value by M3 was not statistically different compared to the other membrane types. In contrast, it was significant when compared to the BIEX column effluent (0.02 ± 0.002 cm^{-1}, mean ± 95% confidence interval, $p < 0.001$). The resins showed good UVA_{254} removal in both the primary and secondary IEX (BIEX mode) regions. At the end of the experiment, the UVA_{254} abatement using the BIEX + GDCM (M3) hybrid process was approximately 94%.

5.4.2.3 Turbidity removal

The effluent turbidities of the BIEX and GDCM sections are shown in Figure 5-3d. Regarding BIEX effluent, the trend started with a sharp decrease from 1.1 NTU to 0.55 NTU at approximately 1,250 BV (day 14). The BIEX effluent turbidity then increased from 0.55 NTU to 0.75 NTU at 3,000 bed volume filtration (day 31) before stabilizing at approximately 0.77 NTU ± 0.06 (mean ± 95% confidence interval) until the end of the experiment.

A similar trend was observed for the membrane permeate turbidity. The turbidity of all permeates started at 0.12 – 0.16 NTU and declined to 0.05, 0.07, 0.08, and 0.06 NTU for M1, M2, M3, and M4, respectively, on day 4. The trend then increased and fluctuated toward a stable value of 0.09 – 0.11 NTU. At the end of experiment (day 65), the permeate turbidities were 0.11, 0.10, 0.09, and 0.11 NTU for M1 – M4, respectively. These performances were consistent with the expected turbidities for low-pressure membrane processes, which are required to provide turbidities lower than 0.15 NTU (USEPA 2001).

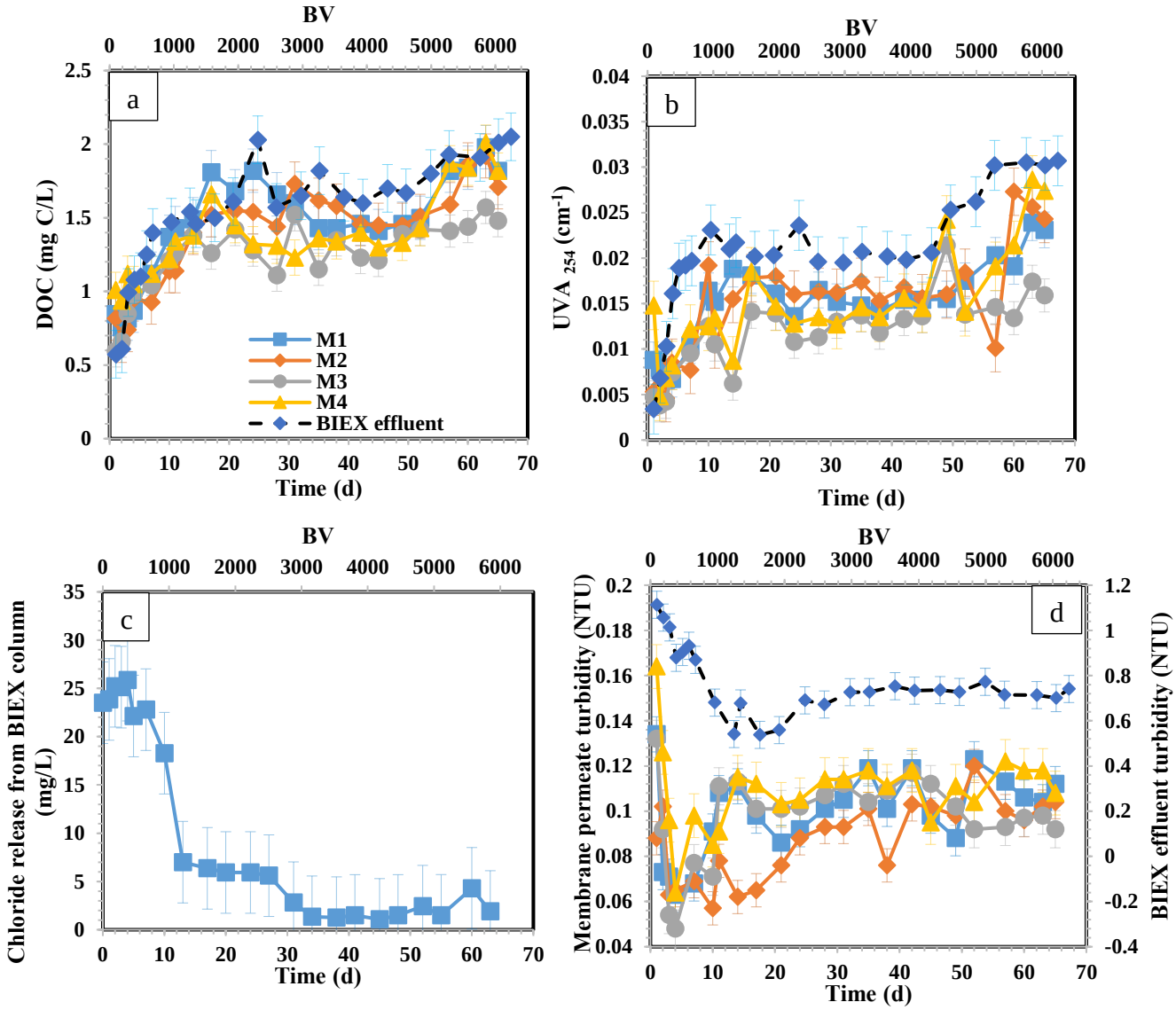

Figure 5-3. The variations of a) DOC, b) UVA_{254}, c) chloride release from the resin, and d) turbidity by M1 (100 wt% kaolin), M2 (75 wt% kaolin, 25 wt% alumina), M3 (50 wt% kaolin, 50 wt% alumina), M4 (0.8 µm commercial), and BIEX column effluent during the operation period. $UVA_{254\,0} = 0.25\ cm^{-1} \pm 0.003$, $DOC_0 = 7.43$ mg C/L ± 0.05, $Turbidity_0 = 2.20$ NTU ± 0.07. Error bars show 95% confidence intervals.

To compare the membrane performance in term of turbidity removal, a bar graph representing the mean of turbidity measurements during the operation was prepared (Figure 5-4c). M2 with 0.09 NTU ± 0.007 turbidity (mean ± 95% confidence interval) was lower than that of the other three

membranes, although the difference was only statistically different when compared to M4 with 0.11 NTU ± 0.008 turbidity (mean ± 95% confidence interval, p = 0.006).

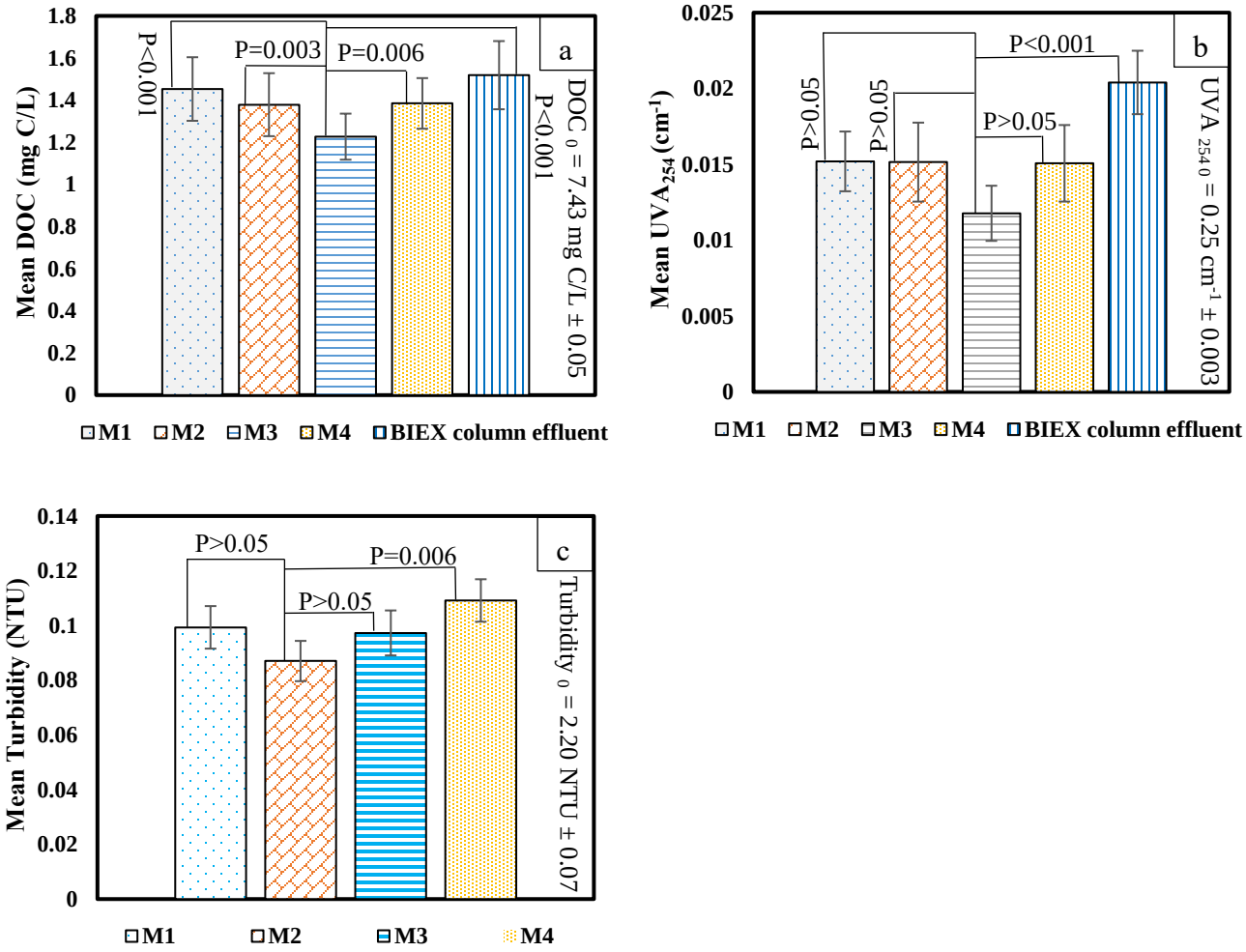

Figure 5-4. a) mean DOC b) mean UVA_{254} c) mean turbidity measurements for M1 (100 wt% kaolin), M2 (75 wt% kaolin, 25 wt% alumina), M3 (50 wt% kaolin, 50 wt% alumina), M4 (0.8 µm commercial), and BIEX column effluent during the operation period (number of samples = 23 in 65 days of operation). The numbers indicate the p-values. Error bars show 95% confidence intervals.

5.4.3 Removal of NOM fractions

The different NOM fractions present in the influent water, BIEX column effluent, and membrane permeates on days 15 (1,440 BV, primary IEX region), 36 (3,456 BV, secondary IEX region), and 65 (6,240 BV, secondary IEX region) of operation are shown in Table 5-3 and Figure B1. As expected, humic substances (HS) were the predominant fraction of NOM in the influent water, with

a concentration of 5,127 µg/L ± 299 (mean ± 95% confidence interval) which were completely removed by the BIEX column and membranes on days 15 and 36. On day 65, the HS concentration reached 293 µg/L ± 72 in the BIEX effluent, which was retained by all membranes. The concentration of biopolymers (BP) was 273 µg/L ± 112 in the influent water. The BIEX effluent showed a slightly higher concentration of BP (295 µg/L ± 40 on day 15); however, the M3 and M4 permeates contained less BP (187 ± 40 and 126 µg/L ± 36 on day 15, respectively). The M3 permeate showed remarkable BP removal at 69 µg/L ± 27 and 79 µg/L ± 12 on days 36 and 65, respectively, compared with the BIEX effluent and influent water. Based on previous results (Rasouli, Maltais-Tariant et al. 2023), the noticeably higher BP removal of M3 was due to BP biodegradation in the biofilm, as evidenced by the higher biological activity and biofilm thickness. The building blocks (BB) concentration in the influent water was 1,074 µg/L ± 270 which was substantially higher than that in the BIEX column effluent (163 µg/L ± 27 on day 15) and membrane permeates (248 – 320 µg/L on day 15). BB concentration was generally slightly higher in the membrane permeate than that of the BIEX column effluent (except for M3 on day 36). The concentration of low molecular weight acids (LMW acids) was slightly higher in the BIEX column effluent and membrane permeates than that of the influent water. The hybrid BIEX + GDCM was used continuously without any cleaning of the foulants; therefore, high-molecular-weight compounds (such as HS) could be retained and accumulated on the membrane surface. Such accumulated biomass can be hydrolyzed to low-molecular-weight compounds by bacteria and living organisms in the biofouling layer (Tang, Ding et al. 2018), which could lead to the higher LMW acids in the BIEX and membrane effluent. Finally, the influent water contained 476 µg/L ± 130 LMW neutrals, which were decreased to approximately 294 ± 36 and 272 µg/L ± 40 on days 15 and 65, respectively, by the BIEX resin. LMW neutrals content of membrane permeates were generally in the same range (250 – 350 µg/L). In summary, the hybrid BIEX + GDCM process removed the total HS because of its high molecular weight (350 – 10,000 g/mol) and charge density (Huber, Balz et al. 2011, Krzeminski, Vogelsang et al. 2019). BB was the second-most-removed NOM fraction in the primary (~ 84%) and secondary IEX regions (day 65, ~77%) in the resin effluent, whereas BP and LMW acids showed no or low removals in either IEX region.

Table 5-3. Fractions of NOM (Mean ± 95% confidence interval) in the influent water, BIEX column effluent, and the membrane permeates.

	Total DOC (µg/L)			**BP (µg/L)**		
	Day 15	Day 36	Day 65	Day 15	Day 36	Day 65
Influent water	7,137 ± 202	-	-	273 ± 112	-	-
BIEX	1,022 ± 144	1,170 ± 193	1,414 ± 386	295 ± 40	346 ± 36	272 ± 148
M1	1,182 ± 27	1,052 ± 67	1,216 ± 292	263 ± 31	229 ± 54	247 ± 36
M2	1,235 ± 18	1,208 ± 22	1,107 ± 126	316 ± 45	296 ± 58	219 ± 85
M3	1,028 ± 72	791 ± 99	940 ± 180	187 ± 40	69 ± 27	79 ± 12
M4	1,525 ± 103	947 ± 148	1,126 ± 220	126 ± 36	128 ± 27	215 ± 54
	HS (µg/L)			**BB (µg/L)**		
	Day 15	Day 36	Day 65	Day 15	Day 36	Day 65
Influent water	5,127 ± 299	-	-	1,074 ± 270	-	-
BIEX	n.d.	n.d.	293 ± 72	163 ± 27	232 ± 24	251 ± 63
M1	n.d.	n.d.	n.d.	320 ± 58	271 ± 85	311 ± 72
M2	n.d.	n.d.	n.d.	279 ± 49	260 ± 54	286 ± 45
M3	n.d.	n.d.	n.d.	248 ± 49	178 ± 72	253 ± 58
M4	n.d.	n.d.	n.d.	289 ± 85	271 ± 54	314 ± 40

n.d = Not detected

Table 5.3. Fractions of NOM (Mean ± 95% confidence interval) in the influent water, BIEX column effluent, and the membrane permeates (cont'd).

	LMW acids (µg/L)			LMW neutrals (µg/L)		
	Day 15	Day 36	Day 65	Day 15	Day 36	Day 65
Influent water	188 ± 117	-	-	476 ± 130	-	-
BIEX	271 ± 40	286 ± 54	327 ± 63	294 ± 36	396 ± 49	272 ± 40
M1	280 ± 94	287 ± 90	367 ± 108	320 ± 31	265 ± 54	291 ± 76
M2	298 ± 49	295 ± 40	340 ± 85	344 ± 58	358 ± 22	263 ± 81
M3	278 ± 18	294 ± 54	333 ± 72	316 ± 45	250 ± 54	276 ± 130
M4	285 ± 67	292 ± 76	335 ± 90	826 ± 220	256 ± 45	262 ± 36

5.4.4 Flux and fouling resistance

The fluxes and fouling resistances of the membranes are shown in Figure 5-5. The fouling dynamics (Figure 5-5a) evolved in two stages. The first stage was a steep flux decline that lasted up to 10 – 30 days, depending on the membrane. The fouling resistance of the membranes is linked to their flux, as shown in Figure 5-5b. The fouling resistance showed a trend reversal similar to that of the flux. During the first 30 days, the flux of M1, M2, M3, and M4 declined from approximately 8.3 LMH to 3.8 LMH, 18.1 LMH to 5.1 LMH, 60 LMH to 5.4 LMH, and 8.6 LMH to 1.8 LMH, respectively. Subsequently, the fluxes stabilized such that at the end of the experiment (day 65), M1, M2, M3, and M4 fluxes were 4.1, 4.5, 5.9, and 2.2 LMH, respectively. The highest mean stabilized flux (day 30 – 65) was obtained for M3 (50 wt% kaolin + 50 wt% alumina, the membrane with enhanced adsorption capacity) which was significant compared to the other three membranes (5.65 LMH ± 0.07, mean ± 95% confidence interval, $p<0.001$, Figure 5-5c). This is related to the larger mean pore size of M3 compared to those of the other three membranes (0.98 µm). Moreover, according to (Derlon, Mimoso et al. 2014, Akhondi, Wu et al. 2015), presence of a biofilm on the membrane surface can improve the permeate flux, as in 5.4.5.1 and 5.4.5.2. In these studies, flux development pattern was reported because of the combined effect of an increased biofilm thickness in dead – end GDM filtration and presence of bacterial activity and predation in

the biofouling layer which are capable of altering biofilm morphology resulting in a more heterogeneous structure. The biofilm on M3 showed the highest mean biofilm thickness and biological activity. These results are consistent with previous findings, in which M3 showed the best stabilized flux in the GDCM process without pre-treatment (Rasouli, Maltais-Tariant et al. 2023). Therefore, a higher flux was achievable without compromising turbidity and NOM removal.

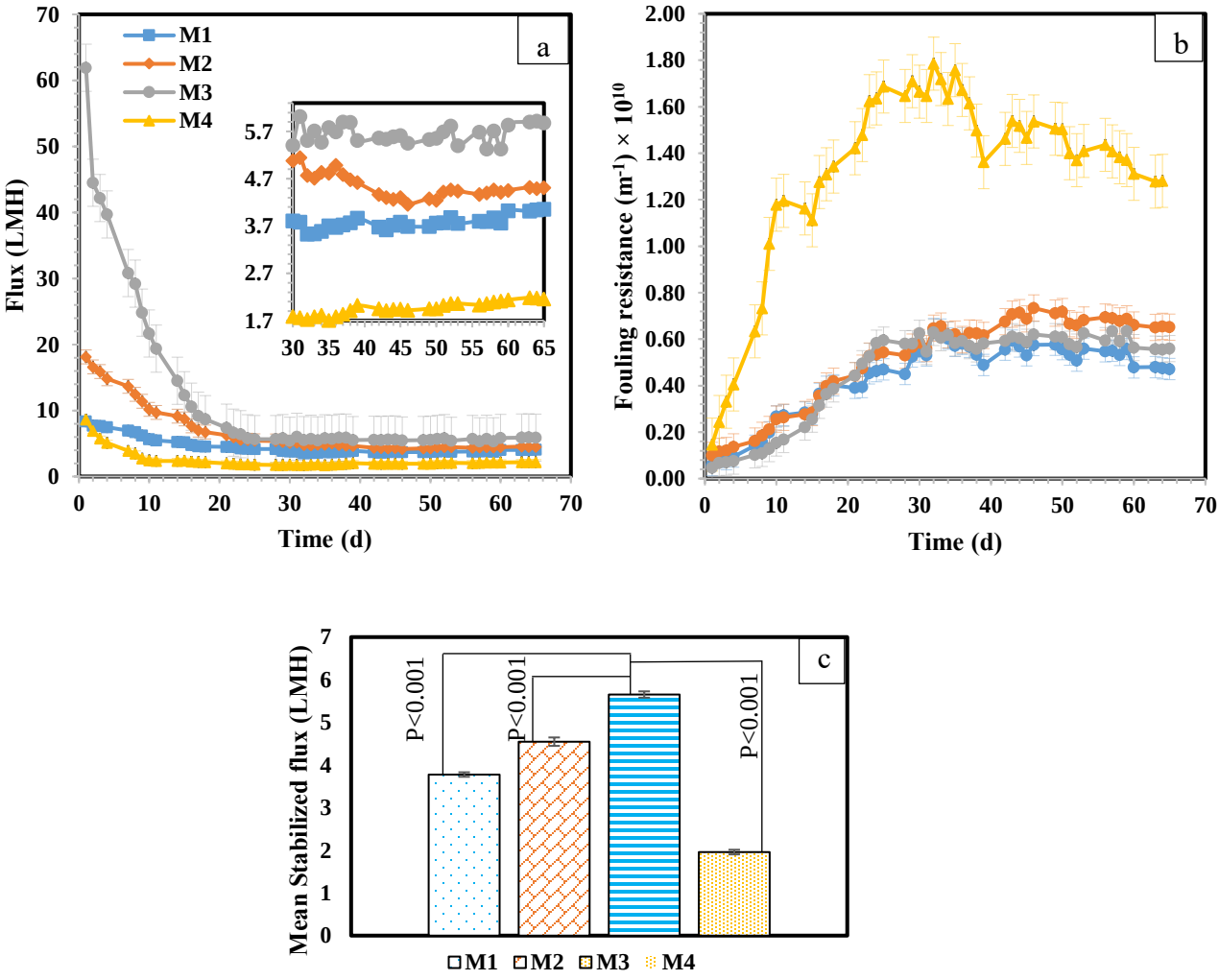

Figure 5-5. a) Flux – time, b) fouling resistance – time, and c) Statistical compare of mean stabilized flux data from day 30 (flux stabilization day) to day 65 for M1 (100 wt% kaolin), M2 (75 wt% kaolin, 25 wt% alumina), M3 (50 wt% kaolin, 50 wt% alumina), M4 (0.8 µm commercial). The numbers indicate the p-values. Error bars show 95% confidence intervals.

5.4.5 Biofouling layer characterization

5.4.5.1 Concentration of active microorganisms and extracellular polymeric substances in the biofouling layer

To quantify the active microorganisms present in the membrane biofilm, ATP concentrations were measured on the surface of each membrane type (Figure 5-6a). Significant differences ($p<0.001$) in ATP concentration (5.0 – 40 ng/cm^2) were observed between membrane types. The highest and lowest ATP concentrations were observed for membranes M3 (40.26 ng/cm^2 ± 2.57, mean ± 95% confidence interval, $p<0.001$) and M1 (5.87 ng/cm^2 ± 0.23, mean ± 95% confidence interval), which also had the highest and lowest DOC removal rates, respectively. Membrane M3 was made of 50% (by weight) alumina, while M1 was 100% kaolin. Given that the M3 membrane has a higher porosity than M1, the increased performance of the M3 membrane lies in the synergy of alumina with biofilm growth. We have previously reported that the use of alumina increases NOM sorption, which appears to be beneficial to biofilm activity, as evidenced by the higher ATP concentrations (Rasouli, Maltais-Tariant et al. 2023). A wide range of ATP concentrations have been reported in the literature for the bioactivity of the biofilm accumulated on filtration media working under gravity-driven mode. For example, rainwater filtration for recycling purpose by a GDM system showed approximately 80 mmol ATP/m^2 (~ 40 × 10^5 ng/cm^2) (Ding, Wang et al. 2017) which is far higher than the data obtained in this study while gravity-driven ultrafiltration of different surface water types and diluted wastewater showed a constant 22 ng/cm^2 of ATP in the biofouling layer (Peter-Varbanets, Hammes et al. 2010) which is in the range of the ATP obtained in this study. Moreover, biomass accumulated on the submerged GDM reactor during filtration of secondary wastewater effluent with two different concentrations showed ~ 4 – 6 ng ATP/cm^2 according to concentration of feed solution (Wang, Fortunato et al. 2017).

EPS concentrations (PN and PS) in the biofouling layers of the synthetic and commercial membranes are shown in Figure 5-6b. Smaller differences in EPS/protein content were observed in cakes recovered from the four membranes compared to ATP. However, membrane M3 had the highest PS and protein content (1.55 mg/cm^2 ± 0.13 of total EPS concentration, mean ± 95% confidence interval) which was statistically different compared to other membrane types, except protein concentration in M2. The membrane with the enhanced adsorption capacity (M3 = 50 wt%

kaolin + 50 wt% alumina) showed the highest biofilm activity, EPS concentration, BP rejection, and maximum biofilm thickness among the tested membranes. Likewise, EPS showed a wide range of values in previous research. In a previous study (Stoquart, Barbeau et al. 2013), ATP and EPS concentrations were measured in biofilms formed on a biological activated carbon (BAC) filter during river water treatment using hybrid activated carbon and membrane filtration (UF). ATP concentration of BAC filter reported as 58.9 ng ATP/g dry BAC. PN and PS showed a concentration of 8.1 and 5.1 mg/g dry BAC, respectively. ATP showed approximately the same range, whereas the EPS concentration was higher than that reported in this study. In another study (Ding, Wang et al. 2017), 2.48 g/m^2 (0.248 mg/cm^2) of EPS during rainwater filtration in a GDM process was reported while lake water filtration using a submerged GDM system showed 200 – 400 g/m^2 (20 – 40 mg/cm^2) of EPS (Shao, Shi et al. 2019).

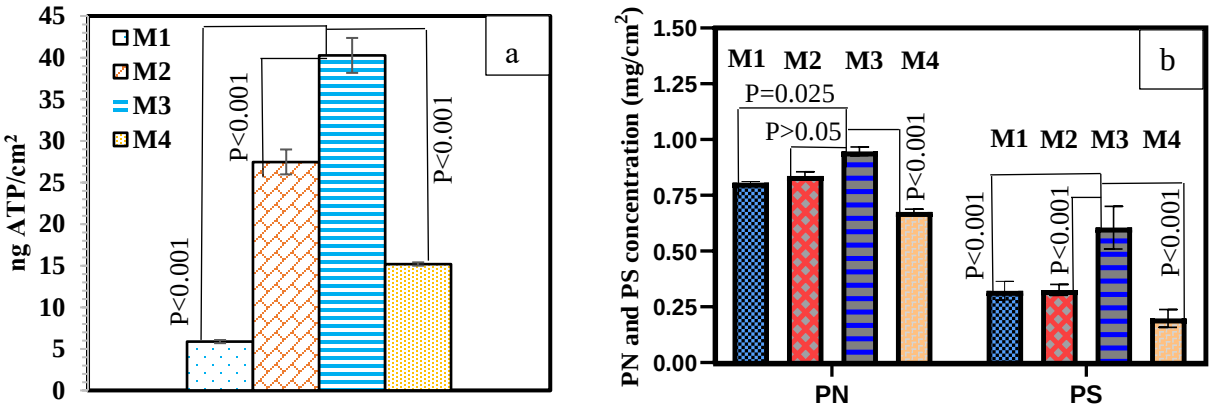

Figure 5-6. a) ATP concentration (active microorganisms), and b) EPS (PN=Proteins and PS=Polysaccharides) concentration in the biofilm of M1 (100 wt% kaolin), M2 (75 wt% kaolin, 25 wt% alumina), M3 (50 wt% kaolin, 50 wt% alumina) and M4 (0.8 µm commercial). Error bars show 95% confidence intervals.

5.4.5.2 Physical characteristics of the biofilm and cake layer formed on the membrane surface

To monitor biofilm growth, OCT images were captured after 10, 25, 38, 52, and 65 days of operation (Figure B2 presents the images). Although the observed layer is a mixture of microorganisms as well as organic and inorganic foulants, we will refer to it as biofilm. Figure B3 shows the progression of biofilm on the membrane surface from days 10 to 52. Figure 5-7 presents the mean biofilm thickness, absolute biofilm roughness, and relative biofilm roughness coefficient

calculated from these images. Mean biofilm thickness increases linearly with time and reaches approximately 200-230 µm after 52 days. The final sampling campaign on day 65 showed a decline in cake accumulation thickness. This has been reported previously in (Akhondi, Wu et al. 2015, Wu, Hochstrasser et al. 2016) and can be attributed to the upper layer detachment of the biofilm (aging biofilm) from the membrane surface because of the shear stress exerted by the transmembrane pressure, water pushing force, and interaction between particles.

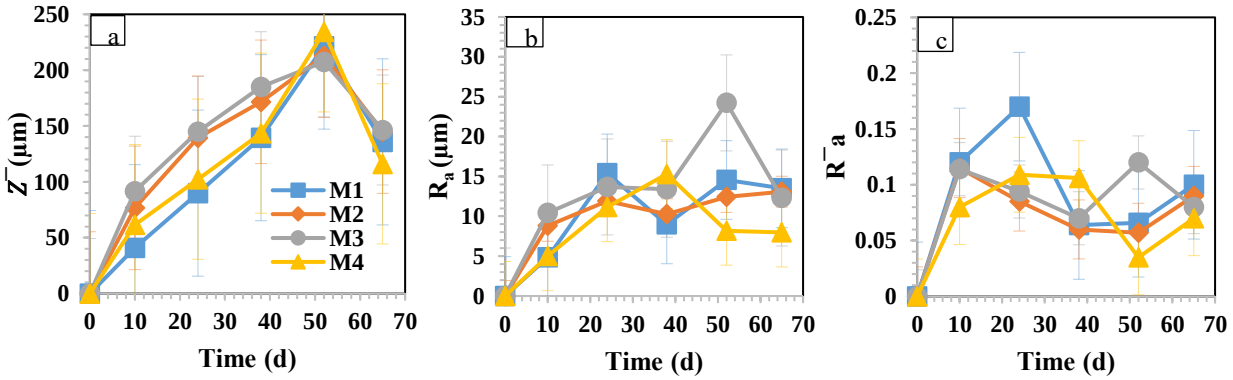

Figure 5-7. a) Mean biofilm thickness ($\bar{Z}$, µm), b) Absolute biofilm roughness (Ra, µm), and c) Relative biofilm roughness coefficient ($\bar{R}$a) during the filtration time for M1 (100 wt% kaolin), M2 (75 wt% kaolin, 25 wt% alumina), M3 (50 wt% kaolin, 50 wt% alumina) and M4 (0.8 µm commercial). The error bars show 95% confidence intervals.

The mean biofilm thicknesses on day 65 were 136, 145, 146, and 116 µm for M1, M2, M3, and M4, respectively. The maximum mean biofilm thickness obtained in this study was higher than the ones reported by Akhondi et al. 2015 (Akhondi, Wu et al. 2015) (max mean thickness ~ 80 µm) during seawater pretreatment by a UF membrane in gravity-driven mode. However, the mean biofilm thickness in the present study is in the range of the thickness obtained during treating primary wastewater (Fortunato, Ranieri et al. 2020). The higher thickness and less bioactivity associated to the biofouling layer formed on the membranes surface in this study, could be attributed to a decreased ratio of viable microorganisms (alive organic cells in the biofilm) to total accumulated biomass (alive + dead organic cells) in the biofilm layer. Young and thin biofilm layer containing higher alive organic cells has been shown to improve the permeate quality due to the degradation of organic fractions such as biopolymers, while aged biofilm comprising less alive organic cells could deteriorate the permeate quality by hydrolysis of organics into smaller-size materials that can permeate through the membrane (Derlon, Mimoso et al. 2014).

As shown in Figure 5-7 b and c, the absolute roughness and relative roughness coefficient exhibit fluctuating trends. Absolute roughness of the biofilm was 4.85, 8.8, 10.42, and 4.99 µm in the case of M1 to M4, respectively. After relatively high fluctuations, it reached approximately 13 µm for the synthetic membranes (M1, M2, and M3) and 8 µm for M4 by the end of filtration. An opposite trend was observed for the relative roughness coefficient of the synthetic membranes. Relative roughness coefficient was calculated approximately to be 0.11 on day 10 for M1, M2, and M3, and then it varied from 0.07 to 0.10 toward the end of the filtration. According to the results, the absolute roughness and relative roughness coefficient of the biofilms in the first and last imaging events (days 10 and 65) were approximately equal, despite fluctuations occurring in the middle of the operation.

5.5 Discussions

5.5.1 Impact of BIEX pre-treatment on the flux and permeate quality of the membrane section

To improve the membrane permeate quality and flux, the GDCM process was integrated with resin pre-treatment operated without regeneration to achieve secondary IEX (BIEX mode). In the hybrid process, the BIEX column mainly removed NOM, and the GDCM retained the turbidity of the influent water while providing additional NOM retention. The BIEX column removed approximately 74% of DOC based on data from day 65, and the membranes retained 10% – 27% of the remaining DOC, which was mainly in the form of HS and BB. DOC removal improves mainly because of primary and secondary IEX and biodegradation (Amini, Papineau et al. 2018). Regarding turbidity data of day 65, BIEX resin decreased the turbidity of influent water from 2.20 NTU to 0.77 NTU, and it was further decreased to 0.09 – 0.11 NTU using different membrane types. Compared to our previous study using the same membranes and influent water in the GDCM process without BIEX pre-treatment (negative control) (Rasouli, Maltais-Tariant et al. 2023), the permeate quality of the hybrid process increased markedly. In GDCM without pre-treatment, the best DOC removal performance (after the initial and temporary high DOC removal periods), M3, was approximately 6% (influent water DOC = 6.51 mg C/L. M3 permeate DOC = 6.12 mg C/L, Figure B4a, Figure 5-8). Turbidity removal in the hybrid process also improved compared to that in GDCM without pre-treatment. Higher turbidity values were observed in the initial filtration days

in the process without pre-treatment. Furthermore, at the end of the filtration, the stable turbidity of the GDCM process without BIEX pre-treatment was approximately 0.25 NTU, which is approximately twice that of the hybrid process (Figure B4b, Figure 5-8). Biologically aerated filters (filled with either granular activated carbon or shredded hollow fiber membranes) combined with PVDF hollow fiber ultrafiltration membranes were developed to treat polluted reservoir water (Wu, Chen et al. 2023). Under optimal conditions, DOC removal and effluent turbidity were approximately 80% and 1 – 3 NTU, respectively, after biologically aerated filtration. Subsequent ultrafiltration membranes provided permeate DOC reduction of 7% and final turbidity of 0.3 NTU compared to that of the effluent of biological filtration. The results of organic removal and turbidity in the present study are fairly similar to the aforementioned research in the pre-treatment sections (BIEX for the present study and biologically aerated filters for the published study). However, in the membrane section, the present study showed a better performance in NOM and turbidity removal.

Regarding the membrane fluxes, the BIEX resin improved the stabilized fluxes approximately two folds compared with the GDCM process without pre-treatment. The membrane stabilized fluxes were reported at 2.5 – 3.0 LMH in GDCM without BIEX pre-treatment, while it was increased to 3.8 – 5.7 LMH using the hybrid process. Notably, flux stabilization occurred approximately on day 24 of filtration in GDCM-only, whereas, in the BIEX + GDCM process, it shifted to day 30, a week longer (Figure B4c, Figure 5-8). This could be related to the effective removal of high molecular weight NOM, such as HS, from the influent water and the reduced fouling effect in the subsequent membrane sections.

The present study results showed that BIEX resin can be a robust, inexpensive, and easy-to-operate pre-treatment method for enhancing the flux in the subsequent membrane section and for increasing the quality of the produced permeate.

5.5.2 Effect of BIEX pre-treatment on the characteristics of biofilm of the membranes

The previous study of the authors (Rasouli, Maltais-Tariant et al. 2023) using the same membranes, influent water and condition in GDCM process without a pre-treatment (negative control) showed a higher biofilm thickness (Maximum biofilm thickness: M1 = 371 µm, M2 = 224 µm, M3 = 315

µm) compared to that in the BIEX + GDCM hybrid process (Maximum biofilm thickness: M1 = 221 µm, M2 = 212 µm, M3 = 207 µm). In the hybrid process, the maximum absolute roughness (R_a) and relative roughness coefficient ($\overline{R_a}$) were markedly lower than those in the GDCM process without BIEX pre-treatment. Maximum R_a and $\overline{R_a}$ in GDCM-only were 104 µm and 0.28, 70 µm and 0.31, 173 µm and 0.55 for M1, M2 and M3, respectively. In BIEX + GDCM process, according to section 5.4.5.2, maximum Ra and $\overline{R_a}$ of 15.4 µm and 0.17, 13.1 µm and 0.12, 12.3 µm and 0.08, 7.97 µm and 0.07 for M1, M2, M3, and M4 were obtained, respectively. In the hybrid process, BIEX resin pre-treatment eliminated NOM from influent water via two mechanisms: ion exchange and biodegradation. Biomass accumulation and biodegradation in BIEX columns have been reported to remove approximately 50% of the NOM and DOC (Catalán, Casas-Ruiz et al. 2017, Amini, Papineau et al. 2018). Nevertheless, IEX is the main NOM removal mechanism (Liu, Solliec et al. 2022, Zimmermann, Li and Mohseni 2022).

In the GDCM process without BIEX pre-treatment, the biological activities of the M1, M2, and M3 biofilms were approximately 2.4, 11.2, and 46 ng ATP/cm^2, respectively (Figure 5-8, Figure B5), whereas, in the BIEX + GDCM hybrid process, the biological activities were roughly 5.8, 28, and 40 ng ATP/cm^2 (Figure 5-8). According to these results, after BIEX pre-treatment, the biological activity of the M3 biofilm in the hybrid process decreased marginally compared to the GDCM-only process, whereas the biological activities of the M1 and M2 biofilms in the hybrid process were more than two times higher than that of the GDCM process without pre-treatment. A lower ATP concentration was expected in the biofilm of all membranes subjected to BIEX pre-treatment because of the lower influent NOM. However, an opposite trend was observed. We suspect that the BIEX mostly removed the poorly biodegradable fractions of NOM (i.e., HS). LMW acids contain biodegradable organic matter. BIEX pre-treatment increased this fraction compared to raw water, which may explain the higher observed biofilm activity on membranes treated with BIEX-pretreated water (Krzeminski, Vogelsang et al. 2019).

5.5.3 Relevance to the industry

The hybrid BIEX + GDCM process, which is intended to be used in the decentralized small water treatment systems, showed high performance in terms of stabilized flux (Max flux ~ 5.7 LMH) and permeate quality (effluent turbidity ~ 0.1 NTU, max DOC removal ~ 81%, effluent DOC < 2.0 mg

C/L) in the long-term operation during treatment of a colored, turbid, and high NOM content river water. Comparing DOC removal, BIEX previously showed (Amini, Papineau et al. 2018) a significant higher performance (~ 62% of DOC removal in warm water condition) compared with GAC and BAC (granular activated carbon under biological mode, ~ 7% of DOC removal in long-term) when treating the same source water as in the present study. Although IEX (ion exchange resin under frequent regeneration) revealed better DOC removal performance (~ 80% DOC removal) than that of BIEX, it cannot be considered as an interesting option in the decentralized systems, because of the chemical use, produced spent brine, and enhanced maintenance requirements, which are undesired characteristics.

The resin manufacturers generally recommend the regeneration after every 48 – 72 h of operation to maintain the resin capacity and control biomass growth on the resin (Amini, Papineau et al. 2018). In this study however, the regeneration process was not performed on the resin during the operation time to promote the BIEX mechanism (secondary IEX) during NOM removal. If a traditional regeneration process was performed on the system, assuming a 72-h regeneration frequency (during 65 days / 6,240 BV of total operation) with a 100 g/L dose of NaCl and 3 BV of the brine consumption during each regeneration process (according to the supplier), 1.06 kg of NaCl per each m^3 of treated water would be required while 10.58 m^3 of spent brine per 1000 m^3 of treated water would be produced. The calculated amount of salt consumption and produced brine (if regeneration was performed) is high enough to increase the operating expense markedly for decentralized applications. In this context, the proposed BIEX + GDCM process represents an opportunity. Likewise, membrane manufacturers advise regular backwash/chemical cleaning to avoid biomass fouling on the membrane surface, while in this GDCM process, the backwash and chemical cleaning are not performed regularly. In the GDCM process without pretreatment (Rasouli, Maltais-Tariant et al. 2023), M3 (50 wt% kaolin + 50 wt% alumina) with a high mean biofilm thickness (315 µm) and microorganism activity (46 ng ATP/cm^2) achieved the highest stabilized flux (~ 3 LMH). Promoting biofilm layer on the membrane surface has previously been shown to improve the organic removal by approximately 80% (Derlon, Mimoso et al. 2014) and affect the stabilized flux positively (Akhondi, Wu et al. 2015). Overall, operating resin and membrane processes in a biologically enhanced mode would lead to a substantial reduction in

operating expenses while increasing the permeate quality, flux, and sustainability toward the decentralized water treatment systems.

Some challenges are associated with the proposed hybrid process when applies to the practical application in the decentralized water treatment systems. Schmutzdecke phenomenon in which a dense and difficult-to-break-up biological layer forms on the upper side of the column, considered as one of the issues in BIEX resin section. Air injection has been proposed to break this layer. Furthermore, a DOC breakthrough at the end of the primary IEX for a short period of time, could be considered as another issue (Amini, Papineau et al. 2018). In the GDCM section, a low stabilized flux and decreased NOM removal could be alleviated by selecting BIEX resin as a pretreatment process as shown in this study.

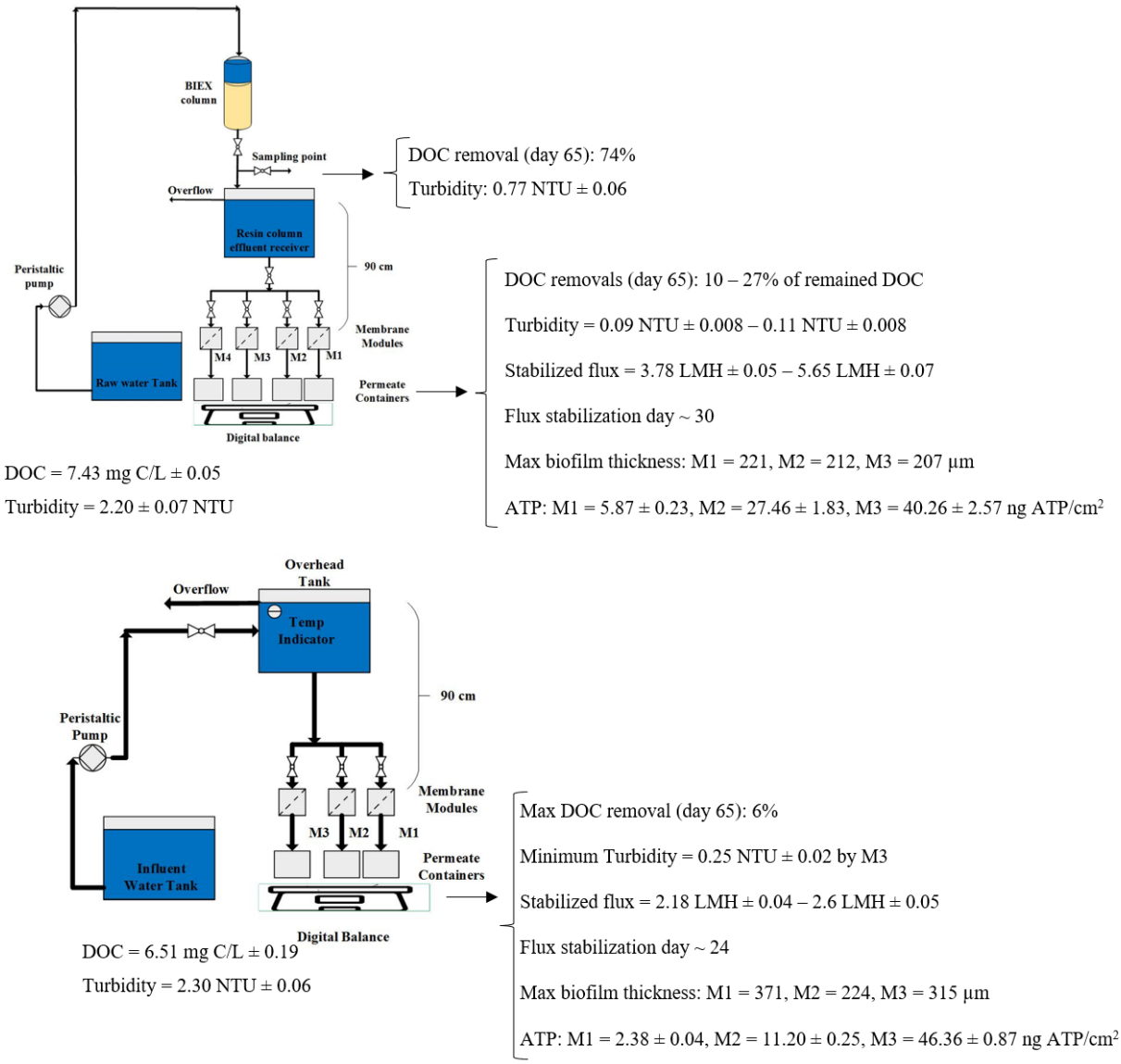

Figure 5-8. Impact of BIEX pre-treatment on the flux, permeate quality and biofilm properties of the membranes. Figure adopted from *(Rasouli, Maltais-Tariant et al. 2023)*. Values show mean ± 95% confidence intervals.

5.6 Conclusions

In this study, a hybrid BIEX + GDCM process was investigated to treat colored and turbid river water for drinking water applications. The performance of BIEX filtration as a pre-treatment stage for the subsequent GDCM process was investigated in terms of water effluent quality, membrane

flux, and physicochemical characterization of the biofilm formed on the membrane surface. The following results were obtained:

- NOM removal was primarily achieved by BIEX pre-treatment. Sustained (> 74% during 65 days = 6,240 BV) NOM removal (mostly HS and BB) was achieved during BIEX pre-treatment without any regeneration.
- Of the four ceramic membranes tested, membrane M3, made of 50% kaolin and 50% alumina, provided the best performance, with an additional 27% removal of DOC at the end of the operation. This is due to the effective removal of the HS fraction. Compared to GDCM without pre-treatment (maximum DOC removal ~ 6%), DOC removal by the membranes increased markedly using the hybrid process (maximum DOC removal ~ 27%).
- Membrane M3 (which had the highest clean water flux) provided an equivalent turbidity (approximately 0.09 NTU) and a higher stabilized flux (approximately 5.7 LMH) than the other three membranes. Notably, M3 membrane exhibited the best DOC removal performance with the highest stabilized flux.
- Mean stabilized fluxes of membranes with BIEX pre-treatment were roughly 3.8 – 5.7 LMH, approximately two-fold higher compared to that of GDCM without a BIEX pre-treatment.
- The physical characteristics of the biofilm on the membranes, such as mean thickness and roughness, were considerably lower in the hybrid process than in the GDCM without the pre-treatment. However, the ATP concentration was higher in the membrane biofilm that received BIEX-pretreated water, possibly due to the biodegradation of the weakly biodegradable fraction of NOM (HS and BB) by BIEX.

5.7 Credit authorship contribution statement

Yaser Rasouli: Conceptualization, Methodology, Formal analysis, Writing original draft, Writing – review & editing. Raphaël Maltais-Tariant: Writing – review & editing. Benoit Barbeau: Supervision, Writing – review & editing, Funding acquisition. Sigrid Peldszus: Writing – review & editing. Caroline Boudoux: Funding acquisition. Dominique Claveau-Mallet: Supervision, Project administration, Writing – review & editing, Funding acquisition.

5.8 Declaration of competing interest

The authors declare that they have no competing financial interests or personal relationships that may have influenced the work reported in this study.

5.9 Acknowledgements

The authors would like to thank to the Polytechnique Montreal technicians and research professionals, Gabriel St-Jean, Julie Philibert, Mélanie Bolduc, Tetiana Elyart, Jacinthe Mailly, and Yves Fontaine for their help in preparing the hybrid BIEX + GDCM setup and influent water and their technical support during this project. We would like to thank Noshin Reza from University of Waterloo for running the LC-OCD samples. This project was funded by the Canada Research Chair for Decentralized and Small-Scale Water Treatment (file number 950-232871).

CHAPTER 6 Article 3: Impact of Cleaning on Membrane Performance during Surface Water Treatment: A Hybrid Process with Biological Ion Exchange and Gravity-Driven Membranes

Yaser Rasouli, Benoit Barbeau, Raphaël Maltais-Tariant, Caroline Boudoux, Dominique Claveau-Mallet. Impact of Cleaning on Membrane Performance during Surface Water Treatment: *A Hybrid Process with Biological Ion Exchange and Gravity-Driven Membranes* (publication date: Jan 25, 2024). Membranes 2024, 14, 33. https://doi.org/10.3390/membranes14020033.

6.1 Abstract

In this study, the hybrid biological ion exchange (BIEX) resin and gravity-driven membrane (GDM) process was employed for the treatment of coloured and turbid river water. The primary objective was to investigate the impact of both physical and chemical cleaning methods on ceramic and polymeric membranes in terms of their stabilised flux, flux recovery after physical/chemical cleaning, and permeate quality. To address these objectives, two types of MF and UF membranes were utilised (M1 = polymeric MF, M2 = polymeric UF, M3 = ceramic UF, and M4 = lab-made ceramic MF). Throughout the extended operation, the resin functioned initially in the primary ion exchange (IEX) region (NOM displacement with pre-charged chloride) and progressed to a secondary IEX stage (NOM displacement with bicarbonate and sulphate), while membrane flux remained stable. Subsequently, physical cleaning involved air/water backwash with two different flows and pressures, and chemical cleaning utilised NaOH at concentrations of 20 and 40 mM, as well as NaOCl at concentrations of 250 and 500 mg Cl_2/L. These processes were carried out to assess flux recovery and identify fouling reversibility. The results indicate an endpoint of 1728 bed volumes (BVs) for the primary IEX region, while the secondary IEX continued up to 6528 BV. At the end of the operation, DOC and UVA_{254} removal in the effluent of the BIEX columns were 68% and 81%, respectively, compared to influent water. This was followed by 30% and 57% DOC and UVA_{254} removal using M4 (ceramic MF). The stabilised flux remained approximately 3.8–5.2 LMH both before and after the cleaning process, suggesting that membrane materials do not play a pivotal role. The mean stabilised flux of polymeric membranes increased after cleaning, whereas that of the ceramics decreased. Enhanced air–water backwash flow and pressure resulted in an increased removal of hydraulic reversible fouling, which was identified as the dominant fouling

type. Ceramic membranes exhibited a higher removal of reversible hydraulic fouling than polymeric membranes. Chemical cleaning had a low impact on flux recovery; therefore, we recommend solely employing physical cleaning.

Keywords: Hydraulic reversible fouling; flux recovery; Permeate quality; Membrane cleaning; Polymeric membranes; Ceramic membranes.

6.2 Introduction

In various parts of the world, rural populations face challenges in accessing simple, cost-effective, and locally produced water treatment technologies. Unfortunately, research on water supply options for rural and remote regions is often overshadowed by the issues encountered in urban areas. Advanced and centralised technologies designed for large-scale operations and skilled personnel cannot be directly applied to smaller systems due to factors such as energy efficiency, robustness, resilience, and staffing requirements, all of which justify the exploration of alternative solutions (Singh, Kazmi and Starkl 2014, Omarova, Tussupova et al. 2019, Lourenço and Nunes 2020). In this context, passive decentralised water treatment systems emerge as an appealing option. They have been developed to reduce maintenance requirements, diminish the reliance on trained operators, simplify design, and allow for potential off-grid operations (Capodaglio, Callegari et al. 2017, Maniam, Zakaria et al. 2022, Lee, Risold et al. 2023).

We recently proposed a passive decentralised treatment option comprising the biological ion exchange (BIEX) process combined with gravity-driven membrane filtration (GDM). This system demonstrated the ability to operate for over 60 days without backwash or regeneration, producing potable water using turbid (5–10 NTU) and coloured (TOC ≈ 7 mg C/L) river water (Rasouli, Maltais-Tariant et al. 2023). The BIEX filtration process involves the operation of an anionic resin with sporadic regeneration to deplete pre-loaded anions (typically chloride). It operates in the secondary ion exchange (IEX) region, taking advantage of the self-regeneration induced by naturally occurring anions in the influent water, such as bicarbonate and/or sulphate anions (Edgar and Boyer 2022, Lee, Noh et al. 2023). These are displaced by NOM from the influent water. Delaying the regeneration stage reduces secondary pollution from spent brine, the transport of regeneration chemicals, maintenance, and costs (Green, Mels and Lahav 1996, McAdam and Judd 2008). However, the BIEX is not a robust treatment for particulate matter. The main challenges

associated with the BIEX filtration process stem from the emergence of a Schmutzdecke phenomenon. This involves the formation of a difficult-to-break-up biological layer on the upper surface of the column, which may be effectively disrupted through the introduction of air injection. A DOC breakthrough during a transition from primary IEX to secondary IEX could also be considered as another issue in BIEX filtration.

GDM filtration, whether utilising ultrafiltration or microfiltration, is considered an efficient removal process. This method necessitates a simple and compact installation, fewer ancillary equipment, lower energy consumption, and operators with lower skill levels (Pronk, Ding et al. 2019, Truttmann, Su et al. 2020, Stoffel, Derlon et al. 2023). Nevertheless, the primary challenges associated with the GDM process, such as achieving a low stabilised flux and a reduction in NOM removal, can be mitigated by opting for BIEX resin as a pre-treatment method. Therefore, BIEX resin pretreatment followed by GDM filtration appears to be a competitive process for eliminating turbidity, colour, and NOM in decentralised surface water treatment applications. For such applications, selecting the right membrane type is essential, maximising productivity and permeate water quality. Comparing the permeability of polymeric and ceramic membranes, it was observed that, for a similar MWCO, polymeric membranes often exhibit higher clean water permeability than ceramic membranes due to the module design (hollow fibre vs. monolithic for ceramics) (Moulin, Bourbigot et al. 1991, Bodzek and Konieczny 1998, Klomfas and Konieczny 2004, Kotobuki, Gu et al. 2021). However, opposite results can be found in the literature. For example, in a study published by Kook et al. (Kook and Park 2022), 0.1- µm ceramic Al_2O_3 membrane (2440 LMH/bar) showed a substantially higher permeability than that of a 0.1 µm polymeric PVDF membranes (992–1621 LMH/bar).

Concerning the fouling tendency, some studies reported similar (Oligny, Bérubé and Barbeau 2016) or slightly lower (Hofs, Ogier et al. 2011) fouling for ceramic membranes. In general, the production cost of ceramic membranes (capital cost) exceeds that of polymeric membranes (Hofs, Ogier et al. 2011, Kurth, Wise and Smith 2018, Li, Sun et al. 2020). However, the higher cost of ceramic membranes can be offset by their longer lifespan, approximately 20 years, which is roughly twice that of polymeric membranes (Fane, Wang and Jia 2011, Arumugham, Kaleekkal et al. 2021, Jarvis, Carra et al. 2022).

A crucial advantage of ceramic membranes is their ability to undergo aggressive chemical and physical cleaning without damaging the membrane materials (Gul, Hruza and Yalcinkaya 2021). For instance, Park et al. (Park, Kang et al. 2018) studied the effect of physical and chemically enhanced backwash on the flux recovery of a 0.1 µm ceramic membranes using DI water injection at 500 kPa and 300 mg/L of NaOCl. The maximum flux recovery obtained was 100% in this study.

Given that GDM processes aim to minimise physical and chemical backwashes, the question arises whether the advantages of ceramic membranes are justified in such applications. Alresheedi et al. (Alresheedi, Barbeau and Basu 2019) demonstrated that backwashes were twice as effective for removing NOM fouling from a ceramic UF (SiC) membrane compared to a polymeric PVDF UF membrane. However, no differences in the removal of irreversible fouling using NaOH and NaOCl were observed between the two membrane types. To date, no equivalent evaluation has been performed to compare the cleaning performances of ceramic and polymeric membranes used in GDM filtration.

A current industry trend involves conducting more frequent yet less aggressive chemical washes to manage fouling (Meng, Zhang et al. 2017). Such a strategy, often referred to as chemically enhanced backwash, contrasts with GDM operation, where low maintenance is desired, and cake filtration is favoured to stabilise the flux. Consequently, the chemical washing strategy necessarily differs for GDM filtration systems installed in small decentralised systems. Research is needed to define the optimal chemical conditions and potential benefits of using ceramic membranes to enable aggressive chemical washes of membranes that have been operated for several months without cleaning.

In the present study, the performances of two ceramics (commercial UF and lab-made MF) and two polymeric membranes (commercial UF and MF) were compared during the treatment of turbid, coloured river water with a high NOM content using a hybrid BIEX resin + GDM filtration process. After approximately 76 days of operation, physical (air/water backwash with enhanced or decreased air/water flow and pressure) and various chemical cleaning conditions (250 or 500 mg Cl_2/L of NaOCl; 20 or 40 mM of NaOH) were tested on the membranes to quantify the removal of different fouling types (reversible/irreversible, physical/chemical). Finally, the effects of the physical cleaning conditions (air/water backwash flow and pressure) and the impact of increasing

the chemical agent concentration during chemical cleaning on the flux recovery and fouling removal of each membrane type are discussed.

6.3 Materials and Methods

6.3.1 Biological ion exchange resin and gravity-driven filtration experiments

Figure 6-1 illustrates the experimental setup consisting of two identical pilots (Sections 1 and 2). Each section comprised a resin column (BIEX column 1 and BIEX column 2) and four parallel membranes. A transparent PVC column (H = 63 cm, ϕ = 1.27 cm) was filled with an approximately 42 cm bed height of resin (resin Bed Volume ≈ 52 mL). The empty bed contact time (EBCT) and filtration rate of the resin column were kept constant at 15 min and 3.47 mL/min (≈ 4 BV/h; linear velocity ≈ 1.64 m/h), respectively, with values chosen based on previous studies in our group. The experiment lasted approximately 76 days (≈ 7300 BV), which was sufficient for achieving secondary IEX (NOM exchange with bicarbonate and/or sulphate). In this study, Purolite A860®, a strong base anion macroporous exchange resin (pre-loaded with chloride), was used. The resin was regenerated after 6530 BV (day 68) using NaCl (100 g/L, 2 BV/h, and 1.5 h). The anions loading of the resin was calculated using Equation (1), where q (eq/L resin) is the cumulative anion loading on the resin, C_{in} and C_{out} are the concentrations of each anion in the inlet and outlet of the resin column (eq/L), V_{resin} is the total resin volume in the column (52 mL), Q is the flow rate (5 L/d), $\Delta t = (t_i - t_{i-1})$ is the time between each anion and the DOC measurement (d), and i is the number of anion measurements during the experiment. The charge balance was calculated only for chloride, sulphate, bicarbonate, DOC, and nitrate, which were the major negatively charged compounds during the IEX (Liu, Lompe et al. 2020).

$$q = \sum_{i=1}^{28} \frac{\left(Average\,(C_{in,i}, C_{in,i-1}) - Average\,(C_{out,i}, C_{out,i-1})\right) \times Q \times (t_i - t_{i-1})}{V_{resin}} \quad (6.1)$$

Four polymeric/ceramic MF/UF membranes were used for the membrane sections. The membrane compositions are listed in Table 6-1. All the membranes used in this study are commercially available, except for M4 (ceramic lab-made MF), which is a flat sheet disk-shaped ceramic MF membrane made in our laboratory, as described in section 6.3.1.1. The equipment in the membrane section was covered with aluminium foil to prevent algal growth. In the receiver of the resin column effluent, an overflow was placed to maintain a transmembrane pressure of 90 cm H_2O (≈ 93 mbar).

The temperature was maintained at 21.2 ± 0.7 °C by the laboratory air conditioning system. The flux of the membranes (in LMH) was calculated by weighing the daily permeate volume and then normalising it to 20 °C.

Table 6-1. Characteristics of the membranes used in the filtration section

Membrane name	**Membrane type**	**Pore size**	**Membrane material**	**Membrane area (cm^2)**	**Suppliers**
M1-1* **M1-2**	Flat-sheet disk-shaped Polymeric	0.1 µm (MF)	Polyether Sulfone (PES)	17	Sterlitech, Auburn, WA, USA
M2-1 **M2-2**	Flat-sheet disk-shaped Polymeric	0.03 µm (UF)	PES	17	Sterlitech, Auburn, WA, USA
M3-1 **M3-2**	Flat-sheet disk-shaped Ceramic	300 kDa (UF)	ZrO_2/ TiO_2	17	Tami Industries, France
M4-1 **M4-2**	Flat-sheet disk-shaped Ceramic	0.62 ± 0.06 µm ** (MF)	Kaolin support + alumina layer	15 ± 0.09 **	Lab-made

* The use of -1 and -2 refer to Sections 1 (pilot 1) and 2 (pilot 2) in Figure 1, respectively. For example, M1-1 represents M1 in Section 1 (pilot 1), and M1-2 represents M1 in Section 2 (pilot 2). ** Mean ± 95% confidence interval.

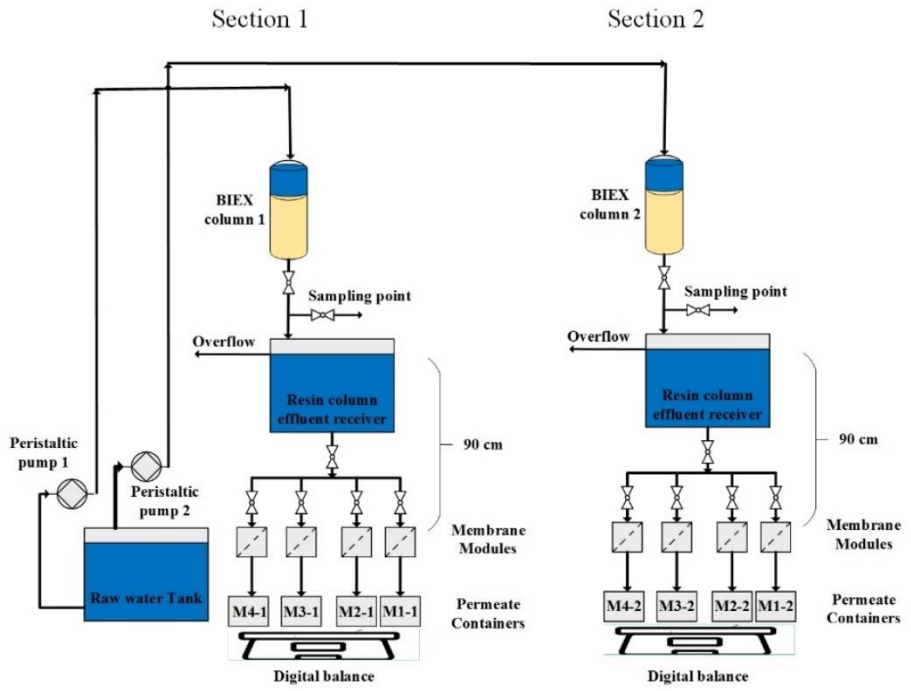

Figure 6-1. Experimental BIEX + GDM filtration pilot setup. BIEX resin operated at a 4 BV/h filtration rate and EBCT = 15 min. M1-1 and M1-2: flat-sheet disk-shaped 0.1 µm (MF) PES, M2-1, and M2-2: flat-sheet disk-shaped 0.03 µm (UF) PES, M3-1, and M3-2: flat-sheet disk-shaped 300 kDa (UF) ceramic, M4-1 and M4-2: lab-made flat-sheet disk-shaped ceramic MF membranes (Kaolin support + alumina layer).

6.3.1.1 M4 membrane synthesis

To fabricate M4 (ceramic MF), deionised (DI) water was incrementally introduced into a mixture of kaolin clay (Ward's Science, Rochester, NY, USA; $Al_2O_3{\cdot}2SiO_2{\cdot}2H_2O$, CAS: 1332-58-7) and boric acid (10 wt%, Ward's Science, Rochester, NY, USA; H_3BO_3, CAS: 10043-35-3, crystals) to make a suitable dough. Subsequently, the dough was mixed at approximately 100 rpm with a mechanical mixer for 10 min. Following this, about 25 g of the mixture was transferred to a disk-shaped mould equipped with a cap. A pressure of 7.3 MPa (Pressure Sensor Product Inc., Madison, NJ, USA) was applied to the cap to compress the mixture and form the disk-shaped membrane, using a clamp (a freezer bag was interposed between the cap and the mould to prevent adhesion during cap removal). After placing the mould on a glass plate, the cap and plastic bag were cautiously removed. Alumina powder (10 wt% of kaolin, Fisher Scientific, Switzerland; Al_2O_3, 40–300 µm, CAS: 1344-28-1, Mw = 101.96 g/mol) was gently poured onto one side of the formed

membrane to cover the entire surface. The membrane was then extracted from the mould after drying for a minimum of 24 h at room temperature. Finally, calcination was carried out at 1100 °C for 2 h using an electric programmable furnace (Ney Vulcan, 3–550). The schematic representing the M4 membrane production steps are shown in Figure C1. Seven membranes were synthesised for each experiment. Characterisations, such as DI water flux, porosity, pore size, SEM images, and Energy Dispersive X-ray (EDX) spectra, are provided in the Supplementary Information (Figure C2, Figure C3, Table C1).

6.3.2 Characteristics of influent water

The experiment was conducted between October and December 2022. A single raw water sample volume of 800 L was collected using 20 L buckets at the entrance of the Pont-Viau water treatment plant (Laval, QC, Canada). Raw water originates from the Des Prairies River. The water was promptly stored at 4 °C after collection. Once a week, approximately 80 L of the collected water was extracted from the refrigerator and allowed to attain room temperature (≈ 22 °C) for at least 5 h before adding it to the influent water tank. The physical and chemical characteristics of the influent water from the Des Prairies River are detailed in Table 6-2, encompassing DOC, turbidity, pH, alkalinity, UVA_{254}, nitrate, sulphate, and chloride. These low uncertainties indicate relatively constant influent water characteristics during storage.

Table 6-2. Characteristics of the influent water from Des Prairies River

Parameters	**Mean ± 95% confidence interval**	**Number of samples**
DOC (mg C/L)	7.04 ± 0.18	27
Turbidity (NTU)	5.09 ± 0.27	27
pH	7.17 ± 0.04	27
Alkalinity (mg $CaCO_3$/L)	23.8 ± 0.4	27
UVA_{254} (cm^{-1})	0.21 ± 0.005	27
Nitrate (mg/L)	2.71 ± 0.11	23
Sulphate (mg/L)	3.57 ± 0.37	23
Chloride (mg/L)	5.04 ± 0.15	23

6.3.3 Physical and chemical cleaning of the membranes

Physical and chemical cleaning was conducted after 30 days of the operation to investigate the dominant fouling type and assess the impact of increasing the chemical cleaning agent concentration (during chemical cleaning) and air/water backwash flow and pressure (during physical cleaning) on membrane flux recovery and the removal of different fouling types. The procedures and steps of the cleaning processes are outlined in Table 6-3 and Figure C4. Physical cleaning involved air and DI water backwashing. After halting the normal filtration process, the fouled membrane surfaces were turned face down (Figure C4a), followed by air backwashing in Section 1 (pilot 1) at P = 30 psi, Q = 5 L/h, and t = 2 min; in Section 2 (pilot 2) at P = 15 psi, Q = 2.5 L/h; and t = 2 min (Figure C4b, c). Subsequently, a DI water backwash was performed for 4 h under the conditions shown in Figure C4d, with back pressures of 120 and 90 cm H_2O for Sections 1 and 2, respectively. The membranes were then returned to their normal filtration position (Figure C4e) to measure the DI water flux (Figure C4f) and calculate the flux recovery using Equation 5.2.

$$\%\, Flux\ recovery = \frac{J_{ac}}{J_v} \times 100 \tag{6.2}$$

In equation 5.2, J_{ac} is the flux after cleaning (physical or chemical), and J_v is the water flux of the virgin membranes, both measured at a 90 cm H_2O pressure and T = 20 °C.

The chemical cleaning procedure commenced by washing membranes with 40 mM of NaOH (pH = 12.40) for t = 6h, T = 21 °C, and 90 cm H_2O pressure in section 1 (pilot 1). For section 2 (pilot 2), 20 mM of NaOH (pH = 12.16) was used for t = 6h, T = 21 °C, and 90 cm H_2O pressure (Figure C4g). After washing with NaOH, the DI water permeability was measured to calculate flux recovery (Figure C4h). Chemical cleaning was then performed by washing the membranes with NaOCl at concentrations of 500 and 250 mg Cl_2/L in sections 1 and 2, respectively, both at t = 6h and 90 cm H_2O pressure (Figure C4i). Finally, the DI water permeability was measured to obtain flux recovery using NaOCl (Figure C4j).

The total fouling resistance (m^{-1}, R) during filtration was obtained using Darcy's law as follows:

$$R_{total} = \left(\frac{\Delta P}{\mu_T\, J_T}\right) - R_{clean} \tag{6.3}$$

where μ_T is the permeate viscosity at temperature T, J_T is the permeate flux measured at temperature T, and ΔP is the hydrostatic pressure. R_{clean} is the clean membrane resistance calculated using the clean water permeability of the virgin membranes.

Total fouling resistance consists of 1) hydraulically reversible fouling, fouling caused by cake layer formation on the membrane surface (biofilm) which is removable by backwash (air + water), 2) hydraulically irreversible fouling, fouling caused by pore blocking which is not removable by backwash (air + water), 3) chemically reversible fouling, fouling caused by pore blocking which is removable by chemical cleaning (NaOCl and NaOH), 4) chemically irreversible fouling, fouling which persists after chemical cleaning.

Table 6-3. Stepwise description of physical and chemical membrane cleaning

No.	Step name	Descriptions	Figure
1	Turning the membranes face down	Membrane positions were faced down according to the inlet flow	Figure C4a
2	Backwash with air	Section 1) P = 30 psi, Q = 5 L/h, t = 2 min Section 2) P = 15 psi, Q = 2.5 L/h, t = 2 min	Figure C4b, c
3	Backwash with DI water	Section 1) Water head = 120 cm, t = 4h Section 2) Water head = 90 cm, t = 4h	Figure C4d
4	Returning the membranes face up	Membrane positions were returned to the normal filtration position.	Figure C4e
5	DI water flux measurement	Measuring DI water flux at water head of 90 cm for 15 min in both sections	Figure C4f
6	Chemical cleaning by NaOH	Section 1) NaOH = 40 mM, Water head = 90 cm, t = 6h Section 2) NaOH = 20 mM, Water head = 90 cm, t = 6h	Figure C4g
7	DI water flux measurement	Measuring DI water flux at water head of 90 cm for 15 min in both sections	Figure C4h
8	Chemical cleaning by NaOCl	Section 1) NaOCl = 500 mg Cl_2/L, Water head = 90 cm, t = 6h Section 2) NaOCl = 250 mg Cl_2/L, Water head = 90 cm, t = 6h	Figure C4i
9	DI water flux measurement	Measuring DI water flux at water head of 90 cm for 15 min in both sections	Figure C4j

6.3.4 Analytical methods for water samples

DOC in the water samples was measured after filtration through a prewashed 0.45 µm filter and analysed with a TOC analyser (Sievers M5310C, Trevose, PA, USA). To convert the concentration from mg C/L to eq/L, the charge density of DOC (NOM) was considered to be 10 meq/g C at pH 6.5 (Boyer, Singer et al. 2008) for the anion charge balance. Turbidity was measured using a turbidity meter (TL2300, Hach, Loveland, Col, USA) after calibration with standard samples. The UVA_{254} was measured using a UV-visible spectrophotometer (Cary 100 Scan, Varian Inc., Palo

Alto, CA, USA) on 0.45 µm filtered samples. pH was measured using a pH meter (Accumet AB 15 basic; Fisher Scientific, Waltham, MA, USA) calibrated with standard solutions. Bicarbonate concentration (alkalinity) was determined using the standard titration method with 0.01 M H_2SO_4 as the titrant. To measure the anions in the BIEX resin column effluent and influent water, samples were filtered through 0.45 µm syringe filters and analysed using an ion chromatography device (ICS 5000 AS-DP DIONEX, Thermo Scientific, Waltham, MA, USA).

6.3.5 Measurement of biofilm thickness

To study the mean biofilm/cake thickness during filtration (especially before and after membrane cleaning), optical coherence tomography (OCT) imaging was routinely performed on the membranes that were removed from the system for approximately 30 min. For each OCT image, three random locations were selected from the membranes. Raw OCT images were obtained using a Thorlabs SL1310V1 laser (Newton, NJ, USA). The mean biofilm thickness was determined using MATLAB (R2023b) and ImageJ 1.54g software (NIH, Bethesda, MD, USA). The details and conditions of the OCT imaging were previously reported (Rasouli, Maltais-Tariant et al. 2023).

6.3.6 Statistical analysis of data

Analysis of variance (ANOVA) was used in Microsoft Excel® (Microsoft 365) and GraphPad Prism® (10.0.02) software before the membrane cleaning day to investigate the effect of the membrane types on the stabilised flux. Moreover, ANOVA was performed after membrane cleaning to determine the effect of the membrane type, chemical agent concentration (in chemical cleaning), and air/water backwash flow (in physical cleaning) on the stabilised flux (as the dependent variable) achieved after the washes. The stabilised flux is defined as a flux data group (from the flux stabilisation day to the end of the operation) in which the slope of the flux–time diagram is no more statistically significant than zero.

6.4 Results and discussions

6.4.1 Operation of the BIEX process

Figure 6-2 illustrates the calculated anion loading on the resin during the 68-day operation (6528 BV) in Column 1. The results for Column 2, depicted in Figure C5, are not discussed as they exhibit similar behaviour to those in Column 1. The primary IEX capacity of the fresh resin, approximately 0.9 eq/L of the resin, was depleted after 18 days of operation (1728 BV). At this juncture, the estimated loadings for DOC, bicarbonate, sulphate, and nitrate were 0.10, 0.45, 0.13, and 0.07 eq/L, respectively. From day 18 to day 68 (1728 to 6528 BV), the secondary IEX (BIEX mode) enabled the displacement of bicarbonate, sulphate, and nitrate anions using DOC. Consequently, the loadings for bicarbonate, sulphate, and nitrate decreased to 0.20, 0.10, and 0.04 eq/L, respectively, while NOM increased from 0.10 to 0.37 eq/L at 6528 BV. After performing regeneration on day 68 (6528 BV), the resin capacity (0.9 eq/L) was fully recovered using chloride (returning to the primary IEX region).

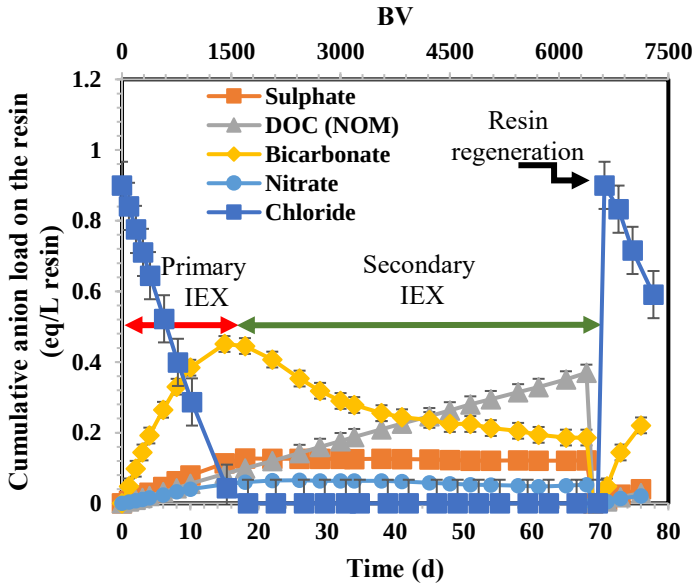

Figure 6-2. Variation in chloride, sulphate, DOC, and bicarbonate loads (as m eq/L of resin) on the BIEX 1 column during the operation. Regeneration was performed on day 68 (6528 BV). The error bars show 95% confidence intervals.

Figure 6-3 displays variations in effluent DOC and chloride release for BIEX-1 (BIEX column in Section 1) and BIEX-2 (BIEX column in Section 2). Both columns exhibited equivalent

performance. Initially, the effluent DOC of the resin columns was 0.4 mg C/L when the chloride release from the columns was 23 mg/L. The chloride release decreased to 1.3 mg/L at approximately 1728 BV (day 18), while the DOC of the column effluent peaked at 1.55 mg C/L. Considering a constant DOC concentration in the influent water (7.04 mg C/L ± 0.18), DOC removal at the end of the primary IEX was 78%. From 1728 BV (day 18) to 6528 BV (day 68), in the secondary IEX region, DOC initially decreased due to the exchange of NOM with bicarbonate and sulphate anions. DOC remained constant from 3000 to 4000 BV and then progressively rose to 2.2 mg C/L after 6528 BV (day 68). DOC removal remained high (68%) after 68 days of the operation. At this point, the resin was regenerated, decreasing the DOC of the BIEX column effluent to 1.05 mg C/L and increasing chloride release back to 23 mg/L. Similar behaviour was observed for UVA_{254} (Figure C6a), except for the higher removal rates compared to DOC, given that humic substances have a higher affinity for the resin. The variation in the turbidity of the BIEX column effluent is shown in Figure C6b.

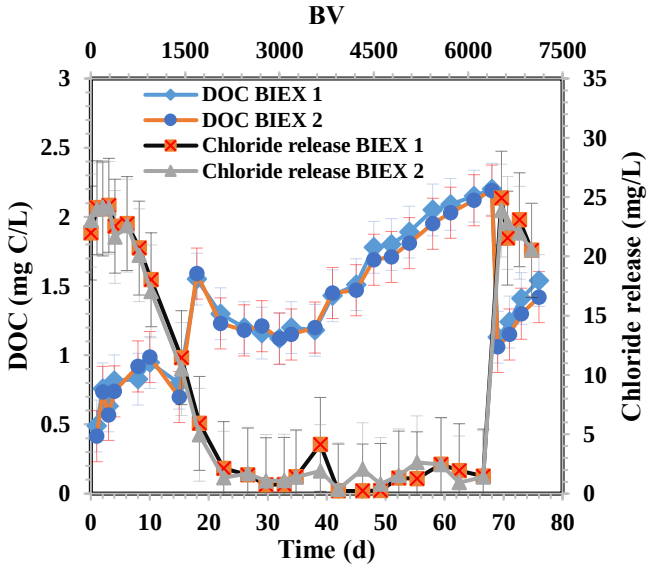

Figure 6-3. DOC concentration and chloride release in the effluent of the BIEX columns during the operation period. Day 68 (6528 BV) is the resin regeneration day. The error bars show 95% confidence intervals.

6.4.2 Effect of membrane type and cleaning process on the stabilised flux and flux recovery

The variation in flux over time is shown in Figure 6-4. In both pilot sections before the membrane cleaning process (days 1–29), the flux stabilised at approximately day 8, after an initial steep flux decline period. To validate the stabilisation in flux, the observed flux between days 8 and 29 for each membrane type in both sections was fitted to linear regression, and the calculated slopes were not statistically higher than zero (the *p*-values of slopes for both sections were >0.05), indicating a stable operating condition. The mean stabilised fluxes of the membranes from days 8 to 29 in sections 1 and 2 (pilot 1 and pilot 2) are shown in Table 6-4. Prior to membrane cleaning (days 1–29), the stabilised flux was affected by the membrane type (polymeric/ceramic, MF/UF), although this difference was fairly modest. For example, the average stabilised flux from day 8 to 29 for the membranes in sections 1 (pilot 1) and 2 (pilot 2) were measured as 4.46–4.56 LMH and 4.46–5.04 LMH, respectively (Table 6-4). The differences in the stabilised flux from the membranes in sections 1 and 2 were not statistically significant (Figure 6-5a, b; $p > 0.05$). This implies that the cleaning conditions described in section 1 can be compared to those described in section 2.

After membrane cleaning (days 30–73), the flux stabilisation period was reached on approximately day 54 in both sections. Similarly, to confirm flux stabilisation, the flux from days 54 to 73 was fitted to linear regression, and the obtained slopes were not statistically different from zero ($p > 0.05$). The average stabilised flux of the membranes for days 54–73 varied between 4.00 and 5.15 LMH (in section 1, Table 6-4) and 3.75 – 5.34 LMH (in section 2).

After cleaning the polymeric membranes (Figure 6-5c), stabilised fluxes increased significantly ($p < 0.001$) from 4.46 (MF)–4.54 (UF) LMH to 5.13 (MF)–4.69 (UF) LMH (after the enhanced cleaning condition in section 1) and from 4.77 (MF)–4.46 (UF) LMH to 5.34 (MF)–5.41 (UF) LMH (using the less stringent cleaning condition in section 2). Although statistically significant ($p < 0.001$), increasing the cleaning intensity did not substantially improve stable fluxes from a practical perspective. The membrane type (UF vs. MF) was equally impacted by the cleaning conditions for the ceramic membranes. After cleaning the ceramic membranes (Figure 6-5d), the stable MF flux declined for both cleaning conditions (sections 1 and 2), while the UF was not impacted by cleaning in section 1, which was subjected to enhanced cleaning conditions.

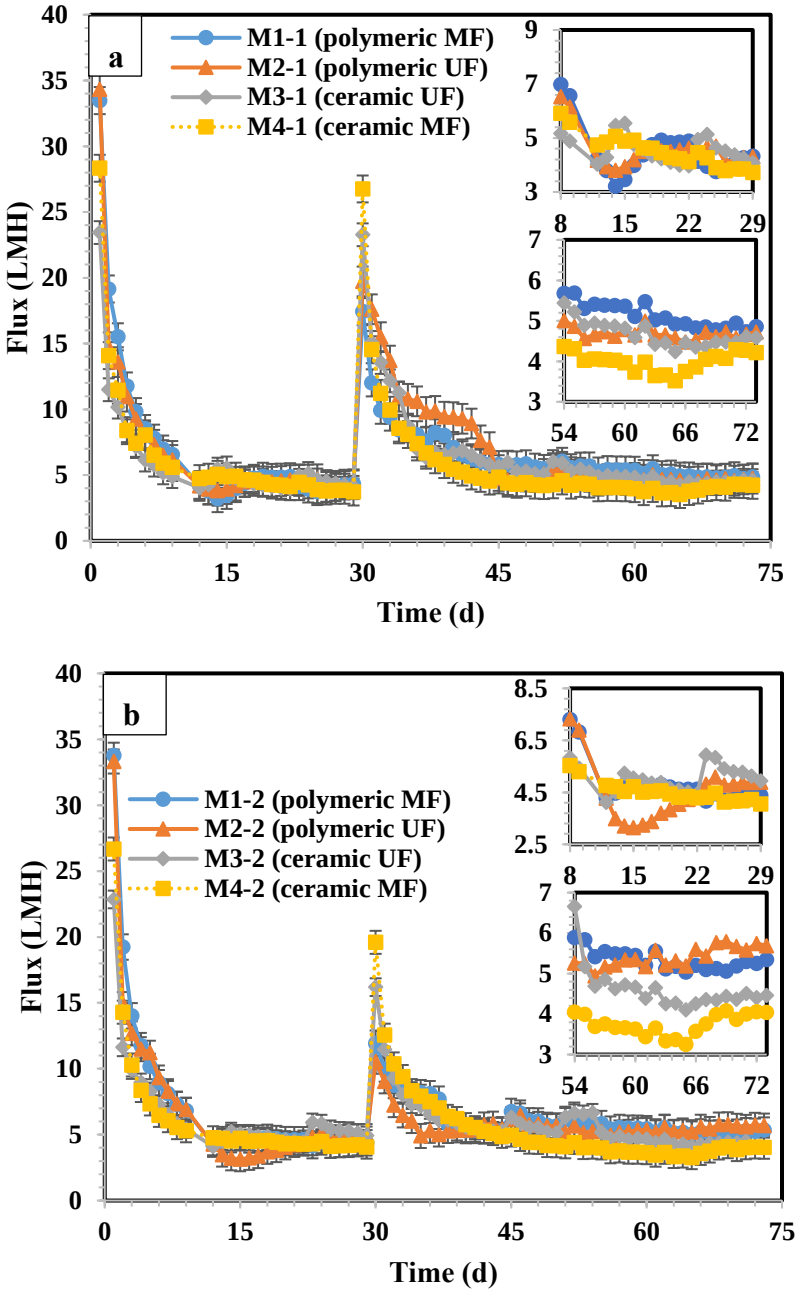

Figure 6-4. (**a**) Flux–time diagram of the membranes in a) Section 1 and (**b**) Section 2. M1 (polymeric 0.1 µm MF), M2 (polymeric 0.03 µm UF), M3 (ceramic 300 kDa UF), and M4 (Lab-made ceramic MF). Day 30 is the physical and chemical cleaning day. The error bars show 95% confidence intervals

In contrast, the ceramic UF in section 2, which was subjected to a lower cleaning condition, exhibited a stabilised flux decline of 8.5%. During the clean-in-place process, some foulants were

solubilised and could penetrate the membrane pores, causing internal clogging when the membranes returned to normal operation. In summary, cleaning the membranes generally led to a fairly modest increase in the stable flux, except for ceramic MF membranes.

Table 6-4. Mean ± 95% confidence interval of the membrane's stabilised flux in both sections before and after membrane cleaning. Before cleaning from day 8 to 29; after cleaning from day 54 to 73.

Membrane type		**Section 1 (enhanced cleaning)**				**Section 2 (decreased cleaning)**			
		Polymeric		Ceramic		Polymeric		Ceramic	
		MF (M1-1)	UF (M2-1)	UF (M3-1)	MF (M4-1)	MF (M1-2)	UF (M2-2)	UF (M3-2)	MF (M4-2)
Stabilised flux (LMH)	Before cleaning (day 8 – 29)	4.46 ± 0.42	4.54 ± 0.31	4.56 ± 0.22	4.50 ± 0.27	4.77 ± 0.37	4.46 ± 0.51	5.04 ± 0.23	4.50 ± 0.17
	After cleaning (day 54 – 73)	5.13 ± 0.14	4.69 ± 0.06	4.67 ± 0.14	4.00 ± 0.11	5.34 ± 0.11	5.41 ± 0.11	4.61 ± 0.25	3.75 ± 0.12
	Change (%)	+15%	+3.3 %	+2.8 %	-11%	+12 %	+21%	-8.5%	-16%

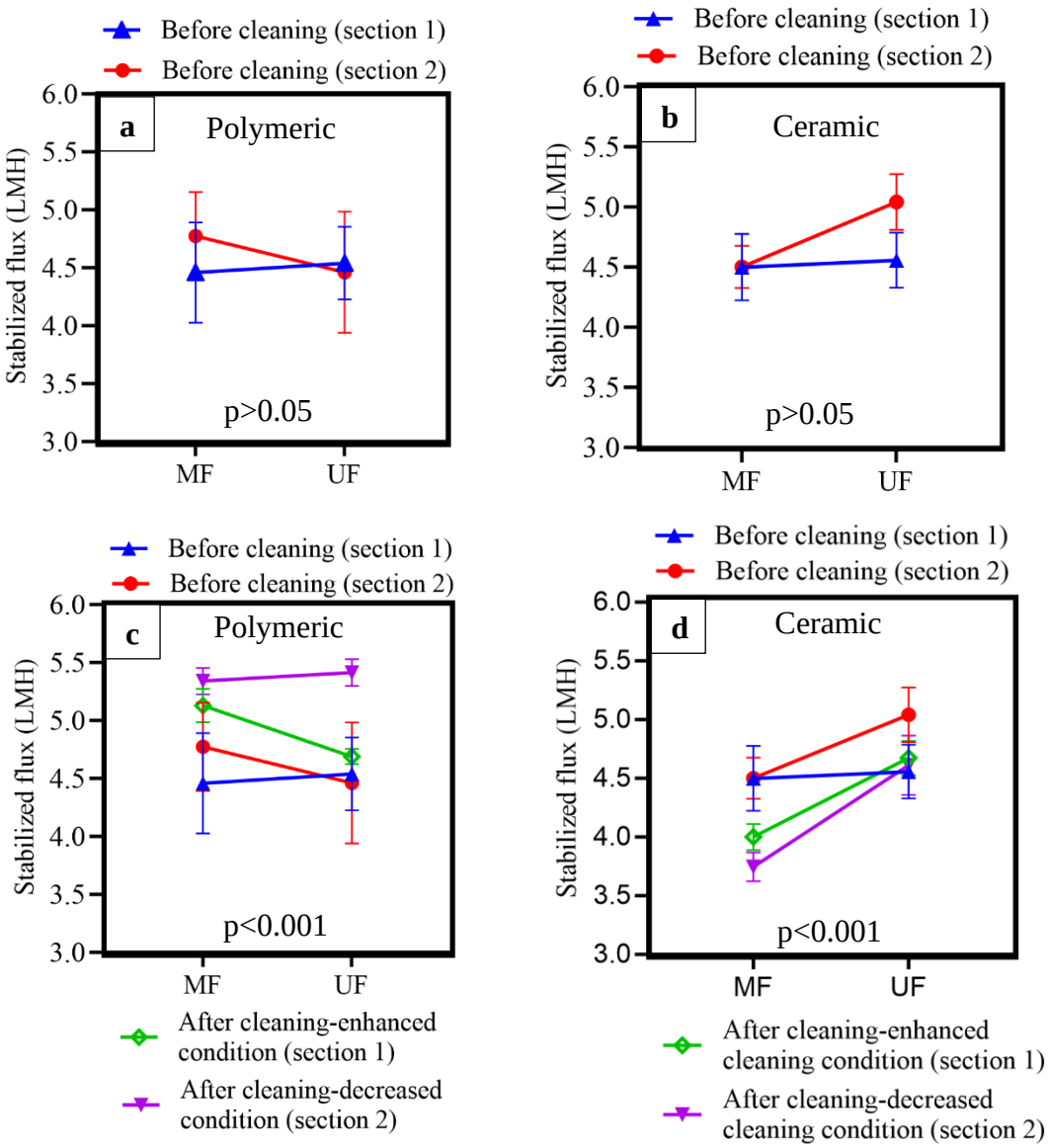

Figure 6-5. (**a**) Comparing the stabilised flux of the polymeric MF/UF membranes in Section 1 with Section 2 before the cleaning process (days 8–29). (**b**) Comparing the stabilised flux of the ceramic MF/UF membranes in Section 1 with Section 2 before the cleaning process (days 8–29). (**c, d**) The effect of membrane type (polymeric/ceramic, MF/UF) and the enhanced (in Section 1) or decreased cleaning condition (in Section 2) on the mean stabilised flux of the membranes after the cleaning process (day 54–73). The error bars represent 95% confidence intervals.

The flux recoveries and foulant reversibility after physical and chemical washes are shown in Table 6-5 and Table 6-6, respectively. According to Table 6-5, most of the membrane fouling was hydraulically reversible (57–80%). The additional recoveries provided by cleaning with NaOH or NaOCl were modest, typically less than 10%. The membranes in section 1 (pilot 1) with enhanced

air/water backwash flow and pressure (enhanced physical cleaning intensity) showed higher flux recoveries (i.e., hydraulic reversible fouling removal, 67–79%) than those in section 2 (pilot 2, 57–75%), which were subjected to a less intense air/water backwash flow and pressure (Table 6-6). The foulants were more hydraulically reversible on the ceramic membranes (70–79%) than on the polymeric membranes (57–69%). These findings suggest that it is simpler to remove foulants from ceramic membranes than from polymeric membranes using a basic backwash method involving air and water. The foulants left on the polymeric membranes after physical cleaning were difficult to remove via chemical cleaning. On average, 26% of the foulants were chemically irreversible. In contrast, the ceramic membranes had the lowest fraction of irreversible fouling (13%), with the UF ceramic (M3) providing the lowest overall irreversible fouling among all the membranes tested (8.8%).

Regarding the impact of chemical wash strength on flux recovery, increasing the NaOH concentration from 20 to 40 mM led to an increase in recovery from 2–4% to 4–6% for the polymeric membranes and from 4–7% to 7–12% for the ceramic membranes. For NaOCl, a lower concentration (250 mg Cl_2/L) led to a flux recovery of 4–6% for polymeric membranes and 1–2% for ceramic membranes, whereas a higher concentration (500 mg Cl_2/L) led to equivalent recoveries of 5–7% for all membranes. Overall, all the chemical washes provided low flux recoveries. According to these results, optimising physical cleaning appears to be a better strategy than using chemical washes to reduce operating costs, simplify operations, and minimise secondary pollution.

Table 6-5. Flux recovery percentages obtained via physical and chemical cleaning (mean ± 95% confidence interval).

Membrane type		**Section 1 (enhanced cleaning)**				**Section 2 (decreased cleaning)**			
		Polymeric		Ceramic		Polymeric		Ceramic	
		MF (M1-1)	UF (M2-1)	UF (M3-1)	MF (M4-1)	MF (M1-2)	UF (M2-2)	UF (M3-2)	MF (M4-2)
Flux recovery %	physical cleaning (air + water)	67.3 ± 8.2	69.7 ± 3.3	79.1 ± 6.0	79.6 ± 4.4	57.0 ± 2.1	61.3 ± 5.3	75.5 ± 10.5	70.8 ± 8.0
	chemical cleaning with NaOH	4.9 ± 4.5	6.1 ± 4.5	12.8 ± 3.2	7.8 ± 4.1	2.5 ± 2.1	3.8 ± 2.8	6.7 ± 6.4	4.6 ± 3.9
	chemical cleaning with NaOCl	7.5 ± 3.9	4.9 ± 2.7	5.3 ± 1.6	5.1 ± 4.0	6.2 ± 4.2	4.4 ± 2.7	3.0 ± 2.0	1.1 ± 0.5

Table 6-6. Percentages of different fouling types causing a flux decline in the filtration.

Membrane type		**Section 1 (enhanced cleaning)**				**Section 2 (decreased cleaning)**			
		Polymeric		Ceramic		Polymeric		Ceramic	
		MF (M1-1)	UF (M2-1)	UF (M3-1)	MF (M4-1)	MF (M1-2)	UF (M2-2)	UF (M3-2)	MF (M4-2)
Different fouling types%	Hydraulically reversible (%)	67.3	69.7	79.1	79.6	57.0	61.3	75.5	70.8
	Hydraulically irreversible (%)	32.7	30.3	20.9	20.4	43.0	38.7	24.5	29.2
	Chemically reversible (%)	12.4	11.0	18.1	12.9	8.7	8.2	9.7	5.7
	Chemically irreversible (%)	20.3	19.3	2.8	7.5	34.3	30.5	14.8	23.5

6.4.3 Mean biofilm thickness formed on the membrane surface during operation

To study the variation in the average thickness of the cake/biofilm accumulated on the membrane during filtration in sections 1 (Figure 6-6a) and 2 (Figure 6-6b), OCT imaging was performed on days 10, 22, 29, 30, 37, and 50. Raw OCT images of all the membranes before (day 29) and after cleaning (day 30) are shown in Figure C8. In section 1, the mean cake/biofilm thickness of M1 (polymeric MF) and M2 (polymeric UF) was measured as 80 µm on day 10. For ceramic membranes of M3 (ceramic UF) and M4 (ceramic lab-made MF), the average thickness was 90 µm on the same day. The cake/biofilm thickness increased by more than 1.5 times for all the membranes until day 22. After that, the thicknesses experienced a slight decrease by approximately 15–20 µm for all the membranes except M2 (polymeric UF), which might be due to the detachment of the aged biofilm on the membrane surface as no cake compression was expected in the GDM process (Akhondi, Wu et al. 2015, Wu, Hochstrasser et al. 2016). On day 30, after the cleaning procedure, the mean thickness decreased substantially to 82, 98, 84, and 75 µm for M1 (polymeric MF), M2 (polymeric UF), M3 (ceramic UF), and M4 (ceramic lab-made MF), respectively. Physical cleaning (increased hydraulic reversible fouling removal) explains the marked decrease in biofilm/cake thickness from the membrane surface. Subsequently, the thickness increased almost linearly by day 50 after the filtration. The mean biofilm thickness was not significantly different between sections 1 and 2 ($p > 0.05$) on day 30. After the membrane cleaning event on day 30 in section 2, the thickness was 97, 86, 75, and 69 µm for M1 (polymeric MF), M2 (polymeric UF), M3 (ceramic UF), and M4 (ceramic MF), respectively. In section 1, which was subjected to an enhanced air/water backwash, which resulted in higher flux recoveries (higher hydraulic reversible fouling removal), a lower mean biofilm thickness was expected for all membranes compared to those in section 2. However, in practice, only two out of four membranes (polymeric MF and ceramic MF) showed lower thicknesses owing to more aggressive cleaning.

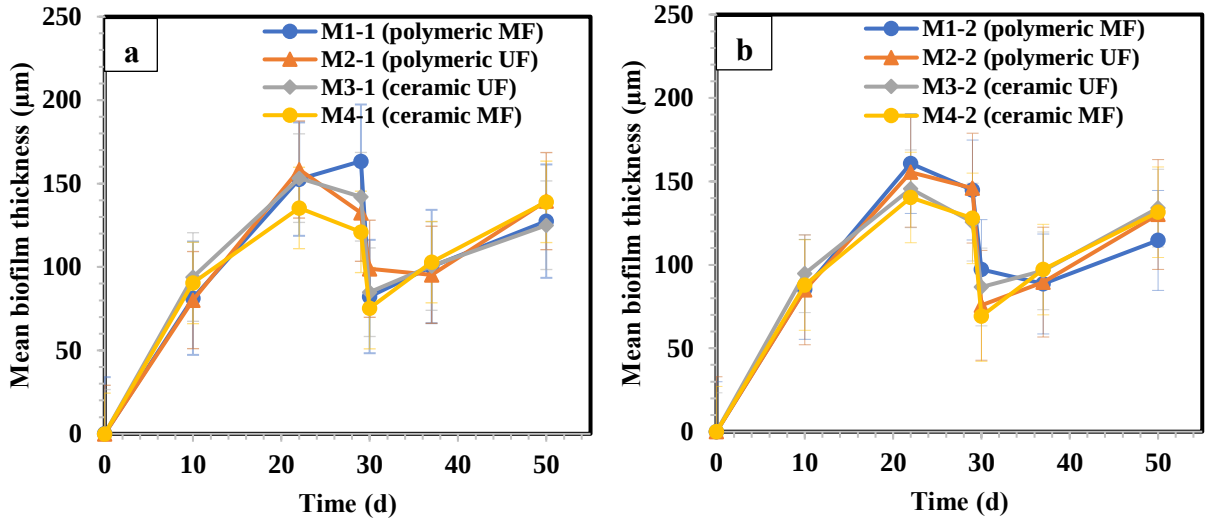

Figure 6-6. Evolution of mean biofilm thickness (µm) of (**a**) the membranes in Section 1 and (**b**) the membranes in Section 2. M1 (polymeric 0.1 µm MF), M2 (polymeric 0.03 µm UF), M3 (ceramic 300 kDa UF), and M4 (Lab-made ceramic MF). Day 30 is the physical and chemical cleaning day. The error bars show 95% confidence intervals.

6.4.4 Permeate quality of the polymeric and ceramic membranes during the operation

The evolution of the permeate DOC of the membranes in sections 1 and 2 is shown in Figure 6-7a, b. In section 1, the DOC concentrations of membrane effluents started at approximately 0.5 mg C/L, and rose progressively to 1.88, 1.55, 1.58, and 1.56 mg C/L for M1 (polymeric MF), M2 (polymeric UF), M3 (ceramic UF), and M4 (ceramic MF), respectively by day 68. M1 (polymeric MF) removed DOC by approximately 15%, whereas DOC removal using M2 (polymeric UF), M3 (ceramic UF), and M4 (ceramic MF) was approximately 30% on Day 68, compared to the DOC of the BIEX column effluents. Based on Figure C9a, the mean DOC of M3 (ceramic UF) from days 1 to 68 showed the lowest concentration (0.94 mg C/L) among all membranes. After resin regeneration on day 68, the permeate DOC of all the membranes decreased markedly to a value slightly higher than that on the initial day. The performance of the membranes for DOC removal in section 2 shows a trend similar to that in section 1. Likewise, according to Figure C9b, M3 (ceramic UF) showed the best performance of DOC removal (mean DOC during days 1–68 = 0.96 mg C/L) in section 2. Therefore, it can be concluded that the increased air/water backwash flow

and pressure (during physical cleaning) and chemical agent (NaOCl, NaOH) concentration (during chemical cleaning) in this study had no visible impact on DOC removal by membrane filtration.

UVA_{254} exhibited the same trend as DOC in both sections (Figure 6-7c, d). UVA_{254} in section 1 started at approximately 0.003 cm^{-1} for all membranes. This figure then increased by a fluctuating trend to 0.023, 0.022, 0.021, and 0.015 cm^{-1} for M1 (polymeric MF), M2 (polymeric UF), M3 (ceramic UF), and M4 (ceramic MF), respectively, by day 68. UVA_{254} removal using M1 (polymeric MF), M2 (polymeric UF), and M3 (ceramic UF) on day 68 was approximately 37%, whereas M4 (ceramic MF) removed approximately 57% of the UVA_{254} compared to the effluent of the BIEX column. According to Figure C9c, d, the mean of UVA_{254} from days 1 to 68 was approximately 0.01 cm^{-1} for all the tested membranes in both sections, which is a very high performance. Similarly, no marked influence of variations in air/water backwash flow, pressure, and chemical agent concentration during physical and chemical cleaning on UVA_{254} removal was observed. As expected, resin regeneration on day 68 decreased UVA_{254} in permeates in both sections to approximately 0.009 cm^{-1}. In section 2, the performance of the membranes in terms of UVA_{254} removal showed a trend very similar to that in section 1.

The evolution of turbidity during filtration in sections 1 and 2 is shown in Figure 6-7e and f, respectively. In section 1, during days 1 – 29 (before membrane cleaning), the polymeric (M1 and M2) and ceramic (M3 and M4) membranes showed similar performances. Turbidity started at approximately 0.05 NTU, followed by a fluctuating upper trend to 0.05 – 0.1 NTU until day 29. Immediately after membrane physical and chemical cleaning on the day 30, turbidity experienced a peak at approximately 0.17 NTU for M1 (polymeric MF) and M2 (polymeric UF), and 0.12 NTU for M3 (ceramic UF) and M4 (ceramic MF). Attributing to the higher mechanical strength of the ceramic membranes during physical cleaning, the turbidity peaked at lower values for these membranes after physical cleaning than for the polymeric membranes. Then, the turbidity of all the membranes decreased and reached a stable value of approximately 0.09 NTU at the end of the filtration time. Based on Figure C9e, f which is plotted using the turbidity data for the entire study, the membranes showed a turbidity of 0.08 – 0.09 NTU (mean of the turbidity during the whole filtration time). Based on the turbidity results, the physical and chemical cleaning processes of the membrane increased permeate turbidity for only a short period. Finally, the enhanced cleaning

conditions (in section 1) had no marked impact on the turbidity of the membrane permeates compared to those in section 2.

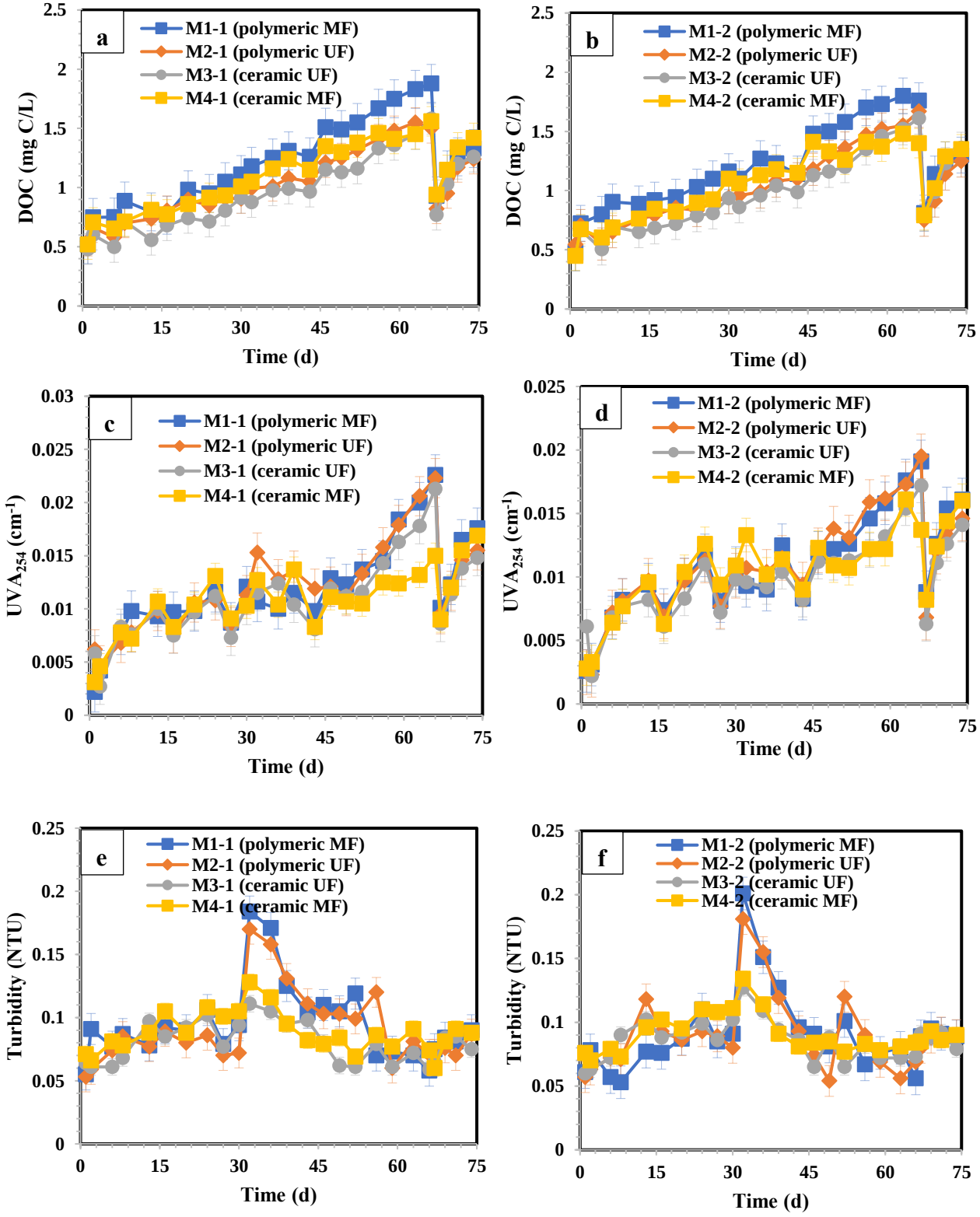

Figure 6-7. Variation in (**a**) DOC in Section 1, (**b**) DOC in Section 2, (**c**) UVA_{254} in Section 1, (**d**) UVA_{254} in Section 2, (**e**) turbidity in Section 1, and (**f**) turbidity in Section 2 during the filtration time. M1 (polymeric 0.1 µm MF), M2 (polymeric 0.03 µm UF), M3 (ceramic 300 kDa UF), and M4 (Lab-made ceramic MF). Days 30 and 68 are the membrane cleaning and resin regeneration days, respectively. The error bars show 95% confidence intervals.

6.5 Conclusions

Two commercial polymeric membranes of 0.1 µm MF (M1) and 0.03 µm UF (M2) and two ceramic membranes (300 kDa commercial UF (M3) and lab-made MF (M4)) were used in the BIEX + GDM hybrid process for treating river water. The performance of both polymeric and ceramic membranes in terms of flux and permeate quality was studied. Furthermore, physical (air + water backwash) and chemical cleaning (NaOH 20 and 40 mM, NaOCl 250 and 500 mg Cl_2/L) were performed to study the dominant fouling type causing the flux decrease in the membranes. Finally, the impacts of increasing the air/water backwash flow and pressure (during physical cleaning) and chemical cleaning agent concentration (during chemical cleaning) on stabilised flux, flux recovery, and permeate quality were investigated. The most important results obtained were as follows:

- BIEX resin column successfully reduced DOC from 7.04 mg C/L to below 2 mg C/L over the 68 days of operation.
- Before membrane cleaning (days 1 – 29), the fluxes of the membranes stabilised after day 8 at approximately 4.5 – 5 LMH. After membrane cleaning (days 30 – 73), the flux was restabilised after 24 days (i.e. on day 54). The new stabilised flux of the membranes was approximately 3.7 – 5.5 LMH at the end of the filtration, which was statistically significant. However, the difference was not substantial, indicating that the membrane material is not a key factor.
- Before cleaning, the ceramic and polymeric membranes showed similar stabilised fluxes. After the cleaning process, the stabilised flux of the ceramic membranes decreased or remained constant, whereas that of the polymeric membranes increased under both enhanced and decreased cleaning conditions compared to that before cleaning.
- The majority of membrane fouling (57%–80%) was hydraulically reversible. The membranes in section 1, with enhanced air/water backwash flow and pressure, showed

higher hydraulic reversible fouling removal than those in section 2. Hydraulically reversible fouling removal was more efficient with ceramic membranes than with polymeric membranes. Chemical cleaning was not effective for removing hydraulically irreversible foulants. Therefore, we recommend performing physical learning and eliminating chemical cleaning steps.

- The ceramic UF (M3) membrane showed the best permeate quality, with DOC and UVA_{254} removals of 30% and 37% on day 68, respectively, as measured against the influent (i.e., the BIEX effluent).
- Physical and chemical cleaning had no measurable impact on DOC and UVA_{254}, whereas physical cleaning increased the turbidity of the membranes for a short period. Resin regeneration decreased the DOC and UVA_{254} of the membrane permeates, whereas it had no significant impact on membrane turbidity.

According to the obtained results, most of the membrane fouling in the hybrid BIEX + GDM process was hydraulically reversible using an air/water backwash. Therefore, future research should focus on optimising physical cleaning to increase flux recovery and stabilise flux.

6.6 Author Contributions

conceptualization, Yaser Rasouli, Dominique Claveau-Mallet, Benoit Barbeau; methodology, Yaser Rasouli, Raphaël Maltais-Tariant; software, Yaser Rasouli, Raphaël Maltais-Tariant; formal analysis, Yaser Rasouli, Dominique Claveau-Mallet, Benoit Barbeau; resources, Caroline Boudoux, Dominique Claveau-Mallet, Benoit Barbeau; writing—original draft preparation, Yaser Rasouli; writing—review and editing, Yaser Rasouli, Dominique Claveau-Mallet, Benoit Barbeau, Raphaël Maltais-Tariant, Caroline Boudoux; supervision, Dominique Claveau-Mallet, Benoit Barbeau; funding acquisition, Caroline Boudoux, Dominique Claveau-Mallet, Benoit Barbeau. All authors have read and agreed to the published version of the manuscript.

6.7 Funding

This research was funded by the Canada Research Chair for Decentralized and Small-Scale Water Treatment (file number 950-232871).

6.8 Acknowledgments

The authors would like to express their gratitude to the Polytechnique Montreal technicians and research professionals who assisted in setting up the hybrid BIEX + GDM system and provided technical support during the project. The individuals named are Gabriel St-Jean, Julie Philibert, Mélanie Bolduc, Tetiana Elyart, Jacinthe Mailly, and Yves Fontaine.

6.9 Conflicts of Interest

Author Caroline Boudoux is employed by the company Castor Optics. The paper reflects the views of the scientists and not the company. The remaining authors declare that the research was conducted in the absence of any commercial or financial relationships that could be construed as a potential conflict of interest.

CHAPTER 7 GENERAL DISCUSSION

This section highlights the primary discoveries stemming from this project concerning the initial research objectives and hypotheses. The general objective of this research was to propose and evaluate a high-performance process during the surface water treatment in the decentralized and passive water treatment systems. We have selected BIEX (with anion exchange resin) and GDM processes (with ceramic and polymeric membranes) for this purpose. The specific objectives focused on the three main sections of I) Application of GDM process without pretreatment using lab-made ceramic membranes. II) BIEX + GDM hybrid process. III) Comparing performance of ceramic and polymeric membranes and membrane cleaning process in BIEX + GDM process. The general and specific objectives of the research are shown in Figure 7-1.

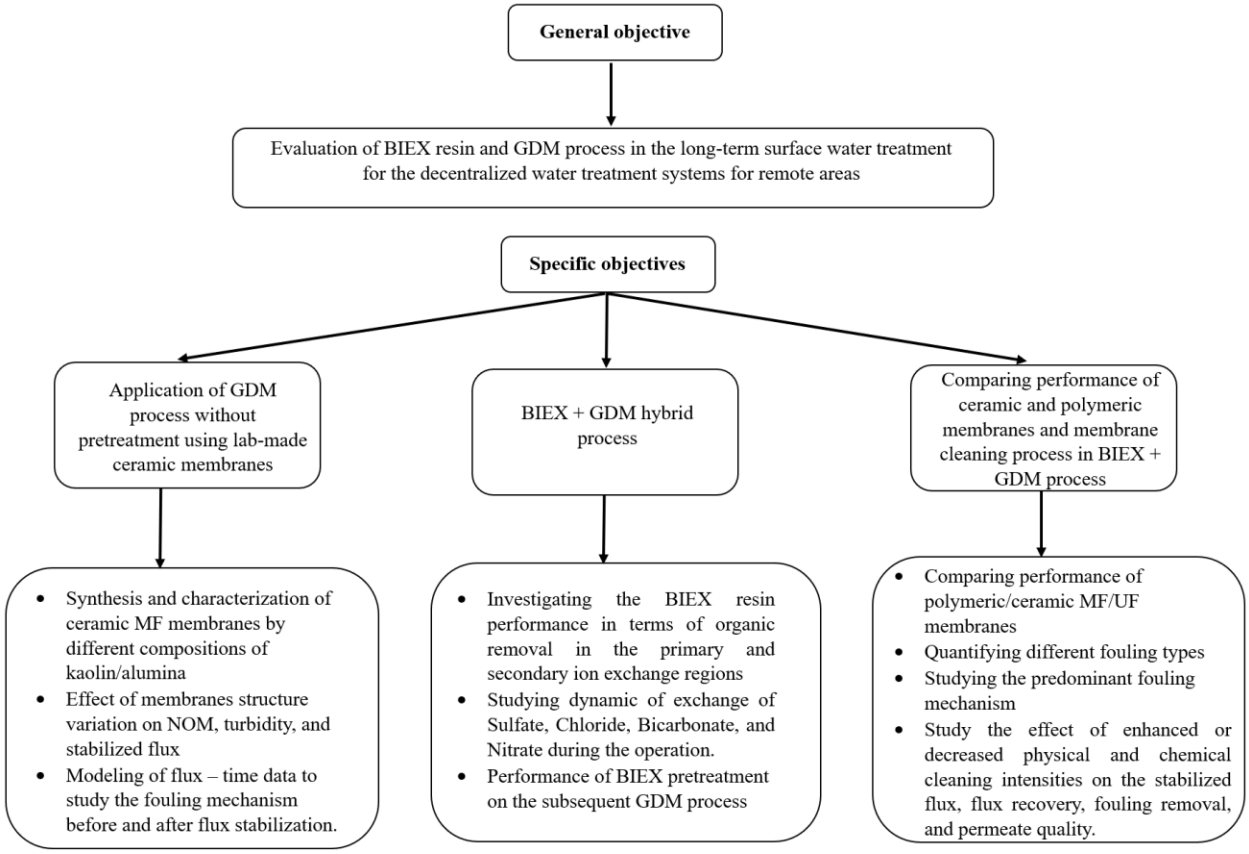

Figure 7-1. Schematic representing the general and specific objectives of the presented thesis.

Firstly, the performance of lab-made kaolin/alumina-based ceramic MF membranes during long-term filtration of a colored and turbid river water was evaluated in the GDM process in terms of stable flux, permeate quality, and biofilm characterization. Moreover, the impact of increasing alumina in the membrane structure on the stabilized flux, water quality, and biofilm characteristics was investigated. It was found that the process effectively removed the turbidity (permeate turbidity ~ 0.15 NTU) while the maximum stabilized flux (~ 3 LMH) and organic removal (~ 6%) can be further improved by employing BIEX resin as a pretreatment step before GDM process. Consequently, a column containing BIEX resin was selected to integrate with the GDM process using the same ceramic membrane types, influent water, and operating conditions. This approach makes it possible to compare the GDM-only process with BIEX + GDM hybrid process, eventually reveals the BIEX performance. In the long-term BIEX + GDM hybrid process, the final effluent of the hybrid process showed a stabilized flux (~ 6 LMH) approximately two-fold of that in GDM-only process as well as increasing organic removal significantly. Finally, MF/UF ceramic/polymeric membranes utilized in the hybrid BIEX + GDM process to compare the performance of polymeric and ceramic membranes, leading to selection of the best membrane type for the decentralized water treatment application. Moreover, enhanced and decreased physical (air – water backwash) and chemical (NaOH and NaOCl) cleaning intensities were employed to investigate the influence of the cleaning intensity on the stabilized flux, flux recovery, removal of different fouling types, biofilm characteristics, and permeate quality.

7.1 Application of GDM process without pretreatment using lab-made ceramic membranes

As shown in chapter 3, the systematic integration of ceramic membranes within the GDM process, particularly for decentralized water treatment systems, remains relatively unexplored in previous research endeavors. Therefore, this study introduces a novel approach by investigating the filtration performance of ceramic membranes within the GDM framework. In contrast to prior studies, our selection of ceramic membrane types was guided by their extended lifespan, aligning perfectly with the requirements of decentralized and passive systems.

The outcomes of this thesis shed light on the efficacy of ceramic MF membranes composed of kaolin (50 – 100 wt%) and alumina (0 – 50 wt%) when employed in the GDM process with a

driving force of 90 cm H_2O. These membranes exhibited exceptional performance in terms of turbidity removal, yielding a permeate turbidity of approximately 0.15 NTU. However, as anticipated for MF membranes, sustained removal of DOC exhibited inferior performance, with M3 (comprising 50 wt% kaolin and 50 wt% alumina) achieving only approximately 6% removal. Furthermore, M3 demonstrated the highest flux recovery, reaching 3 LMH.

The investigation into the impact of increasing alumina concentration within membrane structure revealed notable improvements in stabilized flux, turbidity and DOC removal, and biological activity of the biofilm. In the first objective, a transition in fouling mechanism from pore blocking to cake layer formation was elucidated through OCT observations and flux-time modeling. These findings underscore the importance of considering both membrane composition and fouling mechanisms in optimizing the performance of ceramic membranes within the GDM process.

7.1.1 Is there an optimum alumina concentration within the membrane structure?

In this study, membranes with 0 wt% (M1), 25 wt% (M2), and 50 wt% (M3) alumina composition were produced in the laboratory. Based on the results of chapter 4 (objective 1, paper 1), increasing alumina concentration increased the stabilized flux, permeate quality, and biofilm activity. Additionally, mean biofilm thickness was obtained higher for alumina membranes (M2 and M3) than that of kaolin membrane (M1). This can be attributed to a synergetic effect between biodegradation/biosorption and adsorption.

Based on the findings of chapter 4, it is evident that the composition comprising 50 wt% alumina and 50 wt% kaolin clay (referred to as M3) consistently yielded the highest stabilized flux, superior permeate quality, and enhanced biofilm biological activity which is coherent with the results obtained in chapter 5. Nevertheless, surpassing the 50 wt% threshold for alumina poses challenges, primarily due to the predominant use of kaolin as the primary material for ceramic membrane production. Reducing the kaolin concentration below 50 wt% could compromise the moldability of the mixture, potentially resulting in membrane breakage during the demolding process at room temperature or during subsequent calcination. Further studies should be designed to investigate this issue.

Furthermore, a reduction in kaolin concentration below the established threshold may compromise the overall homogeneity and consistency of the membrane composition. This loss of uniformity could lead to inconsistencies in membrane formation and properties, ultimately affecting filtration performance and operational reliability. Consequently, while optimizing alumina content is desirable for enhancing specific membrane characteristics, such as flux and biofilm activity, careful consideration must be given to the limitations imposed by the critical role of kaolin in the membrane fabrication process.

Therefore, navigating this delicate balance between alumina and kaolin concentrations is essential for achieving optimal membrane Performance while ensuring manufacturability and durability. Future research endeavors may explore innovative strategies to mitigate the challenges associated with increasing alumina content beyond 50 wt%, such as the utilization of alternative additives or refining fabrication techniques to enhance membrane stability and functionality without compromising structural integrity.

7.1.2 Challenges and limitations of GDM process without pretreatment with lab-made ceramic membranes

Fouling in GDM processes without pretreatment is a multifaceted challenge that arises due to the accumulation of suspended solids, microorganisms, and organic matter on the membrane surface or within its pores. This fouling phenomenon can occur through various mechanisms, including cake formation and pore blocking. Understanding the factors influencing fouling, such as feedwater characteristics, membrane properties, and operating conditions, is crucial for mitigating its impact on system performance. Strategies for fouling mitigation may include optimizing hydraulic conditions, implementing periodic backwashing or air scouring, employing membrane surface modification techniques, and integrating pretreatment processes to reduce foulants before reaching the membrane surface. In this thesis, we have selected a BIEX resin pretreatment step in chapter 5 (objective 2, paper 2,) and membrane physical and chemical cleaning approach in chapter 6 (objective 3, paper 3) to overcome this issue. The introduction of a BIEX resin column preceding the GDM process resulted in a notable enhancement in the stabilized flux, indicative of reduced fouling, and a significant improvement in permeate quality for ceramic membranes. Conversely, the application of physical and chemical cleaning procedures generally exhibited either negligible

or adverse effects on the stabilized flux of ceramic membranes while increased the stabilized flux of the polymeric membrane.

The integrity of lab-made ceramic membranes plays a pivotal role in the performance and longevity of GDM processes without pretreatment. Variations in membrane fabrication parameters, such as pore size distribution, porosity, and surface morphology, can impact filtration efficiency, permeate quality, and fouling resistance. Ensuring consistent membrane quality and structural integrity requires stringent quality control measures during the manufacturing process, including precise control of raw material composition, optimized fabrication techniques, and thorough characterization of membrane properties. Therefore, after membrane fabrication in objective 1 (chapter 3) and objective 3 (chapter 6), characterization techniques such as porosity, pore size measurement, SEM, EDX, XRD, and DI water permeability have been applied on the produced membranes and the results are carefully analyzed to ensure their integrity.

GDM processes without pretreatment may encounter challenges in effectively removing certain contaminants, particularly those with small particle sizes or complex molecular structures. The inherent limitations of gravity-driven filtration, such as size exclusion and adsorptive capacity, may restrict the removal efficiency of certain contaminants, including dissolved organics and trace contaminants. As we mentioned before, to address these challenges we have optimized membrane properties by developing BIEX + GDM hybrid treatment process (chapter 5).

7.2 BIEX + GDM hybrid process

chapter 4 demonstrated that enhancements in organic and particulate matter removal, along with improvements in membrane stabilized fluxes, could be achieved through the implementation of a pretreatment stage. Subsequently, in chapter 5, a column filled with resin (BIEX) was selected as the designated pretreatment step for the subsequent GDM process, utilizing identical ceramic membrane types, influent water sources, and operational parameters as in chapter 4. This strategic approach facilitated a direct comparison between the performance of the GDM-only process and the BIEX + GDM process, enabling an assessment of stabilized flux, water quality, and the characteristics of biofilm formation on the membrane surface. According to the results of chapter 5, the maximum stabilized flux of approximately 6 LMH was achieved by M3 (50 wt% kaolin + 50 wt% alumina), representing a doubling of flux compared to the GDM-only process.

Additionally, the hybrid process yielded a final effluent turbidity of approximately 0.1 NTU, which was half that of the GDM process without pretreatment, where turbidity ranged from 0.15 to 0.2 NTU. Regarding organic removal, the BIEX resin column demonstrated the capacity to remove approximately 74% of DOC. Upon integration with the GDM process, the BIEX + GDM hybrid system exhibited even greater efficiency, eliminating over 81% of DOC from the influent water.

The concept of integrating BIEX resin and GDM processes represents a unique aspect of this thesis, as there is a notable dearth of studies specifically exploring the utilization of a BIEX + GDM hybrid process (chapter 3). While both BIEX and GDM processes have been individually investigated for water treatment applications, the synergistic combination of these two technologies in a hybrid treatment system is relatively unexplored in existing literature. This innovative approach capitalizes on the advantages of BIEX, such as delayed regeneration stage, less chemical use and transportation, and decreased secondary pollution which align with the characteristics required by decentralized water treatment systems. By integrating these advantages with the passive filtration capabilities of GDM processes, we have addressed the limitations of individual treatment methods and unlock synergistic benefits for enhanced water treatment efficiency and quality in decentralized settings. For instance, low turbidity removal of BIEX resin section can be mitigated by the membranes in GDM section. In contrast, low organic removal of GDM section can be addressed by BIEX resin column.

The results demonstrated in chapter 5 underscore the efficacy of the BIEX + GDM process, leveraging anion exchange resins in conjunction with lab-made ceramic MF membranes, as a robust and high-performing method for organic and turbidity removal in the decentralized water treatment systems. Notably, this integrated approach exhibits exceptional long-term performance, consistently achieving impressive outcomes. Specifically, the process demonstrates unparalleled efficiency, removing over 80% of organic contaminants while concurrently reducing turbidity to below 0.1 NTU. Such simultaneous achievement of rigorous removal targets for both organics and turbidity is remarkable and indicative of the process efficacy. Moreover, the sustained operation of the system yields a stabilized flux of approximately 6 LMH, underscoring its reliability and suitability for practical applications. This confluence of superior removal efficiency, sustained flux performance, and long-term stability positions the BIEX + GDM process as a noteworthy

advancement in passive water treatment technology, offering a simple yet highly effective solution to complex water quality challenges.

7.2.1 Challenges and limitations of BIEX + GDM hybrid process

The integration of BIEX with GDM in a hybrid process presents distinct challenges and limitations associated with each individual process. In the context of the GDM process without pretreatment employing lab-made ceramic membranes, the challenges and limitations have been meticulously described in section 7.1.2. Consistency in organic removal poses a significant challenge for anion exchange resins operating in biological mode (BIEX). Figure 5-3 highlights a persistent fluctuation in the DOC content of BIEX column effluent over the extended operational period. However, in practical applications within treatment plants utilizing BIEX resin, ensuring reliable and steady organic removal becomes imperative for effective water treatment processes. The GDM process can play a crucial role in stabilizing the fluctuations in DOC content encountered in the BIEX process. By incorporating GDM subsequent to BIEX, the membrane filtration provided by GDM can increase the organic compounds removal that may remain after the BIEX treatment. This additional filtration step helps to ensure more consistent organic removal and enhances the overall performance and reliability of the hybrid BIEX + GDM system.

Moreover, the presence of the Schmutzdecke layer, characterized by its dense and biologically active nature, presents a notable concern within the framework of BIEX resin filtration. This layer, which accumulates atop the filter bed, comprises a complex matrix of microorganisms and organic matter. While essential for effective filtration, as it aids in the removal of contaminants, the Schmutzdecke can also exacerbate operational challenges. Over time, its accumulation can lead to increased pressure differentials across the filtration column. In the most severe instances, this buildup may even impede the flow of water through the column entirely. Thus, managing the formation and impact of the Schmutzdecke is crucial for maintaining the efficiency and longevity of BIEX resin filtration systems. To effectively address the issue of Schmutzdecke formation, implementing air injection and backwash techniques emerges as the most promising approach. Air injection involves introducing air into the filtration system, which helps disrupt and disperse the dense layer of organic material accumulated on the filter bed surface. This process creates agitation within the filter media, facilitating the loosening and detachment of the Schmutzdecke.

Similarly, backwashing involves reversing the flow of water through the filtration system, thereby dislodging and flushing out trapped particles and organic matter, including the Schmutzdecke, from the filter bed. By applying a combination of air injection and backwash cycles, operators can effectively prevent the buildup of the Schmutzdecke, ensuring optimal filtration performance and prolonging the operational lifespan of the system. These proactive maintenance measures are essential for mitigating the adverse effects of Schmutzdecke formation and maintaining the efficiency of BIEX resin filtration systems.

7.3 Comparing performance of ceramic and polymeric membranes and membrane cleaning process in BIEX + GDM process

In order to rigorously evaluate the hypothesis outlined in objective 3 (paper 3, chapter 6), a comprehensive experimental setup was devised. This entailed the establishment of two distinct BIEX + GDM pilot systems, each outfitted with two commercially available polymeric MF/UF membranes and a UF commercial ceramic membrane. Additionally, a MF two-layer ceramic membrane, comprising a kaolin support and an alumina top layer, was fabricated in the laboratory.

Subsequently, after attaining a state of stable flux within each system, a series of physical and chemical cleaning procedures were systematically conducted. These cleaning protocols encompassed both air and water backwash techniques for physical cleaning, complemented by chemical cleaning regimens employing NaOH at concentrations of 20 and 40 mM, as well as NaOCl at concentrations of 250 and 500 mg Cl_2/L. Notably, variations in cleaning intensity were deliberately introduced, with enhanced cleaning measures implemented in Pilot 1, and decreased intensity applied in Pilot 2.

During the experiment, the impact of cleaning intensity on several key parameters was examined. These parameters included stabilized flux, flux recovery, permeate quality, the extent of various fouling types, and the characteristics of biofilm formation. Moreover, a comparative analysis was conducted to evaluate the performance of ceramic membranes compared to polymeric counterparts.

By systematically investigating the multifaceted effects of cleaning intensity on membrane performance and fouling dynamics, this study aimed to provide valuable insights into the

optimization of membrane cleaning protocols and the selection of membrane materials for enhanced water treatment applications.

The findings presented in chapter 6 provide valuable insights into the performance of the BIEX resin columns over an extended period, corroborating the results obtained in chapter 5. Specifically, the effluents from both BIEX resin columns exhibited DOC concentrations consistently below 2 mg C/L for approximately 70 days, indicative of robust and stable operation of the process.

Moreover, the analysis of stabilized fluxes before and after membrane cleaning revealed appealing observations. Across both polymeric and ceramic membrane materials, as well as pore sizes (MF/UF), the stabilized fluxes remained relatively consistent, ranging from approximately 3.7 to 5.5 LMH. This suggests that membrane material composition and pore size do not exert a significant influence on the stable flux within the BIEX + GDM hybrid process.

Furthermore, examination of mean stabilized fluxes before cleaning indicated comparable values for both polymeric and ceramic membranes. However, notable distinctions emerged following cleaning procedures. While the mean stabilized flux of ceramic membranes either remained constant or exhibited a slight decrease under both enhanced and decreased cleaning intensities, polymeric membranes demonstrated an increase in flux.

Interestingly, enhanced cleaning intensities were associated with an elevation in hydraulic reversible fouling, which emerged as the dominant fouling mechanism and could be effectively mitigated through physical cleaning during the BIEX + GDM hybrid process. In contrast, the chemical cleaning performance was found to be negligible in comparison to physical cleaning methods.

Notably, neither physical nor chemical cleaning exerted a measurable impact on DOC and UVA_{254} levels. However, physical cleaning transiently increased membrane turbidity, although this effect was temporary in nature.

Moreover, resin regeneration emerged as a crucial factor in reducing the DOC and UVA_{254} levels of membrane permeates. Conversely, its impact on membrane turbidity was found to be insignificant.

These comprehensive findings shed light on the intricate interplay between membrane cleaning strategies, fouling mechanisms, and effluent quality parameters within the BIEX + GDM hybrid process, thereby contributing to a deeper understanding of its operational dynamics and optimization potential.

In summary, the research conducted in this thesis highlights the feasibility and efficacy of utilizing the BIEX + GDM hybrid process in conjunction with ceramic kaolin/alumina-based membranes over an extended operational period exceeding 70 days. Remarkably, this integrated approach consistently achieved over 81% removal of DOC, maintaining effluent DOC concentrations consistently below 2 mg C/L. Simultaneously, the permeate turbidity was consistently maintained below 0.1 NTU, indicative of exceptional water quality standards achieved by the system.

Moreover, the BIEX + GDM hybrid process demonstrated the capability to sustain a stabilized flux as high as 6 LMH over the long term, without compromise effluent quality. Such sustained relatively high flux rates are a notable achievement, especially considering the demanding conditions often encountered in decentralized water treatment systems serving rural and remote areas, far from urban infrastructure and complex treatment facilities.

This technological advancement holds significant promise for addressing water treatment challenges in underserved regions, where access to clean and safe drinking water remains a pressing concern. By offering a reliable and robust solution capable of achieving stringent water quality standards over extended periods, the BIEX + GDM hybrid process represents a pivotal step towards enhancing the resilience and sustainability of water supply systems in remote and marginalized communities. Ultimately, this research contributes to the advancement of decentralized water treatment technologies, empowering communities to safeguard their health and well-being through access to potable water resources.

7.4 Flux stabilization mechanism in the hybrid process

According to chapter 4, prior to the flux stabilization day, a pore-blocking model was found to be the dominant fouling mechanism of the membranes. However, following the flux stabilization phenomenon, it was demonstrated that the fouling mechanisms of the membranes were attributed to the formation of cake layer and biofilm formation. During the dead-end GDM filtration, the

retained materials are deposited on the membrane surface, resulting in an increased biofouling layer thickness with time. Obviously, there are colonies of microorganisms such as Eukaryotes (such as protists and metazoans) in this biofouling layer. Bacterial activity and predation in the biofouling layer which are capable of altering biofilm morphology and affecting the spatial arrangement of the biofouling layer resulting in a more heterogeneous structure. Therefore, the combined effects of the biofouling layer thickness and structure determine the flux development profile patterns.

7.5 Turbidity and organic removal mechanism in the hybrid process

Three mechanisms of membrane pores, adsorption capacity because of alumina content in the membrane structure, and biosorption/biodegradation due to the biofilm formation contribute to the turbidity removal and organic removal from the influent water using membranes.

On initial days of the filtration before flux stabilization day, the turbidity removal can be related to the membrane pores and adsorption capacity due to the alumina content of the membranes while biosorption/biodegradation does not play a key role in the turbidity removal, as on initial days there not much biofilm formed on the membrane surface. By time, biosorption/biodegradation impact increases because of increasing biofilm thickness and biological activity.

Regarding the organic removal, adsorption capacity (because of alumina concentration in the membranes structure) and membrane pores play an integral role on initial days and before flux stabilization. By time, exhaustion of adsorption capacity and pore blocking disfavours the organic removal while biofilm formation appears to be favorable for the organic removal as biosorption/biodegradation increases.

Finally, in the case of BIEX resin, two mechanisms of ion exchange (in the primary and secondary IEX) and biosorption/biodegradation (mostly in the secondary IEX) contribute to the removal of organics from the influent water, with biodegradation showing a lesser contribution to this process.

7.6 Practical implementation of BIEX + GDM hybrid process

In this section, BIEX + GDM hybrid process is scaled up for a small and isolated community of 25 participants. According to Statistics Canada, mean daily residential water use per capita of the population served in 2021 in Quebec province was 257 L per person per day. Therefore, the total daily water use of this community is 6425 L/d. Given the best stabilized water flux of the

membranes achieved in this thesis is 6 LMH (144 LMD), total membrane area of approximately 45 m^2 is required. We can divide total 45 m^2 area to five sections of membranes with 9 m^2 area at each section. The total number of the required membranes are 500 (100 disk-shaped membranes with diameter of ~ 34 cm and 0.09 m^2 area in each section).

Regarding the BIEX section, considering 9637.5 L/d (1.5 × 6425 = 9637.5 L/d) required flowrate, EBCT of 15 min, total required BV of the resin would be approximately 100 L. This can be achieved using five BIEX resin columns with diameter of 5 inches filled with approximately 1.5 m with resin (each column flowrate and BV are ~ 1927.5 LPD and 20 L, respectively). The schematic of the BIEX + GDM pilot is represented in Figure 7-2.

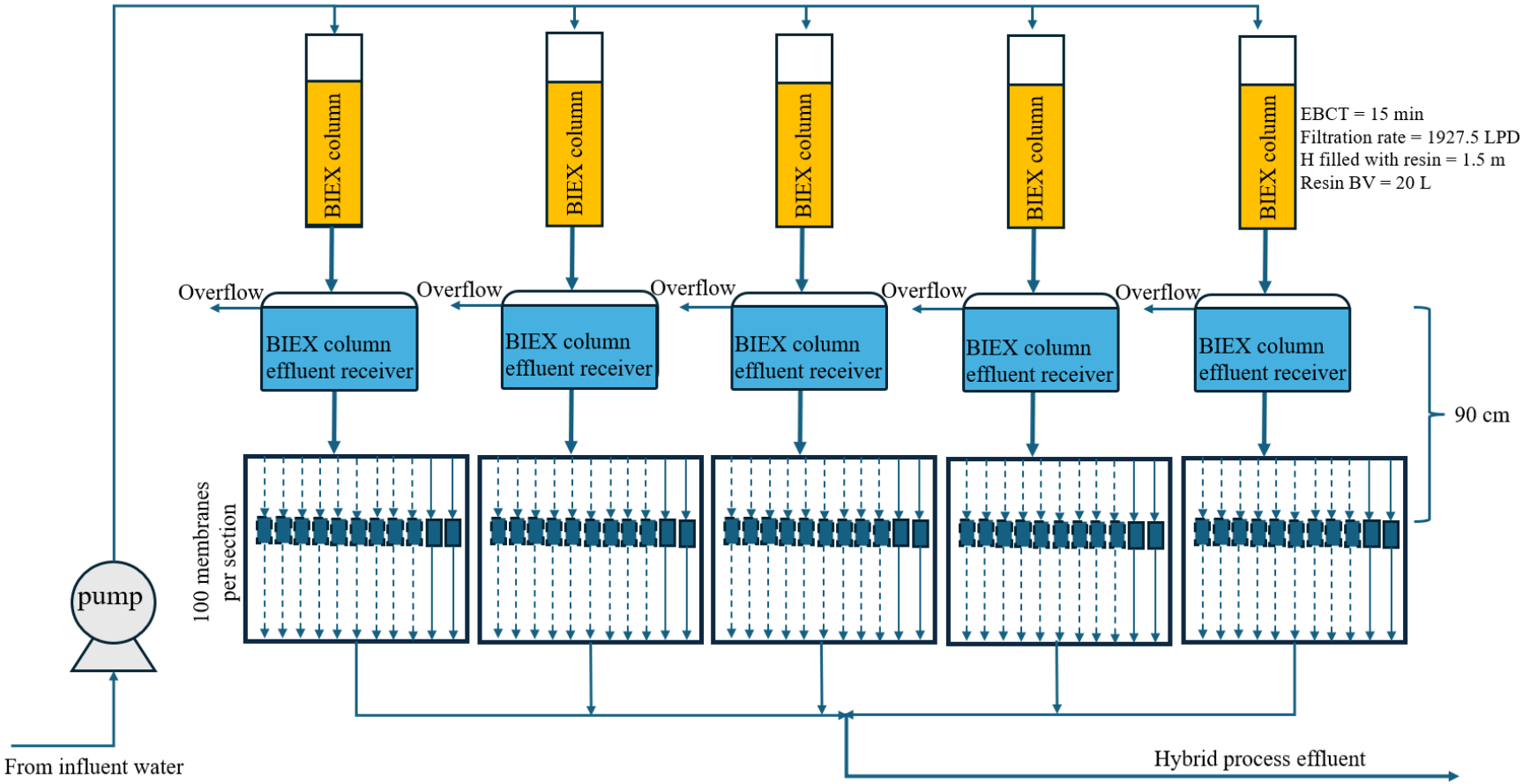

Figure 7-2. Design of the BIEX + GDM hybrid process for a small community consisting of 25 participants.

CHAPTER 8 CONCLUSIONS AND RECOMMENDATIONS

8.1 Conclusions

In the first objective of this research which was covered by paper 1, ceramic MF membranes with the different alumina and kaolin contents (M1 = 0 wt% alumina, M2 = 25 wt% alumina, M3 = 50 wt%) were produced in the laboratory. Then, they were utilized in the GDM process to filter Des Prairies River water which is considered as highly organic content and colored water. The aim was to evaluate the application of the lab-made membranes in the GDM process, investigate the effect of alumina content on the stabilized flux and effluent quality, and research the characteristics of biofouling layer on the membrane surface during long-term filtration. As expected, membranes showed a relatively high turbidity removal (stabilized permeate turbidity ~ 0.15 – 0.2 NTU) while stabilized permeate DOC showed a very low removal (maximum DOC removal ~ 6%). The stabilized process flux obtained 2.5 – 3.0 LMH and this remained unaffected by the alumina content. Pore blocking was the fouling mechanism before flux stabilization which was confirmed by modeling flux – time data and observation of distinct heterogeneous and scattered biofilm layer on the membrane surface. However, fouling mechanism changed from pore blocking model to cake formation layer by modeling flux – time data and observing dense biofouling layer on the membrane surface. The results indicated an increased biofouling layer biological activity and mean biofilm thickness for the membrane with the enhanced adsorption capacity which is associated with the highest alumina content (M3).

In the second objective of the research (paper 2), BIEX resin filtration pre-treatment was introduced to the same GDCM as in objective 1 (with the same operating conditions and ceramic membrane types) to increase the stabilized flux, organic removal, and sustainability of the process. The results of the hybrid BIEX + GDCM process were compared to those of GDCM process without BIEX pre-treatment (objective 1) in terms of stabilized flux, permeate quality, and biofilm characteristics. The results showed a DOC removal of 74% by the BIEX resin column compared to the influent water. Further 27% DOC removal was achieved by M3 when compared to BIEX resin column effluent. The overall DOC removal achieved in the hybrid BIEX + GDCM process was substantially higher than that of the GDCM process without BIEX process (~ 6%). The best effluent turbidity achieved in the GDCM process was 0.15 – 0.2 NTU while BIEX pre-treatment along with

GDCM process decreased the turbidity as low as 0.09 NTU. Moreover, the maximum stabilized flux by BIEX + GDCM hybrid process was approximately 5.7 LMH which is substantially higher than that of the GDCM process without BIEX process (~ 3 LMH). Regarding the biofilm characteristics, a reduced thickness and roughness in the hybrid process compared to those in GDCM without pre-treatment was observed. M3 (50% wt alumina), the membrane with the highest stabilized flux and optimal DOC removal efficiency, displayed elevated EPS concentration and biological activity. These results indicate that the hybrid approach, integrating BIEX and GDCM, is a robust, effective, and user-friendly method that enhances both flux and permeate quality in GDCM systems.

In the third objective which is shown in the paper 3, the impact of physical (air/water backwash with decreased and enhanced intensities) and chemical (NaOH 20 and 40mM; NaOCl 250 and 500 mg Cl_2/L) cleanings on the stabilized flux, flux recovery, different fouling types, and permeate quality of the polymeric (M1 = polymeric MF, M2 = polymeric UF) and ceramic (M3 = ceramic UF, and M4 = lab-made ceramic MF) membranes in the hybrid BIEX + GDM process have been studied. As the stabilized flux of all the tested membranes were approximately between 3.8 LMH and 5.2 LMH, we have concluded that the membrane material is not a key parameter to affect the stabilize flux. Polymeric membranes showed an increased average stabilized flux after the cleaning process. Nevertheless, ceramic membranes experienced a decrease or remained stable. Enhanced air/water backwash flow and pressure led to a greater elimination of hydraulic reversible fouling, identified as the predominant fouling type. Moreover, higher removal of hydraulic reversible fouling is obtained by ceramic membranes than that of polymeric membranes. Given the limited influence of chemical cleaning on flux recovery, it is advisable to exclusively utilize physical cleaning methods.

Overall, this thesis emphasizes the practicality and effectiveness of employing the BIEX + GDM hybrid method with ceramic kaolin/alumina-based membranes for more than two months of continuous operation. Notably, this combined approach consistently achieved over 81% DOC removal, keeping effluent DOC concentrations consistently below 2 mg C/L. Additionally, the permeate turbidity consistently stayed below 0.1 NTU, demonstrating the ability of the process to maintain exceptional water quality standards.

8.2 Recommendations for future work

Throughout this project, based on the obtained results and conclusions, new ideas for future research have emerged. It would be intriguing to:

- Exploring the synthesis of UF ceramic membranes incorporating kaolin/alumina composites to enhance organic matter and turbidity removal in the GDM process simultaneously.
- Producing ceramic membranes with alumina concentrations surpassing 50 wt% to assess whether elevating alumina content beyond this threshold positively influences flux rates and permeate quality, thereby either validating or refuting this hypothesis.
- Changing the operational parameters such as EBCT and filtration rate to examine their impact on organic removal performance, with the objective of identifying the optimal operating conditions.
- Continuing the BIEX + GDM hybrid process operation until reaching the secondary IEX exhaustion point to assess its performance on the subsequent GDM process.
- Developing a BIEX + GDM pilot system equipped with automated air and water backwash capabilities to facilitate regular backwashing intervals. This design aims to investigate whether the implementation of backwashing enhances flux rates and improves permeate quality over the course of operation.
- Studying performance of the hybrid BIEX + GDM process for the removal of micropollutants (e.g., pharmaceutical residues, microplastics, Nano-plastics, PFAS, etc.

REFERENCES

Akanbi, M., L. Hernandez, M. Mobarok, J. Veinot and N. Tufenkji (2018). "QCM-D and NanoTweezer measurements to characterize the effect of soil cellulase on the deposition of PEG-coated TiO 2 nanoparticles in model subsurface environments." Environmental Science: Nano **5**(9): 2172-2183.

Akhondi, E., B. Wu, S. Sun, B. Marxer, W. Lim, J. Gu, L. Liu, M. Burkhardt, D. McDougald and W. Pronk (2015). "Gravity-driven membrane filtration as pretreatment for seawater reverse osmosis: Linking biofouling layer morphology with flux stabilization." water research **70**: 158-173.

Alresheedi, M. T., B. Barbeau and O. D. Basu (2019). "Comparisons of NOM fouling and cleaning of ceramic and polymeric membranes during water treatment." Separation and Purification Technology **209**: 452-460.

Amini, N., I. Papineau, V. Storck, P. R. Bérubé, M. Mohseni and B. Barbeau (2018). "Long-term performance of biological ion exchange for the removal of natural organic matter and ammonia from surface waters." Water research **146**: 1-9.

Arias-Paic, M., K. M. Cawley, S. Byg and F. L. Rosario-Ortiz (2016). "Enhanced DOC removal using anion and cation ion exchange resins." Water Research **88**: 981-989.

Arkhangelsky, E., D. Kuzmenko and V. Gitis (2007). "Impact of chemical cleaning on properties and functioning of polyethersulfone membranes." Journal of Membrane Science **305**(1-2): 176-184.

Arora, M., H. Malano, B. Davidson, R. Nelson and B. George (2015). "Interactions between centralized and decentralized water systems in urban context: A review." Wiley Interdisciplinary Reviews: Water 2 **2**(6): 623-634.

Arumugham, T., N. J. Kaleekkal, S. Gopal, J. Nambikkattu, R. K, A. M. Aboulella, S. Ranil Wickramasinghe and F. Banat (2021). "Recent developments in porous ceramic membranes for wastewater treatment and desalination: A review." Journal of Environmental Management **293**: 112925.

Arzani, M., H. R. Mahdavi, O. Bakhtiari and T. Mohammadi (2016). "Preparation of mullite ceramic microfilter membranes using Response surface methodology based on central composite design." Ceramics International **42**(7): 8155-8164.

Bakke, R., R. Kommedal and S. Kalvenes (2001). "Quantification of biofilm accumulation by an optical approach." Journal of Microbiological Methods **44**(1): 13-26.

Bodzek, M. and K. Konieczny (1998). "Comparison of various membrane types and module configurations in the treatment of natural water by means of low-pressure membrane methods." Separation and Purification Technology **14**(1): 69-78.

Boyer, T. H., P. C. Singer, G. R. J. E. s. Aiken and technology (2008). "Removal of dissolved organic matter by anion exchange: effect of dissolved organic matter properties." Environmental Science & Technology **42**(19): 7431-7437.

Capodaglio, A. G., A. Callegari, D. Cecconet and D. Molognoni (2017). "Sustainability of decentralized wastewater treatment technologies." Water Practice and Technology **12**(2): 463-477.

Catalán, N., J. Casas-Ruiz, D. Von Schiller, L. Proia, B. Obrador, E. Zwirnmann and R. J. J. o. G. R. B. Marcé (2017). "Biodegradation kinetics of dissolved organic matter chromatographic fractions in an intermittent river." Journal of Geophysical Research: Biogeosciences **122**(1): 131-144.

Chawla, C., A. Zwijnenburg, A. Kemperman and K. Nijmeijer (2017). "Fouling in gravity driven Point-of-Use drinking water treatment systems." Chemical Engineering Journal **319**: 89-97.

Derlon, N., N. Koch, B. Eugster, T. Posch, J. Pernthaler, W. Pronk and E. Morgenroth (2013). "Activity of metazoa governs biofilm structure formation and enhances permeate flux during Gravity-Driven Membrane (GDM) filtration." Water research **47**(6): 2085-2095.

Derlon, N., J. Mimoso, T. Klein, S. Koetzsch and E. Morgenroth (2014). "Presence of biofilms on ultrafiltration membrane surfaces increases the quality of permeate produced during ultra-low pressure gravity-driven membrane filtration." Water research **60**: 164-173.

Derlon, N., M. Peter-Varbanets, A. Scheidegger, W. Pronk and E. Morgenroth (2012). "Predation influences the structure of biofilm developed on ultrafiltration membranes." Water research **46**(10): 3323-3333.

Desmond, P., J. P. Best, E. Morgenroth and N. Derlon (2018). "Linking composition of extracellular polymeric substances (EPS) to the physical structure and hydraulic resistance of membrane biofilms." Water Research **132**: 211-221.

Ding, A., H. Liang, G. Li, N. Derlon, I. Szivak, E. Morgenroth and W. Pronk (2016). "Impact of aeration shear stress on permeate flux and fouling layer properties in a low pressure membrane bioreactor for the treatment of grey water." Journal of Membrane Science **510**: 382-390.

Ding, A., H. Liang, G. Li, I. Szivak, J. Traber and W. Pronk (2017). "A low energy gravity-driven membrane bioreactor system for grey water treatment: Permeability and removal performance of organics." Journal of Membrane Science **542**: 408-417.

Ding, A., R. Song, H. Cui, H. Cao, H. H. Ngo, H. Chang, J. Nan, G. Li and J. Ma (2021). "Presence of powdered activated carbon/zeolite layer on the performances of gravity-driven membrane (GDM) system for drinking water treatment: Ammonia removal and flux stabilization." Science of The Total Environment **799**: 149415.

Ding, A., J. Wang, D. Lin, X. Cheng, H. Wang, L. Bai, N. Ren, G. Li, H. Liang and Technology (2018). "Effect of PAC particle layer on the performance of gravity-driven membrane filtration (GDM) system during rainwater treatment." Environmental Science: Water Research & Technology **4**(1): 48-57.

Ding, A., J. Wang, D. Lin, X. Tang, X. Cheng, G. Li, N. Ren and H. Liang (2017). "In situ coagulation versus pre-coagulation for gravity-driven membrane bioreactor during

decentralized sewage treatment: Permeability stabilization, fouling layer formation and biological activity." Water Research **126**: 197-207.

Ding, A., J. Wang, D. Lin, X. Tang, X. Cheng, H. Wang, L. Bai, G. Li and H. Liang (2017). "A low pressure gravity-driven membrane filtration (GDM) system for rainwater recycling: Flux stabilization and removal performance." Chemosphere **172**: 21-28.

Ding, A., J. Wang, D. Lin, R. Zeng, S. Yu, Z. Gan, N. Ren, G. Li and H. Liang (2018). "Effects of GAC layer on the performance of gravity-driven membrane filtration (GDM) system for rainwater recycling." Chemosphere **191**: 253-261.

Discart, V., M. Bilad, L. Marbelia and I. Vankelecom (2014). "Impact of changes in broth composition on Chlorella vulgaris cultivation in a membrane photobioreactor (MPBR) with permeate recycle." Bioresource technology **152**: 321-328.

Dixon, M. C. (2008). "Quartz crystal microbalance with dissipation monitoring: enabling real-time characterization of biological materials and their interactions." Journal of biomolecular techniques: JBT **19**(3): 151.

Do, V. T., C. Y. Tang, M. Reinhard and J. O. Leckie (2012). "Degradation of polyamide nanofiltration and reverse osmosis membranes by hypochlorite." Environmental science & technology **46**(2): 852-859.

Do, V. T., C. Y. Tang, M. Reinhard and J. O. Leckie (2012). "Effects of chlorine exposure conditions on physiochemical properties and performance of a polyamide membrane・Mechanisms and implications." Environmental science & technology **46**(24): 13184-13192.

Drexler, W. and J. G. Fujimoto (2008). Optical coherence tomography: technology and applications, Springer Science & Business Media.

Du, X., Y. Liu, R. Ma, M. Xiao, W. Yang, X. Han, Y. Luo, Z. Wang and H. Liang (2021). "Gravity-driven ceramic membrane (GDCM) filtration treating manganese-contaminated surface water: Effects of ozone (O3)-aided pre-coating and membrane pore size." Chemosphere **279**: 130603.

Dubois, M., K. A. Gilles, J. K. Hamilton, P. t. Rebers and F. J. A. c. Smith (1956). "Colorimetric method for determination of sugars and related substances." Analytical chemistry **28**(3): 350-356.

Edgar, M. and T. H. Boyer (2022). "Nitrate adsorption and desorption during biological ion exchange." Separation and Purification Technology **285**: 120363.

Fane, A., R. Wang and Y. Jia (2011). "Membrane technology: past, present and future." Membrane and desalination technologies: 1-45.

Fortunato, L., L. Ranieri, V. Naddeo and T. Leiknes (2020). "Fouling control in a gravity-driven membrane (GDM) bioreactor treating primary wastewater by using relaxation and/or air scouring." Journal of Membrane Science **610**: 118261.

Frechen, F.-B., H. Exler, J. Romaker and W. Schier (2011). "Long-term behaviour of a gravity-driven dead end membrane filtration unit for potable water supply in cases of disasters." Water Science and Technology: Water Supply **11**(1): 39-44.

Freeman, S. and H. Shorney-Darby (2011). "What's the Buzz About Ceramic Membranes?" Journal-American Water Works Association **103**(12): 12-13.

Graves, P. and D. Gardiner (1989). "Practical raman spectroscopy." Springer.

Green, M., A. Mels and O. Lahav (1996). "Biological-ion exchange process for ammonium removal from secondary effluent." Water Science and Technology **34**(1): 449-458.

Guerra, K. and J. Pellegrino (2013). "Development of a Techno-Economic Model to Compare Ceramic and Polymeric Membranes." Separation Science and Technology **48**(1): 51-65.

Gul, A., J. Hruza and F. Yalcinkaya (2021). "Fouling and Chemical Cleaning of Microfiltration Membranes: A Mini-Review." Polymers (Basel) **13**(6).

Hafeez, A., Z. Shamair, N. Shezad, F. Javed, T. Fazal, S. u. Rehman, A. A. Bazmi and F. Rehman (2021). "Solar powered decentralized water systems: A cleaner solution of the industrial wastewater treatment and clean drinking water supply challenges." Journal of Cleaner Production **289**: 125717.

Hermia, J. (1982). "Constant pressure blocking filtration laws: application to power-law non-Newtonian fluids."

Hernández, M. F., M. A. Violini, M. F. Serra, M. S. Conconi, G. Suarez and N. Rendtorff (2020). "Boric acid (H 3 BO 3) as flux agent of clay-based ceramics, B 2 O 3 effect in clay thermal behavior and resultant ceramics properties." Journal of Thermal Analysis and Calorimetry **139**: 1717-1729.

Hofs, B., J. Ogier, D. Vries, E. F. Beerendonk and E. R. Cornelissen (2011). "Comparison of ceramic and polymeric membrane permeability and fouling using surface water." Separation and Purification Technology **79**(3): 365-374.

Hubadillah, S. K., M. H. D. Othman, T. Matsuura, A. Ismail, M. A. Rahman, Z. Harun, J. Jaafar and M. Nomura (2018). "Fabrications and applications of low cost ceramic membrane from kaolin: A comprehensive review." Ceramics International **44**(5): 4538-4560.

Huber, S. A., A. Balz, M. Abert and W. Pronk (2011). "Characterisation of aquatic humic and non-humic matter with size-exclusion chromatography – organic carbon detection – organic nitrogen detection (LC-OCD-OND)." Water Research **45**(2): 879-885.

Humbert, H., H. Gallard, H. Suty and J.-P. Croué (2005). "Performance of selected anion exchange resins for the treatment of a high DOC content surface water." Water Research **39**(9): 1699-1708.

Issaoui, M. and L. Limousy (2019). "Low-cost ceramic membranes: Synthesis, classifications, and applications." Comptes Rendus Chimie **22**(2-3): 175-187.

Jabornig, S. and S. M. Podmirseg (2015). "A novel fixed fibre biofilm membrane process for on-site greywater reclamation requiring no fouling control." Biotechnology and bioengineering **112**(3): 484-493.

Jarvis, P., I. Carra, M. Jafari and S. J. Judd (2022). "Ceramic vs polymeric membrane implementation for potable water treatment." Water Research **215**: 118269.

Jiang, H., Q. Zhao, P. Wang, J. Ma and X. Zhai (2019). "Improved separation and antifouling properties of PVDF gravity-driven membranes by blending with amphiphilic multi-arms polymer PPG-Si-PEG." Journal of Membrane Science **588**: 117148.

Jiang, Y., Y. Shang, T. Gong, Z. Hu, K. Yang and S. J. C. Shao (2020). "High concentration of Mn2+ has multiple influences on aerobic granular sludge for aniline wastewater treatment." Chemosphere **240**: 124945.

Klein, T., D. Zihlmann, N. Derlon, C. Isaacson, I. Szivak, D. G. Weissbrodt and W. Pronk (2016). "Biological control of biofilms on membranes by metazoans." Water research **88**: 20-29.

Klomfas, G. and K. Konieczny (2004). "Fouling phenomena in unit and hybrid processes for potable water treatment." Desalination **163**(1): 311-322.

Kook, H. and C. Park (2022). "Engineered approaches to facile identification of tiny microplastics in polymeric and ceramic membrane filtrations for wastewater treatment." Membranes **12**(6): 565.

Kotobuki, M., Q. Gu, L. Zhang and J. Wang (2021). "Ceramic-Polymer Composite Membranes for Water and Wastewater Treatment: Bridging the Big Gap between Ceramics and Polymers." Molecules **26**(11): 3331.

Krzeminski, P., C. Vogelsang, T. Meyn, S. J. Köhler, H. Poutanen, H. A. de Wit and W. Uhl (2019). "Natural organic matter fractions and their removal in full-scale drinking water treatment under cold climate conditions in Nordic capitals." Journal of Environmental Management **241**: 427-438.

Kurth, C. J., B. L. Wise and S. Smith (2018). "Design considerations for implementing ceramics in new and existing polymeric UF systems." Water Practice and Technology **13**(4): 725-737.

Kus, B., J. Kandasamy, S. Vigneswaran, H. Shon and G. Moody (2013). "Gravity driven membrane filtration system to improve the water quality in rainwater tanks." Water Science and Technology: Water Supply **13**(2): 479-485.

Lapointe, M., J. M. Farner, L. M. Hernandez and N. Tufenkji (2020). "Understanding and improving microplastic removal during water treatment: impact of coagulation and flocculation." Environmental science & technology **54**(14): 8719-8727.

Lee, D., Y. Lee, S. S. Choi, S.-H. Lee, K.-W. Kim and Y. Lee (2019). "Effect of membrane property and feed water organic matter quality on long-term performance of the gravity-driven membrane filtration process." Environmental Science and Pollution Research **26**: 1152-1162.

Lee, M., Z. Wu and K. Li (2015). Advances in ceramic membranes for water treatment. Advances in membrane technologies for water treatment, Elsevier**:** 43-82.

Lee, S.-J., M. Dilaver, P.-K. Park and J.-H. Kim (2013). "Comparative analysis of fouling characteristics of ceramic and polymeric microfiltration membranes using filtration models." Journal of Membrane Science **432**: 97-105.

Lee, S.-J. and J.-H. Kim (2014). "Differential natural organic matter fouling of ceramic versus polymeric ultrafiltration membranes." Water Research **48**: 43-51.

Lee, S., G. O. Badoux, B. Wu and T. H. Chong (2021). "Enhancing performance of biocarriers facilitated gravity-driven membrane (GDM) reactor for decentralized wastewater treatment: Effect of internal recirculation and membrane packing density." Science of The Total Environment **762**: 144104.

Lee, S., C. Risold, N. Landolt, S. Hube, M. Burkhardt, B. Wu and T. H. Chong (2023). "Gravity-driven membrane reactor for decentralized wastewater treatment: Comparison of reactor configuration and membrane module." Journal of Water Process Engineering **54**: 104055.

Lee, S., S. R. Suwarno, B. W. H. Quek, L. Kim, B. Wu and T. H. Chong (2019). "A comparison of gravity-driven membrane (GDM) reactor and biofiltration + GDM reactor for seawater reverse osmosis desalination pretreatment." Water Research **154**: 72-83.

Lee, Y., J.-H. Noh, J.-W. Park, S.-W. Yoon, S.-Y. Kim, H. J. Son, W. Lee and S. K. Maeng (2023). "Integrating biological ion exchange with biological activated carbon treatment for drinking water: A novel approach for NOM removal, trihalomethane formation potential, and biological stability." Water Research **245**: 120598.

Li, C., W. Sun, Z. Lu, X. Ao and S. Li (2020). "Ceramic nanocomposite membranes and membrane fouling: A review." Water Research **175**: 115674.

Liu, Z., K. M. Lompe, M. Mohseni, P. R. Bérubé, S. Sauvé and B. Barbeau (2020). "Biological ion exchange as an alternative to biological activated carbon for drinking water treatment." Water Research **168**: 115148.

Liu, Z., I. Papineau, M. Mohseni, S. Peldszus, P. R. Bérubé, S. Sauvé, B. J. A. E. Barbeau and T. Water (2021). "Operating bicarbonate-form versus chloride-form ion exchange resins without regeneration for natural organic matter removal." ACS ES&T Water **1**(6): 1456-1463.

Liu, Z., M. Solliec, I. Papineau, K. M. Lompe, M. Mohseni, P. R. Bérubé, S. Sauvé and B. Barbeau (2022). "Elucidating the removal of organic micropollutants on biological ion exchange resins." Science of The Total Environment **808**: 152137.

Lourenço, N. and L. M. Nunes (2020). "Review of Dry and Wet Decentralized Sanitation Technologies for Rural Areas: Applicability, Challenges and Opportunities." Environmental Management **65**(5): 642-664.

Maltais-Tariant, R., C. Boudoux and N. Uribe-Patarroyo (2020). "Real-time co-localized OCT surveillance of laser therapy using motion corrected speckle decorrelation." Biomedical Optics Express **11**(6): 2925-2950.

Maniam, G., N. A. Zakaria, C. P. Leo, V. Vassilev, K. B. Blay, K. Behzadian and P. E. Poh (2022). "An assessment of technological development and applications of decentralized water

reuse: A critical review and conceptual framework." Wiley Interdisciplinary Reviews: Water **9**(3): e1588.

Martin, K., D. Bolster, N. Derlon, E. Morgenroth and R. Nerenberg (2014). "Effect of fouling layer spatial distribution on permeate flux: a theoretical and experimental study." Journal of membrane science **471**: 130-137.

McAdam, E. J. and S. J. Judd (2008). "Biological treatment of ion-exchange brine regenerant for re-use: A review." Separation and Purification Technology **62**(2): 264-272.

Meng, F., S. Zhang, Y. Oh, Z. Zhou, H.-S. Shin and S.-R. Chae (2017). "Fouling in membrane bioreactors: An updated review." Water Research **114**: 151-180.

Metze, F. K., S. Sant, Z. Meng, H.-A. Klok and K. Kaur (2023). "Swelling-Activated, Soft Mechanochemistry in Polymer Materials." Langmuir **39**(10): 3546-3557.

Moulin, C., M. M. Bourbigot, A. Tazi-Pain and F. Bourdon (1991). "Design and performance of membrane filtration installations: Capacity and product quality for drinking water applications." Environmental Technology **12**(10): 841-858.

Murić, A., I. Petrinić and M. L. Christensen (2014). "Comparison of ceramic and polymeric ultrafiltration membranes for treating wastewater from metalworking industry." Chemical Engineering Journal **255**: 403-410.

Ødegaard, H., S. Østerhus, E. Melin, B. J. D. W. E. Eikebrokk and Science (2010). "NOM removal technologies–Norwegian experiences." Drinking Water Engineering and Science **3**(1): 1-9.

Oka, P., N. Khadem and P. Bérubé (2017). "Operation of passive membrane systems for drinking water treatment." Water research **115**: 287-296.

Oligny, L., P. R. Bérubé and B. Barbeau (2016). "Impact of PAC Fines in Fouling of Polymeric and Ceramic Low-Pressure Membranes for Drinking Water Treatment." Membranes **6**(3): 38.

Omarova, A., K. Tussupova, P. Hjorth, M. Kalishev and R. Dosmagambetova (2019). "Water Supply Challenges in Rural Areas: A Case Study from Central Kazakhstan." Int J Environ Res Public Health **16**(5).

Park, S., J.-S. Kang, J. J. Lee, T.-K.-Q. Vo and H.-S. Kim (2018). "Application of physical and chemical enhanced backwashing to reduce membrane fouling in the water treatment process using ceramic membranes." Membranes **8**(4): 110.

Peter-Varbanets, M., F. Hammes, M. Vital and W. Pronk (2010). "Stabilization of flux during dead-end ultra-low pressure ultrafiltration." Water Research **44**(12): 3607-3616.

Peter-Varbanets, M., J. Margot, J. Traber and W. Pronk (2011). "Mechanisms of membrane fouling during ultra-low pressure ultrafiltration." Journal of Membrane Science **377**(1-2): 42-53.

Pronk, W., A. Ding, E. Morgenroth, N. Derlon, P. Desmond, M. Burkhardt, B. Wu and A. G. Fane (2019). "Gravity-driven membrane filtration for water and wastewater treatment: a review." Water research **149**: 553-565.

Rashad, M., G. Logesh, U. Sabu and M. Balasubramanian (2021). "A novel monolithic mullite microfiltration membrane for oil-in-water emulsion separation." Journal of Membrane Science **620**: 118857.

Rasouli, Y., M. Abbasi and S. A. Hashemifard (2017). "Investigation of in-line coagulation-MF hybrid process for oily wastewater treatment by using novel ceramic membranes." Journal of Cleaner Production **161**: 545-559.

Rasouli, Y., M. Abbasi and S. A. Hashemifard (2019). "Fabrication, characterization, fouling behavior and performance study of ceramic microfiltration membranes for oily wastewater treatment." Journal of Asian Ceramic Societies **7**(4): 476-495.

Rasouli, Y., R. Maltais-Tariant, B. Barbeau, M. Lapointe, C. Boudoux and D. Claveau-Mallet (2023). "Synthesis, characterization, and application of gravity-driven ceramic microfiltration membranes for surface water treatment." Journal of Water Process Engineering **51**: 103430.

Rasouli, Y., R. Maltais-Tariant, B. Barbeau, S. Peldszus, C. Boudoux and D. Claveau-Mallet (2023). "Performance of Biological Ion Exchange Resin and Gravity-Driven Ceramic Membrane Hybrid Process for Surface Water Treatment." Separation and Purification Technology: 125769.

Rook, J. J. and R. JJ (1974). "Formation of haloforms during chlorination of natural waters."

Sadrnourmohamadi, M. and B. Gorczyca (2015). "Removal of Dissolved Organic Carbon (DOC) from High DOC and Hardness Water by Chemical Coagulation: Relative Importance of Monomeric, Polymeric, and Colloidal Aluminum Species." Separation Science and Technology **50**(13): 2075-2085.

Samaei, S. M., S. Gato-Trinidad and A. Altaee (2018). "The application of pressure-driven ceramic membrane technology for the treatment of industrial wastewaters – A review." Separation and Purification Technology **200**: 198-220.

Sauerbrey, G. n. (1959). "Use of quartz crystal units for weighing thin films and microweighing." Magzine for Physics **155**(2): 206-222.

Schulz, M., J. Winter, H. Wray, B. Barbeau and P. Bérubé (2017). "Biologically active ion exchange (BIEX) for NOM removal and membrane fouling prevention." Water Science and Technology: Water Supply **17**(4): 1178-1184.

Shao, S., Y. Feng, H. Yu, J. Li, G. Li and H. Liang (2017). "Presence of an adsorbent cake layer improves the performance of gravity-driven membrane (GDM) filtration system." Water research **108**: 240-249.

Shao, S., D. Shi, Y. Li, Y. Liu, Z. Lu, Z. Fang and H. J. C. Liang (2019). "Effects of water temperature and light intensity on the performance of gravity-driven membrane system." Chemosphere **216**: 324-330.

Shi, D., Y. Liu, W. Fu, J. Li, Z. Fang and S. Shao (2020). "A combination of membrane relaxation and shear stress significantly improve the flux of gravity-driven membrane system." Water Research **175**: 115694.

Singh, N. K., A. A. Kazmi and M. Starkl (2014). "A review on full-scale decentralized wastewater treatment systems: techno-economical approach." Water Science and Technology **71**(4): 468-478.

Stoffel, D., N. Derlon, J. Traber, C. Staaks, M. Heijnen, E. Morgenroth and C. Jacquin (2023). "Gravity-driven membrane filtration with compact second-life modules daily backwashed: An alternative to conventional ultrafiltration for centralized facilities." Water Res X **18**: 100178.

Stolov, M. and V. Freger (2019). "Degradation of polyamide membranes exposed to chlorine: an impedance spectroscopy study." Environmental science & technology **53**(5): 2618-2625.

Stoquart, C., B. Barbeau, P. Servais and G. A. Vázquez-Rodríguez (2013). "Quantifying bacterial biomass fixed onto biological activated carbon (PAC and GAC) used in drinking water treatment." Journal of Water Supply: Research and Technology-Aqua **63**(1): 1-11.

Tang, X., A. Ding, W. Pronk, C. Ziemba, X. Cheng, J. Wang, J. Xing, B. Xie, G. Li and H. Liang (2018). "Biological pre-treatments enhance gravity-driven membrane filtration for the decentralized water supply: Linking extracellular polymeric substances formation to flux stabilization." Journal of Cleaner Production **197**: 721-731.

Tang, X., A. Ding, F. Qu, R. Jia, H. Chang, X. Cheng, B. Liu, G. Li and H. Liang (2016). "Effect of operation parameters on the flux stabilization of gravity-driven membrane (GDM) filtration system for decentralized water supply." Environmental Science and Pollution Research **23**(16): 16771-16780.

Truttmann, L., Y. Su, S. Lee, M. Burkhardt, S. Brynjólfsson, T. H. Chong and B. Wu (2020). "Gravity-driven membrane (GDM) filtration of algae-polluted surface water." Journal of Water Process Engineering **36**: 101257.

USEPA (2001). Guidance Manual for Compliance with the Surface Water Treatment Rules: Turbidity Provisions

Vieira, M. and L. F. Melo (1995). Effect of clay particles on the behaviour of biofilms formed by Pseudomonas fluorescens, Elsevier. **32:** 45-52.

Wang, Y., L. Fortunato, S. Jeong and T. Leiknes (2017). "Gravity-driven membrane system for secondary wastewater effluent treatment: Filtration performance and fouling characterization." Separation and Purification Technology **184**: 26-33.

Winter, J., H. E. Wray, M. Schulz, R. Vortisch, B. Barbeau and P. R. Bérubé (2018). "The impact of loading approach and biological activity on NOM removal by ion exchange resins." Water Research **134**: 301-310.

Wu, B., T. Christen, H. S. Tan, F. Hochstrasser, S. R. Suwarno, X. Liu, T. H. Chong, M. Burkhardt, W. Pronk and A. G. Fane (2017). "Improved performance of gravity-driven membrane filtration for seawater pretreatment: Implications of membrane module configuration." Water research **114**: 59-68.

Wu, B., F. Hochstrasser, E. Akhondi, N. Ambauen, L. Tschirren, M. Burkhardt, A. G. Fane and W. Pronk (2016). "Optimization of gravity-driven membrane (GDM) filtration process for seawater pretreatment." Water Research **93**: 133-140.

Wu, B., S. R. Suwarno, H. S. Tan, L. H. Kim, F. Hochstrasser, T. H. Chong, M. Burkhardt, W. Pronk and A. G. Fane (2017). "Gravity-driven microfiltration pretreatment for reverse osmosis (RO) seawater desalination: Microbial community characterization and RO performance." Desalination **418**: 1-8.

Wu, Q., C. Chen, Y. Zhang, P. Tang, X. Ren, J. Shu, X. Liu, X. Cheng, A. Tiraferri and B. Liu (2023). "Safe purification of rural drinking water by biological aerated filter coupled with ultrafiltration." Science of The Total Environment **868**: 161632.

Zhang, X., W.-Z. Lang, H.-P. Xu, X. Yan and Y.-J. Guo (2015). "The effects of hydroxyapatite nano whiskers and its synergism with polyvinylpyrrolidone on poly (vinylidene fluoride) hollow fiber ultrafiltration membranes." RSC Advances **5**(28): 21532-21543.

Zhang, Y., H. Wang, Y. Li, B. Wang, J. Huang, S. Deng, G. Yu and Y. Wang (2020). "Removal of micropollutants by an electrochemically driven UV/chlorine process for decentralized water treatment." Water Research **183**: 116115.

Zhao, Y.-y., X.-m. Wang, H.-w. Yang and F. X. Yue-feng (2018). "Effects of organic fouling and cleaning on the retention of pharmaceutically active compounds by ceramic nanofiltration membranes." Journal of membrane science **563**: 734-742.

Zimmermann, K., S. Li and M. Mohseni (2022). "Biological Activity Offsets Diffusion Limitations of Biofilms in Biological Ion Exchange Water Filters." ACS ES&T Water **2**(12): 2441-2449.

APPENDIX A SYNTHESIS, CHARACTERIZATION, AND APPLICATION OF GRAVITY-DRIVEN CERAMIC MICROFILTRATION MEMBRANES FOR SURFACE WATER TREATMENT

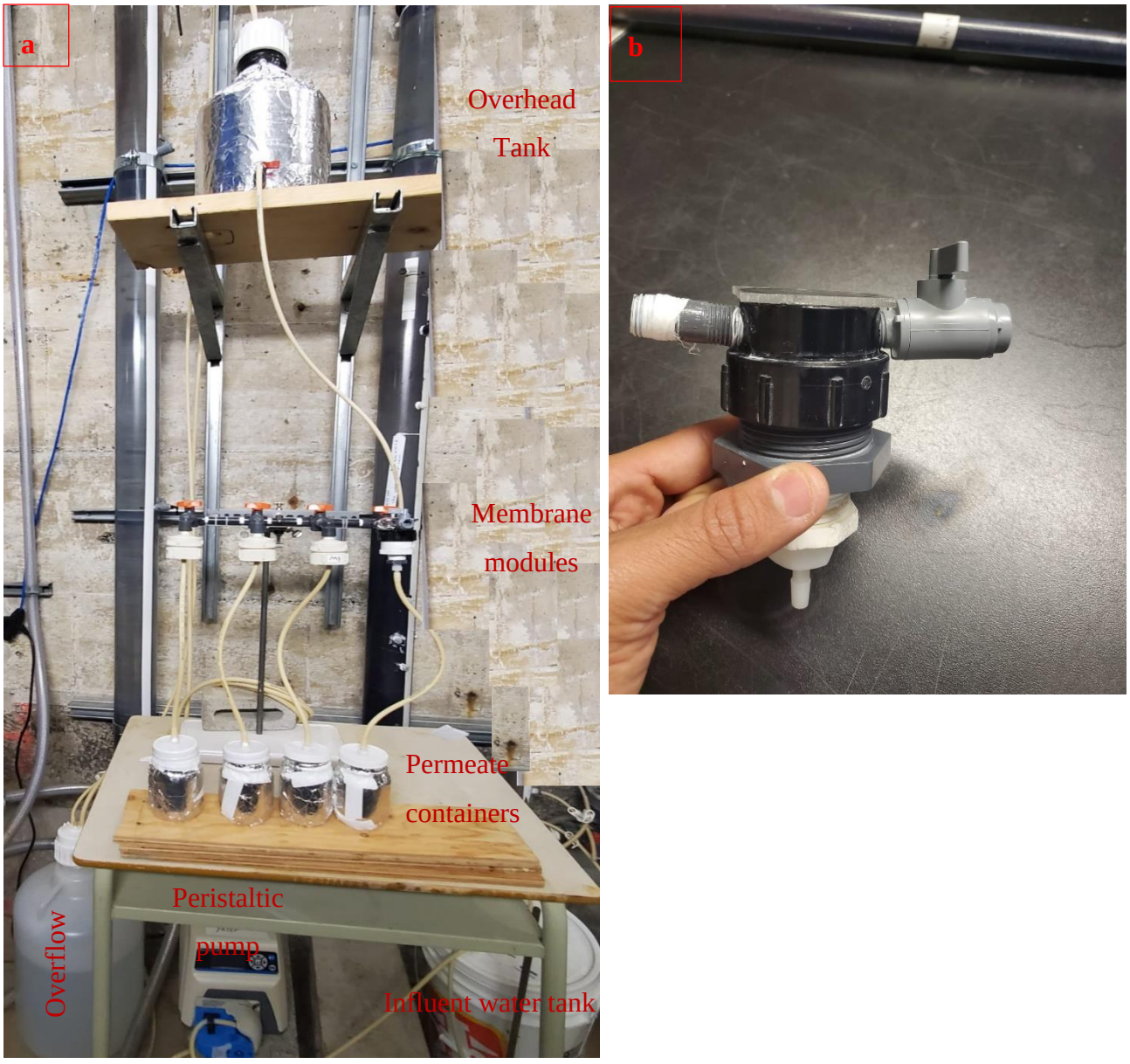

Figure A.1 Photo of the a) filtration setup b) a membrane module

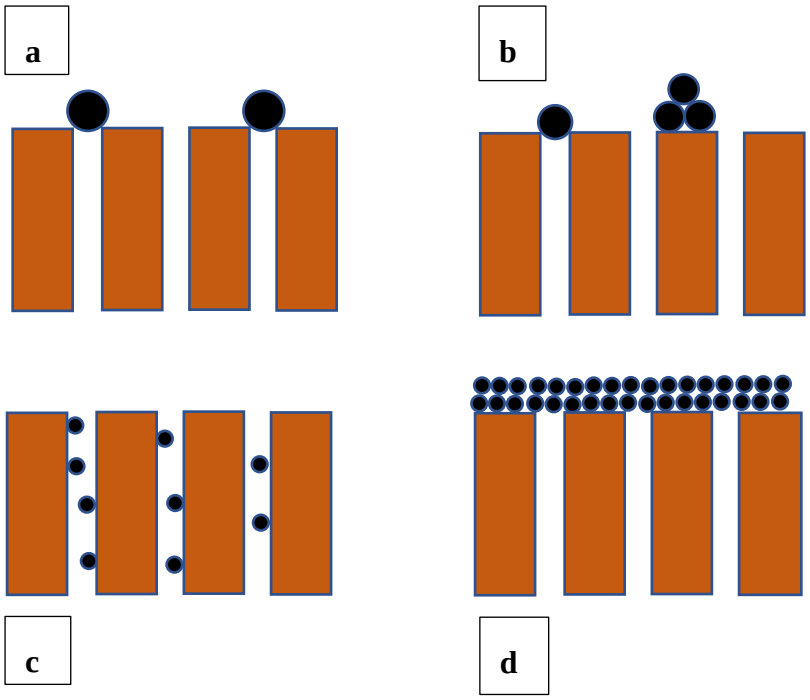

Figure A.2 Schematic representation of blocking mechanisms: a) complete pore blocking, b) intermediate blocking, c) standard blocking, and d) cake layer formation

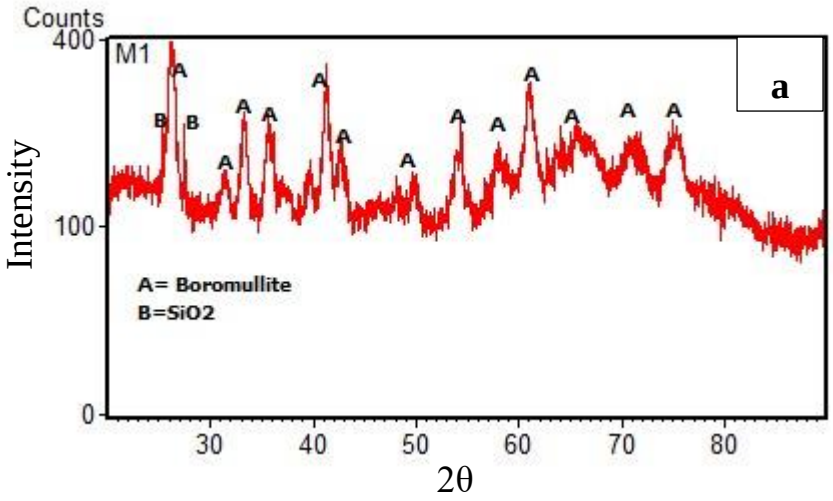
Counts
M1
a
Intensity
A= Boromullite
B=SiO2
2θ

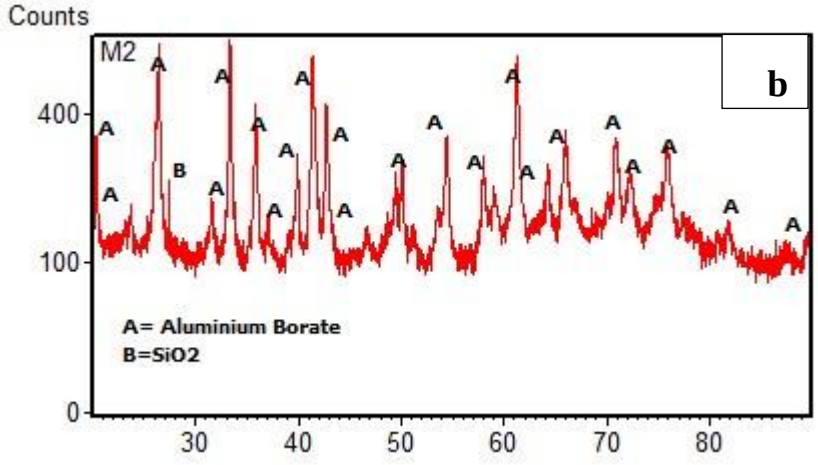
Counts
M2
b
A= Aluminium Borate
B=SiO2

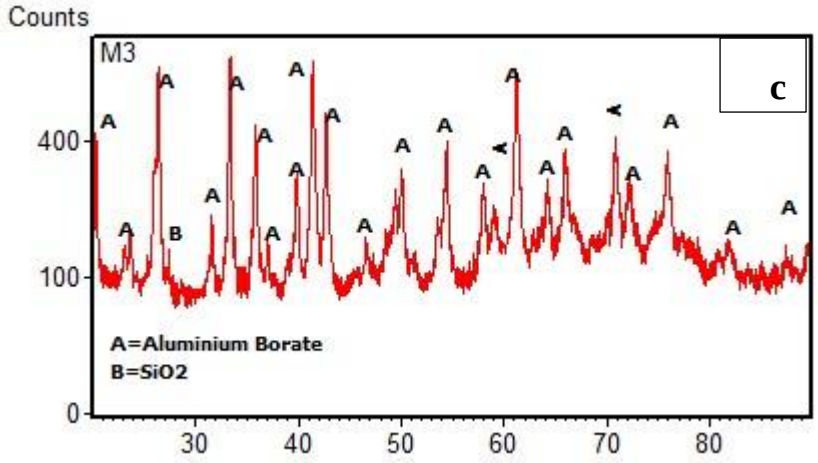
Counts
M3
c
A=Aluminium Borate
B=SiO2

Figure A.3 XRD patterns of M1 (kaolin only), M2 (75 Wt% kaolin + 25 Wt% alumina), and M3 (50 Wt% kaolin + 50 Wt% alumina)

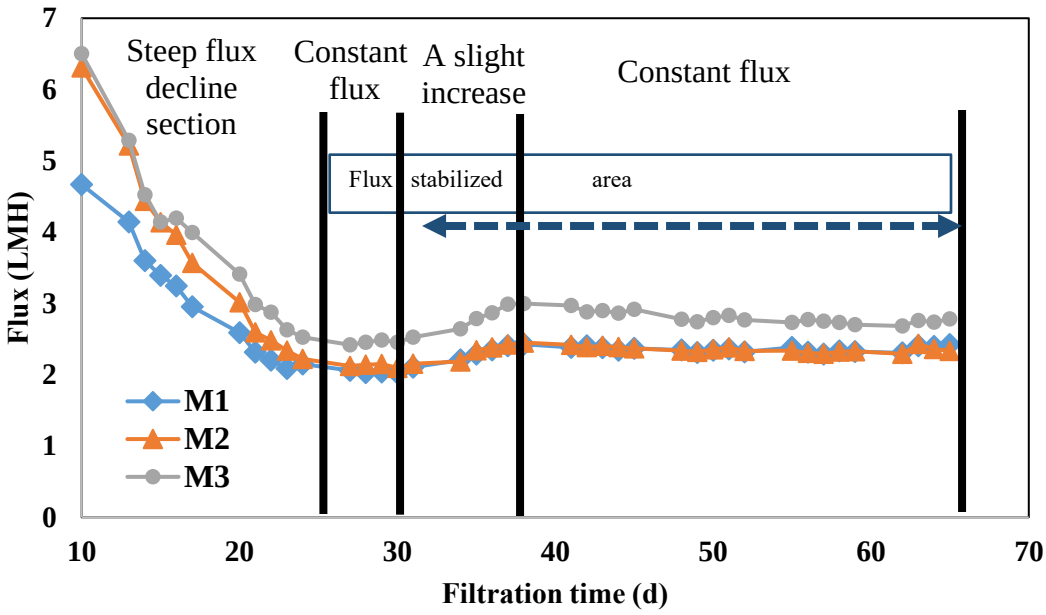

Figure A.4 Zoomed version of Flux-time diagram as shown in Figure 4-4 of the manuscript. Four stages of flux and flux stabilization time are presented in the figure.

Table A.1 Hermia's models (Hermia 1982) to investigate the fouling mechanism

Model name	n	Equation
Cake layer formation	0	$\frac{1}{J_p{}^2} = \frac{1}{J_0{}^2} + K_{gl}\, t$
Intermediate pore blocking	1	$\frac{1}{J_p} = \frac{1}{J_0} + K_i\, t$
Standard pore blocking	1.5	$\frac{1}{\sqrt{J_p}} = \frac{1}{\sqrt{J_0}} + K_s\, t$
Complete pore blocking	2	$Ln\, J_p = Ln\, J_0 - K_C\, t$

Table A.2 Percentage of errors between experimental and modeled fluxes

Membrane type	Cake layer formation model	Intermediate pore blocking model	Standard pore blocking model	Complete pore blocking model
M1	24.36	20.22	17.89	15.17
M2	33.46	23.36	14.45	5.30
M3	33.17	13.33	20.60	89.49

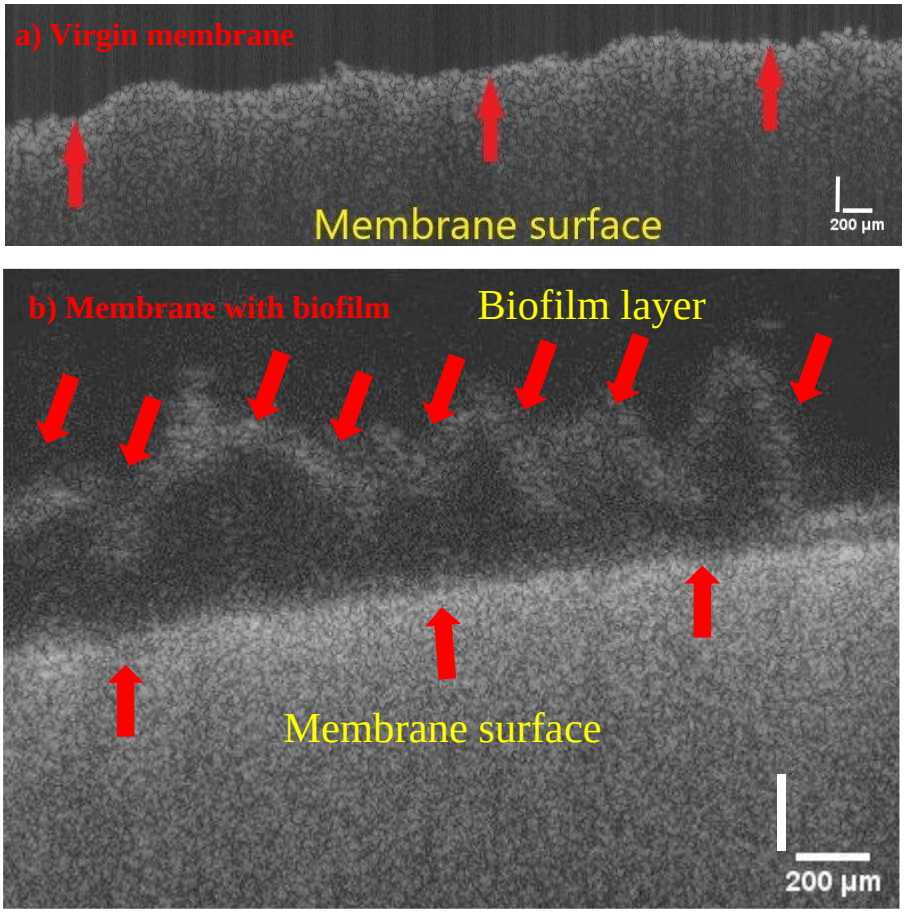

Figure A.5 OCT images of a) a virgin membrane surface and b) a membrane with biofilm formed on its surface

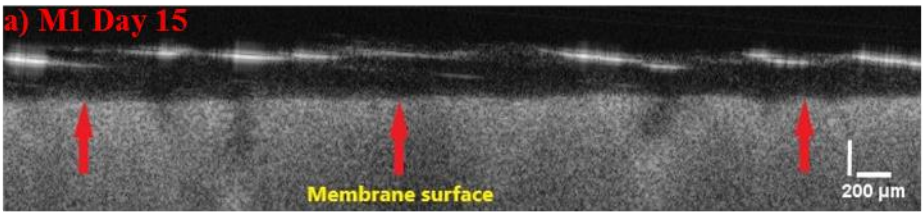
a) M1 Day 15
Membrane surface
200 µm

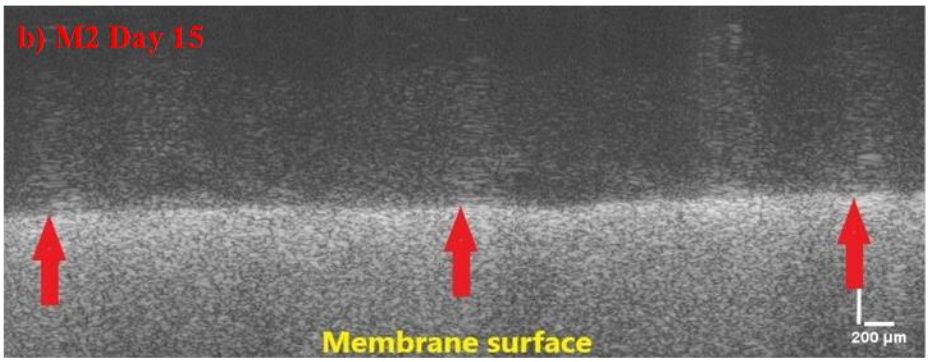
b) M2 Day 15
Membrane surface
200 µm

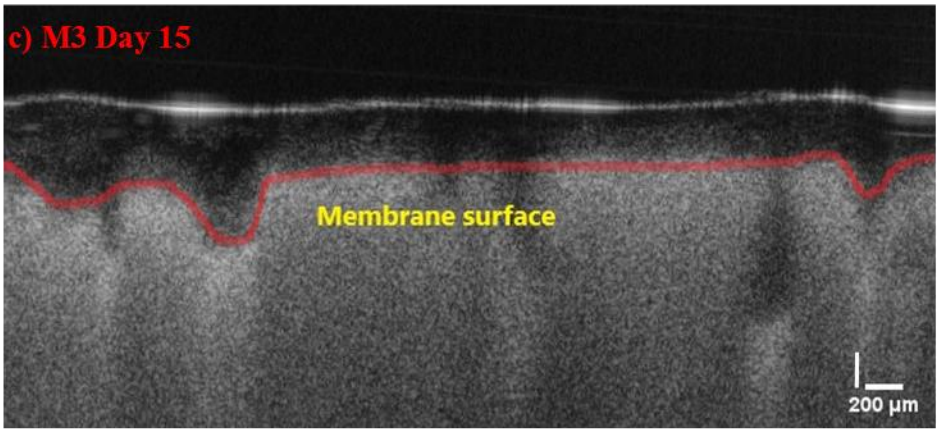
c) M3 Day 15
Membrane surface
200 µm

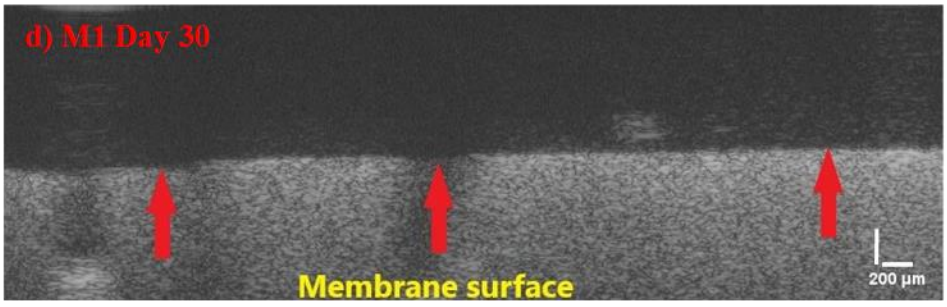
d) M1 Day 30
Membrane surface
200 µm

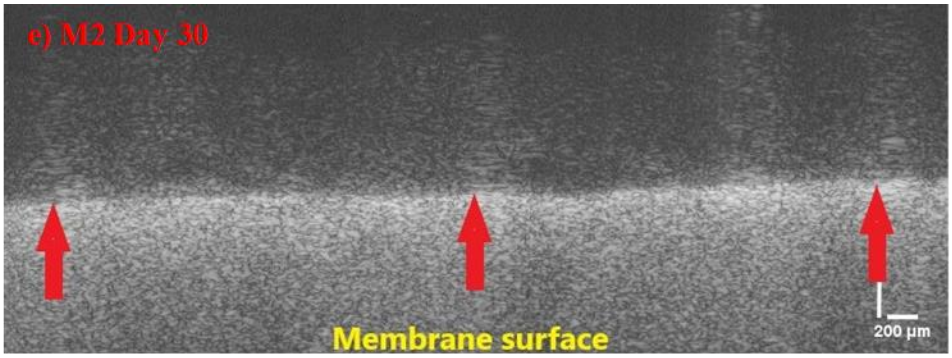
e) M2 Day 30
Membrane surface
200 µm

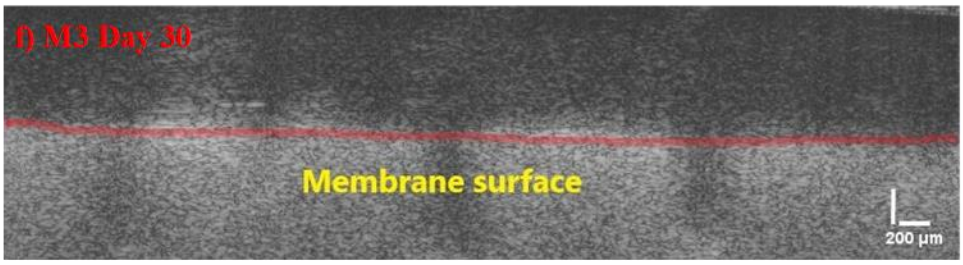
f) M3 Day 30
Membrane surface
200 µm

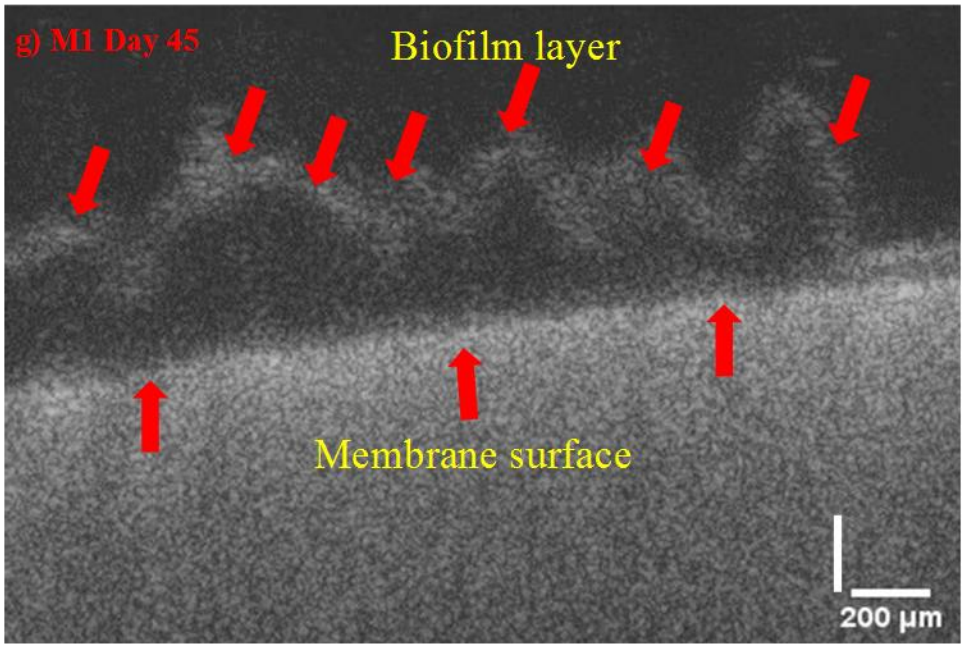
g) M1 Day 45
Biofilm layer
Membrane surface
200 µm

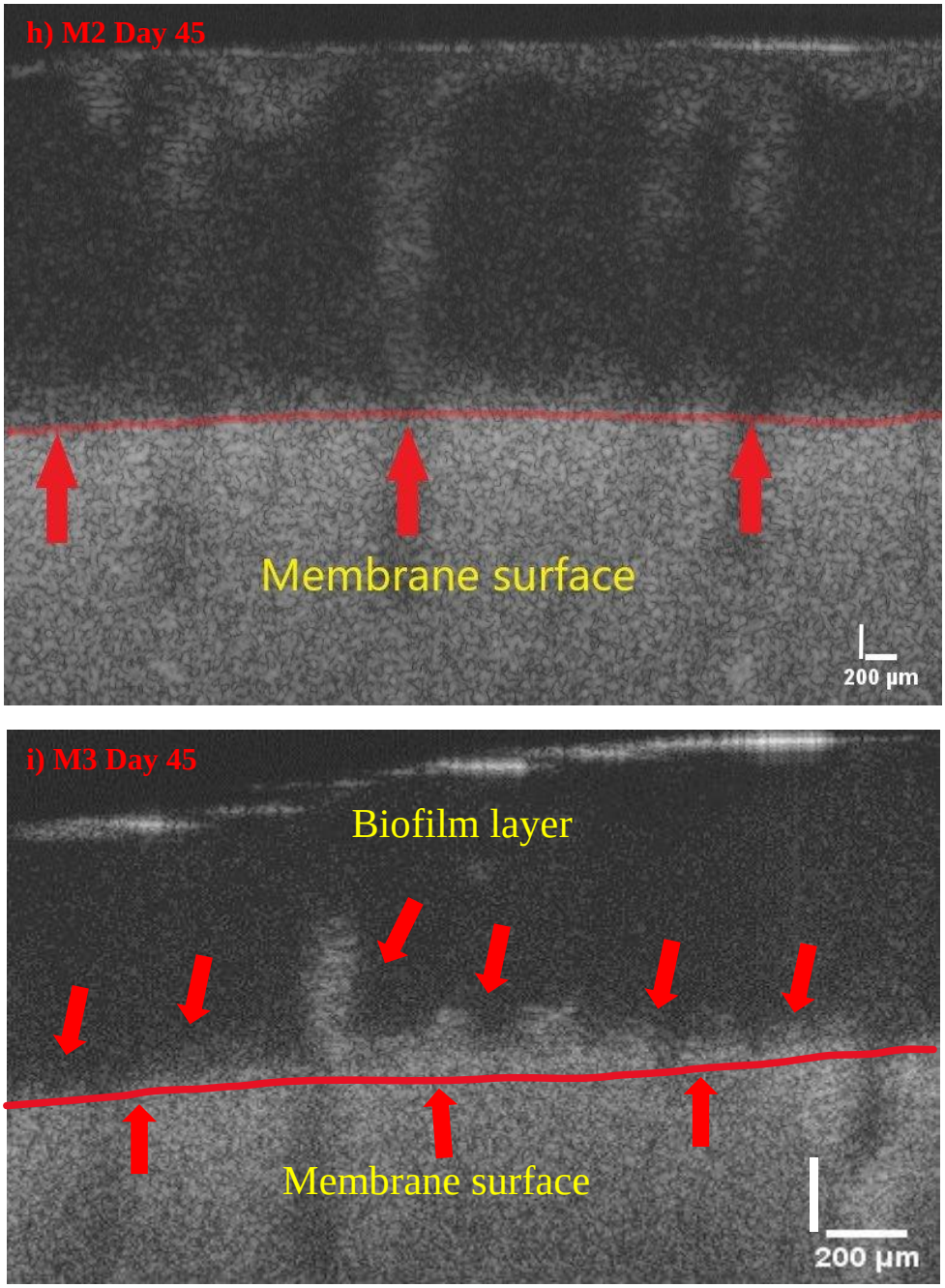

Figure A.6 OCT images of membrane surfaces of a) M1 (kaolin only) day 15, b) M2 (75 Wt% kaolin + 25 Wt% alumina), day 15, c) M3 (50 Wt% kaolin + 50 Wt% alumina), day 15, d) M1 day 30, e) M2 day 30, f) M3 day 30, g) M1 day 45, h) M2 day 45, and i) M3 day 45

APPENDIX B PERFORMANCE OF BIOLOGICAL ION EXCHANGE RESIN AND GRAVITY-DRIVEN CERAMIC MEMBRANE HYBRID PROCESS FOR SURFACE WATER TREATMENT

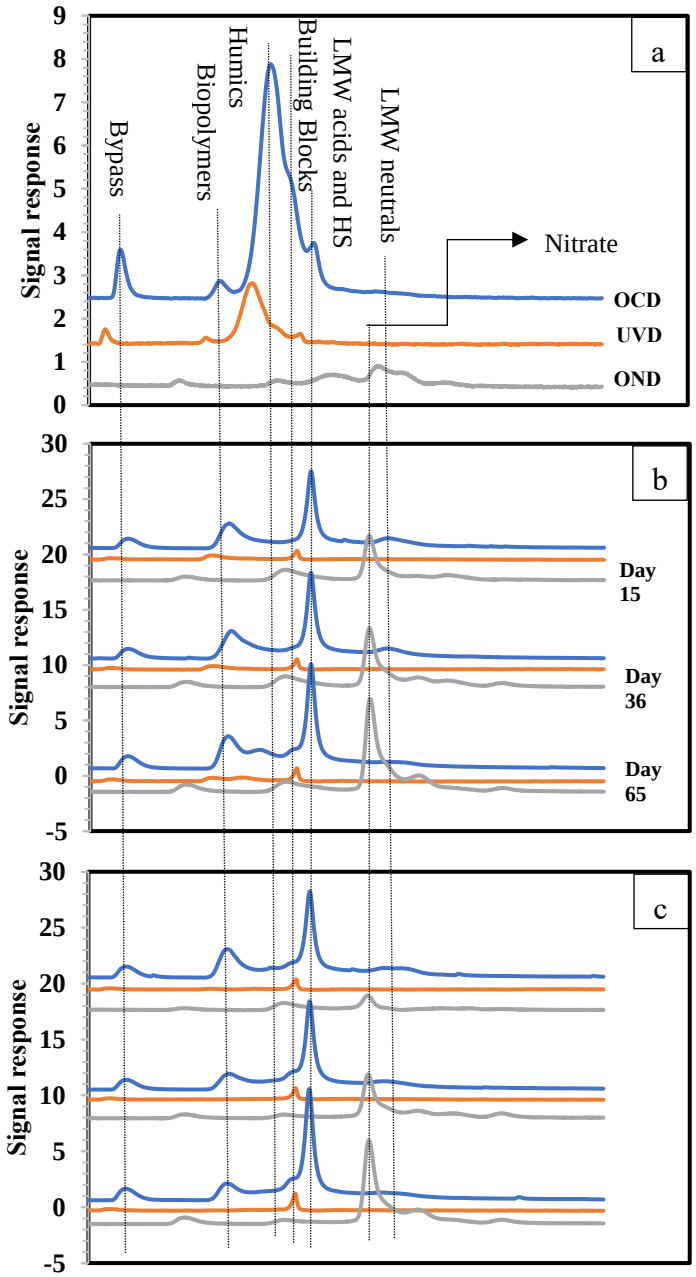

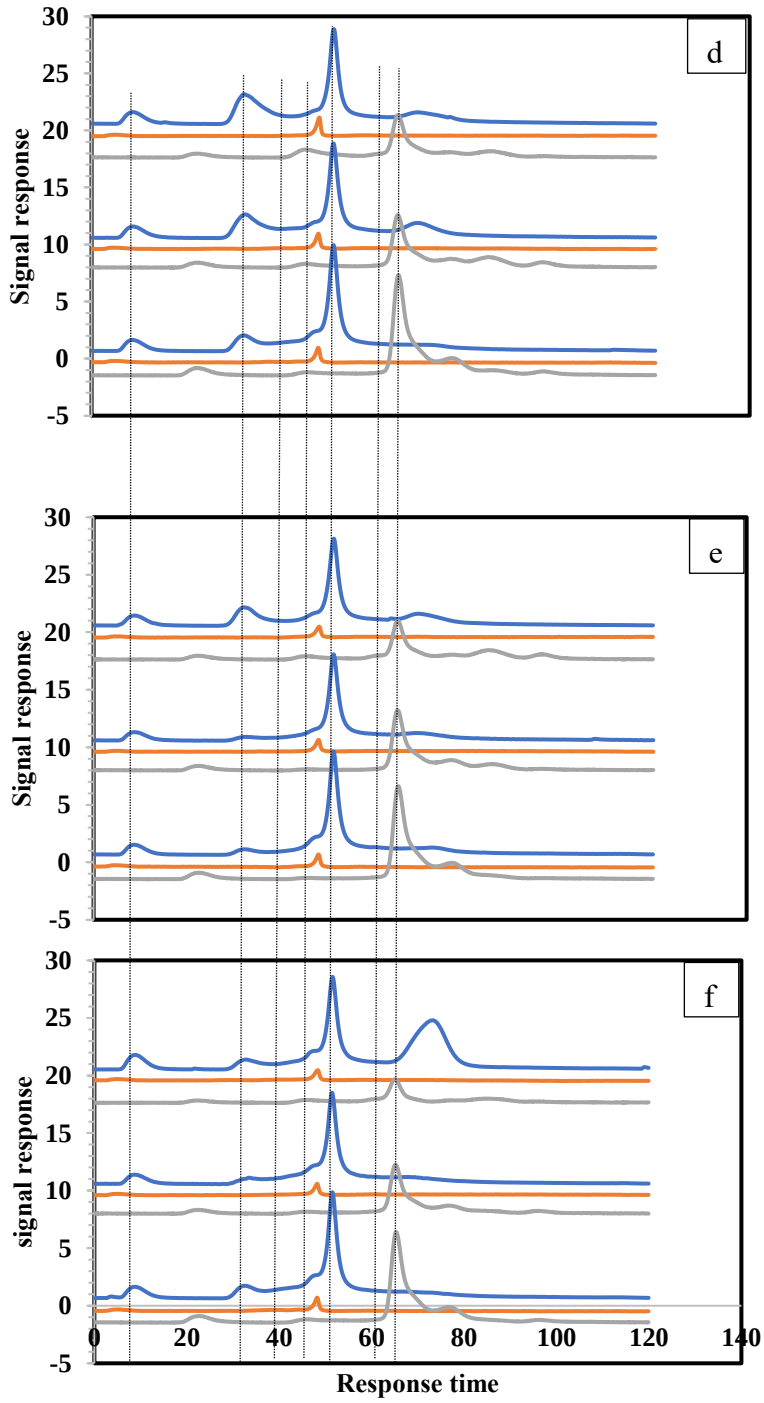

Figure B1. LC-OCD diagram of a) influent water b) BIEX column effluent on days 15, 36 and 65 c) M1 permeate (100 wt% kaolin) on days 15, 36 and 65 d) M2 permeate (75 wt% kaolin, 25 wt%

alumina) e) M3 permeate (50 wt% kaolin, 50 wt% alumina) on days 15, 36 and 65 f) M4 permeate (0.8 µm commercial) on days 15, 36 and 65.

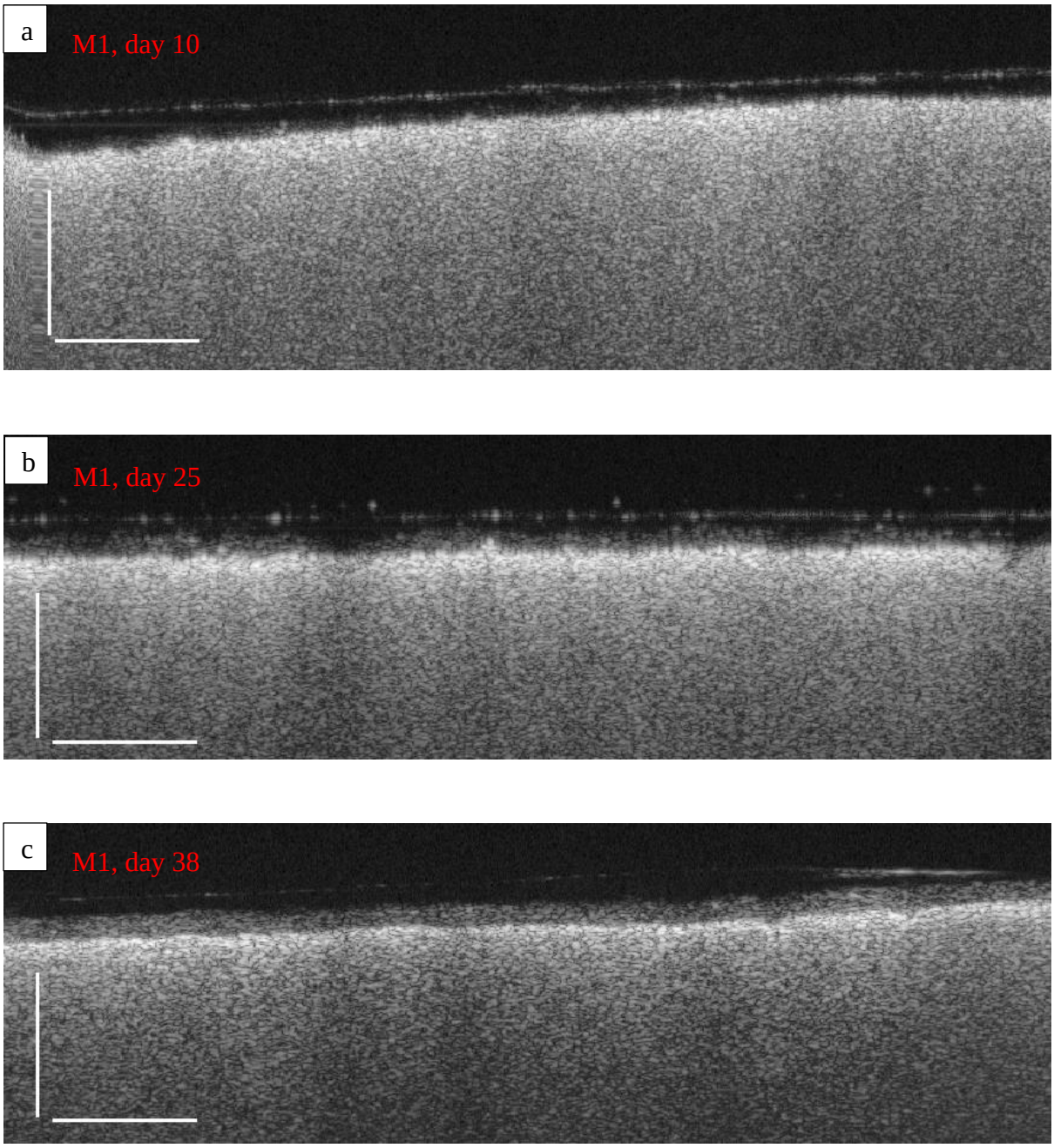

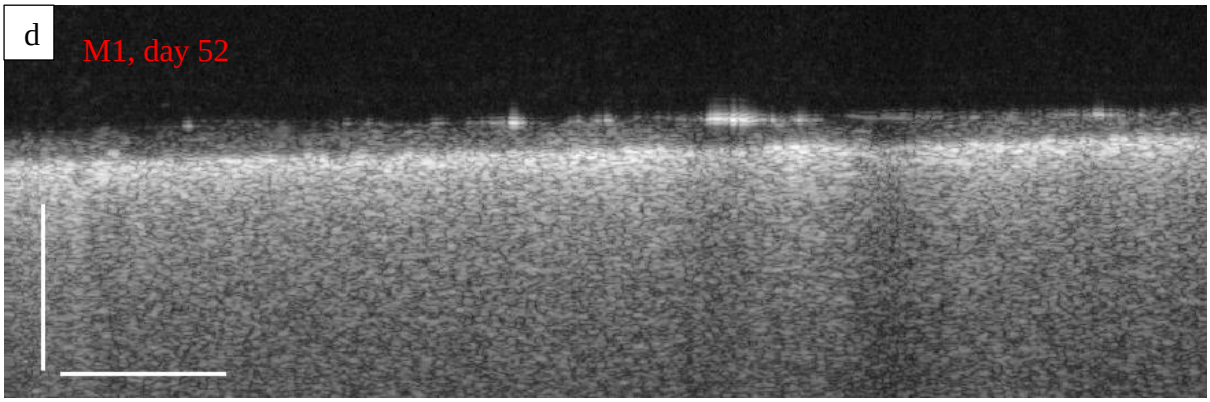
d
M1, day 52

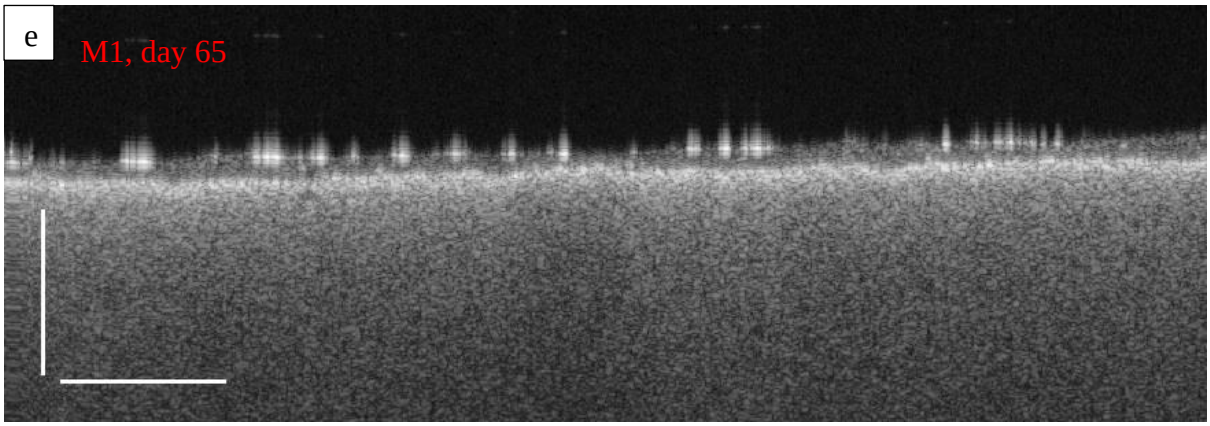
e
M1, day 65

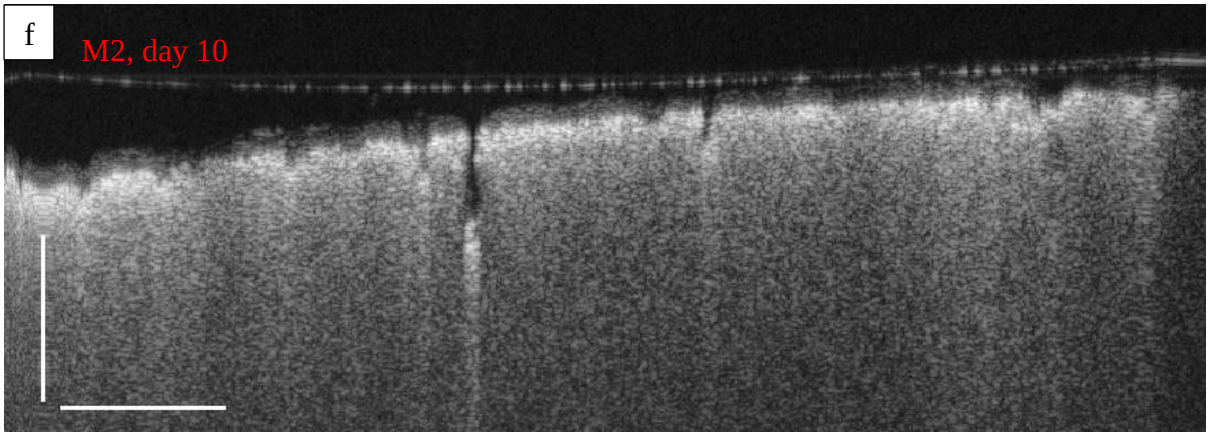
f
M2, day 10

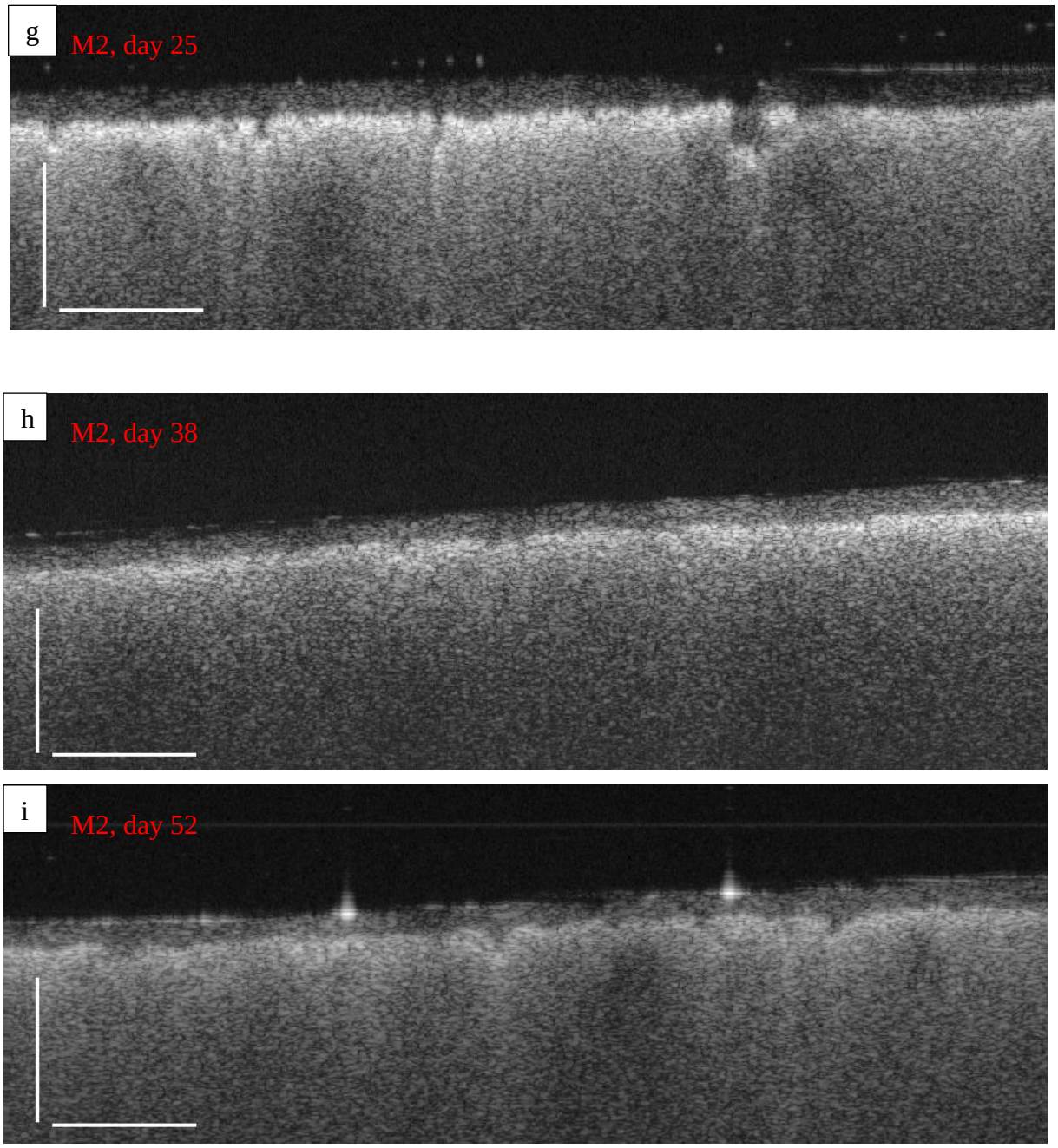
g
M2, day 25
h
M2, day 38
i
M2, day 52

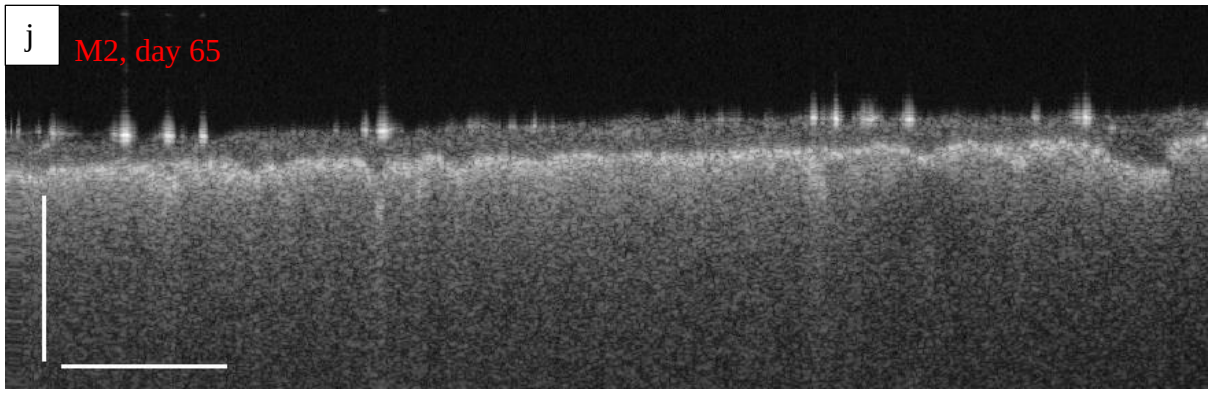
j
M2, day 65

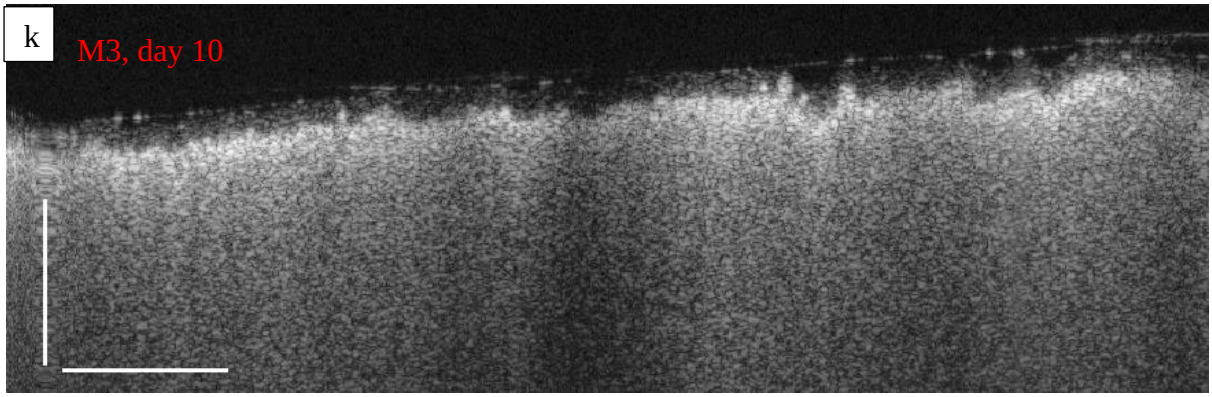
k
M3, day 10

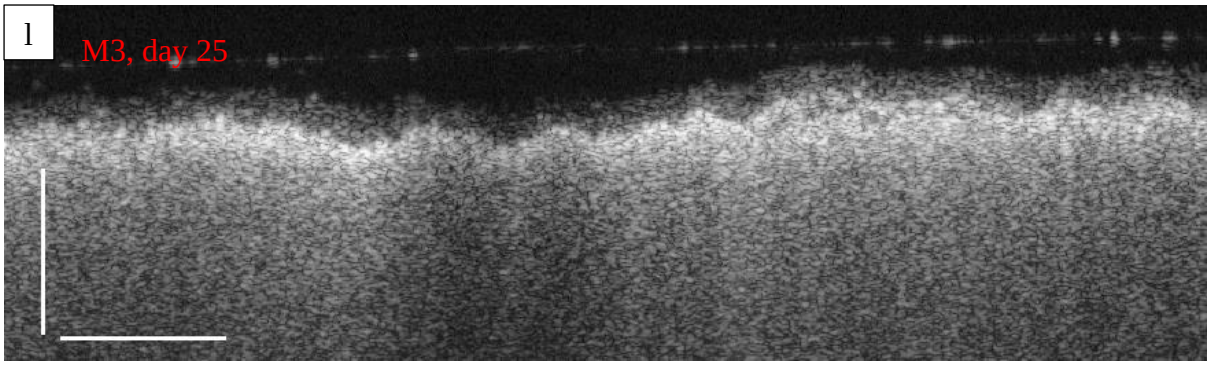
l
M3, day 25

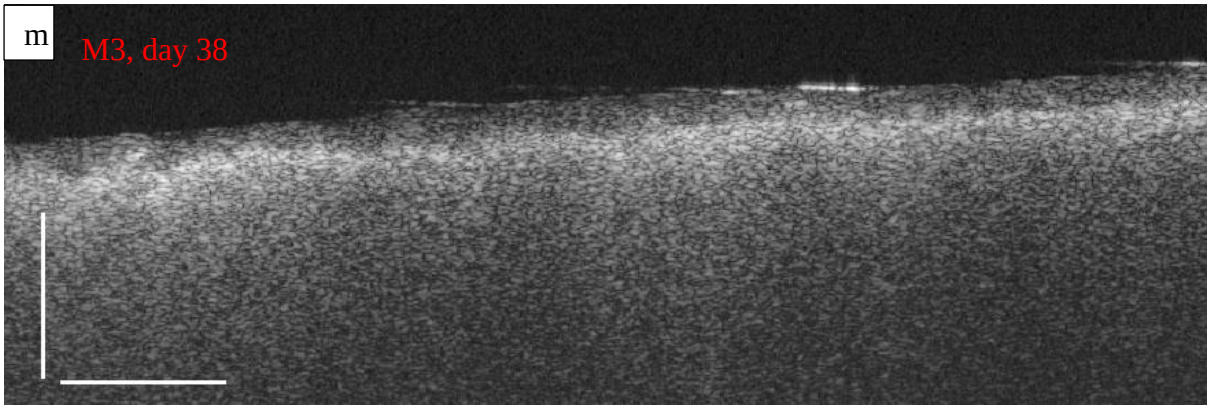
m
M3, day 38

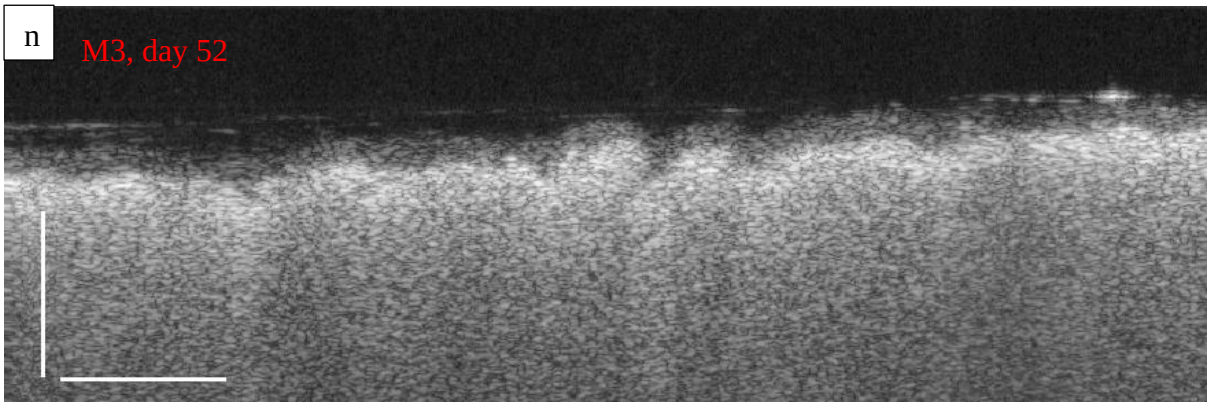
n
M3, day 52

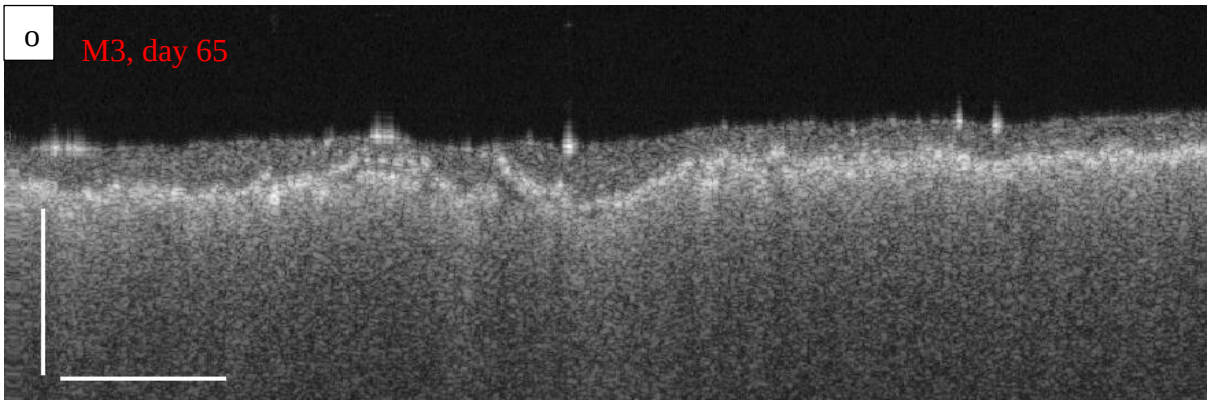
o
M3, day 65

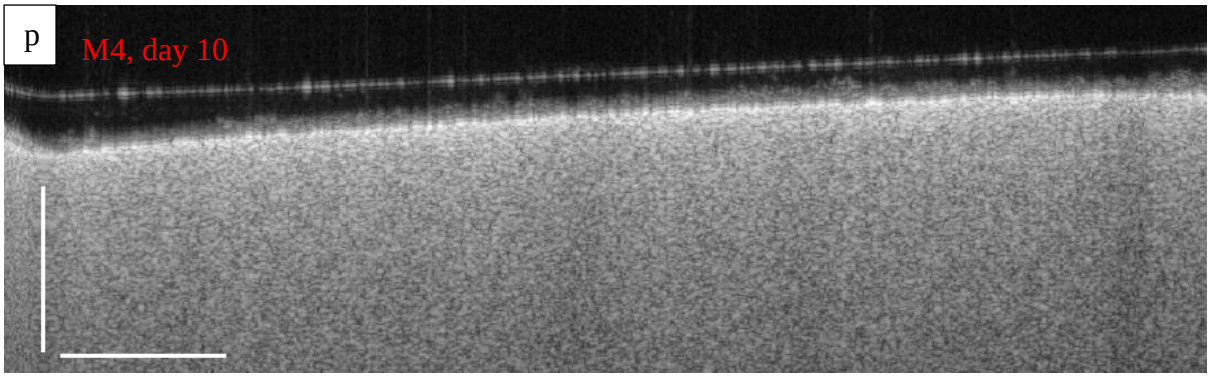
p
M4, day 10

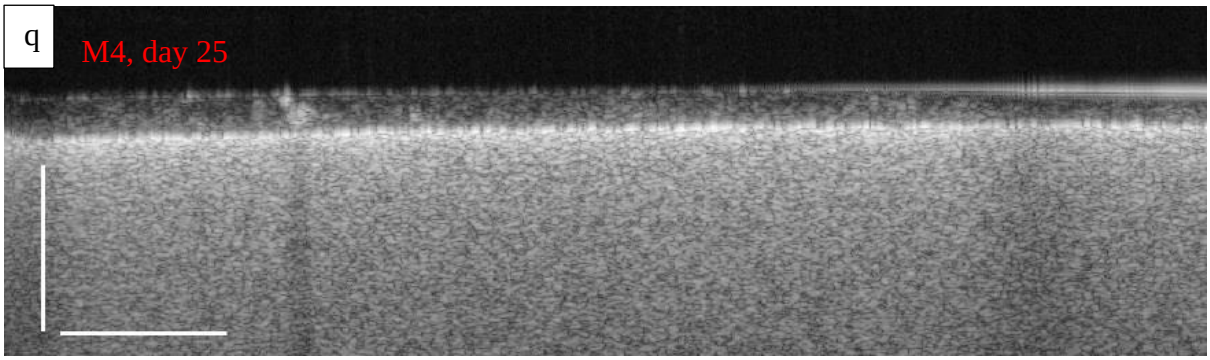
q
M4, day 25

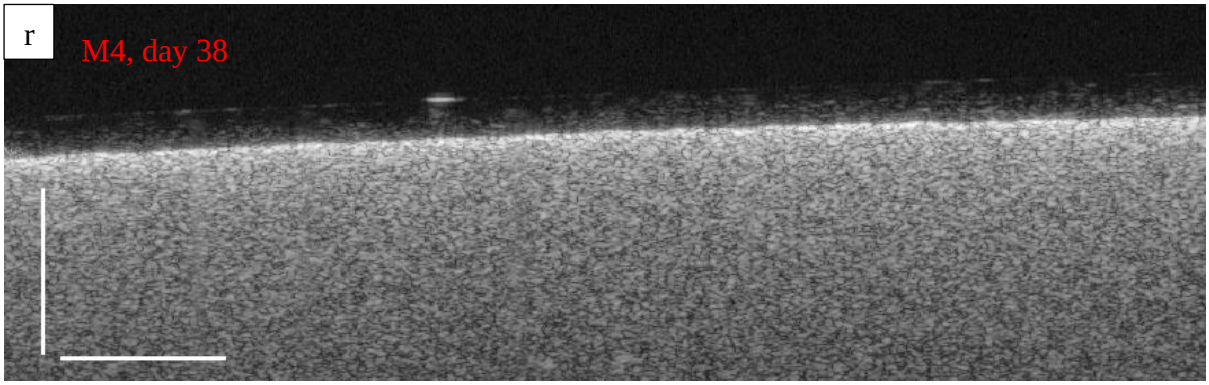
r
M4, day 38

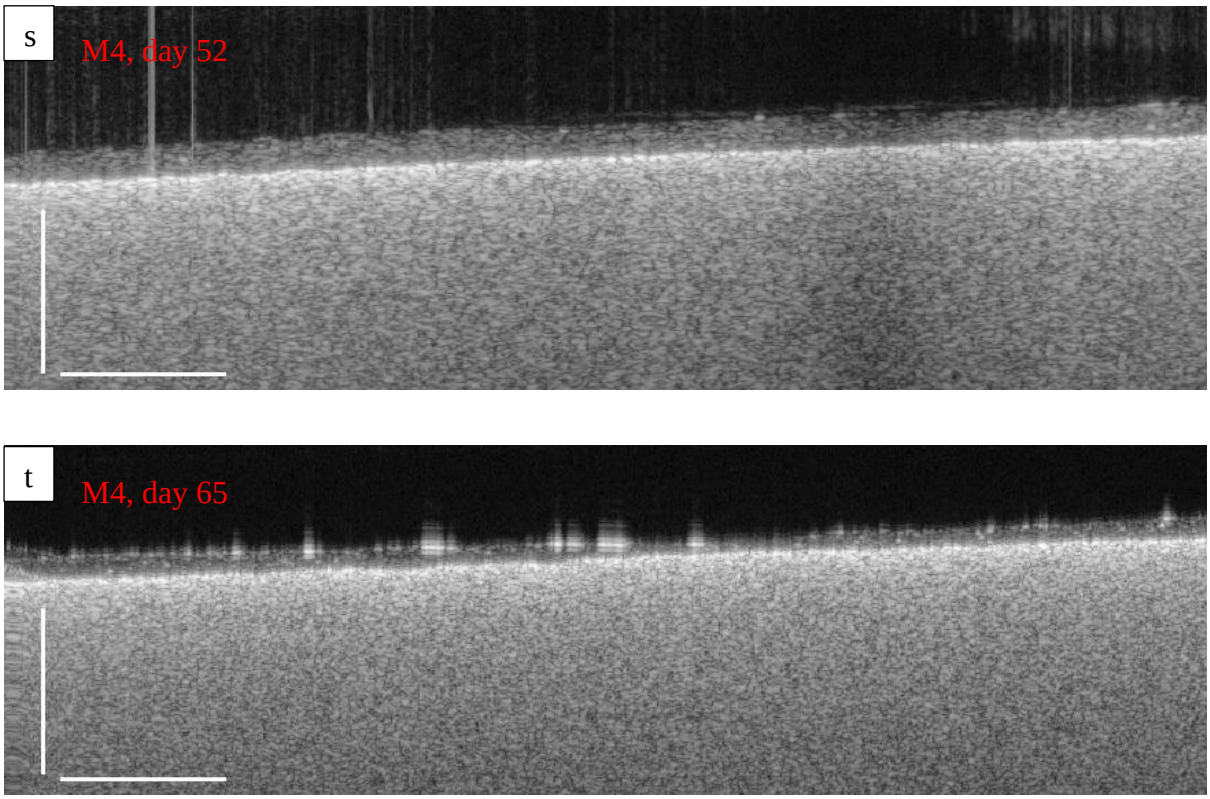

Figure B2. OCT images from biofilm of a, b, c, d, e) M1 (100 wt% kaolin) on days of 10, 25, 38, 52 and 65 f, g, h, I, j) M2 (75 wt% kaolin, 25 wt% alumina) on days of 10, 25, 38, 52 and 65 k, l, m, n, o) M3 (50 wt% kaolin, 50 wt% alumina) on days of 10, 25, 38, 52 and 65 and p, q, r, s, t) M4 (0.8 µm commercial) on days of 10, 25, 38, 52 and 65. The scale bars in the x and y - axis are showing 1 mm distance.

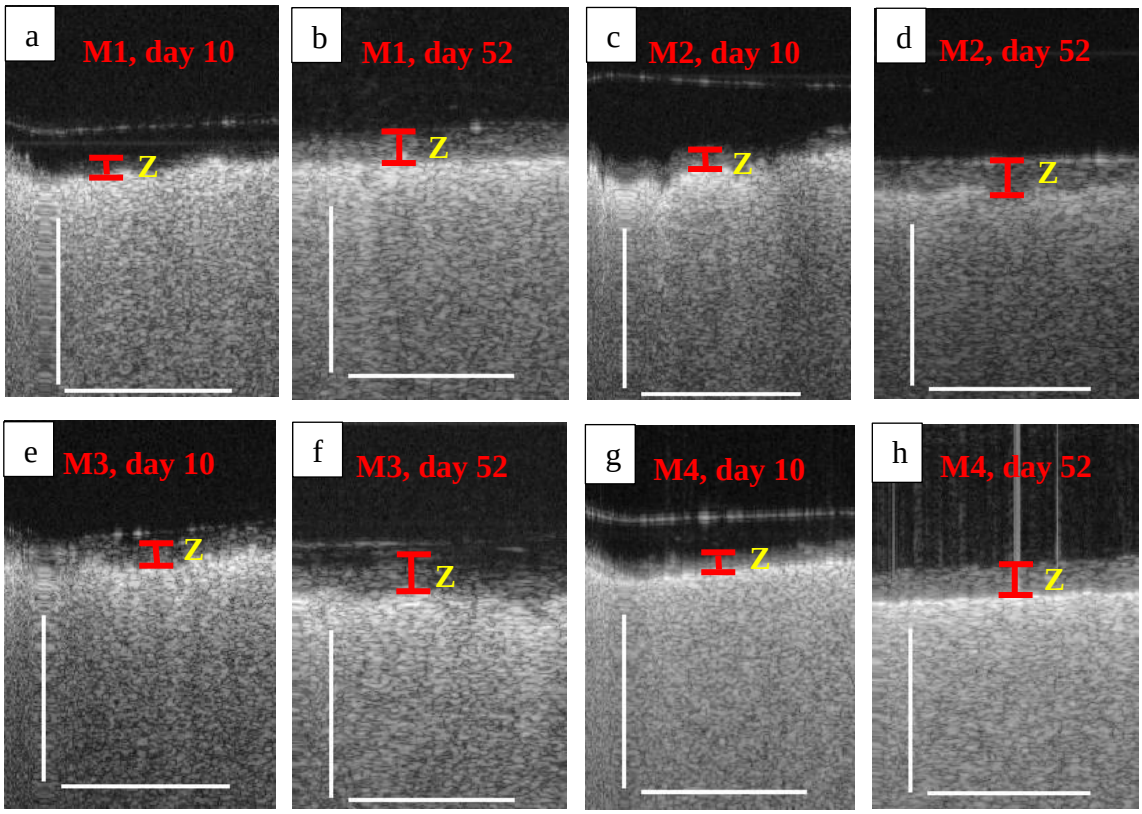

Figure B3. OCT images of a, b) M1 (100 wt% kaolin) day 10 and 52, c, d) M2 (75 wt% kaolin, 25 wt% alumina) day 10 and 52, e, f) M3 (50 wt% kaolin, 50 wt% alumina) day 10 and 52, g, h) M4 (0.8 µm commercial) day 10 and 52. The scale bars in the x and y - axis are showing 1 mm distance. "Z" indicates the OCT biofilm thickness.

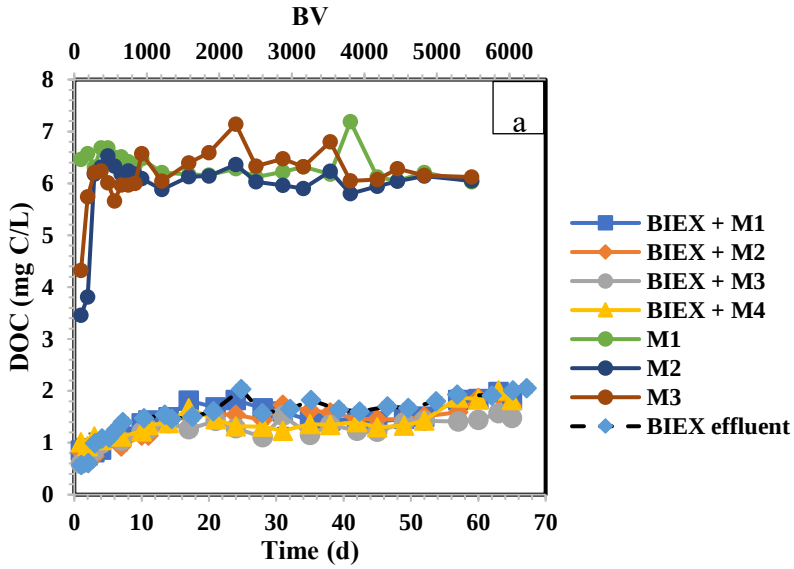
BV
0 1000 2000 3000 4000 5000 6000
a
DOC (mg C/L)
0 1 2 3 4 5 6 7 8
0 10 20 30 40 50 60 70
Time (d)
BIEX + M1
BIEX + M2
BIEX + M3
BIEX + M4
M1
M2
M3
BIEX effluent

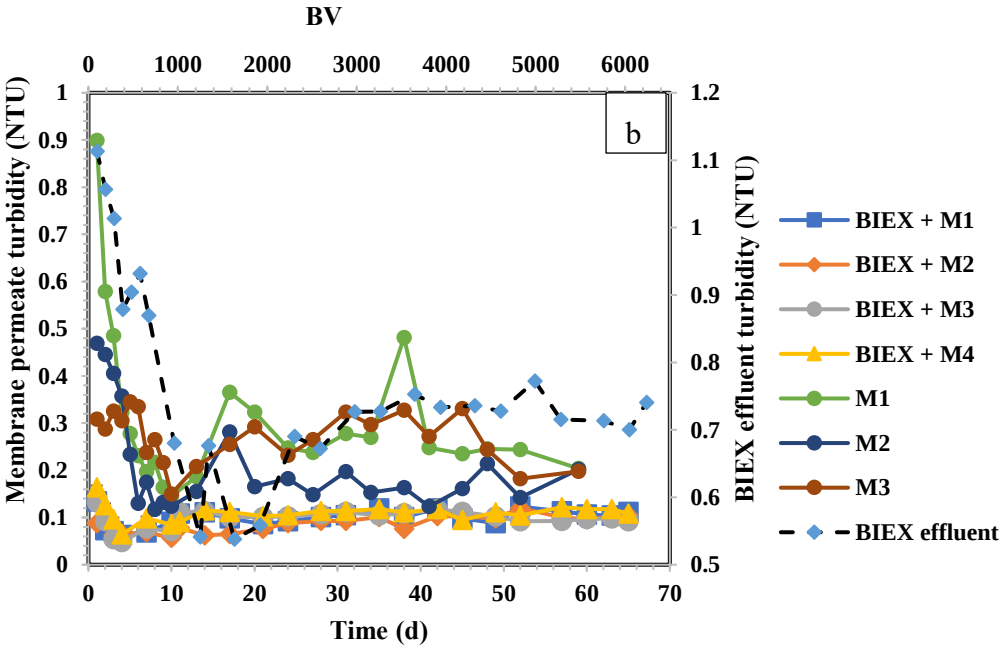
BV
0 1000 2000 3000 4000 5000 6000
b
Membrane permeate turbidity (NTU)
0 0.1 0.2 0.3 0.4 0.5 0.6 0.7 0.8 0.9 1
BIEX effluent turbidity (NTU)
0.5 0.6 0.7 0.8 0.9 1 1.1 1.2
0 10 20 30 40 50 60 70
Time (d)
BIEX + M1
BIEX + M2
BIEX + M3
BIEX + M4
M1
M2
M3
BIEX effluent

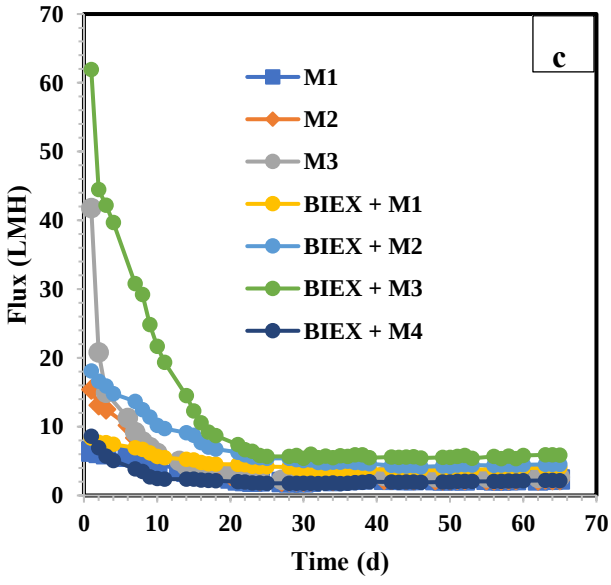
c
Flux (LMH)
0 10 20 30 40 50 60 70
0 10 20 30 40 50 60 70
Time (d)
M1
M2
M3
BIEX + M1
BIEX + M2
BIEX + M3
BIEX + M4

Figure B4. Comparing the a) DOC removal, b) Turbidity removal, and c) flux of GDCM process with and without BIEX pre-treatment using M1 (100 wt% kaolin), M2 (75 wt% kaolin, 25 wt% alumina), M3 (50 wt% kaolin, 50 wt% alumina), and M4 (0.8 µm commercial).

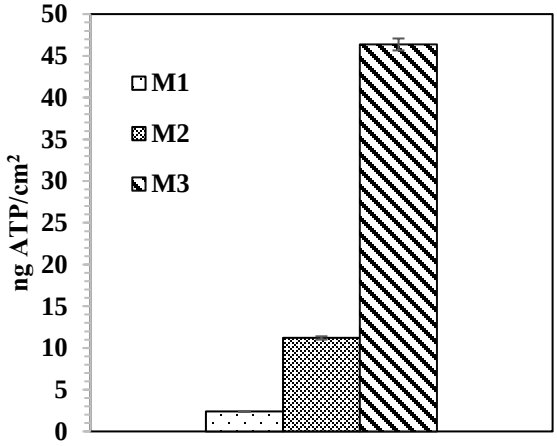

Figure B5. Concentration of active microorganisms in the biofilm of M1 (100 wt% kaolin), M2 (75 wt% kaolin, 25 wt% alumina), and M3 (50 wt% kaolin, 50 wt% alumina) in GDCM process without a pre-treatment. The diagram with a unit of ATP weight / membrane weight previously published (Rasouli, Maltais-Tariant et al. 2023). To compare with the hybrid BIEX + GDCM process (present study), the unit has changed to ng ATP/ cm^2. Error bars show 95% confidence intervals.

APPENDIX C IMPACT OF CLEANING ON MEMBRANE PERFORMANCE DURING SURFACE WATER TREATMENT: A HYBRID PROCESS WITH BIOLOGICAL ION EXCHANGE AND GRAVITY-DRIVEN MEMBRANES

Membrane characterizations

The determination of membrane porosity involved the calculation based on the amount of water absorbed by the membrane structure following immersion in a water bath. Initially, the dry membranes, denoted as "W_1," were weighed. Subsequently, these membranes were immersed in pure water at a consistent ambient temperature for a duration of 72 hours. Following this soaking period, the outer surface of the membranes was dried using Kimwipes™ and subsequently reweighed as "W_2." The formula employed to compute membrane porosity was in accordance with the method outlined by (Arzani, Mahdavi et al. 2016):

$$Porosity = \left(\frac{W_2 - W_1}{\rho_m V_m}\right) \quad \text{(C.1)}$$

where ρ_m and V_m are the density of pure water at the corresponding temperature and membrane volume, respectively.

The membrane mean pore radius (R_m) was calculated using the Guerout-Elford-Ferry equation (Zhang, Lang et al. 2015), where ε is the membrane porosity, L is the membrane thickness, μ is the water viscosity at the filtration temperature, J is the membrane flux, and ΔP is the pressure.

$$R_m = \sqrt{\frac{(2.9 - 1.75\,\epsilon) 8\mu\, L\, J}{\varepsilon\, \Delta P}} \quad \text{(C.2)}$$

Membrane structure characterization using scanning electron microscopy

A small part of the clean membranes was carefully cut and subjected to SEM analyses. The samples were prepared by vacuum coating with a very thin layer of gold (Polaron SC502 sputter coater) at a pressure of approximately 10 bar and current of 10 mA. The samples were observed on a device (Jeol, JSM-7600TFE, JEOL Ltd., Japan) using low electron voltages (5–10 kV).

Characterization results

Table C1. Porosity, mean pore size and water flux of the lab-made membranes. Mean ± 95% confidence interval.

Membrane type	Porosity (%)	Mean pore size (µm)	Water flux at 90 mbar (LMH)
M4 (Ceramic lab-made MF)	35.17 ± 3.55	0.62 ± 0.06	108.04 ± 4.01

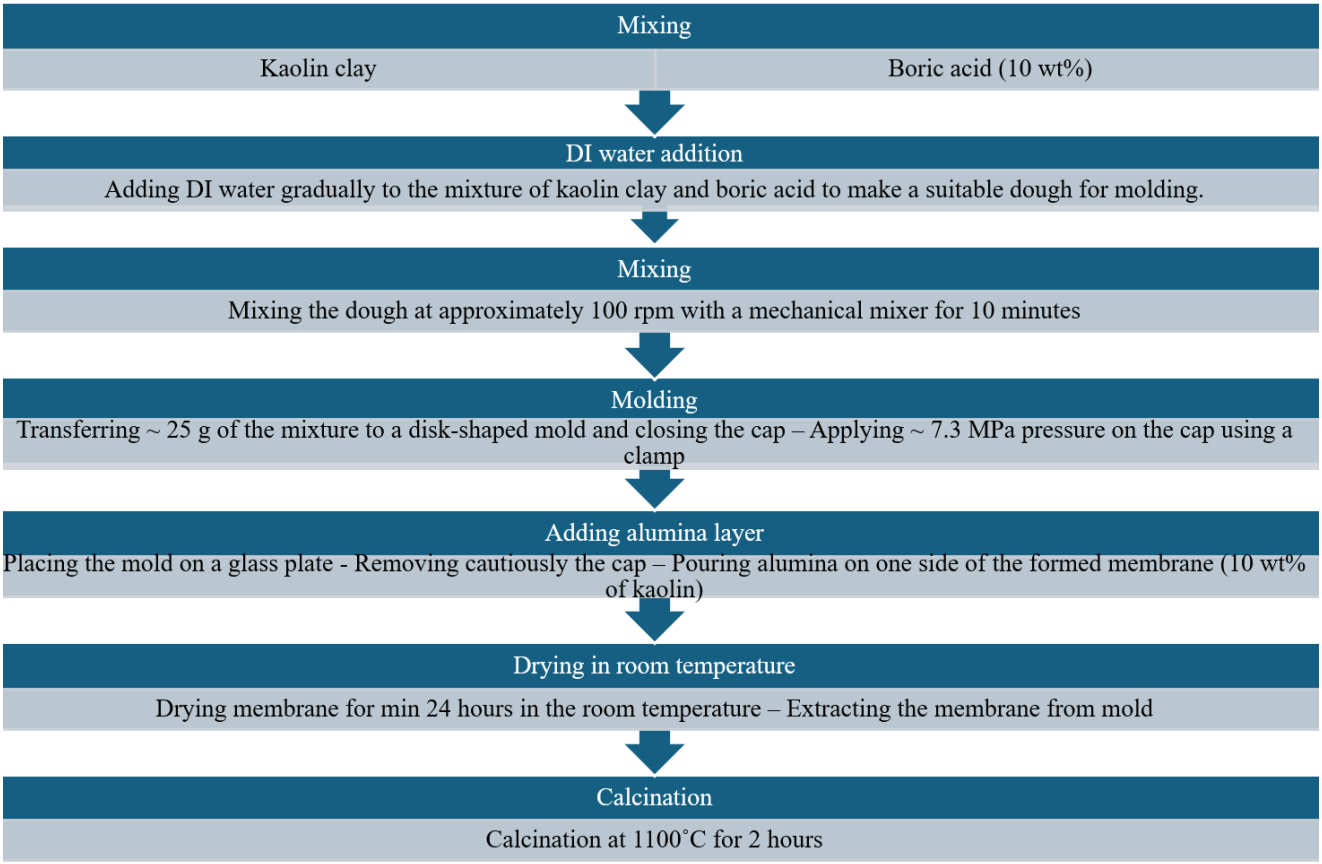

Figure C1. Schematic of M4 (lab-made) production steps

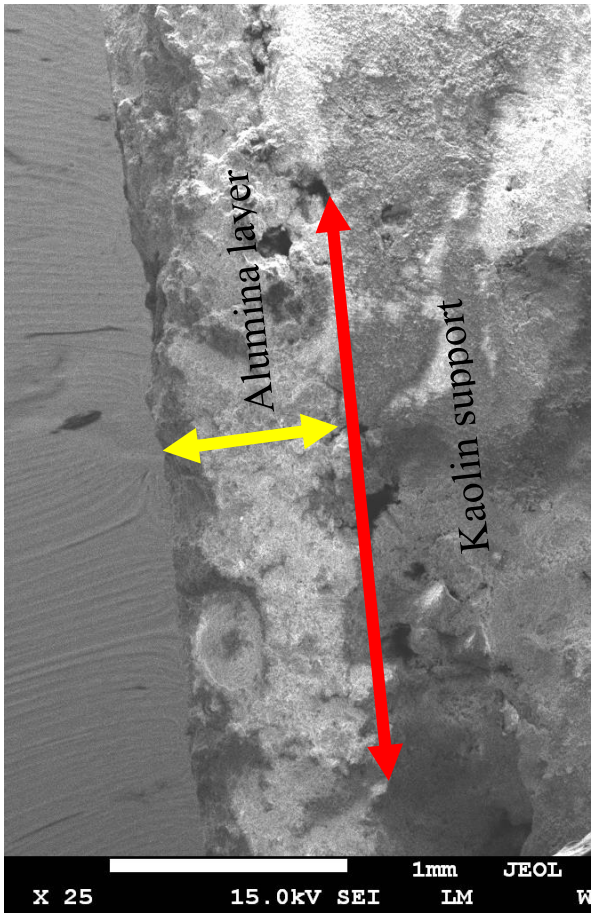

Figure C2. SEM micrograph of the Lab-made membrane, demonstrating the kaolin support and the top alumina layer

According to Figure C3, point 1 which is in the kaolin support, shows more Si and less Al than Point 2 which is located in the alumina layer.

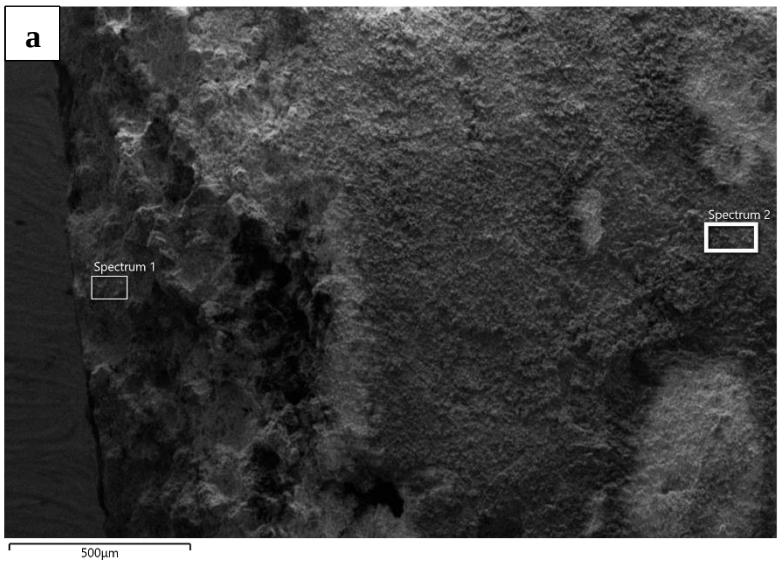

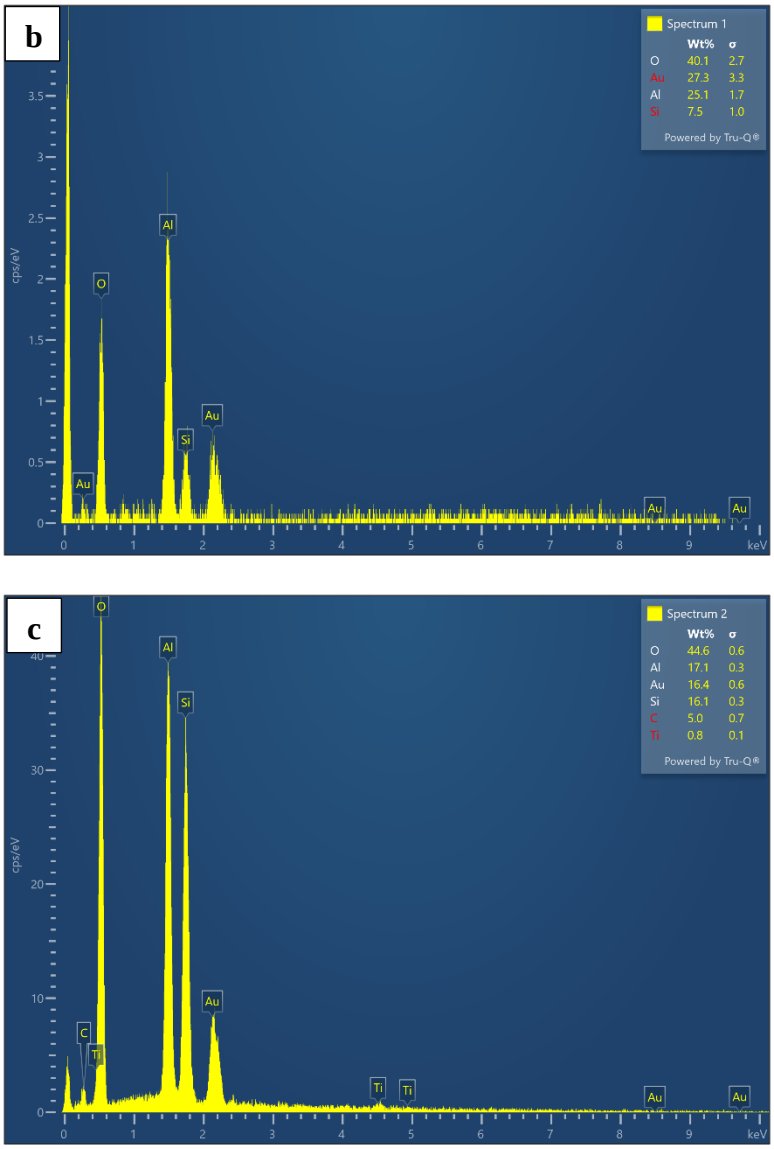

Figure C3. a) SEM micrograph of the Lab-made membrane. Spectrums 1 and 2 show a small area in the kaolin support and alumina top layer. b) The Energy Dispersive X-ray (EDX) spectra of point 1 (in kaolin support), and c) EDX spectra of point 2 (in top alumina layer).

Step 1: Turning the membranes face down – Membranes position was turned to face down according to the inlet flow

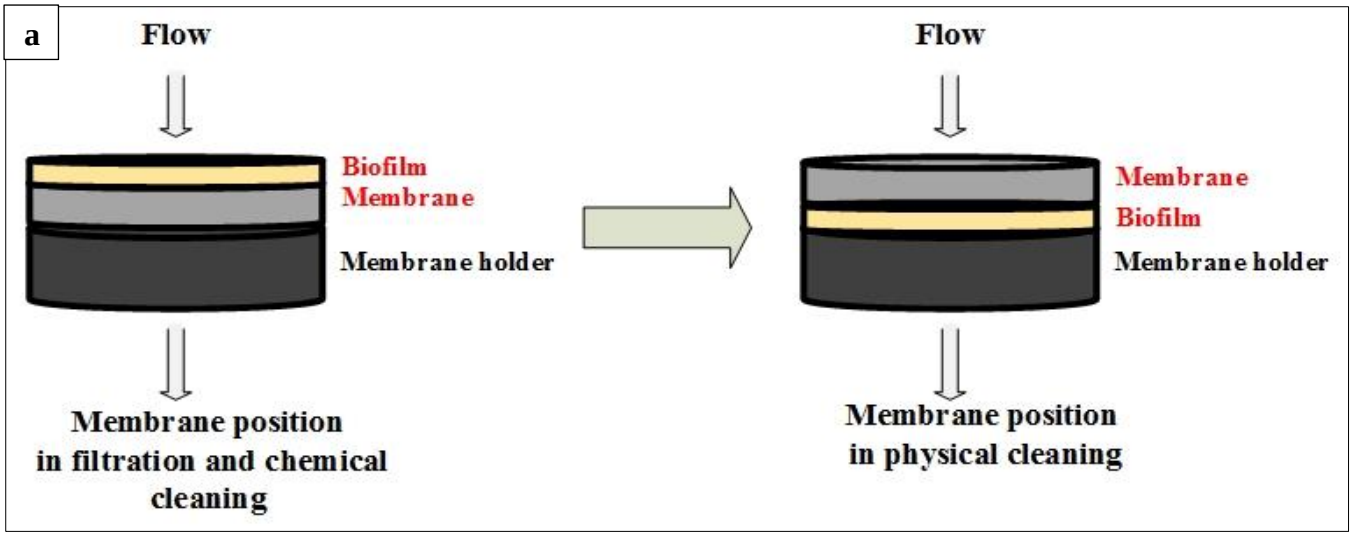

Step 2: Backwash with air at section 1) P = 30 psi, Q = 5 L/h, t = 2 min; section 2) P = 15 psi, Q = 2.5 L/h, t = 2 min.

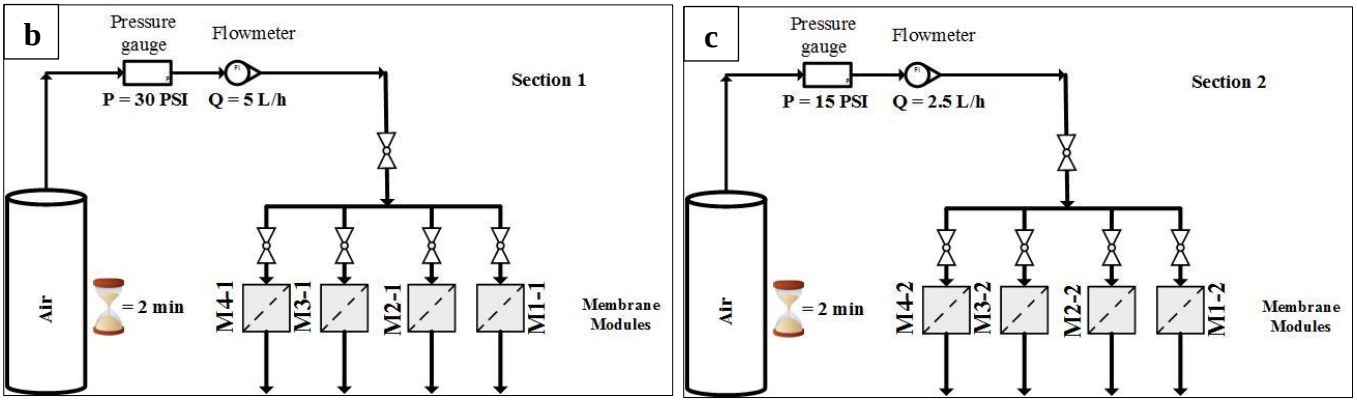

Step 3: Backwash with DI water at section 1) water head = 120 cm, t = 4 h; section 2) water head = 90 cm, t = 4 h.

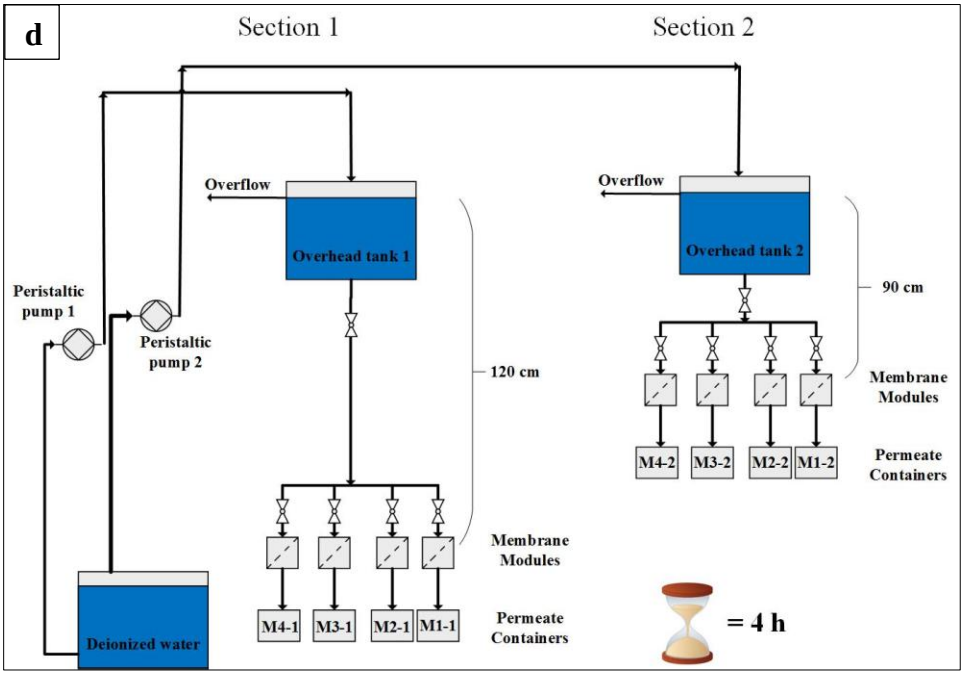

Step 4: Returning the membranes to normal position – Membranes position was turned face up again according to the inlet flow.

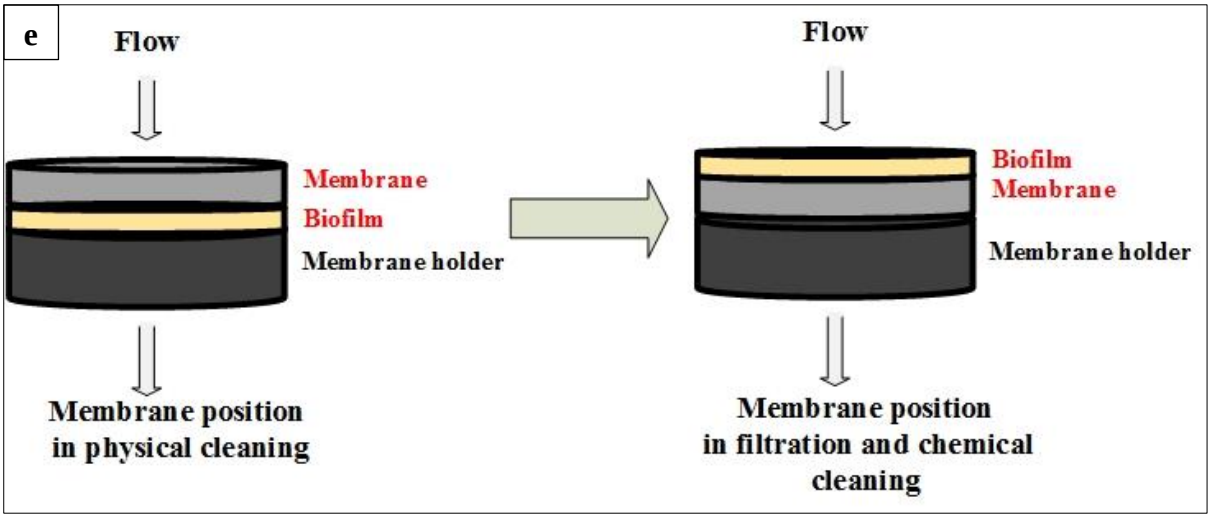

Step 5: Measuring DI water flux at water head of 90 cm for 15 min in both sections.

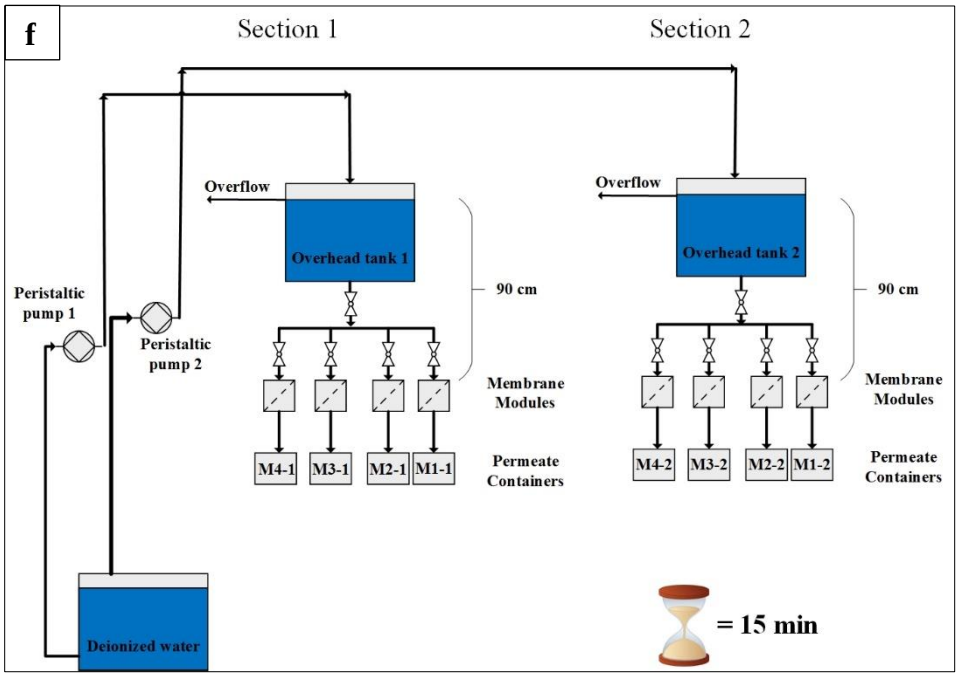

Step 6: Chemical cleaning by NaOH 40 mM in section 1 and 20 mM in section 2 both for 6 h at 90 cm water head.

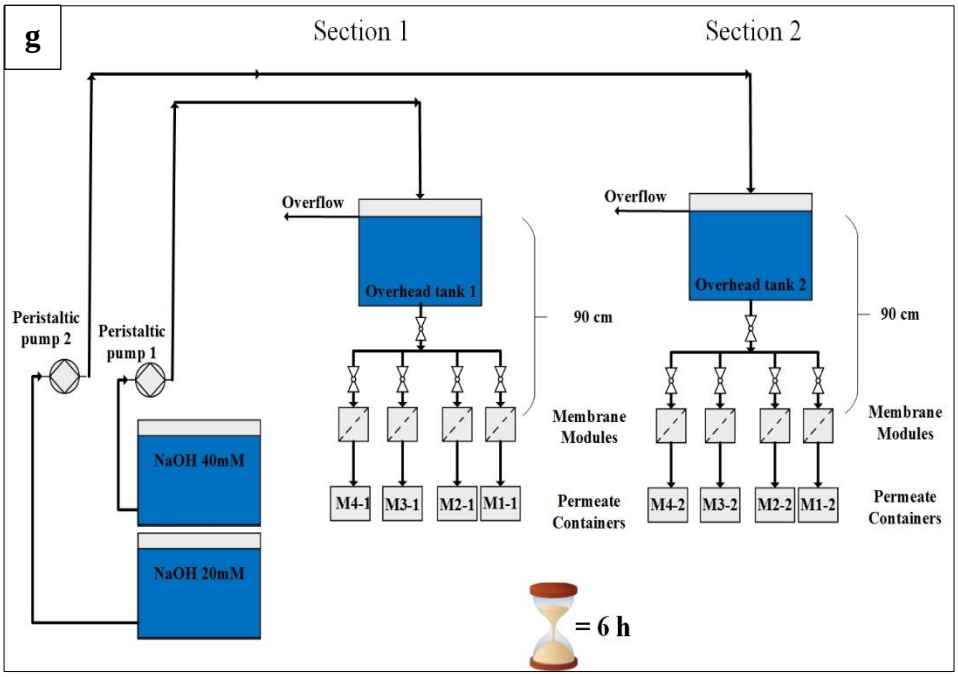

Step 7: Measuring DI water flux at water head of 90 cm for 15 min in both sections.

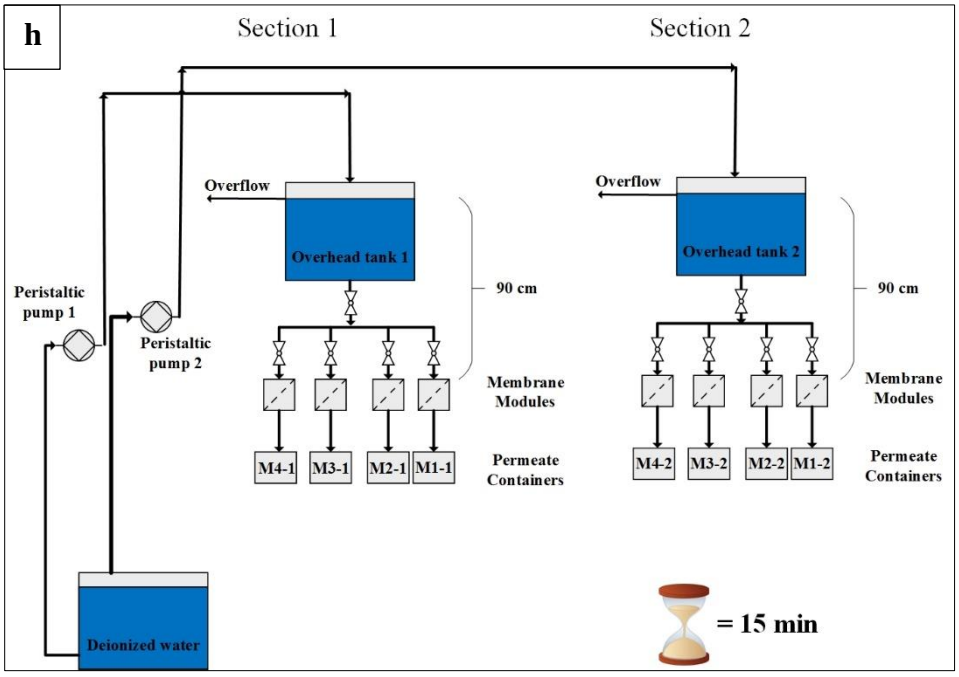

Step 8: Chemical cleaning by NaOCl 500 mg Cl_2/L in section 1 and 250 mg Cl_2/L in section 2 both at 90 cm water head for 6h.

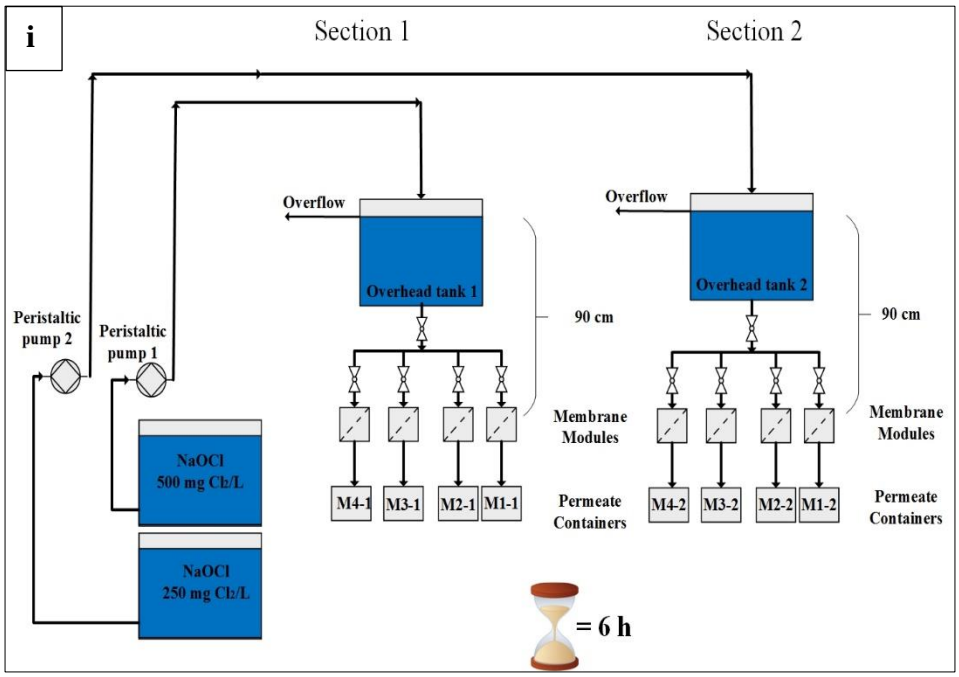

Step 9: Measuring DI water flux at water head of 90 cm for 15 min in both sections.

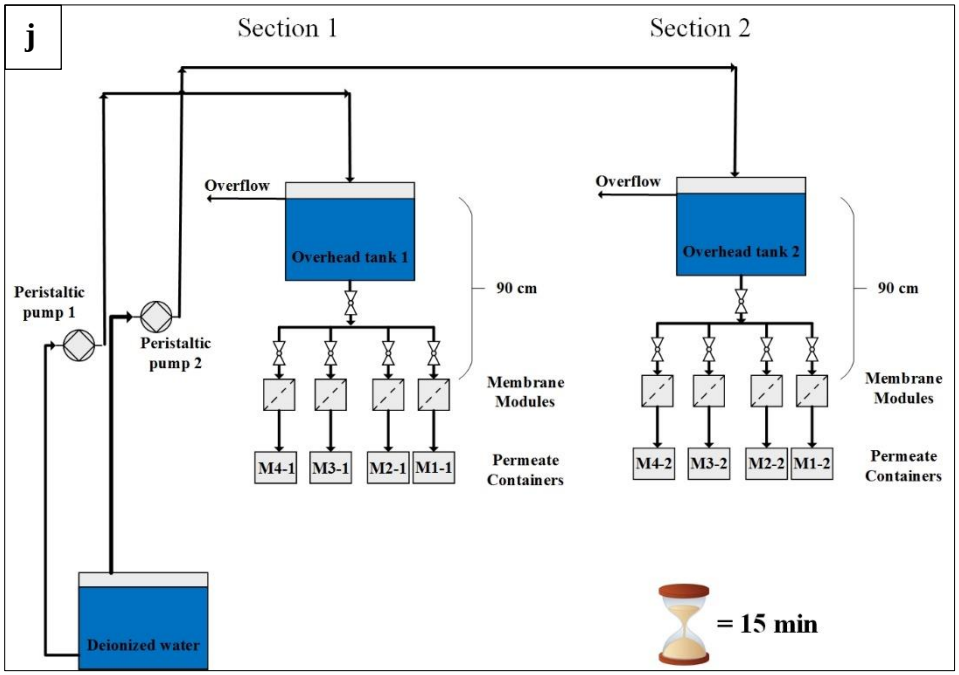

Figure C4. Schematic of the steps in physical and chemical cleaning of the membranes

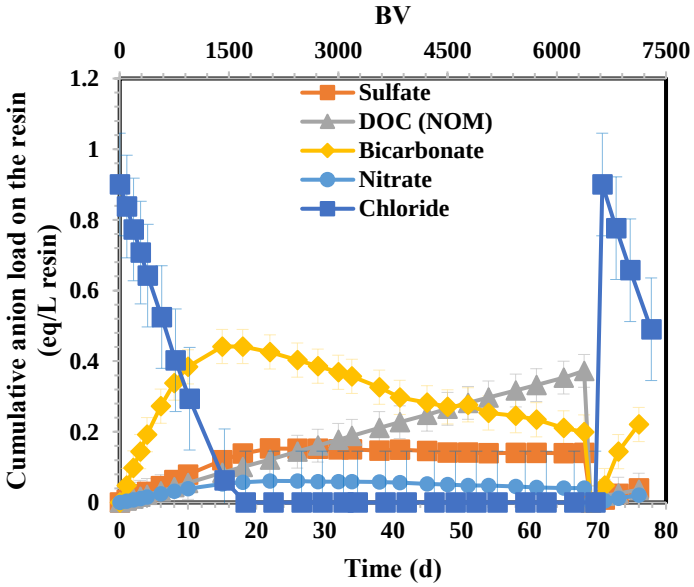

Figure C5. Dynamics of cumulative anion exchange on the resin of BIEX column 2 during the operation. Day 68 and 6,528 BV is the resin regeneration time. The error bars show 95% confidence intervals.

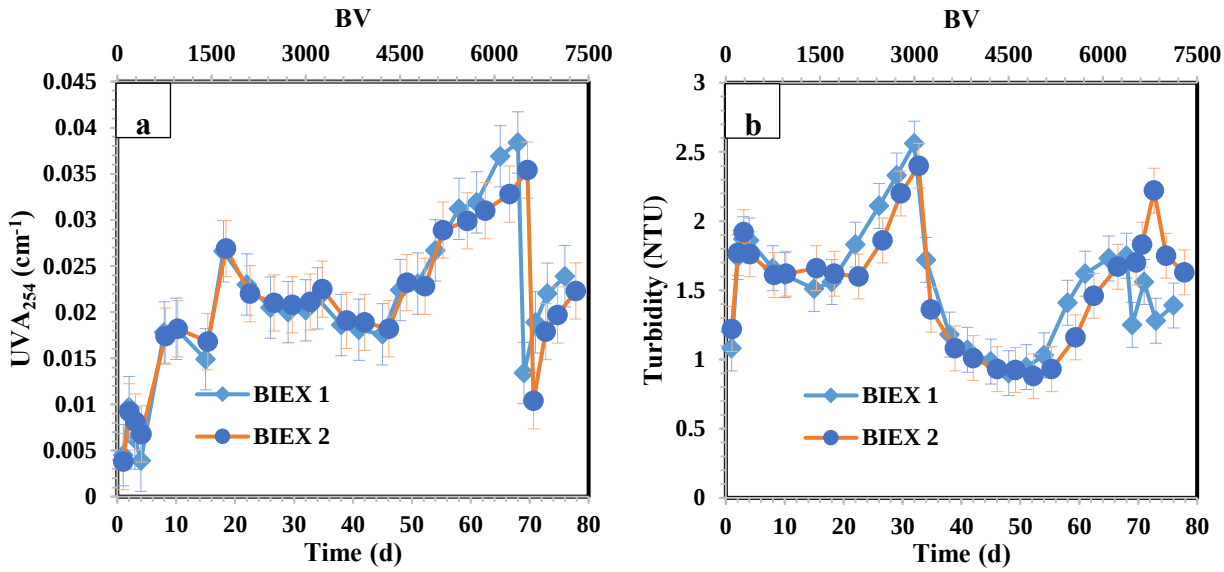

Figure C6. Variations of a) UVA_{254} and b) turbidity of BIEX column effluent during the operation. The error bars show 95% confidence intervals.

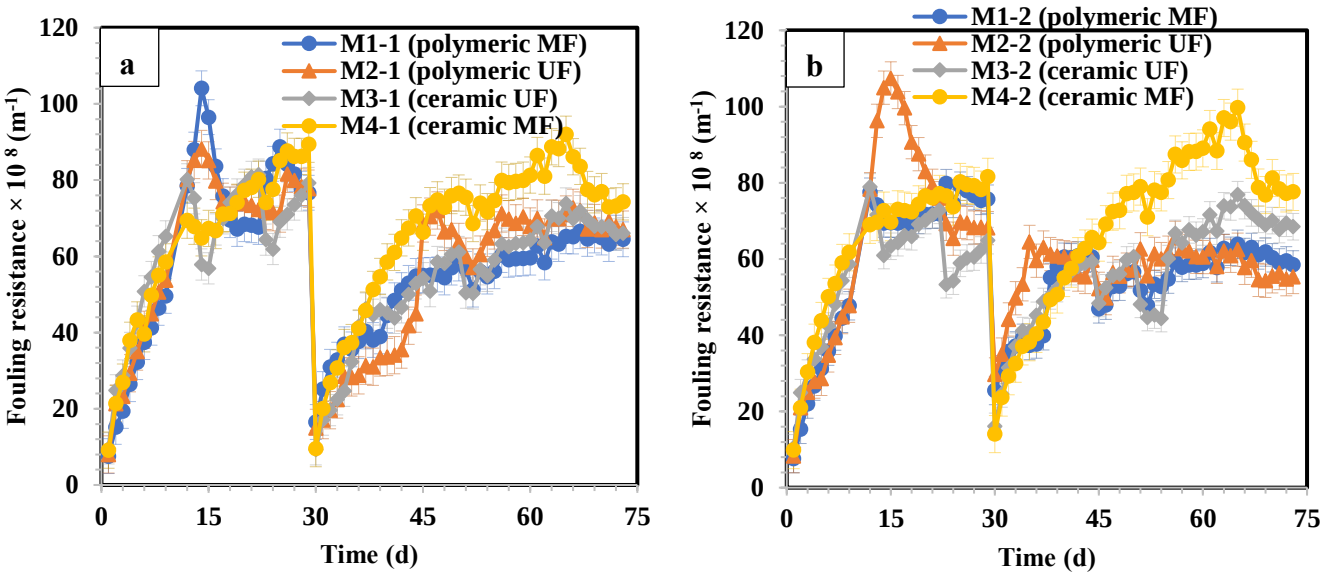

Figure C7. a) Variation of fouling resistance of membranes in section 1 during the filtration, and b) Variation of fouling resistance of membranes in section 2 during the filtration. M1 (polymeric 0.1 µm), M2 (polymeric 0.03 µm), M3 (ceramic 300 kDa), and M4 (Lab-made ceramic). Day 30 is the physical and chemical cleaning day. The error bars show 95% confidence intervals.

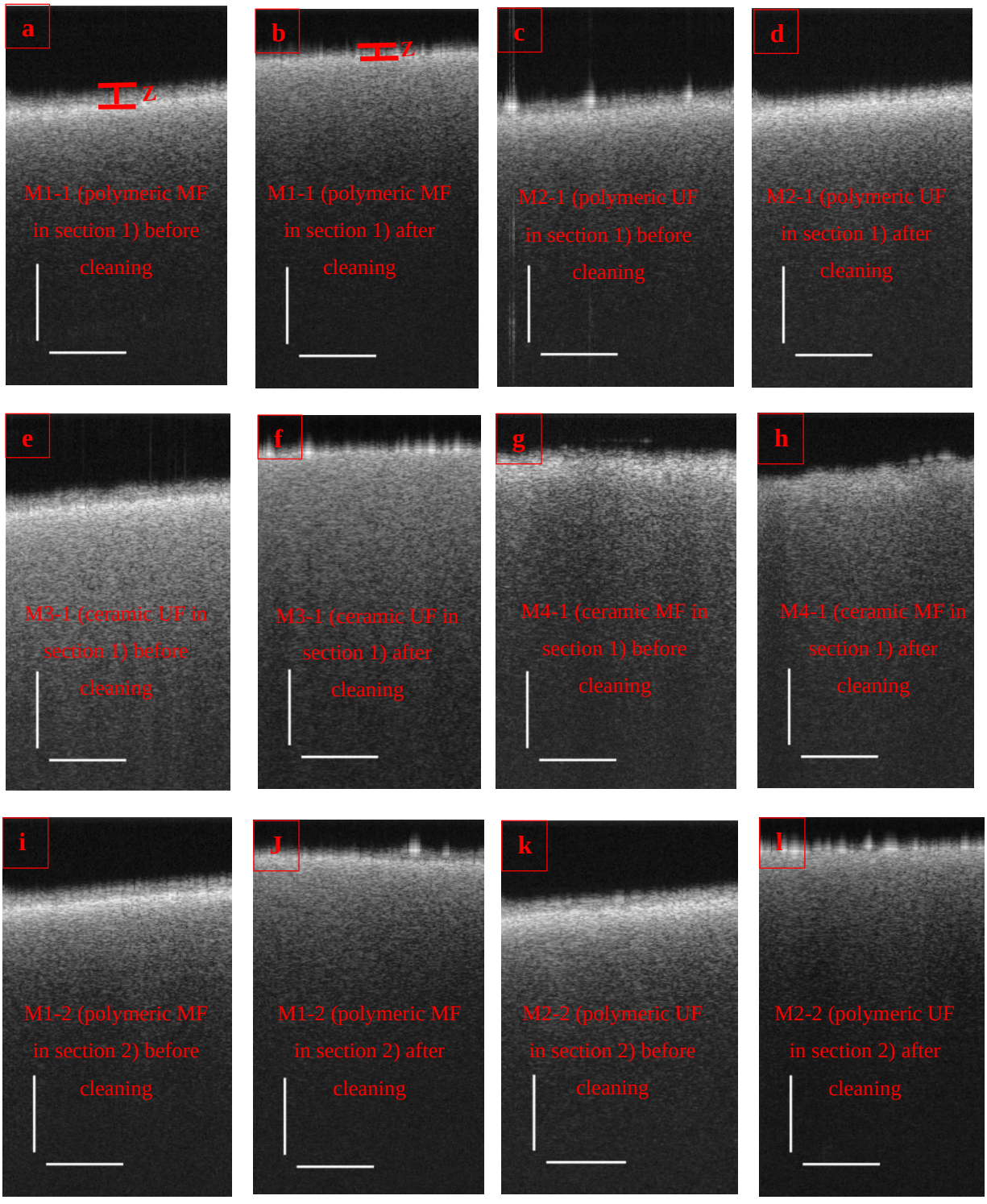
a
M1-1 (polymeric MF in section 1) before cleaning
b
M1-1 (polymeric MF in section 1) after cleaning
c
M2-1 (polymeric UF in section 1) before cleaning
d
M2-1 (polymeric UF in section 1) after cleaning
e
M3-1 (ceramic UF in section 1) before cleaning
f
M3-1 (ceramic UF in section 1) after cleaning
g
M4-1 (ceramic MF in section 1) before cleaning
h
M4-1 (ceramic MF in section 1) after cleaning
i
M1-2 (polymeric MF in section 2) before cleaning
J
M1-2 (polymeric MF in section 2) after cleaning
k
M2-2 (polymeric UF in section 2) before cleaning
l
M2-2 (polymeric UF in section 2) after cleaning

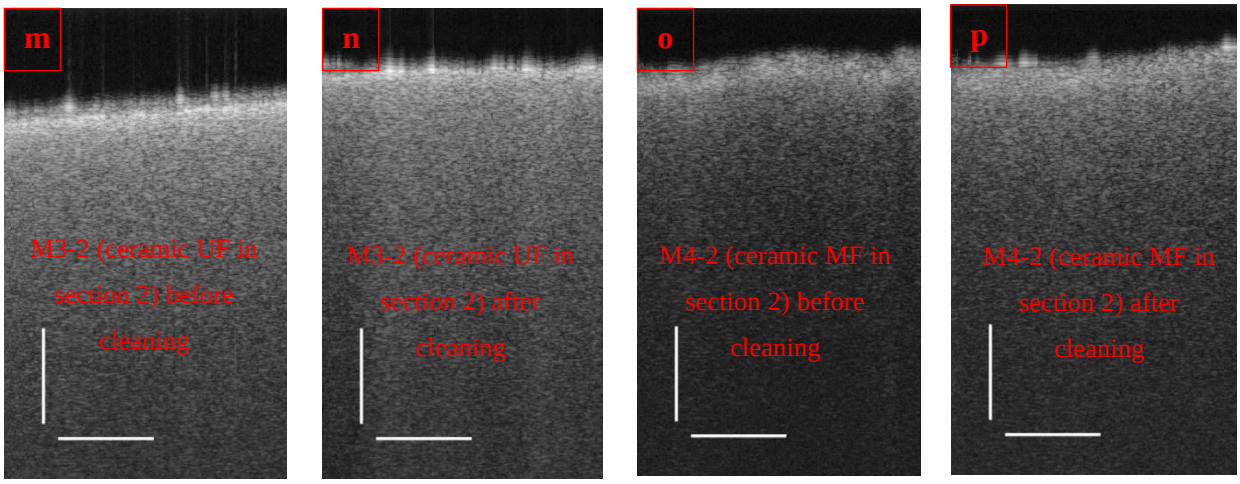

Figure C8. OCT images of a) M1-1 (polymeric MF in section 1) before cleaning, b) M1-1 (polymeric MF in section 2) after cleaning, c) M2-1 (polymeric UF in section 1) before cleaning, d) M2-1 (polymeric UF in section 1) after cleaning, e) M3-1 (ceramic UF in section 1) before cleaning, f) M3-1 (ceramic UF in section 1) after cleaning, g) M4-1 (ceramic MF in section 1) before cleaning, h) M4-1 (ceramic MF in section 1) after cleaning, i) M1-2 (polymeric MF in section 2) before cleaning, j) M1-2 (polymeric MF in section 2) after cleaning, k) M2-2 (polymeric UF in section 2) before cleaning, l) M2-2 (polymeric UF in section 2) after cleaning, m) M3-2 (ceramic UF in section 2) before cleaning, n) M3-2 (ceramic UF in section 2) after cleaning, o) M4-2 (ceramic MF in section 2) before cleaning, and p) M4-2 (ceramic MF in section 2) after cleaning. M1 (polymeric 0.1 µm MF), M2 (polymeric 0.03 µm UF), M3 (ceramic 300 kDa UF), and M4 (Lab-made ceramic MF). X and y-axis bars show 1 mm distance.

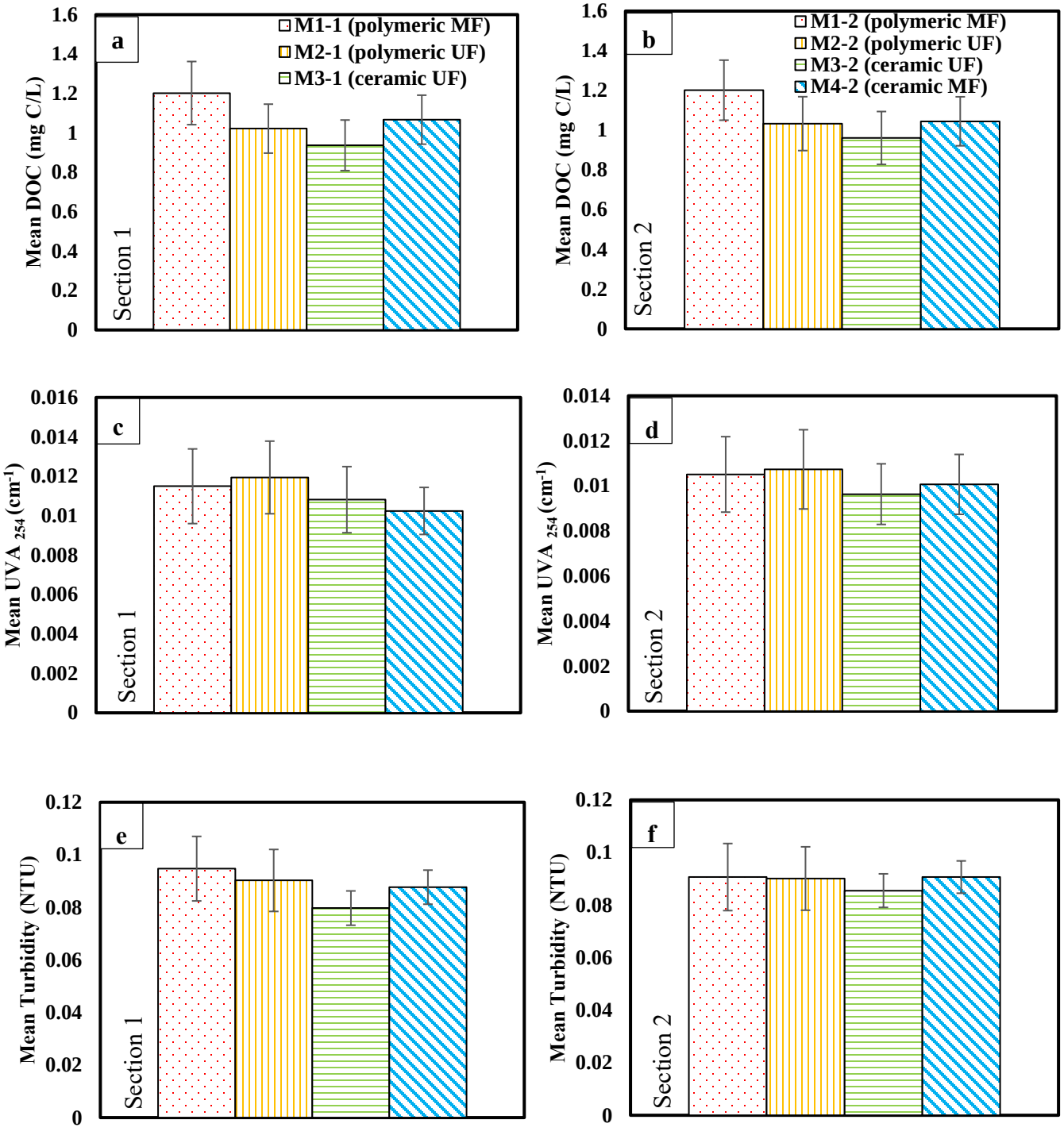

Figure C9. a, b) Mean DOC in section 1and section 2 days 1 – 68 c, d) Mean UVA_{254} in section 1 and section 2 days 1 – 68, e. f) Mean turbidity in section 1 and section 2 during the whole operation

period. M1 (polymeric 0.1 µm MF), M2 (polymeric 0.03 µm UF), M3 (ceramic 300 kDa UF), and M4 (Lab-made ceramic MF). The error bars show 95% confidence intervals.